Removal of H_2S, NH_3, and Tars from the Producer Gas of Biomass Gasification by Secondary Measures

---

A thesis submitted in full fulfilment of the requirements for the

Degree of Doctor of Philosophy

in Chemical and Process Engineering

at the University of Canterbury

by Yanjie Wang

University of Canterbury

2018

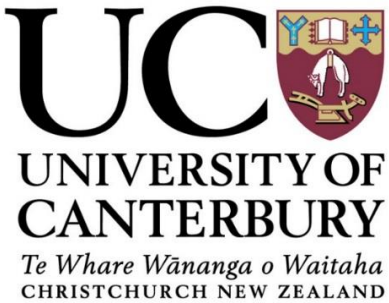

Table of contents

Lists of Figures

Lists of Tables

Acknowledgement

First of all, I would like to express my sincere and deepest appreciation to my principal supervisor professor Shusheng Pang. My academic journey in New Zealand started with him giving me a great opportunity to pursue my doctoral degree at the University of Canterbury. He provides me continuous guidance, patience, motivation and immense knowledge throughout my study. I would also like to thank him for providing me the scholarship, which was an indispensable part of my Ph.D. study. Without the financial support, I couldn't accomplish my goals. His help and support during the first couple of months settling in New Zealand gave me a peace of mind. I am also thankful for his support to let me attend an international conference in Stockholm and a domestic conference in Christchurch which offered me great opportunities for meeting world-renowned experts and contributed valuable ideas for my research.

I would also like to thank my co-supervisor, Dr. Alex Yip, for his valuable guidance for my study. He is especially appreciated for providing me constructive advice for my thesis confirmation.

I would like to offer my special thanks to the technical staff in the Department of Chemical and Process Engineering, Leigh Richardson, Stephen Beuzenberg, Glenn Wilson, Michael Sandridge, Graham Furniss, Frank Weerts, Tim Moore, Graham Mitchell and Rayleen Fredericks. Their technical and analytical support and advice helped me finish my thesis easier and faster.

I wish to acknowledge the help provided by Dr. Matthew Polson and Rob McGregor in the Department of Chemistry, and Stephen Brown, Chris Grimshaw, and Rob Spiers in the Department of Geological Sciences.

I wish to express my sincere gratitude to Mrs. Jingge Li, Dr. Ziyin (Simon) Zhang, Mr. Cheng Li, and Dr. Gaetano Dedual for giving me tremendous help and advice for my study and also life. Thanks to the nice colleagues in my office who accompanied me during my study and the undergraduate students who gave me experimental assistance.

I would like to thank my parents who provide me continuous love and support all the time and also give me encouragement for pursuing a doctoral degree in New Zealand. My grateful thanks also give to my boyfriend's parents for their understandings and kind help in my daily life. The last but definitely not least, I would like to thank my boyfriend, Jack Hu for all his support during my study. Your love, support and accompany make this journey much easier and enjoyable for me.

Publications

[1] Y. Wang and S. Pang, "Investigation of hydrogen sulphide removal from simulated producer gas of biomass gasification by titanomagnetite," *Biomass and Bioenergy*, vol. 109, pp. 61-70, 2018. https://doi.org/10.1016/j.biombioe.2017.12.021 (Chapter 4)

[2] Y. Wang and S. Pang, "Investigation of ammonia removal from the simulated producer gas of biomass gasification by H_2-reduced titanomagnetite," *Fuel*, vol. 220, pp. 800-809, 2018. https://doi.org/10.1016/j.fuel.2018.02.051 (Part of Chapter 5)

[3] Y. Wang and S. Pang, "The effects of temperature and gas species on ammonia removal in the simulated producer gas of biomass gasification by H_2-reduced titanomagnetite," *Energy & Fuels*, vol. 32, pp 5134-5144, 2018. https://pubs.acs.org/doi/10.1021/acs.energyfuels.7b03851 (Chapter 6)

[4] Y. Wang and S. Pang, "Investigation of Ammonia Removal from the Simulated Producer Gas of Biomass Gasification by H_2-Reduced Titanomagnetite," presented at the 25th European Biomass Conference and Exhibition, Stockholm, Sweden, 2017. https://doi.org/10.5071/25thEUBCE2017-2CV.3.65 (Part of Chapter 5)

Abstract

The combination of biomass gasification and Fischer-Tropsch (FT) synthesis is a promising technology for converting biomass to "green" liquid fuel. However, the clean-up process of removing tars, H_2S, NH_3, and the other contaminants from the producer gas of biomass gasification is required because these contaminants are problematic in the downstream processing and some are poisonous to the catalysts used in FT process. A number of methods for the gas cleaning have been reported but these methods either have negative impacts on the environment or are too costly.

This study aims to develop effective and low-cost methods for gas cleaning through experimental studies and fundamental analysis. This thesis describes studies on the removal of H_2S, NH_3, and tars from the producer gas of biomass gasification on a dual fluidised bed (DFB) gasifier via secondary measures with a target of the cleaned producer gas meeting the quality requirements of FT process. The key part of the thesis is the study of H_2S adsorption and NH_3 decomposition from the simulated producer gas by using titanomagnetite as a sorbent/catalyst in a fluidised bed quartz reactor. In addition, studies were also conducted on the modification of an oil scrubber system and preliminary results are also reported on tar removal from the actual producer gas of biomass gasification using the modified oil scrubber system.

Studies on the H_2S and NH_3 removal are divided into two sections. The first section presents the results of H_2S adsorption from the simulated producer gas by titanomagnetite in the fluidised bed quartz reactor. The aims of this section were to determine the effectiveness of titanomagnetite and the most effective operation temperatures for H_2S adsorption, and to examine the effect of steam and CO in the producer gas. In the experiments, H_2S concentration in the gases was controlled at 240±20 ppmv and the test gases were, respectively, (1) Ar gas, (2) simulated producer gas from

biomass steam gasification (CO, CO_2, CH_4 and H_2), (3) mixture of Ar and steam, and 4) mixture of Ar and CO. The unprocessed and H_2-reduced titanomagnetites were used as sorbents and operation temperatures were varied from 350 to 750°C. Results from the experiments show that both of the unprocessed and the H_2-reduced titanomagnetites were effective to remove H_2S in Ar gas at 600°C. However, at the same temperature, the H_2S removal efficiency was reduced in the simulated gas whereas the unprocessed titanomagnetite was more effective than the H_2-reduced titanomagnetite. Therefore, the unprocessed titanomagnetite was further investigated to find the effect of operation temperature on H_2S adsorption, and the results show that the most effective H_2S removal can be achieved at 400 - 450°C. It was also observed that both steam and CO in the gas mixture reduced the removal efficiency significantly although steam in the gas had more significant impacts.

For NH_3 removal, the studies include four parts: a). investigation of performances of both the unprocessed and the H_2-reduced titanomagnetites for NH_3 decomposition in Ar gas; b). investigation of the NH_3 decomposition from the simulated producer gas by the H_2-reduced titanomagnetite at different temperatures; c). examination of the effect of H_2S presence (230 ppmv) in the simulated producer gas on NH_3 decomposition using the H_2-reduced titanomagnetite; d) and analysis of side reactions in the gas cleaning process and examination of the effects of gas species on the NH_3 decomposition. In the last part, six gas mixtures were tested which include 1). H_2 in Ar; 2). CO in Ar; 3). CO_2 in Ar; 4). CH_4 in Ar; 5). H_2, CO and Ar; and 6). H_2, CO, CO_2 and Ar. All the experiments were conducted on the fluidised bed quartz reactor. In the test gases, the NH_3 concentration was 2300±200 ppmv and the operating temperatures were varied from 500 to 850°C.

The results from the NH_3 removal experiments show that in the control Ar gas, the H_2-reduced titanomagnetite had much higher activity than the unprocessed titanomagnetite to decompose NH_3

at all of the temperatures tested, and the efficiency of NH_3 removal increased with reaction temperature. The NH_3 decomposition by the reduced titanomagnetite was 97.8% at 500°C, 99.7% at 600°C, and 100% at 750 and 850°C, in comparison with corresponding values of 31.6%, 34.0%, 83.9% and 93.2% for the unprocessed titanomagnetite. Therefore, the H_2-reduced titanomagnetite was then employed to remove NH_3 in the simulated producer gas in which the NH_3 decomposition was 28.4±3.4%, 94.7±2.8% and 98.4±0.4%, respectively, at 500, 750 and 850°C. During NH_3 decomposition in the simulated producer gas, side reactions have been identified and analysed which played different roles at different temperatures. Side reactions including the reverse water-gas shift reaction, the (reverse) Boudouard reaction, the (reverse) carbon Methanation reaction and the iron oxidization reaction were involved. At 500°C, the carbon formation from the Boudouard reaction significantly suppressed the activity of the reduced titanomagnetite for NH_3 decomposition. In addition, it was found that 230 ppmv H_2S in the simulated producer gas had a significant adverse effect on the H_2-reduced titanomagnetite for NH_3 removal.

Negative effects by gas species in the simulated producer gas on NH_3 decomposition were attributed to equilibrium reduction by H_2, carbon deposition from the Boudouard reaction and carbide formation by CO, and α-Fe phase oxidization by CO_2. However, CH_4 was found to have only slight effect on NH_3 decomposition. H_2 in the simulated producer gas was also found to promote carbon formation by the reverse water gas reaction. In the meantime, H_2 also had favourable effects of protecting α-Fe phase on the catalyst from oxidizing by CO_2 and hindering carbon formation from CH_4 decomposition. Furthermore, CO_2 also had the positive effect of inhibiting carbon formation from the Boudouard reaction.

In the last part of the study, experiments were conducted on a modified oil scrubber to remove tars from the actual producer gas from the DFB gasifier. The results show that without accounting for

an unknown compound, the oil scrubber with either biodiesel or canola oil had the efficiency of removing ~96% GC-detectable tars from the producer gas of biomass gasification. It also illustrates that the oil scrubber with biodiesel or canola oil had the ability to remove the particles, water, and GC-undetectable tars in the producer gas of biomass gasification. However, an unknown compound was detected which concentration in the outlet gas was found to be higher than that in the inlet gas. Further studies will be conducted to identify this compound and to understand the reasons for this unexpected increase in its concentration in the producer gas.

Deputy Vice-Chancellor's Office
Postgraduate Office

UNIVERSITY OF CANTERBURY
Te Whare Wānanga o Waitaha
CHRISTCHURCH NEW ZEALAND

Co-Authorship Form

This form is to accompany the submission of any thesis that contains research reported in co-authored work that has been published, accepted for publication, or submitted for publication. A copy of this form should be included for each co-authored work that is included in the thesis. Completed forms should be included at the front (after the thesis abstract) of each copy of the thesis submitted for examination and library deposit.

Please indicate the chapter/section/pages of this thesis that are extracted from co-authored work and provide details of the publication or submission from the extract comes:

Part of Chapter 4 of this thesis has been published in the journal of "Biomass and Bioenergy".

- *Wang, Y. and Pang, S, "Investigation of hydrogen sulphide removal from simulated producer gas of biomass gasification by titanomagnetite," Biomass and Bioenergy, vol. 109, 61-70, 2018. https://doi.org/10.1016/j.biombioe.2017.12.021*

Part of Chapter 5 has been published in the journal of "Fuel" and was presented at the 25th European Biomass Conference and Exhibition, Stockholm, Sweden.

- *Wang, Y. and Pang, S, "Investigation of ammonia removal from the simulated producer gas of biomass gasification by H_2-reduced titanomagnetite," Fuel, vol. 220, 800-809, 2018. https://doi.org/10.1016/j.fuel.2018.02.051*
- *Wang Y. and Pang S., "Investigation of Ammonia Removal from the Simulated Producer Gas of Biomass Gasification by H_2-Reduced Titanomagnetite," presented at the 25th European Biomass Conference and Exhibition, Stockholm, Sweden, 2017. https://doi.org/10.5071/25thEUBCE2017-2CV.3.65*

Part of Chapter 6 of this thesis has been re-submitted to the journal of "Energy & Fuels" for publication which has been gone through revision and resubmitted.

- *Wang, Y., Pang, S, "The effects of temperature and gas species on ammonia removal in the simulated producer gas of biomass gasification by H_2-reduced titanomagnetite," Energy & Fuels, under review, 23/02/2018.*

Please detail the nature and extent (%) of contribution by the candidate:

The experimental work and writing up was primarily completed by the candidate. The candidate contributed 70-80% of the co-authored works.

Certification by Co-authors:

If there is more than one co-author then a single co-author can sign on behalf of all

The undersigned certifies that:

- The above statement correctly reflects the nature and extent of the PhD candidate's contribution to this co-authored work
- In cases where the candidate was the lead author of the co-authored work he or she wrote the text

Name: Shusheng Pang

Signature:  Date: *23-2-2018*

Glossary

Ar	Archimedes number, dimensionless
A_t	Bed cross-sectional area
C_f	one of the parameters of packing elements
CP	capacity parameter
D	diameter of the column
d_p	particle diameter
d_p^*	dimensionless particle size
d_t	quartz tube reactor inner diameter
F	gas flowrate
F_{LG}	flow parameter
G'	calculated gas flow rate
G	gas flow rate
g	acceleration of gravity
h_L	liquid hold-up
L	liquid flow rate
$Re_{p,mf}$	particle Reynolds number at minimum fluidization
u_L	liquid velocity
u_{mb}	minimum bubbling velocity
u_{mf}	minimum fluidization velocity
u_t	terminal velocity
u_t^*	dimensionless gas terminal velocity
u_V	gas velocity
$u_{v,Fl}$	gas velocity at the flooding point
σ	Surface tension
ε_{mf}	voidage of particle

ϕ_s	sphericity of particle
ρ_g	gas density
ρ_s	particle density
μ	gas viscosity
ρ_L	liquid density
μ_L	liquid viscosity
π	mathematical constant

AC	activated carbon
ACF	activated carbon fiber
BFB	bubbling fluidised bed
BR	Boudouard reaction
BTEX	benzene, toluene, ethyl-benzene and xylenes
BTX	benzene, toluene, and xylene
CAPE	Department of Chemical and Process Engineering, University of Canterbury
CDRR	carbon dioxide reforming reaction
CFB	circulating fluidised bed
CMR	carbon Methanation reaction
DFB	dual fluidised bed
DCM	dichloromethane
ECN	Energy Reach Centre of the Netherlands
ER	Equivalence ratio
EREC	European Renewable Energy Council
ESP	Wet electrostatic precipitators
FFB	fast fluidised bed
FICFB	Fast Internal Circulating Fluidised bed

FT	Fischer-Tropsch
GC	Gas Chromatograph
ID	inner diameter
IGCC	Integrated Gasification Combined Cycle
IPA	isopropyl alcohol
IS	internal standard
ISE	Ion Selective Electrode
L/G	liquid/gas ratio
LPG	liquefied petroleum gas
OD	out diameter
PAHs	polycyclic aromatic hydrocarbons
PFA	Perfluoroalkoxy
RDF	refuse derived fuel
RME	rapeseed oil methyl esther
RPS	rotational particle separator
RWGSR	reverse water-gas shift reaction
S/B	steam to biomass ratio
S/F	steam to fuel ratio
SG	simulated producer gas
SPE	solid phase extraction column
TOC	Total Organic Carbon
VTT	Technical Research Centre of Finland
XRD	X-Ray Diffraction
XRF	X-ray fluorescence
ZF	zinc ferrite
ZT	zinc titanate

1 Introduction

1.1 Introduction

Biomass is one of the most promising alternative energy sources to substitute fossil fuels in the future. It is widely available, renewable, and environmentally friendly. Most importantly, it is the most abundant renewable resource to produce second-generation liquid fuels and biochemicals, which is advantageous over the other clean energy sources such as wind, sun, water, geothermal, and nuclear. Biomass is considered as renewable and clean energy because it can be reproduced and the life-cycle emission of CO_2 (greenhouse gas) can be significantly reduced [1]. Generally, biomass is defined as any organic materials that are derived from plants or animals [2]. It includes forestry and agricultural residues, wood and wood wastes, and organic parts of municipal and sludge wastes [3]. Due to the pressure of global warming, air pollution, and energy crisis, the world energy supply will have a big shift from the fossil fuels to the renewables in the near future. European Renewable Energy Council (EREC) reported that if all of the projections in Table 1.1 are reached, nearly 50% energy consumption in the world will come from renewable energies by 2040 and biomass will contribute more than 50% of the renewables [4].

Table 1.1 Contribution of renewable energy sources to the world energy supply by 2040 [4].

	2001	2010	2020	2030	2040
Total energy consumption	10038.3	10549	11425	12352	13310
Biomass	1080	1313	1791	2483	3271
Large hydro	222.7	266	309	341	358
Small hydro	9.5	19	49	106	189
Wind	4.7	44	266	542	688
Photovoltaic	0.2	2	24	221	784
Solar thermal	4.1	15	66	244	480
Solar thermal electricity	0.1	0.4	3	16	68
Geothermal	43.2	86	186	333	493
Marine (tidal/wave/ocean)	0.05	0.1	0.4	3	20
Total renewables	1364.5	1745.5	2694.4	4289	6351
Renewables contribution	13.6%	16.6%	23.6%	34.7%	47.7%

At present, biomass contributes more than 10% of the world's energy and ranks as the fourth most important energy after coal, petroleum, and natural gas [5]. The global biomass was estimated to provide 33-1135 EJ/year [6-8]. Although there is only 5% of the biomass (13.5 billion metric tons) can be used to produce energy, which is still great enough for supply about 26% energy consumption in the world and equivalent to 6 billion tons of oil [9].

New Zealand has abundant biomass resources, largely from forestry and wood processing industry. At present, there are 1.751 million hectares of exotic plantation forests in New Zealand, which is about 7% of New Zealand's land area [10]. Although New Zealand forestry industry only contributes 1.1% industrial wood of the world's total supply [10], there is still a big quantity of forest residues from log harvesting and wood residues from wood processing. The woody biomass residues from forestry industry in New Zealand are reported to increase from about 3.1 million m^3/year in 2010 to 3.3 million m^3/year in 2020 [11]. However, if the biomass cannot be used efficiently and properly, environmental issues including forest fire and smog caused by biomass direct combustion are still troublesome for human.

Biomass utilization may be through biochemical conversion and thermochemical processes [12]. Biochemical conversion includes biological fermentation and anaerobic digestion, which mainly produce ethanol and gaseous product methane, respectively. Biochemical conversion is one of the popular research topics at this moment; however, it needs pre-treatment to convert the biomass into fermentable sugars before the biochemical conversion. This pre-treatment process will remove lignin thus the process losses over 30% of biomass. In addition, the ethanol from the fermentation process has a low concentration in water thus needs distillation for separation which involves extensive energy use. The biochemical processes are outside the scope of this work, so no more details will be discussed here.

Thermochemical conversion technology mainly includes biomass combustion, biomass pyrolysis and biomass gasification. Biomass combustion is a traditional way to use biomass as energy since mankind started to use energy sources and still available in most of developing countries. However, it has the limitation of low efficiency compared with the other utilization methods and also has the problem of causing air pollution such as smog. Biomass pyrolysis is a popular thermochemical

technology to use biomass and has been studied for a long time. The liquid product from the biomass pyrolysis, commonly termed as bio-oil, may be directly utilized for boiler, furnace, and turbines [13]. However, the bio-oil has a number of shortcomings such as high viscosity and acidity, high water content and content of oxygenated compounds, low heating value, and instability.

Biomass gasification is another useful thermochemical technology to convert biomass to the gaseous product, which is called producer gas or product gas. The producer gas is mainly composed of H_2, CO, CO_2, CH_4, lower concentrations of other gaseous hydrocarbons and contaminants. The producer gas can be used for heat generation after little or no clean-up process if the producer gas is maintained at certain temperatures. The producer gas can also be used for further processes including Fischer-Tropsch (FT) synthesis, alcohols synthesis, and dimethyl ether synthesis to generate liquid fuel. Biomass gasification has the advantages of high efficiency and flexibility for processing various feedstocks [5]. It also has the advantages of converting biomass to the gaseous product, which can be used directly and can also be processed into clean liquid fuel, hydrogen and chemicals [14]. Furthermore, biomass gasification technology has been extensively researched and developed over the past a few of decades, numerous large-scale commercial gasifiers have been built up and invaluable experience has been gained [14]. Therefore, biomass gasification is a promising technology to utilize biomass and realize global CO_2 reduction.

However, the contaminants in the producer gas of biomass gasification are the key barrier for utilizing the producer gas for different downstream processes, especially for the high requirements downstream processes for liquid synthesis. The contaminants can foul and damage the downstream engine, poison the catalysts for synthesizing liquid fuel or chemicals, and also pollute the air after burning. Therefore, the contaminants have to be destructed or removed to meet the required levels of cleanness for different downstream processes.

A 100kW dual fluidised bed (DFB) steam gasifier has been developed in the Department of Chemical and Process Engineering (CAPE) at the University of Canterbury, as sketched in Figure 1.1. The DFB gasifier consists of two columns of a bubbling fluidised bed (BFB) column and a fast fluidised bed (FFB) column. The biomass steam gasification process occurs in the BFB column with biomass continuously being fed into it and steam as gasification agent is introduced from the bottom of it. During the biomass steam gasification process, biomass char is produced and dropped to the FFB column with the bed material via gravity through a chute between the BFB column and the FFB column. In the FFB column, air is injected for combustion of char from the BFB column and the heat is transferred to the bed material. Additionally, supplementary liquefied petroleum gas (LPG) is injected into the FFB column for providing sufficient heat to achieve the target operation temperature for the biomass gasification [15]. Thus, the bed material with heat is carried out by the flue gas from the FFB column and separated by a cyclone and siphon at the top of the gasification system. Then the separated bed material is cycled to the BFB column to provide heat for the biomass steam gasification. More detailed information about the DFB gasifier system can be found elsewhere [15-17].The producer gas generated from the BFB gasifier mainly contains H_2, CO, CO_2, CH_4, low concentration of other gaseous hydrocarbons and impurities. The impurities comprise particles, tars, S-containing compounds (H_2S, COS, and CS_2), N-containing compounds (NH_3 and HCN), halogens (HCl, HBr, and HF), and some volatile inorganic metals [1, 14, 18, 19]. Since the producer gas from the DFB steam gasifier is used for FT synthesis, the impurities have to be removed stringently to meet the requirements of FT synthesis. The requirements are available in Table 1.2.

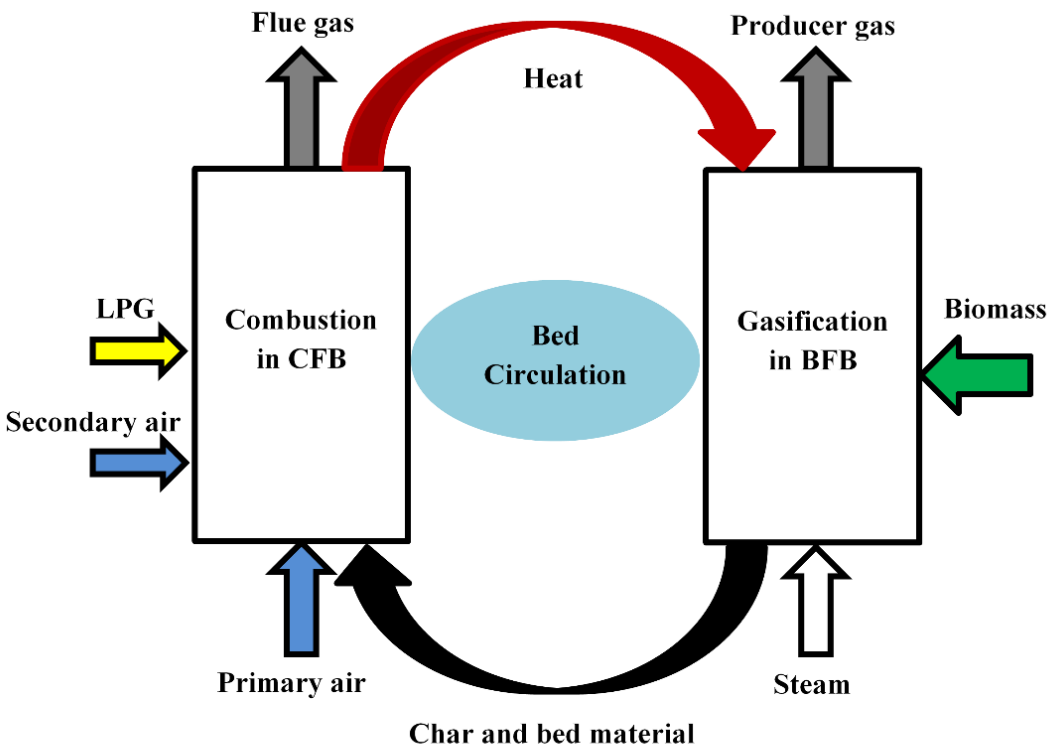

Figure 1.1 Schematic diagram of DFB gasifier [15, 16].

Table 1.2 FT Feed Gas Specifications [1].

Impurity	Removal level
Organic compounds[a] (tars)	Below dew point
N-compounds (NH_3, HCN)	<1 ppmV
S-compounds (H_2S, COS, CS_2)	<1 ppmV
Halogen (HCl, HBr, HF)	<10 ppbV
Alkaline metals	<10 ppbV
Solids (soot, dust, ash)	Essentially completely
-class 2[b] (hetero atoms)	<1 ppmV
CO_2, N_2, CH_4 and larger hydrocarbons	<15 vol%

[a] Organic compounds also include benzene, toluene, and xylene (BTX)

[b] Class 2 tars comprise phenol, pyridine, and thiophene

There are two main methods for clean-up of the producer gas from biomass gasification. The primary measures are conducted in the gasifier for minimising the production of contaminants or converting them into simpler or useful gaseous species, and the secondary measures are used after the gasifier to absorb or convert impurities [19, 20]. The primary measures include optimisation of the operation parameters for biomass gasification and utilization of catalysts in the gasifier. The secondary measures include physical methods, thermal cracking methods, and hot catalytic methods. Since 1980's, it has been realized that it is impossible to clean the producer gas merely

utilizing primary measures to meet the stringent requirements [1, 21]. Therefore, suitable secondary measures should be applied downstream the gasifier to further remove the contaminants.

1.2 Thesis scope and outline

This thesis aims to reduce the concentrations of H_2S and NH_3, tars in the producer gas to meet the requirements of FT synthesis via appropriate secondary measures. This thesis is composed of 8 chapters. Chapter 1 includes an introduction and thesis scope and outline.

Chapter 2 is an extensive literature review which includes three parts. The first part provides a comprehensive understanding of the effects of gasifier type, various gasification conditions, and bed material on the generation and concentrations of tars, H_2S and NH_3 in the producer gas of biomass gasification. This has shown that the concentrations of tars, H_2S and NH_3 in the producer gas can be reduced by primary measures of using suitable gasifier, optimisation of operation conditions and applying catalytic bed material. In the second part, numerous types of secondary measures have been reviewed for removal of tars, H_2S and NH_3, respectively. This leads to a broad and valid comparison and analysis of different secondary measures. The third part introduces the previous works completed in this research group for reducing the concentrations of tars, H_2S and NH_3 in the producer gas from a DFB gasifier by primary measures and secondary measures. Those three parts comprehensive literature review lead to final determinations of using the hot gas cleaning methods for H_2S and NH_3 removal and an oil scrubber for tar removal.

Chapter 3 covers the introduction of the hot gas cleaning methods, equipment, and sorbent/catalyst materials used for H_2S and NH_3 removal. It also presents the determination of feed gas flow rate, and H_2S and NH_3 concentrations in this research. In addition, the development of methodologies

for H_2S and NH_3 sampling and analysis, and analytical techniques for analysing the other gas species are provided. The developed methods and techniques are used in Chapter 4, 5 and 6.

Chapter 4 contains the experimental results and main findings of H_2S removal from the simulated producer gas by titanomagnetite in a fluidised bed quartz reactor. The work in this chapter has been published in the journal of 'Biomass and Bioenergy' [22].

Chapter 5 and Chapter 6 focus on the investigation of NH_3 removal from the producer gas via the hot catalytic reactor with titanomagnetite as the catalyst. Chapter 5 presents the studies of performances of the unprocessed and H_2-reduced titanomagnetites for NH_3 decomposition in Ar gas, the efficiency of the H_2-reduced titanomagnetite for NH_3 decomposition in the simulated producer gas at different temperatures, and the effect of H_2S on NH_3 decomposition in the simulated producer gas. Chapter 6 shows the studies of the effects of temperature and gas species on the NH_3 decomposition in different gas mixtures. Part of the work in Chapter 5 has been published in the journal of 'Fuel' [23]. The work of Chapter 6 has been published in the journal of 'Energy & Fuels' [24].

Chapter 7 details the modification and description of the oil scrubber system for tar removal from the actual producer gas of biomass gasification, the methodology for tar sampling and analysis and the results of the preliminary experiments. Chapter 8 presents the conclusions of this whole thesis and the recommendations for further work.

1.3 Reference

[1] H. P. C. H. Boerrigter, D.J. Slort, H. Bodenstaff, A.J. Kaandorp, H. den Uil, L.P.L.M. Rabou, "Gas Cleaning for Integrated Biomass Gasification (BG) and Fischer-Tropsch (FT)

Systems," in "Energy Research Centre of the Netherlands (ECN), Petten, The Netherlands, report RX-04-041," May 2004.

[2] A. Loppinet-Serani, C. Aymonier, and F. Cansell, "Current and foreseeable applications of supercritical water for energy and the environment," *ChemSusChem,* vol. 1, no. 6, pp. 486-503, 2008.

[3] A. Kumar, D. Jones, and M. Hanna, "Thermochemical Biomass Gasification: A Review of the Current Status of the Technology," *Energies,* vol. 2, no. 3, p. 556, 2009.

[4] "Renewable Energy Scenario to 2040, half of the global energy supply from renewables in 2040," European Renewable Energy Council (EREC)2004.

[5] S. Heidenreich and P. U. Foscolo, "New concepts in biomass gasification," *Progress in Energy and Combustion Science,* no. 0, 2014.

[6] G. Fischer and L. Schrattenholzer, "Global bioenergy potentials through 2050," *Biomass and bioenergy,* vol. 20, no. 3, pp. 151-159, 2001.

[7] M. Hoogwijk, A. Faaij, R. Van Den Broek, G. Berndes, D. Gielen, and W. Turkenburg, "Exploration of the ranges of the global potential of biomass for energy," *Biomass and bioenergy,* vol. 25, no. 2, pp. 119-133, 2003.

[8] M. Parikka, "Global biomass fuel resources," *Biomass and Bioenergy,* vol. 27, no. 6, pp. 613-620, 2004.

[9] P. Basu, "Chapter 1 - Introduction," in *Biomass Gasification, Pyrolysis and Torrefaction (Second Edition)*Boston: Academic Press, 2013, pp. 1-27.

[10] *Ministry for Primary Industries of New Zealand*. Available: http://www.mpi.govt.nz/news-and-resources/open-data-and-forecasting/forestry/

[11] J. Hongrapipat, "Removal of NH_3 and H_2S from biomass gasification producer gas," Doctor of Philosophy, Chemical and Procees Engineering, University of Canterbury, Christchurch, New Zealand, 2014.

[12] A. A. Ahmad, N. A. Zawawi, F. H. Kasim, A. Inayat, and A. Khasri, "Assessing the gasification performance of biomass: A review on biomass gasification process conditions, optimization and economic evaluation," *Renewable and Sustainable Energy Reviews,* vol. 53, pp. 1333-1347, 2016.

[13] F. Abnisa and W. M. A. W. Daud, "A review on co-pyrolysis of biomass: an optional technique to obtain a high-grade pyrolysis oil," *Energy Conversion and Management,* vol. 87, pp. 71-85, 2014.

[14] D. J. Stevens, "Hot gas conditioning: recent progress with larger-scale biomass gasification systerms," National Renewable Energy Laboratory, the U.S. Department of Energy LaboratoryNREL/SR-510-29952, August 2001.

[15] W. Saw and S. Pang, "Influence of mean gas residence time in the bubbling fluidised bed on the performance of a 100-kW dual fluidised bed steam gasifier," *Biomass Conversion and Biorefinery,* vol. 2, no. 3, pp. 197-205, 2012.

[16] W. Saw, H. McKinnon, I. Gilmour, and S. Pang, "Production of hydrogen-rich syngas from steam gasification of blend of biosolids and wood using a dual fluidised bed gasifier," *Fuel,* vol. 93, pp. 473-478, 2012.

[17] Z. Zhang and S. Pang, "Experimental investigation of biomass devolatilization in steam gasification in a dual fluidised bed gasifier," *Fuel,* vol. 188, pp. 628-635, 2017.

[18] H. Boerrigter and R. Rauch, "Review of applications of gases from biomass gasification," *ECN Biomassa, Kolen en Milieuonderzoek,* vol. 20, 2006.

[19] J. Hongrapipat, W. L. Saw, and S. Pang, "Removal of ammonia from producer gas in biomass gasification: integration of gasification optimisation and hot catalytic gas cleaning," *Biomass Conversion and Biorefinery*, vol. 2, pp. 327-348, 2012.

[20] L. Devi, K. J. Ptasinski, and F. J. J. G. Janssen, "A review of the primary measures for tar elimination in biomass gasification processes," *Biomass and Bioenergy*, vol. 24, no. 2, pp. 125-140, 2003.

[21] W. Torres, S. S. Pansare, and J. G. Goodwin Jr, "Hot gas removal of tars, ammonia, and hydrogen sulfide from biomass gasification gas," *Catalysis reviews*, vol. 49, no. 4, pp. 407-456, 2007.

[22] Y. Wang and S. Pang, "Investigation of hydrogen sulphide removal from simulated producer gas of biomass gasification by titanomagnetite," *Biomass and Bioenergy*, vol. 109, pp. 61-70, 2018.

[23] Y. Wang and S. Pang, "Investigation of ammonia removal from the simulated producer gas of biomass gasification by H_2-reduced titanomagnetite," Fuel, vol. 220, pp. 800-809, 2018.

[24] Y. Wang and S. Pang, "The Effects of Temperature and Gas Species on Ammonia Removal in the Simulated Producer Gas of Biomass Gasification by H_2-Reduced Titanomagnetite," *Energy & Fuels*, vol. 32, no. 4, pp. 5134-5144, 2018.

2 Literature Review

2.1 Tars, NH_3 and H_2S in the producer gas of biomass gasification

The producer gas of biomass gasification mainly consists of H_2, CO, CO_2 and CH_4 which can be used for power generation, liquid fuel synthesis, production of pure hydrogen or production of chemicals. Fischer-Tropsch (FT) synthesis is one of the promising processes to generate liquid fuel by using the producer gas of biomass gasification [1]. However, undesirable contaminants also present in the producer gas which include tars, and non-tar contaminants like N-containing compounds, S-containing compounds, particles, alkali and metals and halogens [2-4]. Although CO_2, CH_4, N_2 and larger molecular hydrocarbons in the producer gas are also undesired for the FT synthesis, the requirements for them are less stringent which are much easier to be controlled than the other contaminants [1]. The overall biomass gasification process can be described by the following equation (Eq. 2.1). The concentration of tars in the producer gas is mainly driven by the gasifier type, operation conditions of the gasifier and, to a less extent, the biomass type. However, concentrations of the non-tars contaminants are significantly affected by the contents of N, S, ash, metals and halogen elements in the biomass [2].

$$\begin{aligned} \text{biomass} \xrightarrow{O_2/H_2O} & H_2, CO, CO_2, H_2O, CH_4 + C_{\geq 2} \\ & + \text{tar} + \text{char} + \text{ash} \\ & + NH_3 + HCN + HCl + H_2S + \text{other sulfur gases} \end{aligned} \tag{2.1}$$

The contaminants are highly undesirable for the downstream processes because of their severe impacts on the equipment, downstream catalysts, and environment. Tars are the notorious ones among all of the contaminants in the producer gas from biomass gasification for downstream applications [5, 6]. The contaminants in the producer gas can dramatically foul and clog the

equipment in the system, which significantly increases the cost of repairing and maintenance. Moreover, they can also inactivate or poison the catalysts used in downstream processes and pollute the environment. Therefore, these impurities must be destructed or removed stringently to meet the acceptable levels, which depends on the downstream applications. For example, kilns and co-firing systems have very low requirements for the contaminants concentration, so the producer gas from biomass gasification only needs little or no clean-up process as long as the producer gas is maintained at certain temperatures [7]. However, some applications like FT synthesis process and methanol synthesis process have very stringent requirements for the contaminants in the producer gas and gas composition. Therefore, the contaminants in the producer gas should be removed efficiently, and the gas composition should be adjusted as well.

This chapter will provide a comprehensive review on the removal of tars, N-containing compounds (mainly NH_3) and S-containing compounds (mainly H_2S) which have been known as the most abundant and the most difficult to be removed. Since the producer gas in this research is to be used for FT synthesis process, the contaminants in the producer gas should meet the feed gas specifications of tars being below the dew point (<0.1 mg/Nm^3), and both NH_3 and H_2S being less than 1 ppmv [1, 8-10]. Therefore, this research will primarily focus on the abatement of tars, NH_3 and H_2S in the producer gas of biomass gasification.

2.1.1 Tars

The definition of “tars” has been discussed in literature for a long time but without conclusive result. Normally, “tars” are used to describe the complex oxygenated organic compounds generated from pyrolysis or gasification. They are vaporized matters or as persistent aerosols in the hot gas stream, but condense at reduced temperatures [7]. In this study, “tars” are defined as

the aromatic hydrocarbons with molecular weights more than that of benzene (78 g/mol), and this definition has been accepted elsewhere [7, 11]. Tars in the biomass gasification producer gas are generated through a series of complicated reactions during the biomass gasification process, which are comprised of aromatic compounds ranging from single ring to 5-ring, as well as other oxygen-containing hydrocarbons [12]. Normally, tars produced from biomass gasification can be classified into 5 classes. Class 1 tar compounds are those of Gas Chromatograph (GC)-undetectable tars; Class 2 tars are heterocyclic aromatic compounds; Class 3 tars are aromatic compounds (such as xylene, benzene, and toluene); Class 4 tars are light polyaromatic hydrocarbons (such as naphthalene, fluorine and phenanthrene); and Class 5 tars are heavy polyaromatic hydrocarbons (such as fluoranthene, pyrene, up to coronene) [13]. The formation and the concentration of tars in the biomass gasification producer gas are dependent on the operation temperature, steam/ biomass (S/B) ratio, gasifier type and bed material of biomass gasification.

Among these affecting factors, temperature is the most important parameter significantly influencing the composition of tars and the concentration of tars in the producer gas. Stevens [7] reported that tars were formed from the volatilized material in biomass pyrolysis/ gasification process by dehydration, condensation and polymerization reactions and the tar composition was highly dependent on temperature. Elliott [14], in a comprehensive review, stated that the composition of tars transited when temperature increased, and the transition process from low temperature to high temperature is shown in Figure 2.1. Tars produced in biomass gasification at operation temperatures between 400°C and 600°C mainly comprise molecules with complex structures and have a high proportion of heteroatoms [15, 16], which are normally called “primary tars” [17]. The “primary tars” are thermally unstable when temperature is higher than 600°C, and are easily decomposed and then rearranged into gases or “secondary tars” [18]. The “secondary

tars" are primarily aromatic compounds which are formed from mono-aromatics and polyaromatics. The "secondary tars" are less active and harder to be converted than the "primary tars" under high temperatures [11]. In the extensive literature review of Devi et al. [12], it was also found that temperature not only played an important role on the tar composition but also influenced the tar content in the producer gas. The above findings are consistent with those reported by Baker et al. [19] who found that the tar yield from different biomass gasifiers was significantly reduced with increasing operation temperature as shown in Figure 2.2. Similar results were also found by Meng et al. [20] who performed gasification experiments in a 100 kW oxygen-steam blown circulating fluidised bed (CFB) gasifier with three biomass feedstock (Agrol, willow and residues of dry distiller's grains with solubles). They illustrated that with an increase of the gasification temperature, class 3 tars were converted class 2 tars and 5 tars to class 4 tars, respectively. The authors [20] also reported that the maximum tar concentration was ~12.4 g/Nm^3 in the producer gas from gasification of Agrol. In addition, tar concentration could be minimized by increasing the S/B ratio [20]. Paasen and Kiel [21] also demonstrated that the tar concentration in the producer gas of biomass gasification generated from a lab-scale bubbling fluidised bed (BFB) was reduced when the gasification temperature increased from 750°C to 950°C and the tar composition was converted from alkyl-substituted polycyclic aromatic hydrocarbons (PAHs) to non-substituted PAHs. Moreover, Hernández et al. [22], studied the gasification of dealcoholized marc of grape in a small-scale drop tube gasifier with air and steam as the gasification agents, respectively. The results showed that the tar content and the phenol proportion in the producer gas was reduced significantly when the temperature was increased from 750 to 1200°C. However, with temperature increase, the contents of PAHs, benzene, toluene, ethyl-benzene and xylenes (BTEX) fractions were increased. Narváez et al. [23] studied the effects of different parameters on the tar content in

the producer gas of biomass gasification by using pine sawdust mixed with 2-5 wt% of a calcined dolomite as the feedstock in an air-blown BFB gasifier. The authors [23] also observed that temperature increment had obvious improvement on the producer gas quality and reduction of tar content in the producer gas. However, the selection of operation temperature needs to consider other factors such as gas heating value, bed material sintering, and costs of materials used for the gasification reactor [10, 12].

$$\underset{400°C}{\text{Mixed oxygenates}} \rightarrow \underset{500°C}{\text{Phenolic ethers}} \rightarrow \underset{600°C}{\text{Alkyl phenolics}} \rightarrow \underset{700°C}{\text{Heterocyclic ethers}} \rightarrow \underset{800°C}{\text{PAH}} \rightarrow \underset{900°C}{\text{Larger PAH}}$$

Figure 2.1 Tar transition process with temperature increasing [14].

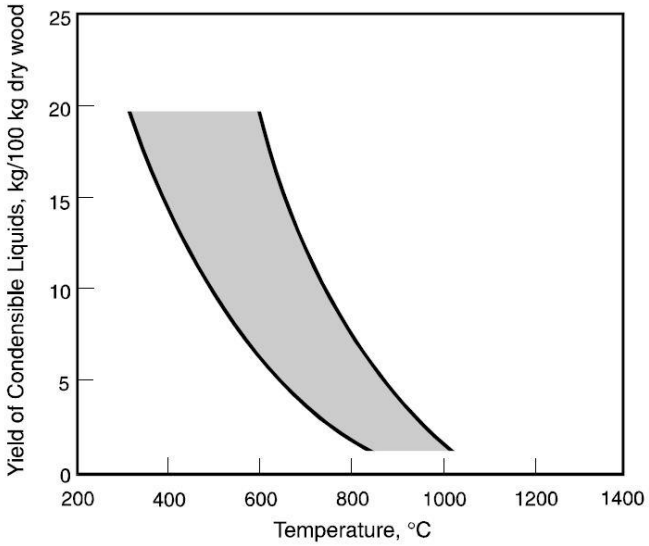

Figure 2.2 The dependency of tar yield on the maximum reaction temperature [19].

In addition to temperature, S/B ratio is another important parameter to impact the tar concentration and formation in biomass gasification process when steam is used as the gasification agent. Meng et al. [20] illustrated that increasing S/B ratio in a steam-oxygen blown CFB gasifier had a positive effect on reducing the total tar concentration by testing three different biomasses (Agrol, willow and dry distiller's grains with solubles). During Agrol gasification, the total tar concentration was

decreased from 10.2 to 7.2 g/Nm^3 when S/B ratio was increased from 0.97 to 1.25 at both 770 and 810°C. By using willow as the feedstock, the total tar concentration was reduced from 6.6 to 4.7 g/Nm^3 when S/B ratio was increased from 0.93 to 1.22 at 780°C [20]. A similar result for gasification of residues of dry distiller's grains with solubles, the total tar decreased from 9.1 to 7.3 g/Nm^3 with S/B ratio increasing from 0.98 to 1.1 at 730°C [20]. For the formation of different class tars, generally, the concentrations of class 3, 4 and 5 tars decreased as S/B ratio was increased, while class 2 tar concentration increased. However, there were also cases where the different trend was observed. Saw and Pang [24] also investigated the influence of S/B ratio on the tar concentration in the producer gas in a 100 kW dual fluidised bed (DFB) steam gasification of radiata pine woody biomass with the bed material of calcite and greywacke mixtures. In this study, S/B ratio had no obvious effect on tar formation when calcite and greywacke (50/50 wt/wt) mixture was used as bed material. However, when 100% calcite was used as the bed material in the gasifier, class 5 tars decreased from 40 to 8 mg/Nm^3 with S/B ratio increased from 0.67 to 0.96, whereas no change was found for class 2 and class 4 tars although class 3 tar concentration was increased from 0.4 to 0.6 mg/Nm^3 [24].

In addition, the tar concentration and tar composition in the producer gas from biomass gasification can also be affected by gasifier type. It has been proven, both theoretically and experimentally, that the producer gas generated from downdraft gasifiers has less tars than that from fluidised bed gasifiers, and much less than that from updraft gasifiers. Milne and Evans [25] explained that in the updraft gasification, when the up-flowing hot gasification agent (air/oxygen/steam) contacts the downward moving biomass at the gasifier bottom, the biomass is pyrolysed and then gasified at the operation temperature. While the producer gas moves upwards, it heats up the biomass and the biomass is then decomposed into volatiles and tars which are carried up by the producer gas.

Therefore, the tar concentration in the final producer gas is high and most of the tars are primary tars.

On the other hand, in the downdraft gasifier, the gasification agent flows downwards with the biomass, with biomass undergoing through drying, pyrolysis and gasification. In this way, the temperature at bottom gasification zone is the highest and most of the tars are cracked and changed to secondary tars when the producer gas go through this high-temperature zone [25].

In the fluidised bed gasifier, when gasification agent flows through the bed comprising bed material and biomass particles, the bed is fluidised and well mixed with the gasification agent [25]. Hence, gasification temperature is uniform within the gasifier and the producer gas does not go through a high-temperature zone. Therefore, the tar concentration in the producer gas from the fluidised bed gasifier is normally between that from downdraft gasifier and that from updraft gasifier.

Warnecke [26] conducted a systematic overview of various gasifier designed and compared their performance in biomass gasification. He found that the tar concentration in the fluidised bed was lower than that in the updraft gasifier. It was proposed that the larger free board in the fluidised bed gasifier than the updraft gasifier was useful for converting the tars [26]. Morf et al. [15] reported that updraft gasifier produced the highest tar concentration of 50 g/Nm^3 in the producer gas from gasification of wood chips, whereas, downdraft fixed bed gasifier had the advantage to lower tar concentration to 0.5 g/Nm^3 in gasification of the same biomass. For the same biomass, the average tar concentration in the producer gas of fluidised bed gasifier ranged from 8 to 12 g/Nm^3. Similar trend can be found in the review report by Stevens [7] that in biomass gasification, the updraft fixed bed gasifier produced the highest tar concentration of 20-200 g/Nm^3, but

downdraft fixed bed gasifier had positive effect to reduce the tar concentration to 0.1-1.2 g/Nm^3. In the producer gas from fluidised bed and CFB gasifiers, tar concentration had similar levels of 1-15 g/Nm^3. Furthermore, Milne and Evans [25] reviewed the influence of gasifier types on tar concentration and composition, and concluded that updraft gasifiers produced higher tar concentration than any other gasifiers and normally had tar concentration of 50 g/Nm^3 in the producer gas, fluidised beds and CFBs had an average tar concentration of 10 g/Nm^3 and downdraft gasifiers produced the least tar with concentration of less than 1 g/Nm^3.

In the fluidised bed gasifiers, bed materials also affect the tar content and tar composition in the producer gas. Olivine as the gasifier bed has been investigated by a number of studies because of its activity for tar reduction and reasonable price. In studies at Güssing gasification plant and Vienna University of Technology, Austria, Kirnbauer et al. [27] reported that the used olivine had higher activity than the fresh olivine to reduce tar formation by 82% for the GC-detectable tars and by 65% for the gravimetric tars (heavy tars). This was attributed to the higher calcium content on the used olivine than the fresh olivine. Moreover, there were fewer components in the tar composition from the biomass gasification catalysed by the used olivine than the fresh olivine [27]. The results showed repeatability between a 100kW gasifier and an 8MW industrial plant at Güssing. In a separate study, Meng et al. [20] reported that the pre-treated Austrian olivine (Bed 1) had higher catalytic reactivity than the natural Austrian olivine (Bed 2) for decomposing class 5 tars. Bed 1 olivine showed higher activity to reduce total tar concentration than its mixture with quartz sand, in which the tar concentrations were 4.5 and 6.9 g/Nm^3, respectively [20]. Virginie et al. [28] also revealed that olivine had high activity to reduce the tar formation in the producer gas of pine wood gasification, in which the tar concentration was reduced from 16.8 g/Nm^3 with silica sand to 5.5 g/Nm^3 with olivine in a bench scale dual fluidised bed (DFB) at 800°C. When Fe was

added onto olivine, the activity was promoted significantly and the tar concentration was further dropped to 3.7 g/Nm^3 [28]. Pfeifer et al. [29] in Vienna University of Technology also reported that a Ni-olivine showed promising ability to reduce the tar content in the producer gas by up to 75% based on experiments on a 100 kW_{th} DFB biomass steam gasifier. Furthermore, calcite also attracts a lot of attention recently because of its flexibility to control H_2/CO ratio and performance to decrease tar concentration in the producer gas. Saw and Pang [24] reported that when calcite was employed as the bed material in a 100 kW_{th} DFB steam gasifier, the total tar concentration can be decreased from 5.0 to 0.7 g/Nm^3 with the calcite loading increasing from 0% to 100%. However, the high attrition rate is the disadvantage of calcite. Apart from the above in-bed materials, calcined dolomites, magnesites and iron catalysts have also been intensively studied to reduce tar concentration [12]. It was reported that calcined dolomite played an important role to crack tars in the gasifier due to steam and dry reforming reactions. Corella et al. [30] revealed that the tar concentration in the producer gas of pine sawdust steam gasification decreased from 29.8 g/Nm^3 with sand as the bed material to 6.0 g/Nm^3 when calcined dolomite was used in the fluidised bed gasifier. A similar conclusion was drawn by Olivares et al. [31] who found that calcined dolomite used in the gasifier bed significantly reduced the tar concentration from 12 to 2-3 g/Nm^3. The authors [31] also found that the main decrease of tar content was achieved when the calcined dolomite amount increased from 0 to 10 wt.% and more dolomite in the gasifier bed only reduced tar concentration slightly. Narváez et al. [23] found that calcined dolomite not only had the ability to crack tars, but also had a promising function to react with contaminants like HCl, SO_2 and PAHs, and thus reducing their concentrations to low levels. It was reported that the tar concentration could be lowered from 6.67 to 4.0 g/Nm^3 when 3 wt.% of calcined dolomite was added to the biomass.

From the above discussion, the tar concentration and composition in the producer gas from biomass gasification are affected by the gasification temperature, the gasifier type, S/B ratio in steam gasification and the bed material in fluidised bed gasifiers. Tar concentration can be reduced through primary measures which are employed during the gasification. However, it is hard or impossible to lower the tar concentration to a level that meets the stringent requirements of downstream applications by only using the primary measures [5]. Therefore, tars in the producer gas have to be further removed to acceptable levels by secondary measures after the gasifier which will be discussed later in this chapter.

2.1.2 Contaminants of nitrogen-containing compounds

Contaminants of nitrogen-containing compounds in the producer gas of biomass gasification mainly include ammonia (NH_3), cyanides ($-C\equiv N$), nitrogen oxides (NO_x), thiocyanates (SCN^-) and various N-tar compounds [32]. NH_3 is the major component among all of the N-containing contaminants [7, 32-35] which concentration ranges from 100 to 5000 ppmv in the producer gas of biomass gasification. However, in most cases, the NH_3 concentration is lower than 2300 ppmv in the producer gas of woody biomass gasification [32, 36-39]. HCN is the second N-containing contaminant in the producer gas of biomass gasification, which concentration is about 20 ppmv and approximately the same as that in coal gasification [2]. The other N-containing contaminants have much lower concentrations thus will not be investigated in this study [32]. Concentrations of N-containing contaminants in the producer gas are strongly dependent on the N contents in the feedstock, gasifier types and gasification operating conditions [32, 37]. Normally, 60-80% of nitrogen in the feedstock was liberated and transformed to NH_3 with the rest nitrogen in the feedstock primarily being converted into N_2 and HCN [40, 41]. NH_3 and HCN are known as the toxin for the catalysts used in downstream processes and the precursor of NO_x when oxidation

process occurs [41]. Therefore, these contaminants must be decomposed or abated strictly to acceptable concentration levels depending on the downstream application requirements. In this work, NH_3 will be mainly reviewed and studied.

The concentration of NH_3 is highly dependent on the feedstock type, more specifically, the N content in the feedstock [32]. In the research on co-gasification of coal and woody biomass on a DFB gasifier, Aigner et al. [42] reported that the NH_3 concentration in the producer gas was linearly increased with the increase of nitrogen content in the feedstock. Similarly, in the publication of Hongrapipat et al. [43] on co-gasification of lignite and wood pellets on a DFB steam gasifier, it was found that the NH_3 concentration in the producer gas was significantly increased with the nitrogen content increasing in the feedstock. In addition, Pinto et al. [44] also reported that the NH_3 concentration in the producer gas of co-gasification of coal and bio-solid wastes was significantly dependent on the nitrogen content. The NH_3 concentration increased rapidly with the increase of the total fuel-N, and the maximum NH_3 concentration was 5000 ppmv when 80% coal and 20% bagasse was used as feedstock. The authors [44] also revealed that dolomite and nickel catalyst had a high activity to decrease the NH_3 concentration. Furthermore, Zhou et al. [41] tested four biomass feedstocks with different nitrogen content between 0.08% and 2.51% in a bench-scale fluidised bed gasification system at 800°. It was found that the NH_3 concentration in the producer gas from gasification of sawdust (0.08% nitrogen content) was only 400 ppmv, whereas that from gasification of leucaena (2.25% nitrogen content) was 18000 ppmv [41].

Gasifier type also affects the concentration of NH_3 in the producer gas. Leppälahti et al. [45] observed from gasification of peat as the feedstock that an air-blown updraft gasifier produced the producer gas with a lower concentration of NH_3 than that using the fluidised bed gasifiers which

include BFB, CFB and DFB. Leppälahti et al. [45] explained that in the updraft gasifier, a significant amount of N in the feedstock was bound in N-containing tars instead of being released into gaseous N-containing compounds in the producer gas. However, in the fluidised bed gasifiers with uniform reaction temperature, most of the N in the feedstock was decomposed and liberated to form gaseous N-containing compounds like NH_3, HCN and N_2 [45]. In further studies, Leppälahti et al. [46] confirmed the above findings from gasification of wood as the feedstock.

The gasification temperature, bed material, steam to fuel (S/F) ratio in steam gasification and equivalence ratio (ER) in air/O_2 gasification also affect the NH_3 concentration, to various extents. However, there was no general agreement on the extent of the temperature effect on the NH_3 concentration in the producer gas. In the research of Zhou et al. [41], temperature showed significant influence on the NH_3 concentration which decreased from 31240 ppmv to 6060 ppmv when the temperature was increased from 750°C to 900°C. Pinto et al. [47], from co-gasification of coal and sewage sludge, also revealed that NH_3 concentration in the producer gas was significantly reduced when the gasification temperature or air flow rate increased. Furthermore, Kurkela and Staåhlberg [48] conducted experiments on gasification of peat, wood and brown coal, respectively, in a small fluidised bed gasifier under 0.4-1.0 MPa pressure and at gasification temperatures ranging from 800 to 995°C. They [48] found that the nitrogen in the feedstock was mainly converted into NH_3 with a small amount of HCN and N-containing tar compounds and the NH_3 concentration was slightly reduced with the temperature increasing. However, Hongrapipat et al. [3] found that increasing the DFB gasifier temperature promoted the NH_3 formation which increased from 130 to 330 ppmv when the gasification temperature was increased from 750 to 850°C. Farzam et al. [49] conducted tests on gasification of lignite and sub-bituminous coals in a steam-oxygen pressurised fluidised bed gasifier, and found that the temperature effect was

insignificant on NH_3 concentration when the gasification temperature was changed between 795 and 980°C. A possible reason for the inclusive results on the influences of gasification temperature on NH_3 concentration could be due to the different type of gasifiers and the different catalytic effects of ash elements in the feedstocks [33].

Application of catalytic bed material in fluidised bed gasifiers is another method which could affect the NH_3 concentration in the producer gas from biomass gasification [32]. Normally, the catalytic bed materials containing Fe, Ca, Mg or Ni have been found to have a functional effect on conversion and decomposition of NH_3 in the producer gas. Such catalytic bed materials include olivine, dolomite, ilmenite and limestone which have been investigated in past studies. Hongrapipat et al. [3, 50] found that ilmenite and calcined olivine had much higher activities to reduce the NH_3 concentration in the producer gas than silica due to the much higher Fe, Ca and Mg contents in ilmenite and calcined olivine. Corella et al. [36] conducted experiments using sintered olivine, raw olivine and dolomite as the in-bed materials in air gasification of biomass on a CFB gasifier at 850°C. They found that the raw olivine showed much better performance to reduce NH_3 in the producer gas than the sintered olivine and the dolomite. The authors [36] also compared the Ni-olivine, dolomite and raw olivine and reported that the raw olivine showed the best performance as well. However, different results were reported by Jeremiáš et al. [39] who found that dolomitic limestone had positive impact to increase the conversion of N in fuel into NH_3 in both coal and biomass gasification on a fluidised bed reactor. Furthermore, different results have also been reported about the effects of dolomite and lime in the biomass gasifier which were found to be favourable for the formation of NH_3 by catalysing HCN into NH_3 in the gasification environment [51].

S/F ratio in steam gasification is another influencing factor on the NH_3 concentration in the producer gas. It was reported by Hongrapipat et al. [50] that the NH_3 concentration increased from 273 to 582 ppmv when the S/F ratio was increased from 0.6 to 1.0 in a DFB steam gasifier at 800°C by using radiata pine sawdust as feedstock. The authors [50] explained that the increase in NH_3 concentration was probably due to the increased H radicals from steam reforming in the atmosphere which promoted the availability to react with N-based volatile compounds and hydrogenation reactions of N in the char [39, 52]. However, Farzam et al. [49] reported that the temperature, pressure and steam-to-carbon feed ratio in a fluidised bed gasifier had negligible effect on the N-containing compounds production rate in coal gasification. The different effects of S/F ratio on the NH_3 concentration in the above two studies may be due to the different sources of N and different structures of N binding between biomass and coal. Nitrogen in wood is mainly in proteins and alkaloids, however the source of nitrogen in coal came from the plant and bacterial proteins, chlorophyll and plant alkaloids remain after the stage of coalification [46].

The definition of ER in air/O_2 gasification is the ratio of the actual oxygen-to-fuel ratio divided by the stoichiometric oxygen-to-fuel ratio [41]. In a similar way to the effect of S/F ratio in steam gasification, there is no conclusive trend regarding the effect of ER on the NH_3 concentration in the producer gas. From a comprehensive review by Hongrapipat et al. [32], most studies that the increase of ER in the biomass gasification facilitated the conversion of fuel-N to NH_3 and, subsequently, increased the NH_3 concentration in the producer gas [33, 53-55]. However, there was also evidence that the ER in biomass gasification had insignificant influence on the concentrations of nitrogenous compounds in the producer gas [41].

Overall, the feedstock, gasifier types and a few of gasification operating conditions can affect the level of NH_3 concentration in the producer gas from biomass gasification. These parameters can

be adjusted or controlled to reduce the NH_3 concentration, and these actions are called primary measures.

2.1.3 Sulphur contaminants

Sulphur-containing compounds are also regarded as the gaseous contaminants in the producer gas from biomass gasification. The concentration of sulphur contaminants is normally lower than the concentration of N-containing contaminants because the sulphur content in most of the biomass feedstock is low [7, 56] which is <0.1 wt.% in woody biomass and 0.3-0.4 wt.% in herbaceous crops [57]. The fuel-S is largely converted into H_2S, with very low concentrations of COS, CS_2, CH_3SH, CH_3CH_3SH, C_4H_4S, and S_x during the process of gasification [56]. The formation and conversion of sulphur-containing compounds during the biomass gasification process were summarized by Meng et al. [56] as the following steps and reactions.

Fuel devolatilization:

$$\text{Fuel} - \text{S} \xrightarrow{\text{Heat}} \text{H}_2\text{S} + \text{COS} + ... + \text{Char} - \text{S} \quad (2.2)$$

Char oxidation:

$$\text{Char} - \text{S} + \text{CO}_2 \rightarrow \text{COS} \quad (2.3)$$

$$\text{Char} - \text{S} + \text{H}_2\text{O} \rightarrow \text{H}_2\text{S} \quad (2.4)$$

$$\text{Char} - \text{S} + \text{O}_2 \rightarrow \text{SO}_2 \quad (2.5)$$

Gas phase reactions:

$$\text{H}_2\text{S} + \frac{3}{2}\text{O}_2 \rightarrow \text{SO}_2 + \text{H}_2\text{O} \quad (2.6)$$

$$CO_2 + H_2S \leftrightarrow COS + H_2O \quad (2.7)$$

$$H_2S + CO \leftrightarrow H_2 + COS \quad (2.8)$$

$$COS + H_2S \leftrightarrow CS_2 + H_2O \quad (2.9)$$

$$CS_2 \leftrightarrow C + \frac{2}{x}S_x \quad (2.10)$$

Further sulphur compounds oxidation:

$$SO_2 + 0.5O_2 \leftrightarrow SO_3 \quad (2.11)$$

$$H_2O + SO_3 \leftrightarrow H_2SO_4 \quad (2.12)$$

H_2S is the most stable sulphur-containing compounds in the producer gas from biomass gasification while a low concentration of COS may also be found in the producer gas [58, 59]. This finding was confirmed by other researchers who reported that sulphur-containing compounds contained mainly H_2S, and minor quantities of COS and CS_2 [2, 60, 61]. Chao et al. [62] studied the sulphur distribution during downdraft gasification of corn straw and found that most of the sulphur was converted into gaseous sulphides including H_2S, COS, CH_3SH and SO_2, as well as the condensed phase of sulphur such as fly ash and collectable ash. Gai et al. [62] found that the concentration of H_2S in the producer gas from downdraft gasification of corn straw was in the range of 300-500 ppmv, COS in the range of 20-40 ppmv, CH_3SH in the range of 0.1-2.3 ppmv, and SO_2 in range of 0.03-5ppmv. However, most studies show that the H_2S concentration in the producer gas from biomass gasification is the range of 20-230 ppmv [3, 56, 59, 63-65] which is affected by feedstock type (sulphur content in the feedstock), gasification temperature, bed material in gasifier, and S/F ratio in steam gasification.

Sulphur content in the feedstock is a dominant factor on the H_2S concentration in the producer gas of gasification as most of the fuel-S is liberated and formed gaseous sulphur-containing compounds with a small amount in the ash. Furthermore, H_2S is the primary species in the gaseous sulphur-containing compounds, which conversion can be up to 95% [59]. Pinto et al. [44] studied different types of feedstocks with different sulphur contents and confirmed that the concentrations of sulphur-containing compounds in the producer gas were linearly correlated to the S content in the feedstock. In the research of Pinto et al. [44], Puertollano coal, Colombian coal, refuse derived fuel (RDF), pine and bagasse which have sulphur contents of 2.4%, 0.9%, 0.22%, 0.20% and 0.13% daf, respectively, were used for gasification or co-gasification in a pilot-scale fluidised bed gasifier at 850°C. It was found that the highest H_2S concentration of 2700 ppmv was in the producer gas from gasification of the Puertollano coal, which was followed with 1585 ppmv H_2S in the producer gas from gasification of Colombian coal. The H_2S concentration in the producer gas was the lowest at a value of 200 ppmv from gasification of pine [44]. These results are consistent with the sulphur content in the feedstocks. Co-gasification of coal and bagasse blends led to H_2S concentration in the producer gas around 26% lower than that obtained from gasification of mixed coal and pine at the same ratio as coal and bagasse. This was because the sulphur content in pine was higher than bagasse. However, co-gasification of coal and RDF mixtures had lower H_2S concentration in the producer gas than that from co-gasification of coal and pine blends at the same blending ratio [44]. The authors [44] explained that even though there were similar sulphur contents in RDF and pine, there was higher mineral content in RDF than in pine which had favourable activity to crack H_2S. In a separate research, Pinto et al. [66] also showed that the H_2S concentration in the producer gas from co-gasification of sewage sludge and straw bends was increased with the proportion of sewage sludge in the blend increased because the sulphur content in the sewage sludge was much

higher than that in the straw. In addition, Kuramochi et al. [67] developed an equilibrium model and predicted the H_2S concentrations in the producer gases for gasification of six types of feedstocks. From this study, a linear relationship was proposed between the H_2S concentration in the producer gas and the sulphur content in the feedstock. Furthermore, Dias and Gulyurtly [68] illustrated that in co-gasification of coal and RDF on a BFB gasifier at 850°C, the H_2S concentrations in the producer gas increased from 320 to 2681 ppmv when the coal percentage in the blend increased from 0% to 100%. Similarly, Hongrapipat et al. [69] found that increasing the proportion of lignite in the mixture of lignite and wood pellets (feedstock) led to linear increase in S content in the feedstock which resulted in corresponding increase in the H_2S concentration in the producer gas when the mixtures were gasified in a 100 kW_{th} DFB gasifier at 800°C.

Gasification temperature has an adverse impact on the H_2S yield in gasification of biomass and coal. Hongrapipat et al. [50] reported that the H_2S concentration in the producer gas was increased when the gasifier temperature increased from 750 to 850°C for gasification of woody biomass on a DFB steam gasifier. Dias and Gulyurtly [56] had a similar finding that the H_2S concentration increased from 808 to 1081 ppmv in the producer gas from co-gasification of RDF (70%) and coal (30%) on a BFB gasifier when the temperature increased from 720 to 850°C. Furthermore, Pinto et al. [66] also reported that rising temperature from 750 to 850°C led to 30% higher H_2S concentration in the producer gas from co-gasification of blended coal (60%) and sewage (40%) in a bench-scale atmospheric fluidised bed gasifier. The above results can be explained by the concept that increasing of gasification temperature enhanced the release of volatile S-compounds from the solid fuel to the gas atmosphere which then reacted with the H radicals in the system to form H_2S [67, 68]. Furthermore, the metal sulphides such as FeS, ZnS, MnS, PbS, Ni_3S_2 and Cu_2S

were formed at low temperatures which may remain in ash and thus reducing the H_2S concentration in the producer gas at low gasification temperatures [67].

For fluidised bed gasification, catalytic bed materials also have influences on H_2S concentration in the producer gas. Therefore, employing appropriate bed material in the gasifier is useful to decrease the S-containing compounds for gas cleaning purpose. Normally, the bed materials which are abundant of elements Ca, Fe, and Mg have higher activity to adsorb or crack the sulphur compounds in the gasification atmosphere [50]. The calcium-based material is one of the well-known bed materials used in the gasifier to abate H_2S because of its relatively low cost. Natural calcium-based sorbents such as limestone, dolomite, and dolomitic limestone and commercial calcium-based sorbents such as calcium acetate and calcium magnesium are commonly used in the gasifier to capture sulphur [56]. The desulfurization reactions by calcium-based sorbents were summarized by Meng et al. [56] and are shown as follows.

Direct desulfurization:

$$CaCO_3 + H_2S \rightarrow CaS + CO_2 + H_2O \quad (2.13)$$

$$CaCO_3 \cdot MgO + H_2S \rightarrow CaS \cdot MgO + CO_2 + H_2O \quad (2.14)$$

Calcination:

$$CaCO_3 \rightarrow CaO + CO_2 \quad (2.15)$$

$$CaCO_3 \cdot MgO \rightarrow CaO \cdot MgO + H_2O \quad (2.16)$$

Desulfurization of calcined sorbents:

$$CaO + H_2S \rightarrow CaS + H_2O \quad (2.17)$$

$$CaO \cdot MgO + H_2S \rightarrow CaS \cdot MgO + H_2O \quad (2.18)$$

Side reaction:

$$CaS + 2O_2 \rightarrow CaSO_4 \quad (2.19)$$

Abbasian et al. [70] investigated limestone and dolomite as the bed materials for desulfurization in a fluidised bed gasifier and they found that these two bed materials had effective performance for sulphur capture. It was also found that the sulphur capture ability of these two materials was independent of temperature when the gasification temperature ranged from 925 to 1040°C, and dolomite had almost twice rapid rate than limestone due to the difference of pore matrix [70]. However, different findings were reported by Husmann et al. [71] who tested four in-bed materials, including lime, limestone, dolomite and calcined dolomite, in an air-blown BFB gasifier with wood pellets as the feedstock. The authors [71] manually increased the H_2S concentration in the producer gas by adding CS_2 to the bottom of the gasifier thus up to 1200 ppmv of H_2S was tested. It was found that lime, limestone and un-calcined dolomite had higher sulphur capture activity than calcined dolomite [71]. It was elucidated that there was much higher MgO content in the un-calcined dolomite than the other three bed materials, and MgO was thus considered as an inert component for desulfurization. Furthermore, since the lower price of limestone than lime, the authors recommended limestone as the most advisable bed material for desulfurization in biomass gasification [71]. Commercial calcium-based bed materials are also available for H_2S removal and normally had higher activity than the natural ones as reported. García-Labiano et al. [72] studied 12 different calcium-based materials including natural, commercially available and modified limestone for H_2S reduction, and found that the commercially available calcium-based sorbents had the highest activity for desulfurization. However, it was reported that H_2S removal by calcium-

based materials was limited by thermodynamic constraints and only approximately 90% of H_2S can be removed [73]. Furthermore, it was also found that CO_2, H_2S, H_2 and HCl in the gas atmosphere had adverse effects on desulfurization by limestone [56, 73]. In addition to the above mentioned calcium-based materials, Fe-rich materials were also investigated in biomass gasification for H_2S reduction. Hongrapipat et al. [50] tested three types of bed materials, including silica sand, ilmenite and calcined olivine, in a 100 kW_{th} DFB steam gasifier at 800°C for wood pellet gasification. It was found that ilmenite and calcined olivine had the much better performance to reduce H_2S concentration in the producer gas than that of silica sand because of the much higher contents of Fe, Mg, Ca and Mn in the ilmenite and calcined olivine [50].

The other parameters in the gasifier such as residence time and S/F ratio also have effects on H_2S removal. Hongrapipat et al. [50] reported that increasing the mean gas residence time in the biomass gasifier had a positive effect on H_2S reduction. Even though the effect was not as significant as the other parameters in the research, the H_2S concentration is still decreased from 30 to 19 ppmv when the mean gas residence time was increased from 0.19 to 0.25 s. The authors also found that higher S/F ratio had a strong negative effect for the H_2S reduction in which the H_2S concentration increased from 19 to 122 ppmv when the S/F ratio was increased from 0.6 to 1.4 [50]. This finding was interpreted as the increase of H_2O in the system at high S/F ratio increased the availability of H radicals for reacting with the S- volatile compounds which resulted in higher H_2S concentration in the producer gas [50]. Similarly, Husmann et al. [71] also found that higher S/F ratio in the biomass gasification system could increase the H_2S concentration by using both lime and dolomite as in-bed materials.

Therefore, the in-situ measures for H_2S reduction for biomass gasification include using low sulphur content feedstock, reducing the gasification temperature and using suitable bed materials.

If the concentration of the H_2S is still higher than the requirements for the downstream applications, secondary measures have to be implemented for further removal of S-containing contaminants.

2.2 Downstream gas cleaning technologies in biomass gasification

Methods for cleaning the producer gas from biomass gasification are classified into two main categories: primary methods (in-situ methods) and secondary methods (downstream methods). The primary methods include using suitable biomass and gasifier type, controlling gasification conditions and utilizing appropriate bed material which have been studied extensively in the past [11, 24, 32, 50, 74] and was discussed in Section 2.1 of this chapter. However, for satisfying the stringent requirements of FT synthesis process, utilizing primary methods in the biomass gasifier alone is impossible. Therefore, development and application of appropriate secondary methods are necessary for meeting the gas quality requirements for the FT synthesis. It is commonly agreed that effective tars removal from the producer gas of biomass gasification should be realized by applying both primary and secondary methods [75], which is shown in Figure 2.3. This research is mainly focused on development and application of secondary gas cleaning methods for removal of tars, NH_3 and H_2S from the producer gas generated from biomass gasification in a DFB gasifier. The downstream gas cleaning technologies in the literature for removing tars, NH_3 and H_2S will be reviewed in the following sections.

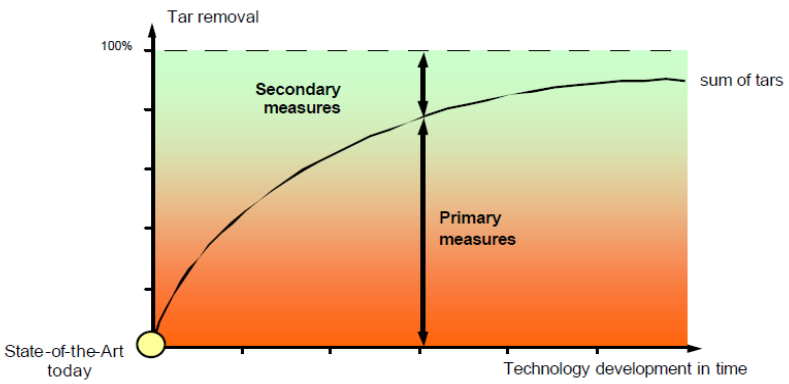

Figure 2.3 Necessary of utilizing both primary and secondary measures in biomass gasification technology [75].

2.2.1 Secondary methods for tar removal

The secondary methods for tar removal can be physical or chemical methods [1, 2, 7]. In literature, the chemical methods have been further divided into catalytic and non-catalytic methods. In this way, the secondary methods can be classified into three categories of physical, non-catalytic and catalytic methods [76]. Based on operation temperature, the secondary gas cleaning methods can be classified as cold gas cleaning methods and hot gas cleaning methods [10, 77-79]. The physical methods include dry gas cleaning and wet gas cleaning [10]. Dry gas cleaning methods include cyclone, rotational particle separator (RPS) and filters (ceramic filter, fabric filter, and activated carbon filter). Wet gas cleaning methods include wet electrostatic precipitators (wet ESP) and wet scrubbers (water scrubber and oil scrubber). The chemical methods include thermal cracking, plasma cracking and catalytic cracking. Classic methods used for tar cleaning from the producer gas will be introduced and their advantages and disadvantages will be discussed.

2.2.1.1 Physical methods for tar removal

Dry gas cleaning methods

I. Cyclone

Cyclone uses centrifugal force to separate matters with different densities in which solids and aerosols are separated from gases [2]. It was reported that for effective separation, particles with diameters no less than 5 μm thus it may not be suitable for fine particulates and tars [2]. However, deposition of particulates and tars on the surface of the cyclone is problematic for tar removal [2]. Therefore, the cyclone is not an ideal method for the tar removal from the biomass producer gas.

II. RPS

Rotational particle separator (RPS) uses a rotating cylinder that centred in a single cyclone to separate dust or particles from the target gases [2]. For this method, there are two methods to remove the tars from the producer gas. One is condensing the tars by low temperature and removing the droplets from the producer gas subsequently. Another is injecting solvent to the producer gas then removing the saturated solvent subsequently [2]. However, it is reported that the performance of both methods was unsatisfied. The efficiency of using the first method was only 30-70% [2, 80, 81]. There was also a serious fouling issue caused by the heavy tars in the producer gas [2]. Therefore, the RPS method is more applicable for particulate removal rather than tar removal.

III. Filters

There are several types of filters that are reported for tar removal which include ceramic filter, fabric filter, activated carbon filter, barrier filter and sand bed filter [2, 82, 83]. However, the problems of low efficiency, filter cleaning and waste disposal inhibits the utilization of these filters. The tar removal efficiency reported for various filters are summarized in Table 2.1. It was mentioned that filters coated with catalytic materials had much better performance [2, 84, 85], and this type of filters fall into the category of the catalytic method.

Table 2.1 The efficiencies of different filters for tar removal from the producer gas of biomass gasification.

Filter type	Efficiency of tar removal	Literature
Quartz ceramic filter	77-97.9%	[86]
Fibre ceramic filter	75.6-94%	[86]
Fabric filter	0-50%	[80]
Sand bed filter	50-97% for heavy tars	[80, 81]
Sieved lignite coke filter	50-97% for heavy tars	[81]
Sawdust filter	83-85% for tars is condensable at 5°C	[81]
Barrier filter	Not suitable for tars removal because of fouling issue	[2, 86]

Wet gas cleaning methods

I. Wet electrostatic precipitators (Wet ESP)

The ESP uses the electric field to separate the charged particles and droplets of tar and water. The charged particles and droplets are generated by attaching ions from a corona discharge [2, 83]. It was noted that the electrostatic forces are 100 times higher than gravitational force when acting upon fine particles with a diameter less than 30 μm [83]. However, the targets of wet ESP technology are for fine solids and liquid droplets, and it is not functional for high-temperature gases because tar exists in the gaseous phase [2]. Therefore, it is necessary to have a quenching process before the producer gas entering the wet ESP equipment.

There are some reports about using wet ESP technology for tar removal, but its efficiency of tar removal is uncertain. A wet ESP in Energy Reach Centre of the Netherlands (ECN) was tested after a water scrubber and it showed very high ability to remove the tars in the producer gas from an air blown CFB gasifier with the removal efficiency of 99% for heavy tars, 74% for light tars and 79% for hetero-cyclic tars [2, 87]. Its efficiency for tar removal was reported lower than that of "OLGA" system [2]. However, another report showed that the wet ESP could only remove 0-60% of heavy tars in the producer gas [80]. Furthermore, it was reported that the tube type wet EPS had a maximum efficiency of 83% for particle removal and 62% for tar removal [88].

II. Wet scrubbers

The efficiencies of wet scrubbers are strongly dependent on the solubility of the solvent for tars. Therefore, solvent selection is crucial for maximizing the tar reduction efficiency. In addition, the price of the solution and the environmental influence also need to be considered for applications in a commercial plant.

Water has been widely used as a solvent for tar removal because of the cheap price of water. It was reported that a water scrubber was employed for tar removal of the raw producer gas from a wood chips updraft gasifier at the Harboøre in Denmark [2]. The tar concentration in the producer gas was reduced from 80 g/m^3 to 25 mg/m^3 through that water scrubber and a wet ESP [2]. However, there was a great amount of wastewater generated that gasification of 1 kg of wood chips could produce 0.6 kg wastewater. Moreover, light tar compounds such as phenol and acid content in the water were hard to be separated and posed hazards for environment [2]. Although the water scrubber technology demonstrated the ability of reducing tar concentration to low levels for some downstream applications, wastewater treatment is the potential dilemma for its wide application.

Furthermore, it was also reported that using water scrubber for cleaning tars in the biomass producer gas also had saponification, equipment clogging and fouling problems [82, 89, 90].

Another type of solvent, oil, has attracted a lot of attention because it has the advantages of high efficiency for tar reduction, low price, waste-solution free and easy operation [91]. The most famous oil scrubber system is "OLGA" technology in ECN [75]. It was comprised of three sections of heavy tar absorption section, light tar absorption section, and stripper section [2]. The heavy tars in the producer gas were cleaned by a "special scrubbing oil" during the heavy tar absorption stage. Hence, the condensed heavy tars could be separated from the oil and recycled to the gasifier. During the light tar absorption, another "secret oil" was used for the light tar absorption, after which a stripper was followed and the light tars were stripped by hot air. Furthermore, the hot air with light tars was recycled back to the gasification system for maximizing energy utilization and minimizing environmental pollution [2]. It was demonstrated that the "OLGA" system had extremely high efficiency for the tar removal from the producer gas of different gasifiers. The heavy tars were completely removed, and 99% light tars and hetero-cyclic could also be removed. After the OLGA system, the tar dew point was lowered down to 10°C, which met the requirements of numerous downstream applications [2, 92].

Another successful tar removal solvent with the wet scrubber is the rapeseed oil methyl ester (RME) which has been applied in the scrubber for tar removal at the Fast Internal Circulating Fluidised bed (FICFB) gasifier in Güssing, Austria [93]. The RME scrubber had a remarkable ability to reduce the tar concentration from 1.5-4.5 g/m^3 to 10-40 mg/m^3, which met the requirement of the gas engine [93]. The condensed tars were separated and recycled to the combustor of the indirect gasifier [2], which resulted in no waste liquid treatment and high efficiency of energy utilization. However, in comparison with the "OLGA" technology, it had a limitation that the tar concentration

in the inlet gas of REM scrubber cannot be high, as otherwise there would be a massive amount of RME required [2].

Furthermore, in Tokyo Institute of Technology, Japan, other oily sorbents were also investigated on their possibility and efficiency for tar removal from the biomass producer gas. Phuphuakrat et al. [94] tested diesel fuel, biodiesel fuel, vegetable oil, engine oil and water for absorbing the tars produced from wood chip pyrolysis in a pyrolyzer and a reformer both at 800°C to simulate the tars produced from biomass gasification. It was found that the rank of absorption efficiency for gravimetric tars (heavy tars) was vegetable oil> engine oil> water> biodiesel fuel> diesel fuel. However, the rank of light PAH tars absorption efficiency was diesel fuel> vegetable oil>biodiesel fuel> engine oil >water [94]. It can be observed that vegetable oil had a relatively better performance than the other oily sorbents for removing both gravimetric and light PAH tar. Moreover, a bio-oil scrubber and a char bed were investigated by Nakamura et al. [95] for removing tars in the producer gas from an updraft gasifier. The bio-oil scrubber had tar removal efficiencies of 63.6%, 64.5% and 51.6% at 40, 50 and 60°C, respectively, whereas, the tar removal efficiency was 98% when the bio-oil scrubber and the char bed were utilized together [95]. Furthermore, a waste cooking oil scrubber was tested by Tarnpradab et al. [91] for abating the tars generated from rice husk pyrolysis in a pyrolyzer at 800°C and reformed at the same temperature to simulate the tars generated from rice husk gasification. It was reported that the waste cooking oil had as high as 88% efficiency in the first 20 min for gravimetric tar absorption; however, it was lowered gradually to 25.3% after 10 hours. This waste cooking oil scrubber had a higher efficiency for light tar removal in the first two hours of the experiment which was more than 74% absorption efficiency for benzene, toluene, styrene, phenol, indene and naphthalene [91]. In a separate research, vegetable oil scrubber and waste cooking oil scrubber were tested for gravimetric tar

removal [77]. It was illustrated that vegetable oil scrubber had higher efficiency (63.6%) for gravimetric tar removal than that of waste cooking oil scrubber (56.4%). It was explained that the waste cooking oil was non-uniform and contaminated after being used for cooking, and the contaminants in it blocked the absorbent surface area of the oil molecules [77]. The authors [77] also found that increasing the vegetable oil mixing speed to 1000 rpm during the tar absorption process could improve its ability to 89.8% for gravimetric tar absorption. A similar finding for waste cooking oil that the efficiency was increased to 81.4% for gravimetric tar absorption when the mixing speed was 750 rpm.

Overall, oil-based scrubbers have shown the high ability for tar removal and are likely to lower the tar concentration to meet the requirements of downstream applications such as FT synthesis. Moreover, the used tars containing oil can be recycled and burned to recover energy for the gasification system which solves the problems of waste treatment and environmental pollution. Therefore, this study will investigate the tar removal using different oily solvents including bio-diesel and vegetable oil.

However, it is well noted that the oil scrubber may have lower energy efficiency because the hot producer gas after gasifiers should be cooled down before entering the oil scrubber for effective tar removal.

2.2.1.2 Chemical methods for tar removal

The non-catalytic method or thermal cracking method is one of the chemical methods which uses high temperature to crack tar molecules into light gases [96-98]. Bridgwater [99] had shown that thermal cracking had the ability to reduce tar, but biomass-derived tars were very refractory and hard to crack by thermal treatment alone. In addition, the thermal cracking temperature was

proposed to be as high as 900~1300°C [100-102], which needs high-temperature resistant materials for the system. Moreover, thermal cracking of the tars may produce extremely fine soot [103]. Due to the above reasons, thermal cracking is not chosen for removing tars in this research.

The catalytic method is a classic chemical method for tar cracking and destruction. Catalysts can reduce the tar cracking activation energy, thus reduce the reaction temperatures dramatically. David [104] summarized the criteria for tar removal catalyst as follows:

1. High efficiency for tar removal;
2. Capable of reforming methane if the target product is syngas (H_2 and CO) ;
3. Resistant to deactivation;
4. Easy to regenerate;
5. Strong;
6. Inexpensive.

El-Rub et al. [76] reviewed nine groups of catalysts and showed the advantages and disadvantages of each group of catalysts, which are shown in Table 2.2. Based on the characteristics, price, and efficiency of different catalysts, a suitable catalyst is important for tar removing system.

Table 2.2 The advantages and disadvantages of the catalysts for tar removal [76].

	Catalyst	Advantages	Disadvantages
Minerals	Calcined rocks	Abundant, cheap, and popular; dolomite has high efficiency for tar conversion ~95%; often used as guard beds for expensive catalysts.	Fragile and easily eroded.
	Olivine	Cheap and high attrition resistance.	Reduced catalytic performance than dolomite.
	Clay minerals	Abundant and cheap; easy disposal.	Reduced catalytic performance than dolomite; lower resistance to high temperature.
	Iron Ores	Abundant and cheap.	Rapidly deactivated without of H_2; lower catalytic activity than dolomite.
Synthetic catalysts	Char	Cheap and easily obtained from the gasifier; high tar conversion; competitive to dolomite.	Easily consumed by gasification reactions.
	FCC	Relatively inexpensive but still more expensive than the above catalysts	Rapid deactivation by coke, lower catalytic activity than dolomite.

	Alkali-metal-based	Easily obtained from the gasification ash, then reduce ash-handling problems.	Agglomerated at high temperatures; lower catalytic activity than dolomite.
	Activated alumina	High tar conversion.	Rapidly deactivated by coke.
	Transition metal-based	High possibility to eliminate tar completely at ~900°C; boost the yield of CO_2 and H_2; Ni-based catalysts are 8~10 times more active than dolomite.	Rapidly deactivated by sulphur and high tar content in the gas atmosphere; expensive.

There are a few ways to classify the catalysts used for tar cracking and destruction. In this research, catalysts are categorized into two main groups, and they are alkaline earth metal catalysts and transition metal-based catalysts, which will be reviewed in the following sections.

Alkaline earth metal catalysts

Natural alkaline earth metal catalysts including dolomite and olivine have been studied extensively for tar destruction in biomass gasification system. These catalysts are normally inexpensive and disposable so they have attracted a lot of attention [105].

I. Dolomite

Dolomite has been used both in-situ as a bed material of gasifier and downstream as a catalyst to reduce the tar concentration in the producer gas. The natural dolomite with a chemical formula of $CaMg(CO_3)_2$ has a lower activity for tar destruction [105]. However, calcined dolomite showed improved activity as the calcination increased surface area and oxide contents of the dolomite which led to higher tar conversion [106]. Olivares et al. [31] found that the calcined dolomite also increased the H_2/CO ratio of the producer gas. Similar findings were found in the other studies as well [107, 108]. However, catalyst deactivation could be a problem of the calcined dolomite after long time use [105]. Moreover, since the complete dolomite calcination occurs at 800-900°C, effective use of dolomite is constrained at this high-temperature range [105]. Furthermore, calcination makes dolomite more friable, thus inducing severe catalyst attrition and reactor blocking by fine particulate [105].

To increase the activity of calcined dolomite, adding other metal oxides and metal elements such as Fe_2O_3 and Ni has been investigated. Wang et al. [109] compared the activities of calcined natural dolomite, Fe_2O_3 added dolomite, and Ni impregnated dolomite for tar reduction. It was found that the activity of Fe_2O_3-dolomite was slightly higher than that of

natural dolomite; however, the Ni-dolomite had much higher activity than both natural dolomite and Fe_2O_3-dolomite and the difference was more substantial at lower temperatures.

II. Olivine

Olivine is another natural mineral catalyst which has chemical formulas of Fe_2SiO_4 or Mg_2SiO_4 and has been extensively investigated as well. Rapagna et al. [110] found that calcined olivine had comparable activity to the calcined dolomite for tar reforming. In comparison with dolomite, olivine is more attractive because it has much stronger resistance to the attrition in fluidised bed reactor [105], however, both of them have the disadvantage of carbon deposition [111-113].

Like dolomite, calcined olivine and Fe/Ni-doped olivine showed higher activity for tar destruction than the natural olivine [112-114]. It was interpreted that there was more Fe on the calcined olivine than un-calcined olivine, which was a potential reason for higher tar conversion by calcination [112]. Virginie et al. [28] revealed that the Fe-olivine had a higher activity for tar destruction than olivine and that the tar concentration can be reduced by 65% by using Fe-olivine. Michel et al. [115] demonstrated that Ni-olivine had higher efficiency (30%) for converting α-methylnaphthalene (model tar) than that of olivine (4%). This conclusion was supported by Świerczyński et al [111] who found that Ni-olivine had higher activity and selectivity for toluene destruction and lower carbon deposition than olivine alone.

Transition metal-based catalysts

Transition metal-based catalysts have also been used for tar destruction in the producer gas of biomass gasification which include Fe-based catalysts, Ni-based catalysts and noble metals based catalysts.

I. Fe-based catalysts

Fe-based catalysts have attracted more and more attention because of their affordable price and high activity for tar cracking or conversion. Limonite is a natural iron ore and has been applied for tar destruction in some studies. Two types of inexpensive limonite ore, Australian limonite and Brazilian limonite, had been used by Tsubouchi et al. [116] for catalytic decomposition of toluene and benzene (model tars) from a simulated producer gas in a fixed-bed quartz reactor. It was shown that those two limonite ores had an extremely high catalytic activity for destructing the model tars when the temperature was 500°C or higher and tars were almost completely converted [116]. In a separate research [117], the above two limonite ores were also used to decompose asphaltene from Marlim vacuum residue and their performance was compared with a conventional NiMo catalyst ($NiO\text{-}MoO_3\text{-}Al_2O_3$). It was found that those two limonite ores had higher tar cracking activity than that of the NiMo catalyst at the tested temperature range of 430-450°C. Another type of limonite ore, Indonesia limonite, was also tested by Kannari et al. [118] to decompose phenol as a model biomass tar in a fluidised bed. It was found that the calcinated limonite at 900°C had the long-term durability for decomposing phenol to H_2 and CO with repeated O_2 treatment for removing the deposited carbon [118].

In KTH Royal Institute of Technology, Sweden, a pre-reduced hematite (Fe_2O_3) was tested in a reactor in the downstream of a fluidised bed gasifier for cracking tars in the producer gas from gasification of Swedish birch and it was found that tars were decomposed almost completely at 900°C [119]. However, iron oxides, FeO, Fe_2O_4 and Fe_3O_4 showed very low activity for tar decomposition [119].

II. Ni-based catalysts

A wide variety of commercial Ni-based catalysts were also available for tar removal which are used in petrochemical industry. Ni-based catalysts are not suitable for tar reduction within the gasifier because they are likely to be deactivated by coking [105], but they are promising

catalysts with high activity for tar decomposition when used as the secondary tar removal method [98, 120].

Sutton et al. [121] compared several types of Ni-based catalysts for tar destruction at 800°C where the tars were generated from peat gasification at 550°C. Ni was supported by Al_2O_3, ZrO_2, TiO_2, SiO_2 and MOR 1 by using wet-impregnation or co-precipitation methods. It was found that the Ni-TiO_2 catalyst had the best performance with 98.1% tar conversion at 800°C, which was followed by Ni-ZrO_2 with 95.2% tar conversion at the same temperature. Dou et al. [120] used five catalysts in a fixed-bed reactor to test their performance for tar reduction by using 1-Methylnaphthalene as the model tar. A NiMo catalyst with 4% NiO doped on Y-zeolite showed the most effective performance with 100% tar conversion. Dayton [105] reviewed 13 types of commercial Ni-based catalysts with different NiO contents which were used for tar destruction at different operational conditions. It was found that most of the Ni-based catalysts could reduce nearly tars in the gases by up to 99%, and the least effective catalyst, BASF G1-25S with 15% NiO, still had tar conversion of higher than 88%.

However, in the real producer gas from biomass gasification, there are S-containing gases, chlorine and alkali metals which are poisonous to Ni-based catalysts [105]. Furthermore, during the tar cracking or destruction process, carbon or coke formation would suppress the activity of Ni-based catalysts as well. Although the carbon or coke formation problem can be solved by catalyst regeneration, prolonged exposure of the Ni-based catalysts to high-temperature environment may lead to catalyst sintering, phase transformation, and nickel volatilization [105].

III. Noble metal-based catalysts

Noble metal (Rh, Ru, Pd, Pt) based catalysts have also been investigated for tar removal as the secondary method in biomass gasification. Although the noble metal-based catalysts had high efficiency for tar destruction, the high price of them restricted their applications.

Anis and Zainal [82] reviewed a number of noble metal-based catalysts for tar reduction and found that a Rh-based catalyst had better performance than the commercial catalysts. They also found that the order of the performance for different catalysts was Rh> Pt> Pd> Ni=Ru and concluded that Rh was the most effective among those examined. In the research of Asadullah et al [122], CeO_2 was added to the catalyst to improve the catalytic performance of Rh-based catalyst because CeO_2 had high redox properties. It was found that 35% CeO_2 loading on the catalyst achieved the best results while higher CeO_2 loading decreased the catalytic performance due to CeO_2 sintering during reaction [122]. Miyazawa et al. [123] reported that $Rh/CeO_2/SiO_2$ was more stable than Ni-based catalyst due to its high resistance to coke formation. However, due to the expensive price of noble metal-based catalysts, they will not be considered for tar destruction in this research.

2.2.2 Secondary methods for NH_3 removal

In a similar manner to the tar removal, the secondary methods used for NH_3 removal can also be clarified into physical and chemical methods. In some review papers, the physical methods are termed as cold gas clean-up methods and the chemical methods are called hot gas clean-up methods [79].

2.2.2.1 Physical methods

The key physical method used for NH_3 removal from the biomass producer gas is a wet scrubber. Due to the high solubility of NH_3, water and acid solutions are normally regarded as the conventional solvents for the wet scrubber of NH_3 removal. The wet scrubber method has

the advantage that the solvents are also capable to remove other gaseous contaminants such as HCN and H_2S in addition to NH_3. Moreover, the dissolved acidic gaseous contaminants could further increase the capability for NH_3 absorption [79]. However, the main obstacle of using the wet scrubber for NH_3 reduction is coexisting of tars in the producer gas, which will end up in the scrubber solution as well [2]. Therefore, in the wet scrubber method, the tar concentration of the inlet gas is required to be below a certain level so that the tar dew point is below the scrubber temperature. For example, if the operation temperature of the NH_3 removal scrubber is 20°C, the tars dew point in the inlet producer gas should be lower than 20°C. "OLGA" system was capable of achieving this target and a conventional water scrubber was used downstream of it [2].

Another disadvantage of using the wet scrubber is that the NH_3 concentration of the inlet gas should be below a certain level to achieve required HN_3 removal efficiency. Abdoulmoumine et al. [79] reported that the wet scrubber had low NH_3 removal efficiency if the inlet NH_3 concentration was higher than 500 ppmv. However, the producer gas from gasification of N-rich biomasses (such as herbaceous) has NH_3 concentrations high than this value. In this case, the wet scrubber may not be suitable or multi-step wet scrubbers are needed. In literature, different NH_3 removal efficiencies for wet scrubber have been reported. Boerrigter et al. [1] reported that a water scrubber following the "OLGA" system had an NH_3 removal efficiency of higher than 99% which reduced the NH_3 concentration from 1304 to 8.5 ppmv. Pino et al. [47] used a scrubber system to cool down the producer gas and, at the same time, to remove NH_3 in the producer gas using the condensed water, and they found that the NH_3 removal efficiency could be higher than 90%. Loipersböck et al. [124] also found that a biodiesel scrubber at low temperatures with the assistance of condensed water from the producer gas from a DFB steam blown gasifier had a remarkable capacity to absorb NH_3 in the producer gas with removal efficiency of 99.7%. However, in a separate study by Pröll et al. [125], only 50%

of 500 ppmv NH_3 in the producer gas of biomass gasification was removed by using a wet scrubber using a mixture of an organic solvent with condensed water from the same producer gas. In the study of Pröll et al. [125], when the NH_3 concentration was increased to 2000 ppmv, the NH_3 removal efficiency was reduced to 30%. Furthermore, waste solvent treatment or regeneration should be implemented which can be a stripper, a biological process ("ANAMMOX" process) or integrated treatment with waste solvent from tar removal ("TARWATC" reactor) [2]. It should be noted that all of these supplementary treatment processes incur additional equipment, energy and costs.

2.2.2.2 Chemical methods

Chemical methods for NH_3 removal may include thermal cracking and catalytic cracking. Thermal cracking method for NH_3 decomposition requires extremely high temperature due to the high activation energy of the NH_3 decomposition reaction [126, 127]. Hongrapipat et al. [32] reviewed several different thermal cracking methods for decomposing NH_3. The authors [32] illustrated that at 900°C, the NH_3 decomposing efficiency in an empty reactor was only 10% or less. When the reactor was packed with inert materials such as silicon carbide (SiC) or quartz sand, the NH_3 decomposition enhancement was very limited and the cleaned gas was still unable to meet the downstream requirements [32]. Therefore, thermal cracking methods will not be considered in this study for NH_3 decomposition in the producer gas from biomass gasification.

However, catalytic methods have attracted more attention because of their high efficiency for NH_3 removal. Compared with the thermal methods, catalysts used in the catalytic reactor can decrease the activated energy of the NH_3 decomposition reaction significantly, which make the NH_3 decomposition to happen at lower temperatures. In literature, a number of the alkaline earth metal catalysts have been investigated for the NH_3 removal [32] which include dolomite,

limestone and olivine [45, 128-132], transition metal based catalysts such as Fe-based catalysts and Ni-based catalysts [35, 38, 133-136], and activated carbon [136-138]. In the following section, catalysts used for the NH_3 decomposition will be introduced in more details, and disadvantages and advantages will be discussed.

Alkaline earth metal catalysts

The alkaline earth metal catalysts have been used for tar abatement and for NH_3 reduction. It was reported that limestone and dolomite had catalytic activity for decomposing NH_3 into H_2 and N_2 in the inert gas atmosphere at operation temperatures of higher than 450°C [131]. The calcined limestone and dolomite also showed higher activity for NH_3 decomposition in inert gases than pure CaO and pure MgO [126, 139]. However, when H_2, CO_2, CO, CH_4 and H_2O gases were present in the gas atmosphere, activity of the alkaline earth metal catalysts was significantly suppressed for NH_3 decomposition [32, 132, 140]. Leppälahti et al. [45] demonstrated that limestone and dolomite had no catalytic effect for NH_3 decomposition in the real producer gas from a 5 MW updraft gasifier. In a separate study by Corella et al. [141], it was found that when dolomite served as a primary catalyst for tar destruction in the gasifier, the NH_3 concentration in the producer gas was actually increased. It was interpreted that the dolomite in the gasifier bed released the N from the N-containing tars during tars destruction and increased the availability to form NH_3 [141]. Therefore, alkaline earth metal catalysts have their limitations and are not suitable for the NH_3 decomposition in producer gas with complicated gas composition from biomass gasification.

Transition metal-based catalysts

I. Fe-based catalysts

Fe-based catalysts used for NH_3 decomposition have been well documented which include iron sinter, iron pellet, ferrous dolomite [45], magnetite [142], hematite [142], limonite [133, 142-

144], titanomagnetite [145], and iron catalysts with supporting materials [136, 138, 146, 147]. The investigations have shown that the Fe-based catalysts had high NH_3 decomposition efficiency in the inert gases at high temperatures. However, their high NH_3 removal activity can be inhibited by the presence of H_2, CO, and H_2S which could be due to equilibrium reduction, carbon deposition, and sulphur poisoning.

Leppälahti et al. [45] tested three different iron catalysts (iron sinter, iron pellet and ferrous dolomite) for NH_3 decomposition in real biomass producer gas. The authors [45] found that even a fairly low iron content on the catalysts had sufficient catalytic activity for NH_3 decomposition. However, the activity of the iron catalysts for NH_3 decomposition was appearing at temperatures of 900°C and higher because the formation of metallic iron occurred at the high temperatures. The authors [45] also revealed that at the same temperature 900°C, iron sinter had better performance than ferrous dolomite but much better performance than iron pellet for NH_3 removal. It was explained that the different specific surface area and calcium contents of the iron catalysts led to different NH_3 decomposition activities. However, none of the catalysts could remove the NH_3 in the biomass producer gas completely. In the study of Tsubouchi et al. [142], NH_3 decomposition efficiencies were compared for three reduced iron catalysts, hematite (α-Fe_2O_3) and magnetite (Fe_3O_4) and limonite (90 mass% of α-FeOOH), which were tested in helium gas at 750°C. It was found that all of them demonstrated catalytic activity for NH_3 decomposition; however, the reduced limonite had much smaller size of α-Fe than those of reduced hematite and magnetite which led to much higher NH_3 decomposition (>99%) than those of magnetite (<90%) and hematite (<20%) [142]. Overall, the activity of the iron catalyst for NH_3 decomposition depends both on the iron content of the catalyst and on other properties such as the specific surface area, catalytic structure, and the other elements on the catalysts.

Since limonite has shown high efficiency for NH_3 decomposition in the inert gas atmosphere, it was extensively investigated to explore the possibility of using it in the real producer gas. Tsubouchi et al. [142] illustrated that limonite had lower efficiency for NH_3 decomposition in simulated producer gas (20% CO, 10% H_2 and 70% He) in comparison with that in inert helium gas. This was due to the carbon deposition from CO decomposition [142] and NH_3 decomposition equilibrium reduction by H_2 [147]. However, with the limonite, the addition of 10% CO_2 or 3% H_2O into the simulated gas increased the NH_3 decomposition efficiency significantly, which was interpreted that CO_2 or H_2O in the atmosphere suppressed carbon deposition [142]. In addition, the sulphur tolerance ability of limonite was also investigated by Tsubouchi et al. in a separate research [133]. It was reported that the α-Fe phase on the reduced limonite could be poisoned by H_2S to form FeS which reduced its activity for NH_3 decomposition at low temperatures. However, increasing NH_3 decomposition temperature to 750°C or higher could significantly improve the sulphur tolerance of the reduced limonite and almost complete NH_3 decomposition was achieved in the gas where NH_3 (2000 ppm) and H_2S (50-500 ppm) [133]. Furthermore, Tsubouchi et al. [144] also found that the addition of 3 mass% Mg on the limonite could suppress carbon deposition and substantially improve the NH_3 decomposition ability.

Another type of natural form iron sand, titanomagnetite, was also investigated to decompose NH_3 in the biomass producer gas cleaning purpose. It was found that the titanomagnetite could achieve almost complete NH_3 decomposition in an inert gas argon (Ar) at an operation temperature of 700°C and higher [3]. Moreover, even with the coexistence of H_2S at a concentration of 230 ppmv, its activity for NH_3 decomposition could be maintained as high as 96% at the above-mentioned operation temperatures. However, the other gas species of H_2, CO, CO_2 and CH_4 present in the producer gas had severely negative impacts on the NH_3 decomposition by the titanomagnetite catalyst [3].

In addition to the above-mentioned iron catalysts, some lab-made iron catalysts were also tested for NH_3 decomposition. Sarioğlan et al. [146] made a zeolite beta supported iron catalyst via wet impregnation method which achieved 97.3% of NH_3 decomposition in the N_2 atmosphere at 700°C. However, its NH_3 decomposition ability was adversely impacted by the addition of H_2, CO and CO_2 into the gas which was due to the side reactions during the NH_3 decomposition [146]. Furthermore, a coal char supported iron catalyst was prepared in the lab by precipitating Fe on pyrolysis char which could decompose NH_3 completely at 850°C in helium gas [147]. However, again, the addition of H_2 and CO into the inert gas atmosphere deactivated its NH_3 decomposition activity remarkably. It was also found that the addition of CO_2 to the syngas (H_2 and CO) could restore the catalytic activity of the catalyst again [147].

From the above observations, effective NH_3 decomposition could be achieved by Fe-based catalysts, although their activities could be impacted by some gaseous species in the producer gas such as H_2, CO and H_2S. Fe-based catalysts also showed the possibility of removing NH_3 effectively in the biomass producer gas by modifying catalysts. Therefore, Fe-based catalysts will be selected for further investigation to decompose NH_3 for biomass producer gas cleaning purpose.

II. Ni-based catalysts

Nickel catalysts have been investigated extensively because of their high abilities to decompose NH_3 in most of the gas conditions and the possibility to remove tars and NH_3 simultaneously. However, high cost and catalyst poisoning by sulphur are the key barriers for the application of the Ni-based catalysts in commercial-scale plants.

In the earlier 1990s, the Technical Research Centre of Finland (VTT) conducted some researches on NH_3 removal from peat/coal gasification producer gas by using different types of catalysts [45, 128, 130]. It was reported that two commercial Ni-based catalysts could

achieve almost complete NH_3 removal in producer gas from peat gasification both on an updraft gasifier and on a fluidised bed gasifier at 900°C [45, 128]. Moreover, those two commercial Ni-based catalysts also showed higher NH_3 removal activity than dolomite, limestone and three types of Fe-based catalysts including Fe-dolomite, iron sinter and iron pellet [128]. Furthermore, it was also observed that temperature had a significant impact on the activity of the nickel catalyst for NH_3 reduction which was reduced rapidly when the temperature was decreased from 900 to 800°C [128]. Therefore, the authors [128] proposed that the nickel catalysts should be used at high temperatures of higher than 900°C.

However, the performance of Ni-based catalysts for NH_3 reduction in the biomass/coal gasification producer gas could be seriously impacted by the other contaminants in the producer gas. Mojtahedi et al. [40] tested three different Alumina-supported nickel catalysts in a reactor after a pressurized fluidised bed gasifier, and only 48%-85% NH_3 conversion was achieved by the aged nickel catalysts. The authors [40] concluded that the contaminants in the producer gas such as H_2S, HCl, alkali metals, tars, trace elements reduced the activity of the Ni-based catalysts significantly. In addition, high pressure and temperatures lower than 900°C were unfavourable conditions for the NH_3 decomposition with the presence of H_2S in the producer gas because of the formation of NiS [40]. Corella et al. [148] also found that the sulphur poisoning of Ni-based monolith by H_2S could reduce the NH_3 conversion considerably.

Extensive studies have been performed on removing NH_3 and tars simultaneously by Ni-based catalysts as these catalysts have effective activities of reducing NH_3 and tars at high temperatures. A nickel catalyst named Ni-3, which was composed of 4.0 wt% NiO, 14.3 wt% MoO_3 and Al_2O_3, showed high efficiency to remove NH_3 and the tar model compound of 1-Methylnaphthalene simultaneously [149]. Similar results have been reported by Simell et al. [130] who found that the nickel catalyst decomposed the tar and NH_3 effectively from the

biomass gasification producer gas at operation conditions of 900°C and 5 bar with a residence time of 1 s. At these conditions, carbon deposition and sulphur poisoning were avoided.

However, the activities of Fe-based and Ni-based catalysts for NH_3 removal are significantly reduced when tars and H_2S are both present at high concentrations in the producer gas. Therefore, Fe-based and Ni-based catalysts should be applied for NH_3 decomposition after tar removal and H_2S adsorption. If necessary, the other contaminants with high concentrations should be abated as well. Nevertheless, it is found that the Fe-based and Ni-based catalysts may, to a certain extent, tolerate tar and H_2S in the producer gas if concentrations of these contaminants are sufficiently low. Therefore, even though the tar and H_2S cannot be removed completely during their cleaning processes, NH_3 reduction process by Fe-based and Ni-based catalysts can still be effective.

Activated carbon (AC)

AC was also used for NH_3 removal due to its large surface area per unit volume [32, 140]. However, the experimental results showed that commercial ACs and AC-supported metal catalysts had poor performance for NH_3 reduction [136-138] and less activity than other catalysts such as dolomite, olivine, Fe-based and Ni-based catalysts for NH_3 decomposition [147]. In a separate study, Xu et al. [137] investigated a commercial AC with <0.05 wt.% Fe content and five different chars from low-rank coals for decomposing NH_3 in helium gas. It was observed that only 11-13% NH_3 conversion was achieved with the AC loaded with Fe which was lower than that by using the other five chars [137]. Furthermore, Fortier et al. [150] also reported that the AC alone had a very low capability for NH_3 adsorption, but the capability was improved by increasing the $ZnCl_2$ loading on the AC. It can be concluded that ACs have a very low activity for NH_3 decomposition in the producer gas from biomass gasification, therefore, it is not suitable for application in NH_3 removal in the producer gas.

2.2.3 Secondary methods for H_2S removal

For the secondary methods for H_2S removal from the producer gas of biomass gasification, both physical and chemical methods can be applied. Physical methods including alkaline solutions (such as aqueous diethanolamine and NaOH solutions) and physical sorbents such as polyethylene glycol) have shown their suitability for absorbing H_2S in high volume gas streams [151]. However, the physical sorbents demonstrated less economic competitiveness than the chemical sorbents when the partial pressure of H_2S in the gas stream was low because the H_2S solubility in the physical sorbents is strongly dependent on its partial pressure [151]. Since the H_2S concentration is as low as at 20-230 ppmv levels in the producer gas from most of the biomass species [64], chemical sorbents are more suitable for H_2S adsorption of biomass producer gas cleaning.

Metal oxide-based sorbents are the main sorbents for chemical adsorption of H_2S, which include oxides of iron, zinc, copper, manganese, cerium, and so on [152, 153]. The general desulfurization reactions for metal oxides with H_2S and the regeneration reactions of the metal oxides are as follows [56, 152]:

$$M_xO_y(s) + xH_2S(g) + (y - x)H_2(g) \rightarrow xMS + yH_2O(g) \quad (2.20)$$

$$MS(s) + H_2O(g) \rightarrow MO(s) + H_2S(g) \quad (2.21)$$

$$xMS(s) + (y/2)SO_2(g) \rightarrow M_xO_y(s) + (x + y/2)S(g) \quad (2.22)$$

$$xMS(s) + (x + y/2)O_2(g) \rightarrow M_xO_y(s) + xSO_2(g) \quad (2.23)$$

$$MS(s) + 2O_2(g) \rightarrow MSO_4(s) \quad (2.24)$$

The general factors considered on selecting metal oxide sorbents for H_2S reduction are summarized as follows [154]:

- High thermodynamic equilibrium for sulphur capture and fast kinetics for sulphidation reaction;
- High selectivity for sulphur adsorption;
- Resistance to reduction by H_2;
- High mechanical stability;
- High regeneration capabilities.

2.2.3.1 Iron oxide based sorbents

Iron oxide is well-known sorbents for sulphur capture used in coal gasification plants before the 1980s in the United States of America (USA), but the applications have been less common at present in the coal gasification plants due to its limitation at low temperatures [152, 155]. However, due to its advantages of low price, no need for chemical processing, disposability after desulfurization, and regenerability, it is still applied in power plants of Integrated Gasification Combined Cycle (IGCC) [152, 155, 156]. The principal reactions occurring during the desulfurization by iron oxides and its regeneration reactions were summarized as follows [157]:

Sorbent reduction:

$$3Fe_2O_3(s) + H_2(g) \rightarrow 2Fe_3O_4(s) + H_2O(g) \quad (2.25)$$

Desulfurization:

$$Fe_3O_4(s) + 3H_2S(g) + H_2(g) \rightarrow 3FeS(s) + 4H_2O(g) \quad (2.26)$$

Sorbent regeneration:

$$2FeS(s) + 7/2O_2(g) \rightarrow Fe_2O_3(s) + 2SO_2(g) \quad (2.27)$$

SO_2 reduction:

$$xCO(g) + (2-x)H_2(g) + SO_2(g) \rightarrow xCO_2(g) + (2-x)H_2O(g) + S(g) \quad (2.28)$$

In general, iron oxide is likely to be chosen as a sorbent for sulphur reduction because of its ability for regeneration and relatively low cost [152]. It was reported that the iron oxide after the desulfurization step can be readily regenerated by air or N_2-diluted air to oxidize the iron sulphide at relatively lower temperature than other metal oxides [152, 158]. Moreover, the iron sulphide has the ability to react with SO_2 gas to form Fe_3O_4, which provides a promising route of iron oxide regeneration using the waste gas of SO_2 [152]. In addition, it was also found that a number of cheap iron-containing materials with high capability to remove H_2S at moderate temperatures are available for selection, and these materials include taconite, ilmenite, iron ores, and red and brown muds from aluminium refining residues [152, 159].

The operation temperature for H_2S removal using iron oxide sorbent is limited in a range of 350-550°C [152]; however, different interpretations were shown in literature. Meng et al. [56] reported that iron oxide sorbent was severely decrepitated and had the lower capability for desulfurization than oxides of Zn, Cu, and Mn when the temperature was higher than 550°C owing to the excessive reduction and iron carbide formation. Moreover, Tseng et al. [160] illustrated that high temperatures above 600°C can cause reduction of oxide iron to Fe and FeO which had lower desulphurization equilibrium. Furthermore, Newby and Bannister [153] demonstrated that iron oxides had reduced thermodynamic sulphur removal potential with temperature increasing and suitable application temperature was less than 649°C.

From the above discussion, utilizing iron oxide at relatively low temperatures (350-550°) and mixing with the other metal oxides should be considered to improve the efficiency of iron oxides for H_2S adsorption. Hongrapipat et al. [145] developed a novel hot gas cleaning process by using a natural and cheap iron sand, titanomagnetite, for simultaneously removing NH_3 and H_2S from biomass producer gas. Experimental results from their study showed that the iron

sand could achieve the H_2S reduction by more than 98% in the Ar gas at the operation temperatures of 700 and 800°C even though NH_3 coexisted at 2000 ppmv in the gas [145]. Moreover, it was found that the H_2S adsorption by titanomagnetite was favoured at lower temperatures while at 500°C, the H_2S was almost completely removed [145]. De Wild et al. [161] reported that a sorbent with iron oxide (Fe_2O_3) and molybdenum oxide (MoO_3) with the support of alumina was effective and regenerable for the removal of H_2S and COS gases. Interestingly, these two metal oxides showed synergistic effects on H_2S removal that Fe_2O_3 played the main role for the desulphurization reaction and MoO_3 prevented the formation of metallic iron during the reduction of Fe_2O_3. Hence, carbon formation was avoided due to the limited catalytic effect of metallic iron [161].

2.2.3.2 Zinc oxide based sorbents

Zinc oxide (ZnO) is the most common and basic sorbent among zinc oxides, which also shows high desulfurization efficiency. However, vaporization of elemental Zn at high reduction temperatures limits the application of ZnO. Extensive research has been conducted on other two improved sorbents, zinc ferrite (ZF) and zinc titanate (ZT) [56].

Zinc ferrite (ZF)

ZF ($ZnFe_2O_4$) was considered as an activated sorbent for H_2S removal at an applicable temperature range of 450~600°C [162]. If the temperature is higher than 600°C, the activity of zinc ferrite will be lowered due to the following reasons: 1) decrepitation; 2) ZF decomposition into individual oxides/metals (Fe_2O_3 is reduced to FeO and Fe and ZnO is reduced to Zn); 3) and formation of iron carbides [163]. High calcination temperature also limited the sorbent's performance due to the decrease of specific surface area and reduction of the kinetics of desulphurization [164]. For enhancing the structural strength and increasing the porosity of the sorbent, support materials can be used. For example, the stability of ZnO could be improved

by adding Titanium (Ti) to the sorbent. In addition, the stabilized structure of the sorbent was also enhanced by the inclusion of Ti in the ferrite lattice thus preventing decomposing the sorbent into the two-component oxide. Moreover, the addition of Cu to ZF could improve the performance of sorbent due to the increase of ferrite formation and the migration of Zn and O to the surface of the sorbent during both calcination and regeneration stages [165]. Furthermore, when ZF is supported by carbon material, such as AC and activated carbon fiber (ACF), the desulfurization capacity was enhanced. In the study of Ikenaga et al. [166], it was found that with the application of the carbon supported ZF, the H_2S concentration in a simulated coal gasification producer gas was reduced from initial 4000 ppmv to less than 1 ppmv at an operation temperature of 500°C. The chemical reactions of ZF in a desulfurization process are summarized as follows [164]:

Reduction:

$$ZnOFe_2O_4(s) + 1/3H_2(g) \rightarrow ZnO(s) + 2/3Fe_3O_4(s) + 1/3H_2O(g) \quad (2.29)$$

Sulphidation:

$$ZnO(s) + 2/3Fe_3O_4(s) + 3H_2S(g) + 2/3H_2(g) \rightarrow ZnS(s) + 2FeS(s) + 11/3H_2O(g) \quad (2.30)$$

Regeneration:

$$ZnS(s) + 2FeS(s) + 5O_2(g) \rightarrow ZnOFe_2O_3(s) + 3SO_2(g) \quad (2.31)$$

For the regeneration stage, low concentration of O_2 (~2%) can be used. Kobayashi et al. [167] reported that the ZF and silicon dioxide sorbent ($ZnFe_2O_4$-SiO_2) could be regenerated successfully in the gas medium of 1.6 vol% oxygen in nitrogen at the temperature of 450°C. However, high operation temperature for ZF regeneration led to the loss of sorbent activity due to thermal sintering [168, 169].

Zinc titanate (ZT)

ZT is another regenerable sorbent for H_2S removal which has better performance than ZF in most cases. The three major components in ZT are $ZnTiO_3$, Zn_2TiO_4 and $Zn_2Ti_3O_8$ with different ZnO/TiO_2 ratios. ZnO in ZT is the active chemical for desulfurization, while TiO_2 serves as a support for improving the stability of ZT [162]. The chemical reactions occurring for desulfurization and regeneration was summarized as follows [162, 170]:

Desulfurization:

$$Zn_2TiO_4(s) + 2H_2S(g) \rightarrow 2ZnS(s) + TiO_2(s) + 2H_2O(g) \quad (2.32)$$

$$ZnTiO_3(s) + H_2S(g) \rightarrow ZnS(s) + TiO_2(s) + H_2O(g) \quad (2.33)$$

Regeneration:

$$2ZnS(s) + TiO_2(s) + 3O_2(g) \rightarrow Zn_2TiO_4(s) + 2SO_2(g) \quad (2.34)$$

In comparison with ZnO, ZT sorbent can be applied at higher operation temperatures due to its lower ZnO reduction rate and resistance to the formation of fine particles/cracks that affect the structure of sorbent [56]. For improving the stability, reactivity, and regenerability of the ZT sorbent, some metal oxides such as LaO_3, ZrO, Co_3O_4 and Cu/Mn metal oxides were added to it. Poston [171] reported that by adding La_2O_3 to the sorbent, the sorbent spalling was reduced but its H_2S removal performance was maintained. Sasaoka et al. [172] reported that the addition of ZrO_2 into ZT sorbent enhanced the reactivity of desulfurization and regenerability of the sorbent, while the specific surface area of the $ZnO\text{-}TiO_2\text{-}ZrO_2$ sorbent was lost after sintering during regeneration. Jun et al. [173] found that the ZT sorbents had higher stability and reactivity by the addition of Co_3O_4 but SO_2 slippage during desulfurization was also increased as a result of the $CoSO_4$ formation. The authors tried to solve this problem by addition of cobalt

and nickel oxides together and found that nickel oxide reduced the sulphate formation and SO_2 slippage during desulfurization process [174].

2.2.3.3 Other metal oxide based sorbents

Sorbents of copper oxide, manganese oxide, and cerium oxide have also been studied for H_2S removal. Copper oxide-based sorbent is an effective sorbent for decreasing the H_2S concentration from thousands ppmv level to below 1 ppmv. However, the sorbent has the disadvantage that it could be reduced to metallic copper by H_2 or CO in the biomass producer gases thus leading to low desulfurization performance [56]. To improve the performance of copper oxide-based sorbent, dispersed and blended sorbent with other additives and support materials have been studied which include zeolites, SiO_2, CeO_2, and Cr_2O_3 [175, 176].

Manganese oxide-based sorbent has also attracted attention in the past decades and its major advantage is that it can be utilized at high operation temperatures (>800°C). Westmoreland et al. [177] reported that MnO had higher reactivity than CaO, ZnO, and V_2O_3 for H_2S removal. In addition, mixed and supported manganese oxide-based sorbent has also been reported in the literature. Turkdogan et al. [178] studied the mixture of manganese ore and alumina and found that the mixture sorbent maintained high capability at 800°C for removing H_2S and could also be effectively regenerated by air. Furthermore, Slimane and Hepworth [179] reported that the combination of manganese carbonate and Moanda manganese ore supported by alumina showed high desulfurization capacity, kinetics, and strength. MnO sorbent supported with γ-Al_2O_3 has the improved pore structure and can be regenerated with gas-steam mixture [180].

Cerium oxides attracted less attention than the above sorbents because of its high price and low desulfurization equilibrium. However, it has shown good reducibility and regenerability. Zeng et al. [181] demonstrated that the Ce_2O_2S could be regenerated completely to CeO_2 even after ten desulfurization-regeneration cycles without apparent activity loss. Some researchers also

reported that the reducibility, desulfurization, activity, specific surface area, and sulphur retention capacity of cerium oxide-based sorbent could be enhanced by adding other metal elements such as Cu, La, Zr, and Mn. Kobayashi et al. [182] showed that the desulfurization and reducibility of cerium oxides were improved with the addition of copper even at a low content. However, the addition of copper increased the sintering of ceria during oxidative and reductive treatments at 800°C [183]. ZrO_2 doping cerium oxide sorbent has the advantages of high reducibility, specific surface area, and sintering resistance [184]. Yasyerli [185] found that the sulphur retention capacity and H_2S removal rate of cerium oxide-based sorbent were improved by incorporation of Mn.

2.2.3.4 The disadvantages and advantages of different H_2S removal sorbents

Meng et al. [56] reviewed the sorbents used for desulfurization of hot gases in detail. The authors [56] also suggested the situations for application of each sorbent as reproduced Table 2.3. Furthermore, the authors [56] also suggested that additives and supporters could be used for overcoming the limitations of the sorbents. These additives include Si, Al, Fe, Ni, Ti, Si, Zr, and Co, and the promoters are Fe, Ni, and Co. The mesoporous materials and zeolites can be served as supporters to create and maintain the required sorbent structure.

Table 2.3 The advantages and disadvantages of the sorbents used for H_2S removal [56].

	Sorbents		Advantages	Disadvantages
In situ sulphur capture	Calcium-based sorbents	Limestone and dolomite	Widespread; inexpensive; have immense effects on the quality of gas.	Have attrition and incomplete conversion problems below the calcining temperatures; the produced stable sulphate layer leads to a loss of activation of sorbents.
		Calcium magnesium acetate and calcium acetate	Better sulphur capture capability than limestone and dolomite; better resistance to attrition.	Sulphur capture efficiency depends on the partial pressure of stream, CO_2 and temperature.
Downstream sulphur capture	Zinc-based sorbents	ZnO	Has the most favourable thermodynamic property with H_2S.	Has zinc migration and agglomeration problems at high temperature; limited to the temperature around 600°C.
		ZF		
		ZT		
	Copper oxide		Can reduce H_2S from several thousand ppmv to sub-ppmv.	Disunited CuO is tending to be reduced to metallic copper by H_2 and CO.
	Manganese oxide		High sulphur reactivity and capacity at moderate temperatures; no requirement for sorbent activation.	Be apt to form Manganese sulphate; regeneration at extremely high temperature.

	Iron oxide	Conveniently regenerated by N_2-diluted air and air at a lower temperature than other metal oxides; the product of FeS_x can react with SO_2 to form Fe_3O_4 and S_x.	Lower desulfurization ability.
	Cerium oxide	Good regeneration property; sulphur removal increase when desulfurization temperature and CO/CO_2 ratio increase.	Lower sulphur capture ability than zinc oxide sorbents; expensive.

2.3 Secondary gas cleaning technologies selection for tars, NH_3 and H_2S removal in this research

In the secondary methods for cleaning the biomass producer gas, downstream process requirements, contaminants' concentrations in the raw producer gas and the system capacity should be considered for the method selection and system design [186, 187]. In this study, in choosing the methods for removal of tars, NH_3 and H_2S, the gas quality requirements for FT liquid fuel synthesis and contaminant concentrations in the raw producer gas from the DFB steam gasification of biomass will be taken into account. Moreover, the efficiency, cost, operability, environmental issue, and industrial applications of the methods will be considered as well.

The concentrations of tars, NH_3 and H_2S in the producer gas from the 100kW DFB steam gasifier in this research team are available in literature and can be found elsewhere [43, 50, 69, 188]. It is reported that from the steam gasification of woody biomass on the DFB gasifier, the tar concentration in the producer gas ranged from 0.7 to 12.7 g/Nm^3 [43, 74, 188]. The NH_3 and H_2S concentrations in the producer gas varied from 130 to 582 ppmv, and 19-122 ppmv, respectively, depending on the gasification temperature and steam to biomass (S/B) ratio [50]. However, in co-gasification of blended lignite and woody biomass, the NH_3 and H_2S concentrations in the producer gas varied from 525 to 5590 ppmv, and 104 to 2175 ppmv, respectively, depending on the blending ratio of the lignite and biomass [69].

In the gas cleaning for the above-mentioned gasification system, dry gas cleaning methods are suitable for particulate removal but these methods are not considered to be appropriate for tar removal. Moreover, the wet ESP and water scrubber are also considered inappropriate due to the inconclusive efficiency for tar removal and the waste solution treatment issues. Eventually, the oil scrubber and catalytic methods are chosen in this study because of their high efficiency

for tar removal and minimum environmental impact. Moreover, oil scrubber method also has the advantage of removing tars including GC-detectable and GC-undetectable tars, water, part of the gaseous contaminants, and particulates simultaneously, which is necessary for the downstream gas cleaning processes (adsorption of H_2S and catalytic removal of NH_3) after the oil scrubber. Therefore, oil scrubber method will be used for the tar removal in this research and it will be applied before the sulphur removing process and NH_3 removing process.

For removing the NH_3 in the producer gas, Fe-based catalysts are more preferred because of its low cost and reasonably high activity. A cheap natural form iron sand, titanomagnetite, has been studied by Hongrapipat et al. [3, 145] previously, which showed high activity for decomposing NH_3 in Ar gas. Therefore, titanomagnetite will be further investigated in this study for the NH_3 decomposition and various gas mixtures will be tested including the simulated producer gas which has a similar composition to that from a practical gasification process.

For removal of H_2S, iron oxides such as titanomagnetite are the primary option in this research. Titanomagnetite has been tested by Hongrapipat et al. [3, 145] who has found that the titanomagnetite had a high capability for removing H_2S in the Ar gas. Furthermore, titanomagnetite is naturally abundant and widely distributed in New Zealand. Therefore, titanomagnetite will be investigated in this research to find its activity for H_2S adsorption in various gas mixtures including simulated producer gas from biomass gasification.

Overall, oil scrubber for tar removal and hot catalytic method by using titanomagnetite for NH_3 decomposition and H_2S adsorption will be studied in this research for the purpose of cleaning the producer gas from a 100kW DFB steam gasifier. The preliminary schematic layout of the gas cleaning system is shown in Figure 2.4.

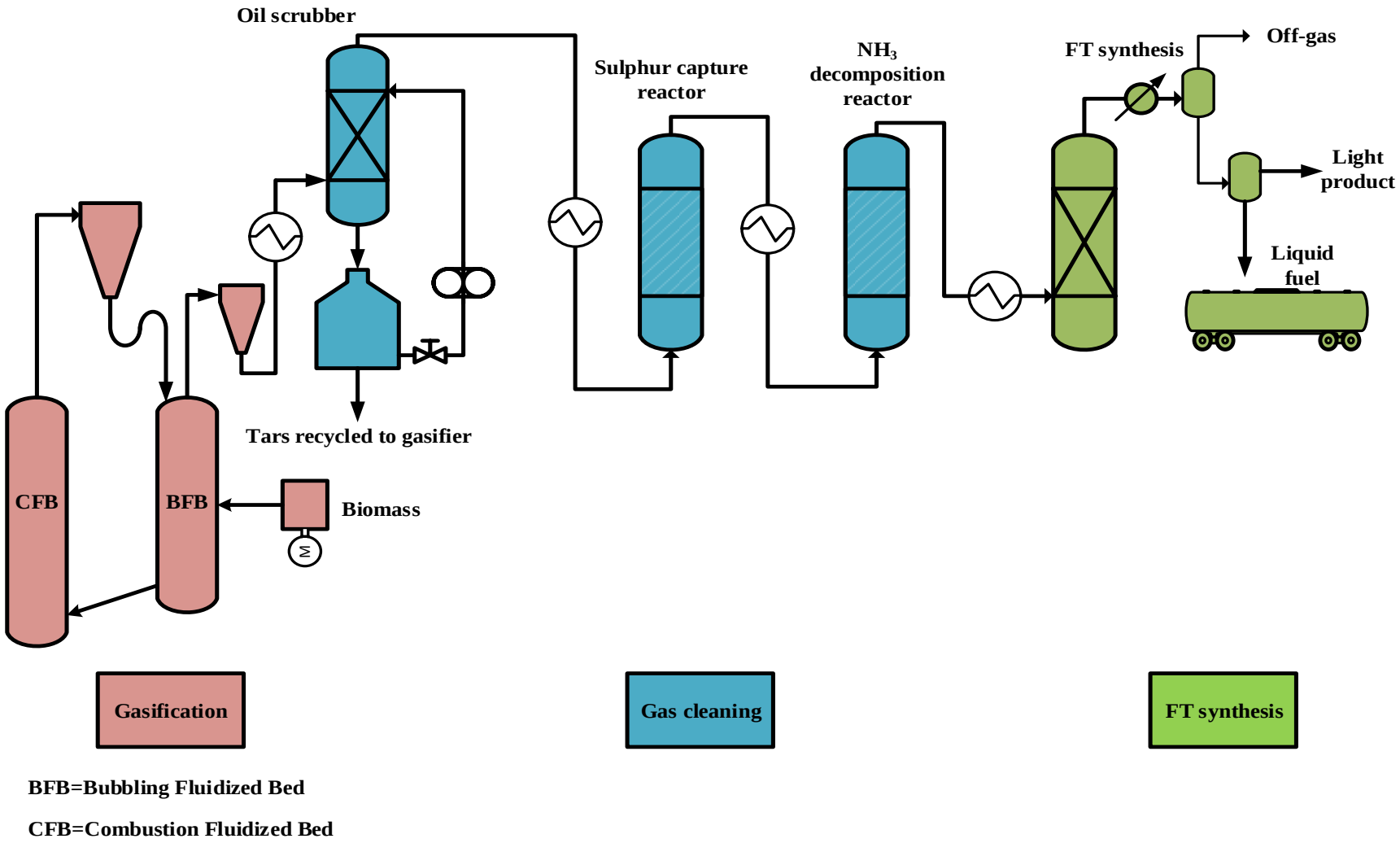

Figure 2.4 The preliminary schematic layout of the gas cleaning system.

2.4 Reference

[1] H. P. C. H. Boerrigter, D.J. Slort, H. Bodenstaff, A.J. Kaandorp, H. den Uil, L.P.L.M. Rabou, "Gas Cleaning for Integrated Biomass Gasification (BG) and Fischer-Tropsch (FT) Systems," in "Energy Research Centre of the Netherlands (ECN), Petten, The Netherlands, report RX-04-041," May 2004.

[2] Z. RWR, "Gas cleaning downstream biomass gasification: status report 2009," the Energy research Centre of the Netherlands (ECN), the NetherlandsECN-E-08-078, 2009.

[3] J. Hongrapipat, "Removal of NH_3 and H_2S from biomass gasification producer gas," Doctor of Philosophy, Chemical and Procees Engineering, University of Canterbury, Christchurch, New Zealand, 2014.

[4] C. Li and K. Suzuki, "Tar property, analysis, reforming mechanism and model for biomass gasification—an overview," *Renewable and Sustainable Energy Reviews,* vol. 13, no. 3, pp. 594-604, 2009.

[5] W. Torres, S. S. Pansare, and J. G. Goodwin Jr, "Hot gas removal of tars, ammonia, and hydrogen sulfide from biomass gasification gas," *Catalysis reviews,* vol. 49, no. 4, pp. 407-456, 2007.

[6] R. L. Bain *et al.*, "Evaluation of catalyst deactivation during catalytic steam reforming of biomass-derived syngas," *Industrial & engineering chemistry research,* vol. 44, no. 21, pp. 7945-7956, 2005.

[7] D. J. Stevens, "Hot gas conditioning: recent progress with larger-scale biomass gasification systerms," National Renewable Energy Laboratory, the U.S. Department of Energy LaboratoryNREL/SR-510-29952, August 2001.

[8] P. L. Spath and D. C. Dayton, "Preliminary screening-technical and economic assessment of synthesis gas to fuels and chemicals with emphasis on the potential for biomass-derived syngas," National Renewable Energy Lab Golden Co2003.

[9] T. Bui, R. Loof, and S. Bhattacharya, "Multi-stage reactor for thermal gasification of wood," *Energy*, vol. 19, no. 4, pp. 397-404, 1994.

[10] M. Asadullah, "Biomass gasification gas cleaning for downstream applications: A comparative critical review," *Renewable and sustainable energy reviews*, vol. 40, pp. 118-132, 2014.

[11] D. Fuentes-Cano, A. Gómez-Barea, S. Nilsson, and P. Ollero, "The influence of temperature and steam on the yields of tar and light hydrocarbon compounds during devolatilization of dried sewage sludge in a fluidized bed," *Fuel*, vol. 108, pp. 341-350, 2013.

[12] L. Devi, K. J. Ptasinski, and F. J. J. G. Janssen, "A review of the primary measures for tar elimination in biomass gasification processes," *Biomass and Bioenergy*, vol. 24, no. 2, pp. 125-140, 2003.

[13] P. S. Kiel JHA, Neeft JPA, Devi L, Ptasinski KJ, Janssen FJJG, Meijer R, Berends RH, Temmink HMG, Brem G, Padban N, Bramer EA, "Primary measures to reduce tar formation in fluidised-bed biomass gasifiers," 2004.

[14] D. C. Elliott, "Relation of reaction time and temperature to chemical composition of pyrolysis oils," ACS Publications, 1988.

[15] P. Morf, P. Hasler, and T. Nussbaumer, "Mechanisms and kinetics of homogeneous secondary reactions of tar from continuous pyrolysis of wood chips," *Fuel*, vol. 81, no. 7, pp. 843-853, 2002.

[16] H. N. Stiles and R. Kandiyoti, "Secondary reactions of flash pyrolysis tars measured in a fluidized bed pyrolysis reactor with some novel design features," *Fuel,* vol. 68, no. 3, pp. 275-282, 1989.

[17] R. J. Evans and T. A. Milne, "Molecular characterization of the pyrolysis of biomass," *Energy & Fuels,* vol. 1, no. 2, pp. 123-137, 1987.

[18] J. Hayashi, T. Kawakami, T. Taniguchi, K. Kusakabe, S. Morooka, and M. Yumura, "Control of molecular composition of tar by secondary reaction in fluidized-bed pyrolysis of a subbituminous coal," *Energy & fuels,* vol. 7, no. 1, pp. 57-66, 1993.

[19] E. Baker, M. Brown, D. Elliott, and L. Mudge, "Characterization and treatment of tars and biomass gasifiers," Pacific Northwest Lab., Richland, WA (USA)1988.

[20] X. Meng, W. de Jong, N. Fu, and A. H. M. Verkooijen, "Biomass gasification in a 100 kWth steam-oxygen blown circulating fluidized bed gasifier: Effects of operational conditions on product gas distribution and tar formation," *Biomass and Bioenergy,* vol. 35, no. 7, pp. 2910-2924, 2011.

[21] S. van Paasen and J. Kiel, "Tar formation in a fluidised-bed gasifier. Impact of fuel properties and operating conditions. 2004," ECN-C-04-013.

[22] J. J. Hernández, R. Ballesteros, and G. Aranda, "Characterisation of tars from biomass gasification: Effect of the operating conditions," *Energy,* vol. 50, pp. 333-342, 2013.

[23] I. Narváez, A. Orío, M. P. Aznar, and J. Corella, "Biomass Gasification with Air in an Atmospheric Bubbling Fluidized Bed. Effect of Six Operational Variables on the Quality of the Produced Raw Gas," *Industrial & Engineering Chemistry Research,* vol. 35, no. 7, pp. 2110-2120, 1996/01/01 1996.

[24] W. L. Saw and S. Pang, "The influence of calcite loading on producer gas composition and tar concentration of radiata pine pellets in a dual fluidised bed steam gasifier," *Fuel,* vol. 102, pp. 445-452, 2012.

[25] T. A. Milne, R. J. Evans, and N. Abatzaglou, "Biomass Gasifier"Tars": Their Nature, Formation, and Conversion," National Renewable Energy Laboratory, Golden, CO (US)1998.

[26] R. Warnecke, "Gasification of biomass: comparison of fixed bed and fluidized bed gasifier," *Biomass and bioenergy,* vol. 18, no. 6, pp. 489-497, 2000.

[27] F. Kirnbauer, V. Wilk, H. Kitzler, S. Kern, and H. Hofbauer, "The positive effects of bed material coating on tar reduction in a dual fluidized bed gasifier," *Fuel,* vol. 95, pp. 553-562, 2012.

[28] M. Virginie *et al.*, "Effect of Fe–olivine on the tar content during biomass gasification in a dual fluidized bed," *Applied Catalysis B: Environmental,* vol. 121-122, pp. 214-222, 2012.

[29] C. Pfeifer, R. Rauch, and H. Hofbauer, "In-bed catalytic tar reduction in a dual fluidized bed biomass steam gasifier," *Industrial & engineering chemistry research,* vol. 43, no. 7, pp. 1634-1640, 2004.

[30] J. Corella, J. Herguido, J. Gonzalez-Saiz, F. J. Alday, and J. L. Rodriguez-Trujillo, "Fluidized Bed Steam Gasification of Biomass with Dolomite and with a Commercial FCC Catalyst," in *Research in Thermochemical Biomass Conversion*, A. V. Bridgwater and J. L. Kuester, Eds.: Springer Netherlands, 1988, pp. 754-765.

[31] A. Olivares, M. P. Aznar, M. A. Caballero, J. Gil, E. Francés, and J. Corella, "Biomass gasification: produced gas upgrading by in-bed use of dolomite," *Industrial & Engineering Chemistry Research,* vol. 36, no. 12, pp. 5220-5226, 1997.

[32] J. Hongrapipat, W. L. Saw, and S. Pang, "Removal of ammonia from producer gas in biomass gasification: integration of gasification optimisation and hot catalytic gas cleaning," *Biomass Conversion and Biorefinery,* vol. 2, pp. 327-348, 2012.

[33] M. Berg, B. G. Espenas, P. Vriesman, E. Heginuz, and K. Sjöström, "Fuel‐Bound Nitrogen Conversion: Results from Gasification of Biomass in Two Different Small Scale Fluidized Beds," *Progress in Thermochemical Biomass Conversion,* pp. 322-332, 2001.

[34] J. Leppälahti, "Formation and behaviour of nitrogen compounds in an IGCC process," *Bioresource technology,* vol. 46, no. 1-2, pp. 65-70, 1993.

[35] W. Mojtahedi and J. Abbasian, "Catalytic decomposition of ammonia in a fuel gas at high temperature and pressure," *Fuel,* vol. 74, no. 11, pp. 1698-1703, 1995.

[36] J. Corella, J. M. Toledo, and R. Padilla, "Olivine or dolomite as in-bed additive in biomass gasification with air in a fluidized bed: which is better?," *Energy & Fuels,* vol. 18, no. 3, pp. 713-720, 2004.

[37] W. Wang, N. Padban, Z. Ye, G. Olofsson, A. Andersson, and I. Bjerle, "Catalytic hot gas cleaning of fuel gas from an air-blown pressurized fluidized-bed gasifier," *Industrial & engineering chemistry research,* vol. 39, no. 11, pp. 4075-4081, 2000.

[38] H. Cui, S. Q. Turn, V. Keffer, D. Evans, T. Tran, and M. Foley, "Contaminant estimates and removal in product gas from biomass steam gasification," *Energy & Fuels,* vol. 24, pp. 1222-1233, 2010.

[39] M. Jeremiáš, M. Pohořelý, P. Bode, S. Skoblia, Z. Beňo, and K. Svoboda, "Ammonia yield from gasification of biomass and coal in fluidized bed reactor," *Fuel,* vol. 117, pp. 917-925, 2014.

[40] W. Mojtahedi, M. Ylitalo, T. Maunula, and J. Abbasian, "Catalytic decomposition of ammonia in fuel gas produced in pilot-scale pressurized fluidized-bed gasifier," *Fuel processing technology,* vol. 45, no. 3, pp. 221-236, 1995.

[41] J. Zhou, S. M. Masutani, D. M. Ishimura, S. Q. Turn, and C. M. Kinoshita, "Release of fuel-bound nitrogen during biomass gasification," *Industrial & engineering chemistry research,* vol. 39, no. 3, pp. 626-634, 2000.

[42] I. Aigner, C. Pfeifer, and H. Hofbauer, "Co-gasification of coal and wood in a dual fluidized bed gasifier," *Fuel,* vol. 90, no. 7, pp. 2404-2412, 2011.

[43] W. L. Saw and S. Pang, "Co-gasification of blended lignite and wood pellets in a 100kW dual fluidised bed steam gasifier: The influence of lignite ratio on producer gas composition and tar content," *Fuel,* vol. 112, pp. 117-124, 2013.

[44] F. Pinto *et al.*, "Co-gasification of coal and wastes in a pilot-scale installation. 2: Effect of catalysts in syngas treatment to achieve sulphur and nitrogen compounds abatement," *Fuel,* vol. 89, no. 11, pp. 3340-3351, 2010.

[45] J. Leppälahti, P. Simell, and E. Kurkela, "Catalytic conversion of nitrogen compounds in gasification gas," *Fuel Processing Technology,* vol. 29, no. 1, pp. 43-56, 1991.

[46] J. Leppälahti and T. Koljonen, "Nitrogen evolution from coal, peat and wood during gasification: Literature review," *Fuel Processing Technology,* vol. 43, no. 1, pp. 1-45, 1995.

[47] F. Pinto, H. Lopes, R. N. André, M. Dias, I. Gulyurtlu, and I. Cabrita, "Effect of experimental conditions on gas quality and solids produced by sewage sludge cogasification. 1. Sewage sludge mixed with coal," *Energy & Fuels,* vol. 21, no. 5, pp. 2737-2745, 2007.

[48] E. Kurkela and P. Staåhlberg, "Air gasification of peat, wood and brown coal in a pressurized fluidized-bed reactor. II. Formation of nitrogen compounds," *Fuel processing technology,* vol. 31, no. 1, pp. 23-32, 1992.

[49] A. Z. Farzam, R. M. Felder, and J. K. Ferrell, "Analysis of nitrogenous compounds in the effluent streams from a fluidized bed coal gasification reactor," *Fuel processing technology,* vol. 10, no. 3, pp. 249-259, 1985.

[50] J. Hongrapipat, S. Pang, and W. L. Saw, "Removal of NH_3 and H_2S from producer gas in a dual fluidised bed steam gasifier by optimisation of operation conditions and application of bed materials," *Biomass Conversion and Biorefinery,* vol. 6, no. 1, pp. 105-113, 2016.

[51] J. Leppälahti, "Behaviour of fuel-bound nitrogen in gasification and in high-temperature NH~ 3 removal processes," *VTT PUBLICATIONS,* 1998.

[52] L. Chang *et al.,* "Formation of NOx precursors during the pyrolysis of coal and biomass. Part VI. Effects of gas atmosphere on the formation of NH_3 and HCN," *Fuel,* vol. 82, no. 10, pp. 1159-1166, 2003.

[53] W. Wang and G. Olofsson, "Reduction of ammonia and tar in pressurized biomass gasification," in *5th International Symposium on Gas Cleaning at High Temperature,* 2002.

[54] I. De Bari, D. Barisano, M. Cardinale, D. Matera, F. Nanna, and D. Viggiano, "Air gasification of biomass in a downdraft fixed bed: a comparative study of the inorganic and organic products distribution," *Energy & Fuels,* vol. 14, no. 4, pp. 889-898, 2000.

[55] P. Vriesman, E. Heginuz, and K. Sjöström, "Biomass gasification in a laboratory-scale AFBG: influence of the location of the feeding point on the fuel-N conversion," *Fuel,* vol. 79, no. 11, pp. 1371-1378, 2000.

[56] X. Meng, W. de Jong, R. Pal, and A. H. M. Verkooijen, "In bed and downstream hot gas desulphurization during solid fuel gasification: A review," *Fuel Processing Technology*, vol. 91, no. 8, pp. 964-981, 2010.

[57] D. L. Klass, *Biomass for renewable energy, fuels, and chemicals*. Academic press, 1998.

[58] J. Hepola, *Sulfur transformations in catalytic hot-gas cleaning of gasification gas*. Espoo, 2000.

[59] M. Jazbec, K. Sendt, and B. S. Haynes, "Kinetic and thermodynamic analysis of the fate of sulphur compounds in gasification products," *Fuel*, vol. 83, no. 16, pp. 2133-2138, 2004.

[60] C. H. Boerrigter H, Slort DJ, Bodenstaff H, Kaandorp AJ, denUil H, Rabou LPLM, "Gas cleaning for integrated biomass gasification (BG) and Fischer-Tropsch (FT) systems: experimental demonstration of two BG-FT systems ("Proof-of-Principle")," the Energy research Centre of the Netherlands (ECN), the NetherlandsECN-C-04-056, 2004.

[61] H. Cui, S. Q. Turn, V. Keffer, D. Evans, T. Tran, and M. Foley, "Contaminant Estimates and Removal in Product Gas from Biomass Steam Gasification," *Energy & Fuels*, vol. 24, no. 2, pp. 1222-1233, 2010/02/18 2010.

[62] C. Gai, Y. Dong, and T. Zhang, "Distribution of sulfur species in gaseous and condensed phase during downdraft gasification of corn straw," *Energy*, vol. 64, pp. 248-258, 2014.

[63] W. Torres, S. S. Pansare, and J. G. Goodwin, "Hot Gas Removal of Tars, Ammonia, and Hydrogen Sulfide from Biomass Gasification Gas," *Catalysis Reviews*, vol. 49, no. 4, pp. 407-456, 2007.

[64] A. Van der Drift, J. Van Doorn, and J. Vermeulen, "Ten residual biomass fuels for circulating fluidized-bed gasification," *Biomass and Bioenergy*, vol. 20, no. 1, pp. 45-56, 2001.

[65] H. Boerrigter and R. Rauch, "Review of applications of gases from biomass gasification," *ECN Biomassa, Kolen en Milieuonderzoek,* vol. 20, 2006.

[66] F. Pinto, R. N. André, H. Lopes, M. Dias, I. Gulyurtlu, and I. Cabrita, "Effect of experimental conditions on gas quality and solids produced by sewage sludge cogasification. 2. Sewage sludge mixed with biomass," *Energy & Fuels*, vol. 22, no. 4, pp. 2314-2325, 2008.

[67] H. Kuramochi, W. Wu, and K. Kawamoto, "Prediction of the behaviors of H 2 S and HCl during gasification of selected residual biomass fuels by equilibrium calculation," *Fuel,* vol. 84, no. 4, pp. 377-387, 2005.

[68] M. Dias and I. Gulyurtlu, "H 2 S and HCl formation during RDF and coal co-gasification: a comparison between the predictions and experimental results," in *Proceedings of the biomass gasification technologies workshop, MRC Gebze Campus-Tü rkiye,* 2008.

[69] J. Hongrapipat, W. Saw, and S. Pang, "Co-gasification of blended lignite and wood pellets in a dual fluidized bed steam gasifier: the influence of lignite to fuel ratio on NH 3 and H 2 S concentrations in the producer gas," *Fuel,* vol. 139, pp. 494-501, 2015.

[70] J. Abbasian, A. Rehmat, D. Leppin, and D. D. Banerjee, "Desulfurization of fuels with calcium-based sorbents," *Fuel processing technology,* vol. 25, no. 1, pp. 1-15, 1990.

[71] M. Husmann, C. Zuber, V. Maitz, T. Kienberger, and C. Hochenauer, "Comparison of dolomite and lime as sorbents for in-situ H_2S removal with respect to gasification parameters in biomass gasification," *Fuel,* vol. 181, pp. 131-138, 2016.

[72] F. Garcia-Labiano, L. De Diego, and J. Adanez, "Effectiveness of natural, commercial, and modified calcium-based sorbents as H2S removal agents at high temperatures," *Environmental science & technology,* vol. 33, no. 2, pp. 288-293, 1999.

[73] S. Cheah, D. L. Carpenter, and K. A. Magrini-Bair, "Review of mid-to high-temperature sulfur sorbents for desulfurization of biomass-and coal-derived syngas," *Energy & Fuels,* vol. 23, no. 11, pp. 5291-5307, 2009.

[74] Z. Zhang and S. Pang, "Experimental investigation of biomass devolatilization in steam gasification in a dual fluidised bed gasifier," *Fuel*, vol. 188, pp. 628-635, 2017.

[75] P. C. Bergman, S. V. van Paasen, and H. Boerrigter, "The novel “OLGA” technology for complete tar removal from biomass producer gas," in *Pyrolysis and Gasification of Biomass and Waste, Expert Meeting, Strasbourg, France*, 2002, vol. 30.

[76] Z. Abu El-Rub, E. A. Bramer, and G. Brem, "Review of Catalysts for Tar Elimination in Biomass Gasification Processes," *Industrial & Engineering Chemistry Research,* vol. 43, no. 22, pp. 6911-6919, 2004/10/01 2004.

[77] A. Paethanom, S. Nakahara, M. Kobayashi, P. Prawisudha, and K. Yoshikawa, "Performance of tar removal by absorption and adsorption for biomass gasification," *Fuel Processing Technology,* vol. 104, pp. 144-154, 2012.

[78] P. Aravind and W. de Jong, "Evaluation of high temperature gas cleaning options for biomass gasification product gas for solid oxide fuel cells," *Progress in Energy and Combustion Science,* vol. 38, no. 6, pp. 737-764, 2012.

[79] N. Abdoulmoumine, S. Adhikari, A. Kulkarni, and S. Chattanathan, "A review on biomass gasification syngas cleanup," *Applied Energy,* vol. 155, pp. 294-307, 2015.

[80] P. Hasler and T. Nussbaumer, "Gas cleaning for IC engine applications from fixed bed biomass gasification," *Biomass and Bioenergy,* vol. 16, no. 6, pp. 385-395, 1999.

[81] J. Neeft, H. Knoef, and P. Onaji, *Behaviour of tar in biomass gasification systems: tar related problems and their solutions*. Novem, 1999.

[82] S. Anis and Z. A. Zainal, "Tar reduction in biomass producer gas via mechanical, catalytic and thermal methods: A review," *Renewable and Sustainable Energy Reviews,* vol. 15, no. 5, pp. 2355-2377, 2011.

[83] M. K. Karmakar, P. Chandra, and P. K. Chatterjee, "A review on the fuel gas cleaning technologies in gasification process," *Journal of Environmental Chemical Engineering,* vol. 3, no. 2, pp. 689-702, 2015.

[84] D. Draelants, H.-B. Zhao, and G. Baron, "Catalytic conversion of tars in biomass gasification fuel gases with nickel-activated ceramic filters," *Studies in surface science and catalysis,* vol. 130, pp. 1595-1600, 2000.

[85] L. Ma, H. Verelst, and G. Baron, "Integrated high temperature gas cleaning: tar removal in biomass gasification with a catalytic filter," *Catalysis Today,* vol. 105, no. 3, pp. 729-734, 2005.

[86] E. Simeone, M. Siedlecki, M. Nacken, S. Heidenreich, and W. De Jong, "High temperature gas filtration with ceramic candles and ashes characterisation during steam–oxygen blown gasification of biomass," *Fuel,* vol. 108, pp. 99-111, 2013.

[87] H. Könemann and S. Van Paasen, "OLGA tar removal technology: 4 MW commercial demonstration," in *Dahlman, Paper presented at the 15th European biomass conference in Berlin*, 2007.

[88] A. K. S. Parihar, T. Hammer, and G. Sridhar, "Development and testing of plate type wet ESP for removal of particulate matter and tar from producer gas," *Renewable Energy,* vol. 77, pp. 473-481, 2015.

[89] F. Lettner, H. Timmerer, and P. Haselbacher, "Biomass gasification–State of the art description," *Intelligent Energy Europe, Austria,* 2007.

[90] B.-K. Lee, K.-R. Jung, and S.-H. Park, "Development and application of a novel swirl cyclone scrubber—(1) Experimental," *Journal of Aerosol Science,* vol. 39, no. 12, pp. 1079-1088, 2008.

[91] T. Tarnpradab, S. Unyaphan, F. Takahashi, and K. Yoshikawa, "Tar removal capacity of waste cooking oil absorption and waste char adsorption for rice husk gasification," *Biofuels,* vol. 7, no. 4, pp. 401-412, 2016.

[92] R. Zwart, A. Van der Drift, A. Bos, H. Visser, M. Cieplik, and H. Könemann, "Oil-based gas washing—Flexible tar removal for high-efficient production of clean heat and power as well as sustainable fuels and chemicals," *Environmental progress & sustainable energy,* vol. 28, no. 3, pp. 324-335, 2009.

[93] H. Hermann, R. Reinhard, B. Klaus, K. Reinhard, and A. Christian, "Biomass CHP Plant Güssing–a success story," ed: Vienna, 2001.

[94] T. Phuphuakrat, T. Namioka, and K. Yoshikawa, "Absorptive removal of biomass tar using water and oily materials," *Bioresource Technology,* vol. 102, no. 2, pp. 543-549, 1// 2011.

[95] S. Nakamura, S. Kitano, and K. Yoshikawa, "Biomass gasification process with the tar removal technologies utilizing bio-oil scrubber and char bed," *Applied Energy,* vol. 170, pp. 186-192, 2016.

[96] B. JD, "Low tar and high efficient gasification concept," presented at the Proceedings of the conferences ECOS, 2000.

[97] C. Di Blasi, "Modeling intra- and extra-particle processes of wood fast pyrolysis," *AIChE Journal,* vol. 48, no. 10, pp. 2386-2397, 2002.

[98] J. Han and H. Kim, "The reduction and control technology of tar during biomass gasification/pyrolysis: An overview," *Renewable and Sustainable Energy Reviews*, vol. 12, no. 2, pp. 397-416, 2// 2008.

[99] A. V. Bridgwater, "The technical and economic feasibility of biomass gasification for power generation," *Fuel*, vol. 74, no. 5, pp. 631-653, 5// 1995.

[100] P. Brandt and U. B. Henriksen, "Decomposition of tar in gas from updraft gasifier by thermal cracking," in *1st World Conference and Exhibition on Biomass for Energy and Industry*, 2000.

[101] A. Beenackers and K. Maniatis, "Gasification technologies for heat and power from biomass," in *Fuel and Energy Abstracts*, 1998, vol. 39, no. 1: Elsevier Science.

[102] M. Houben, *Analysis of tar removal in a partial oxidation burner*. Technische Universiteit Eindhoven, 2003.

[103] E. Rensfelt, "Atmospheric pressure gasification process for power generation," Analysis and coordination of the activities concerning a gasification of biomass, ESpoo Finiland1996.

[104] D. Sutton, B. Kelleher, and J. R. Ross, "Review of literature on catalysts for biomass gasification," *Fuel Processing Technology*, vol. 73, no. 3, pp. 155-173, 2001.

[105] D. Dayton, "Review of the literature on catalytic biomass tar destruction: Milestone completion report," National Renewable Energy Lab., Golden, CO (US)2002.

[106] A. Donnot, P. Magne, and X. Deglise, "Experimental approach to the catalysed cracking reaction of tar from wood pyrolysis," *Journal of analytical and applied pyrolysis*, vol. 21, no. 3, pp. 265-280, 1991.

[107] P. A. Simell, E. K. Hirvensalo, V. T. Smolander, and A. O. I. Krause, "Steam reforming of gasification gas tar over dolomite with benzene as a model compound," *Industrial & Engineering Chemistry Research,* vol. 38, pp. 1250-1257, 1999.

[108] S. Rapagna, N. Jand, and P. Foscolo, "Catalytic gasification of biomass to produce hydrogen rich gas," *International Journal of Hydrogen Energy,* vol. 23, no. 7, pp. 551-557, 1998.

[109] T. Wang, J. Chang, P. Lv, and J. Zhu, "Novel catalyst for cracking of biomass tar," *Energy & Fuels,* vol. 19, no. 1, pp. 22-27, 2005.

[110] J. N. Rapagná S, Kiennemann A, Foscolo PU, "Steam-gasification of biomass in a fluidized-bed of olivine particles," *Biomass and Bioenergy,* vol. 19, pp. 187-197, 2000.

[111] D. Świerczyński, S. Libs, C. Courson, and A. Kiennemann, "Steam reforming of tar from a biomass gasification process over Ni/olivine catalyst using toluene as a model compound," *Applied Catalysis B: Environmental,* vol. 74, no. 3, pp. 211-222, 2007.

[112] L. Devi, K. J. Ptasinski, and F. J. Janssen, "Decomposition of naphthalene as a biomass tar over pretreated olivine: effect of gas composition, kinetic approach, and reaction scheme," *Industrial & engineering chemistry research,* vol. 44, no. 24, pp. 9096-9104, 2005.

[113] G. Hu, S. Xu, S. Li, C. Xiao, and S. Liu, "Steam gasification of apricot stones with olivine and dolomite as downstream catalysts," *Fuel Processing Technology,* vol. 87, no. 5, pp. 375-382, 2006.

[114] Z. Zhao *et al.*, "Characterization of olivine-supported nickel silicate as potential catalysts for tar removal from biomass gasification," *Applied Catalysis A: General,* vol. 489, pp. 42-50, 2015.

[115] R. Michel *et al.*, "Steam reforming of α-methylnaphthalene as a model tar compound over olivine and olivine supported nickel," *Fuel,* vol. 109, pp. 653-660, 2013.

[116] N. Tsubouchi, Y. Mochizuki, E. Byambajav, S. Takahashi, Y. Hanaoka, and Y. Ohtsuka, "Catalytic Performance of Limonite Ores in the Decomposition of Model Compounds of Biomass-Derived Tar," *Energy & Fuels,* vol. 31, no. 4, pp. 3898-3904, 2017.

[117] A. Matsumura, T. Kondo, S. Sato, I. Saito, and W. F. de Souza, "Hydrocracking Brazilian Marlim vacuum residue with natural limonite. Part 1: catalytic activity of natural limonite," *Fuel,* vol. 84, no. 4, pp. 411-416, 2005.

[118] N. Kannari, C. Satomi, Y. Oyama, and T. Takarada, "Durability studies of limonite ore for catalytic decomposition of phenol as a model biomass tar in a fluidized bed," *Biomass and Bioenergy,* vol. 107, pp. 86-92, 2017.

[119] T. Nordgreen, T. Liliedahl, and K. Sjöström, "Metallic iron as a tar breakdown catalyst related to atmospheric, fluidised bed gasification of biomass," *Fuel,* vol. 85, no. 5, pp. 689-694, 2006.

[120] B. Dou, J. Gao, X. Sha, and S. W. Baek, "Catalytic cracking of tar component from high-temperature fuel gas," *Applied thermal engineering,* vol. 23, no. 17, pp. 2229-2239, 2003.

[121] D. Sutton, B. Kelleher, A. Doyle, and J. Ross, "Investigation of nickel supported catalysts for the upgrading of brown peat derived gasification products," *Bioresource Technology,* vol. 80, no. 2, pp. 111-116, 2001.

[122] M. Asadullah, T. Miyazawa, S.-i. Ito, K. Kunimori, M. Yamada, and K. Tomishige, "Catalyst development for the gasification of biomass in the dual-bed gasifier," *Applied Catalysis A: General,* vol. 255, no. 2, pp. 169-180, 12/8/ 2003.

[123] T. Miyazawa, T. Kimura, J. Nishikawa, K. Kunimori, and K. Tomishige, "Catalytic properties of Rh/CeO 2/SiO 2 for synthesis gas production from biomass by catalytic partial oxidation of tar," *Science and technology of Advanced Materials,* vol. 6, no. 6, pp. 604-614, 2005.

[124] J. Loipersböck, M. Lenzi, R. Rauch, and H. Hofbauer, "Hydrogen production from biomass: The behavior of impurities over a CO shift unit and a biodiesel scrubber used as a gas treatment stage," *Korean Journal of Chemical Engineering,* vol. 34, no. 8, pp. 2198-2203, 2017.

[125] T. Pröll, I. G. Siefert, A. Friedl, and H. Hofbauer, "Removal of NH3 from biomass gasification producer gas by water condensing in an organic solvent scrubber," *Industrial & engineering chemistry research,* vol. 44, no. 5, pp. 1576-1584, 2005.

[126] E. Bjoerkman and K. Sjoestroem, "Decomposition of ammonia over dolomite and related compounds," *Energy & fuels,* vol. 5, no. 5, pp. 753-760, 1991.

[127] M. Yumura and T. Asaba, "Rate constants of chemical reactions in the high temperature pyrolysis of ammonia," in *Symposium (International) on Combustion*, 1981, vol. 18, no. 1, pp. 863-872: Elsevier.

[128] J. Leppälahti, E. Kurkela, P. Simell, and P. Ståhlberg, "Formation and removal of nitrogen compounds in gasification processes," in *Advances in thermochemical biomass conversion*: Springer, 1993, pp. 160-174.

[129] A. Chambers, Y. Yoshii, T. Inada, and T. Miyamoto, "Ammonia decomposition in coal gasification atmospheres," *The Canadian Journal of Chemical Engineering,* vol. 74, no. 6, pp. 929-934, 1996.

[130] P. Simell, E. Kurkela, P. Ståhlberg, and J. Hepola, "Catalytic hot gas cleaning of gasification gas," *Catalysis Today*, vol. 27, no. 1, pp. 55-62, 1996.

[131] M. Abul-Milh and B.-M. Steenari, "The effect of calcination on the reactions of ammonia over different carbonates and limestones in fluidized bed combustion conditions," *Energy & fuels*, vol. 15, no. 4, pp. 874-880, 2001.

[132] T. Shimizu, E. Karahashi, T. Yamaguchi, and M. Inagaki, "Decomposition of NH3 over calcined and uncalcined limestone under fluidized bed combustion conditions," *Energy & fuels*, vol. 9, no. 6, pp. 962-965, 1995.

[133] N. Tsubouchi, H. Hashimoto, and Y. Ohtsuka, "Sulfur tolerance of an inexpensive limonite catalyst for high temperature decomposition of ammonia," *Powder Technology*, vol. 180, pp. 184-189, 2008.

[134] Y. Ozawa and Y. Tochihara, "Catalytic decomposition of ammonia in simulated coal-derived gas over supported nickel catalysts," *Catalysis Today*, vol. 164, pp. 528-532, 2011.

[135] H. Rönkkönen, P. Simell, M. Reinikainen, O. Krause, and M. V. Niemelä, "Catalytic clean-up of gasification gas with precious metal catalysts–A novel catalytic reformer development," *Fuel*, vol. 89, no. 11, pp. 3272-3277, 2010.

[136] J. Donald, C. C. Xu, H. Hashimoto, E. Byambajav, and Y. Ohtsuka, "Novel carbon-based Ni/Fe catalysts derived from peat for hot gas ammonia decomposition in an inert helium atmosphere," *Applied Catalysis A: General*, vol. 375, pp. 124-133, 2010.

[137] C. Xu, N. Tsubouchi, H. Hashimoto, and Y. Ohtsuka, "Catalytic decomposition of ammonia gas with metal cations present naturally in low rank coals," *Fuel*, vol. 84, no. 14, pp. 1957-1967, 2005.

[138] C. Xu, J. Donald, H. Hashimoto, E. Byambajav, and Y. Ohtsuka, "Ammonia decomposition with metal catalysts supported on Canadian peat-derived carbons," in *8th World Congress on Chemical Engineering, Montreal, Canada*, 2009, pp. 23-27.

[139] D. Cooper, S. Ghardashkani, and E. Ljungström, "Decomposition of ammonia over calcined and sulfated limestone at 725-950. degree. C," *Energy & fuels,* vol. 3, no. 3, pp. 278-283, 1989.

[140] C. C. Xu, J. Donald, E. Byambajav, and Y. Ohtsuka, "Recent advances in catalysts for hot-gas removal of tar and NH_3 from biomass gasification," *Fuel,* vol. 89, pp. 1784-1795, 2010.

[141] J. Corella, A. Orió, and J.-M. Toledo, "Biomass gasification with air in a fluidized bed: exhaustive tar elimination with commercial steam reforming catalysts," *Energy & Fuels,* vol. 13, no. 3, pp. 702-709, 1999.

[142] N. Tsubouchi, H. Hashimoto, and Y. Ohtsuka, "Catalytic performance of limonite in the decomposition of ammonia in the coexistence of typical fuel gas components produced in an air-blown coal gasification process," *Energy & Fuels,* vol. 21, pp. 3063-3069, 2007.

[143] N. Tsubouchi, H. Hashimoto, and Y. Ohtsuka, "High catalytic performance of fine particles of metallic iron formed from limonite in the decomposition of a low concentration of ammonia," *Catalysis letters,* vol. 105, pp. 203-208, 2005.

[144] N. Tsubouchi, H. Hashimoto, and Y. Ohtsuka, "High catalytic performance of magnesium cations-added limonite in the decomposition of ammonia in a simulated syngas-rich fuel gas," *Journal of Molecular Catalysis A: Chemical,* vol. 407, pp. 75-80, 2015.

[145] J. Hongrapipat, A. C. K. Yip, A. T. Marshall, W. L. Saw, and S. Pang, "Investigation of simultaneous removal of ammonia and hydrogen sulphide from producer gas in biomass gasification by titanomagnetite," *Fuel,* vol. 135, pp. 235-242, 2014.

[146] A. Sarıoğlan, Y. Durak-Çetin, H. Okutan, and F. Akgün, "Decomposition of ammonia: The effect of syngas components on the activity of zeolite Hβ supported iron catalyst," *Chemical Engineering Science,* vol. 171, pp. 440-450, 2017.

[147] Y. Ohtsuka, C. Xu, D. Kong, and N. Tsubouchi, "Decomposition of ammonia with iron and calcium catalysts supported on coal chars," *Fuel,* vol. 83, pp. 685-692, 2004.

[148] J. Corella, J. M. Toledo, and R. Padilla, "Catalytic hot gas cleaning with monoliths in biomass gasification in fluidized beds. 3. Their effectiveness for ammonia elimination," *Industrial & engineering chemistry research,* vol. 44, no. 7, pp. 2036-2045, 2005.

[149] B. Dou, M. Zhang, J. Gao, W. Shen, and X. Sha, "High-temperature removal of NH_3, organic sulfur, HCl, and tar component from coal-derived gas," *Industrial & engineering chemistry research,* vol. 41, no. 17, pp. 4195-4200, 2002.

[150] H. Fortier, P. Westreich, S. Selig, C. Zelenietz, and J. Dahn, "Ammonia, cyclohexane, nitrogen and water adsorption capacities of an activated carbon impregnated with increasing amounts of $ZnCl_2$, and designed to chemisorb gaseous NH_3 from an air stream," *Journal of colloid and interface science,* vol. 320, no. 2, pp. 423-435, 2008.

[151] S. v. Paasen, M. Cieplik, and N. Phokawat, "Gasification of non-woody biomass," *Petten, Netherlands: Energy Research Centre of the Netherlands (ECN),* 2006.

[152] R. B. Slimane and J. Abbasian, "Utilization of metal oxide-containing waste materials for hot coal gas desulfurization," *Fuel Processing Technology,* vol. 70, no. 2, pp. 97-113, 2001.

[153] R. Newby and R. Bannister, "Advanced hot gas cleaning system for coal gasification processes," in *ASME 1993 International Gas Turbine and Aeroengine Congress and Exposition,* 1993, pp. V03BT16A094-V03BT16A094: American Society of Mechanical Engineers.

[154] W. J. Bakker, F. Kapteijn, and J. A. Moulijn, "A high capacity manganese-based sorbent for regenerative high temperature desulfurization with direct sulfur production: Conceptual process application to coal gas cleaning," *Chemical Engineering Journal,* vol. 96, no. 1, pp. 223-235, 2003.

[155] J. Swisher and K. Schwerdtfeger, "Review of metals and binary oxides as sorbents for removing sulfur from coal-derived gases," *Journal of Materials Engineering and Performance,* vol. 1, no. 3, pp. 399-407, 1992.

[156] S. Araki, "R & D of an IGCC system by the 200 t/d pilot plant at Nakoso," presented at the 1995 APEC experts' group on clean coal technology seminar, Teajon, Korea, 1995.

[157] K. Kamei *et al.*, "Recent development of a simultaneous sulfur and dust removal process for IGCC power generation system," 1996: Pittsburgh Coal Conference, Pittsburgh, PA (United States).

[158] R. B. Slimane and J. Abbasian, "Regenerable mixed metal oxide sorbents for coal gas desulfurization at moderate temperatures," *Advances in Environmental Research,* vol. 4, no. 2, pp. 147-162, 2000.

[159] E. Sasaoka, T. Ichio, and S. Kasaoka, "High-temperature hydrogen sulfide removal from coal-derived gas by iron ore," *Energy & Fuels,* vol. 6, no. 5, pp. 603-608, 1992.

[160] T. K. Tseng, H. C. Chang, H. Chu, and H. T. Chen, "Hydrogen sulfide removal from coal gas by the metal-ferrite sorbents made from the heavy metal wastewater sludge," *Journal of Hazardous Materials,* vol. 160, no. 2–3, pp. 482-488, 2008.

[161] P. De Wild, J. Kiel, and E. Schenk, "Iron oxide/molybdenum oxide sorbents for high temperature fuel gas desulfurization," 1996: Pittsburgh Coal Conference, Pittsburgh, PA (United States).

[162] S. C. Mitchell, *Hot gas cleanup of sulphur, nitrogen, minor and trace elements*. IEA Coal Research, 1998.

[163] E. Sasaoka, Y. Iwamoto, S. Hirano, M. A. Uddin, and Y. Sakata, "Soot formation over zinc ferrite high-temperature desulfurization sorbent," *Energy & fuels,* vol. 9, no. 2, pp. 344-353, 1995.

[164] M. Kobayashi, H. Shirai, and M. Nunokawa, "Investigation on desulfurization performance and pore structure of sorbents containing zinc ferrite," *Energy & fuels,* vol. 11, no. 4, pp. 887-896, 1997.

[165] M. Pineda, J. G. Fierro, J. Palacios, C. Cilleruelo, E. García, and J. Ibarra, "Characterization of zinc oxide and zinc ferrite doped with Ti or Cu as sorbents for hot gas desulphurization," *Applied surface science,* vol. 119, no. 1, pp. 1-10, 1997.

[166] N.-o. Ikenaga, Y. Ohgaito, H. Matsushima, and T. Suzuki, "Preparation of zinc ferrite in the presence of carbon material and its application to hot-gas cleaning," *Fuel,* vol. 83, no. 6, pp. 661-669, 2004.

[167] M. Kobayashi, M. Nunokawa, and H. Shirai, "Development of regenerable desulfurization sorbent for coal gas sulfur removal below ppm level," *Schmidt E., Gang P., Pilz T., Dittler A,* pp. 618-629, 1996.

[168] E. García, C. Cilleruelo, J. V. Ibarra, M. Pineda, and J. M. Palacios, "Kinetic study of high-temperature removal of H_2S by novel metal oxide sorbents," *Industrial & engineering chemistry research,* vol. 36, no. 3, pp. 846-853, 1997.

[169] L. Yanxu, L. Chunhu, G. Hanxian, and Z. Bing, "Modeling of hydrogen sulfide removal using zinc oxide desulfurizer," 1997: Pittsburgh Coal Conference, Pittsburgh, PA (United States).

[170] J. Yang and J. Swisher, "The phase stability of $Zn_2Ti_3O_8$," *Materials characterization,* vol. 37, no. 2, pp. 153-159, 1996.

[171] J. A. Poston, "A reduction in the spalling of zinc titanate desulfurization sorbents through the addition of lanthanum oxide," *Industrial & engineering chemistry research,* vol. 35, no. 3, pp. 875-882, 1996.

[172] E. Sasaoka, N. Sada, A. Manabe, M. A. Uddin, and Y. Sakata, "Modification of ZnO-TiO_2 high-temperature desulfurization sorbent by ZrO_2 addition," *Industrial & engineering chemistry research,* vol. 38, no. 3, pp. 958-963, 1999.

[173] H. K. Jun, T. J. Lee, S. O. Ryu, and J. C. Kim, "A study of Zn-Ti-based H_2S removal sorbents promoted with cobalt oxides," *Industrial & engineering chemistry research,* vol. 40, no. 16, pp. 3547-3556, 2001.

[174] H. K. Jun *et al.*, "A study of Zn-Ti-based H_2S removal sorbents promoted with cobalt and nickel oxides," *Energy & fuels,* vol. 18, no. 1, pp. 41-48, 2004.

[175] T. Kyotani, H. Kawashima, A. Tomita, A. Palmer, and E. Furimsky, "Removal of H_2S from hot gas in the presence of Cu-containing sorbents," *Fuel,* vol. 68, no. 1, pp. 74-79, 1989.

[176] Z. Li and M. Flytzani-Stephanopoulos, "Cu-Cr-O and Cu-Ce-O regenerable oxide sorbents for hot gas desulfurization," *Industrial & engineering chemistry research,* vol. 36, no. 1, pp. 187-196, 1997.

[177] P. R. Westmoreland and D. P. Harrison, "Evaluation of candidate solids for high-temperature desulfurization of low-Btu gases," *Environmental science & technology,* vol. 10, no. 7, pp. 659-661, 1976.

[178] E. Turkdogan and R. Olsson, "Desulfurization of hot reducing gases with manganese oxide pellets," in *Third International Iron and Steel Congress,* 1978, pp. 277-288.

[179] R. Ben-Slimane and M. Hepworth, "Desulfurization of hot coal-derived fuel gases with manganese-based regenerable sorbents. 1. Loading (sulfidation) tests," *Energy & Fuels,* vol. 8, no. 6, pp. 1175-1183, 1994.

[180] H. Atakül, J. P. Wakker, A. W. Gerritsen, and P. J. van den Berg, "Removal of H_2S from fuel gases at high temperatures using $MnO/\gamma\text{-}Al_2O_3$," *Fuel,* vol. 74, no. 2, pp. 187-191, 1995.

[181] Y. Zeng, S. Zhang, F. Groves, and D. Harrison, "High temperature gas desulfurization with elemental sulfur production," *Chemical engineering science,* vol. 54, no. 15, pp. 3007-3017, 1999.

[182] M. Kobayashi and M. Flytzani-Stephanopoulos, "Reduction and sulfidation kinetics of cerium oxide and Cu-modified cerium oxide," *Industrial & engineering chemistry research,* vol. 41, no. 13, pp. 3115-3123, 2002.

[183] Z. Wang and M. Flytzani-Stephanopoulos, "Cerium oxide-based sorbents for regenerative hot reformate gas desulfurization," *Energy & fuels,* vol. 19, no. 5, pp. 2089-2097, 2005.

[184] K. B. Yi, E. J. Podlaha, and D. P. Harrison, "Ceria-zirconia high-temperature desulfurization sorbents," *Industrial & engineering chemistry research,* vol. 44, no. 18, pp. 7086-7091, 2005.

[185] S. Yasyerli, "Cerium–manganese mixed oxides for high temperature H_2S removal and activity comparisons with V–Mn, Zn–Mn, Fe–Mn sorbents," *Chemical Engineering and Processing: Process Intensification,* vol. 47, no. 4, pp. 577-584, 2008.

[186] K. Engvall, H. Kusar, K. Sjöström, and L. J. Pettersson, "Upgrading of raw gas from biomass and waste gasification: challenges and opportunities," *Topics in catalysis,* vol. 54, no. 13-15, p. 949, 2011.

[187] R. Sadegh-Vaziri, M. Amovic, R. Ljunggren, and K. Engvall, "A Medium-Scale 50 MWfuel Biomass Gasification Based Bio-SNG Plant: A Developed Gas Cleaning Process," *Energies*, vol. 8, no. 6, pp. 5287-5302, 2015.

[188] W. Saw, H. McKinnon, I. Gilmour, and S. Pang, "Production of hydrogen-rich syngas from steam gasification of blend of biosolids and wood using a dual fluidised bed gasifier," *Fuel*, vol. 93, pp. 473-478, 2012.

3 Equipment and Materials for H_2S and NH_3 Removal

This chapter will firstly introduce the selected hot catalytic clean-up methods, sorbent and catalyst for H_2S and NH_3 removal in the producer gas from biomass gasification. Then equipment setup and gas sampling and analysis methods will be described. Finally, experimental procedures will be presented. Thus, the chosen sorbent will be applied in Chapter 4 for the examination of H_2S adsorption, and the selected catalyst will be used in Chapter 5 and 6 for the investigation of NH_3 removal. The equipment system will be utilized for both of the H_2S and NH_3 removal in Chapter 4, 5, and 6.

3.1 Introduction

3.1.1 Hot catalytic clean-up method

As the discussion in Chapter 2, hot/thermal catalytic clean-up method has been selected for removing H_2S and NH_3 in the producer gas from biomass gasification. Although some physical methods, such as wet scrubbers, can be used to reduce the H_2S and NH_3 in the biomass producer gas, the removal efficiency of these methods is relatively low. Furthermore, environmental issue posted by the waste solvent disposal is a serious concern. However, hot catalytic clean-up technology has advantages of removing H_2S and NH_3 efficiently and potential of transforming contaminants into useful products. In previous studies of this research group, a lab-scale fluidized bed reactor has been designed and constructed by Hongrapipat which has shown flexibility and suitability for removing H_2S and NH_3 in Ar gas effectively [1]. Therefore, this hot catalytic system has been improved and modified in this research, and thus used to further investigate the removal of H_2S and NH_3 from various gases. Detailed information of this fluidized bed reactor will be described in Section 3.2 of this chapter.

3.1.2 Sorbent selected for H_2S adsorption

From the literature review in Section 2.2.3 of Chapter 2, metal oxide sorbents are normally used in the catalytic desulfurization process, which include iron oxides [2-5] and zinc oxides [6-8]. Expensive sorbents have also been reported for H_2S removal which are copper oxides [9-11], manganese oxides [12, 13] and cerium oxides [14-17]. Criteria for selection of suitable sorbents for H_2S adsorption include the requirement of Fischer-Tropsch (FT) synthesis process (H_2S concentration <1ppmv), H_2S concentration in the raw producer gas, conversion efficiency, cost and issues of industrial application of the sorbents. Based on these selection criteria, a Fe-based sand in natural form, named titanomagnetite, was selected in this research for H_2S adsorption due to its abundance in New Zealand, low price, and high efficiency for H_2S removal in Ar gas (almost 100% at 500°C) [1, 18]. Furthermore, although it was found by Hongrapipat that the reduced titanomagnetite had lower efficiency for H_2S adsorption in simulated biomass producer gas than in Ar gas at both 500 and 800°C [1], the author only used reduced titanomagnetite in her study. However, it was reported that the oxidized form of iron sorbents have better performance for H_2S adsorption than the reduced form [19-21]. Therefore, both reduced and un-processed titanomagnetites were experimentally investigated in this research to compare their performance differences and suitability for H_2S removal. In addition, the most effective temperatures and the mechanisms for H_2S removal in biomass producer gas were also explored.

3.1.3 Catalysts selected for NH_3 decomposition

As the discussion presented in section 2.3 of Chapter 2, both Fe-based catalysts and Ni-based catalysts have shown high efficiency for NH_3 removal in the biomass producer gas. Titanomagnetite has been found to be capable of NH_3 removal in Ar gas with high efficiency

(almost 100% when the temperature was higher than 700°C). In addition, it is cheap and widely available in New Zealand [1, 18]. Therefore, it is the primary choice for NH_3 removal from the biomass producer gas of this research.

In a similar way to the H_2S removal, this study will investigate the differences between H_2-reduced and unprocessed titanomagnetites, find out the effective operation temperatures and explore the mechanisms for the NH_3 removal by using the two different types of titanomagnetite.

3.1.4 Characterization of titanomagnetite

For investigation the performance of titanomagnetite for removal of H_2S and NH_3 in the producer gas from biomass gasification, analysis of its relevant characteristics is important. The titanomagnetite sand composition was measured using X-ray fluorescence (XRF) and the results show it consists of 86.2 wt.% Fe_2O_3, 7.4 wt.% TiO_2, 3.5 wt.% Al_2O_3, 2.7 wt.% MgO and 1.7 wt.% SiO_2. The BET surface area, BJH, as well as sorption cumulative pore volume and average pore diameter of the titanomagnetite were also measured which values are, respectively, 1.1 m^2/g, 0.002 cm^3/g and 10.6 nm [1]. Particle density and bulk density of the titanomagnetite were provided by the supplier as 4540 and 2810 kg/m^3, respectively. Other properties of the titanomagnetite can be found elsewhere [18].

3.2 Hot catalytic clean-up system in this research

The reactor for removal of H_2S and NH_3 to be used in this study is a lab scale bubbling fluidised bed (BFB) reactor which has the advantages of uniform mixing solids and gases, enhanced heat and mass transfer between gases and solids, and uniform temperature distribution in the reactor. This reactor was designed and constructed by Hongrapipat previously for H_2S and NH_3 removal in Ar gas [1]. For avoiding reactions between the equipment inner materials and NH_3/H_2S, the hot

catalytic reactor and gas outlet pipe were made of fused quartz; gas flow meters and a flame arrester used at room temperature were made of glass and stainless steel, which were impossible to react with NH_3 and H_2S; and the other components were constructed by Perfluoroalkoxy (PFA) material [1].

In this study, the reactor system was modified by adjusting the positions of ABB rotameters, adding instrumentations, and improving the gas sampling system for solving some issues and for improving the performance of the system, which will be described later in this section. The schematic diagram of the modified system is shown in Figure 3.1 and its pictures are given in Figure 3.2. The system can be divided into four parts: 1). gas supply; 2). reactor and heat supply furnace; 3). gas sampling system and gas analysis instrument (micro-GC); and 4). gas extraction system.

The gas supply part includes a series of gas bottles for different gases and gas mixtures, gas pipelines, pressure sensors, rotameters, valves, a mass flow controller and a gas mixer. The reactor and heat supply furnace part includes a quartz tube reactor, a three-zone heating tube furnace, and a temperature controller and monitor. A vertical quartz tube reactor placed in the centre of the furnace was the key part of the system used for H_2S/NH_3 removal. The reactor was 40 mm for inner diameter, 46 mm for the outer diameter and 1020 mm for length [1]. The sorbent/catalyst was distributed on a porous quartz frit at the position of 580 mm above the bottom of the reactor. For a clear view, the schematic diagram of the quartz tube reactor is shown in Figure 3.3. A Lenton tube furnace was used to heat up the reactor which can be operated up to 1150°C [1]. The inside temperature of the reactor was measured by two sets of K-type thermocouples which were placed at different heights and radial positions. The previous study confirmed that the temperature

difference along the reactor height was less than 2°C, which showed high level of uniformity of this reactor [1].

The gas sampling system includes a gas sampling train as to be described in Section 3.4.3 of this chapter, and the gas was analysed by using a micro-Gas Chromatography (micro-GC) which will be described in Section 3.5 of this chapter. The gas extraction system is comprised of an afterburner and fume hoods. More detailed information about the hot catalytic gas clean-up system is available elsewhere [1].

In this study, the system was firstly assessed on its performance and then modified accordingly. The aims of these modifications were to control the gas flow rates more accurately, to enable for testing more gases and gas mixtures, and to add pressure sensors. These modifications are indicated in Figure 3.1 as numbered in the red rectangles from (1) to (6). In red rectangle (1) of Figure 3.1, an ABB rotameter was moved from before to after the check valve, and further down on the line a pressure sensor was added, which is shown in red rectangle (2) of Figure 3.1. These two modifications applied to all of the gases and gas mixtures except for the LPG. The adjustments were to measure the gas pressures more appropriately and accurately which are required for gas flow rate calculations by the ABB software (CAL-AP3). In red rectangle (3) of Figure 3.1, a specified Alicat scientific mass flow controller was added on the gas mixture lines to precisely control the gas flow rates of simulated gas and mixture of Ar, CO, CO_2 and CH_4. In red rectangle (4) of Figure 3.1, a removable steam generation system was added to inject steam into the test gas when steam was required in the experiment. In the steam supply system, a syringe pump was used for accurately controlling the water flow rate (very low value), and then a micro steam generator was used for steam generation when needed. In red rectangle (5) of Figure 3.1, top of the quartz tube reactor was filled with quartz wool before each experiment, which served as a filter to prevent

the fine particulates from flying out of the reactor. In red rectangle (6) of Figure 3.1, a liquid condenser in an ice bath was added to the gas sampling system to condense the vapour produced from the reactor during the experiments. By using this improvement, vapour produced from the reactor can be condensed, collected and analysed. Additionally, this careful design of condensate collection could prevent absorption of NH_3 or H_2S in the gas, and thus concentrations of NH_3 and H_2S were not affected.

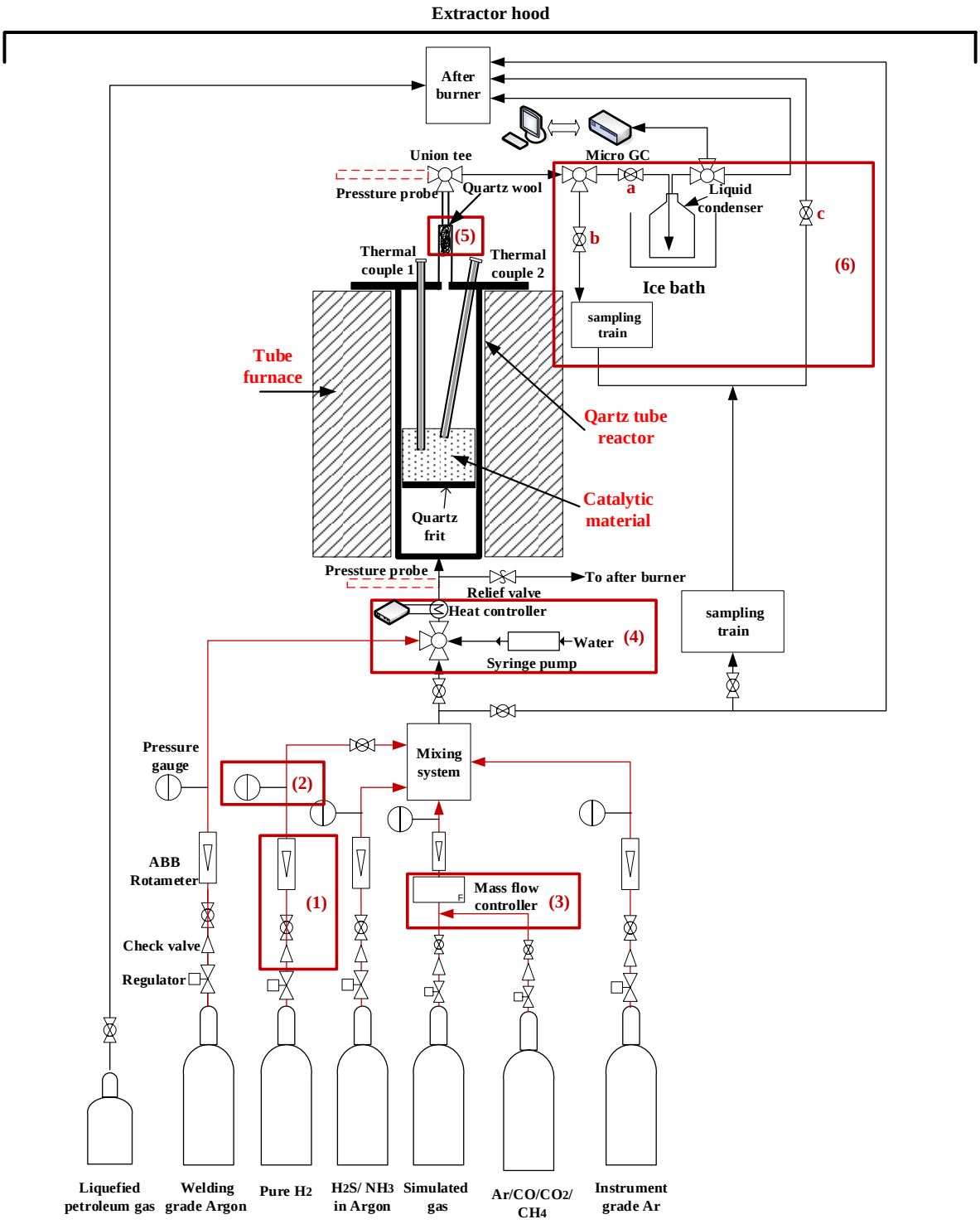

Figure 3.1 The hot catalytic gas cleaning system for H_2S/NH_3 removal. The highlighted rectangles and corresponding numbers indicate improvements in this study.

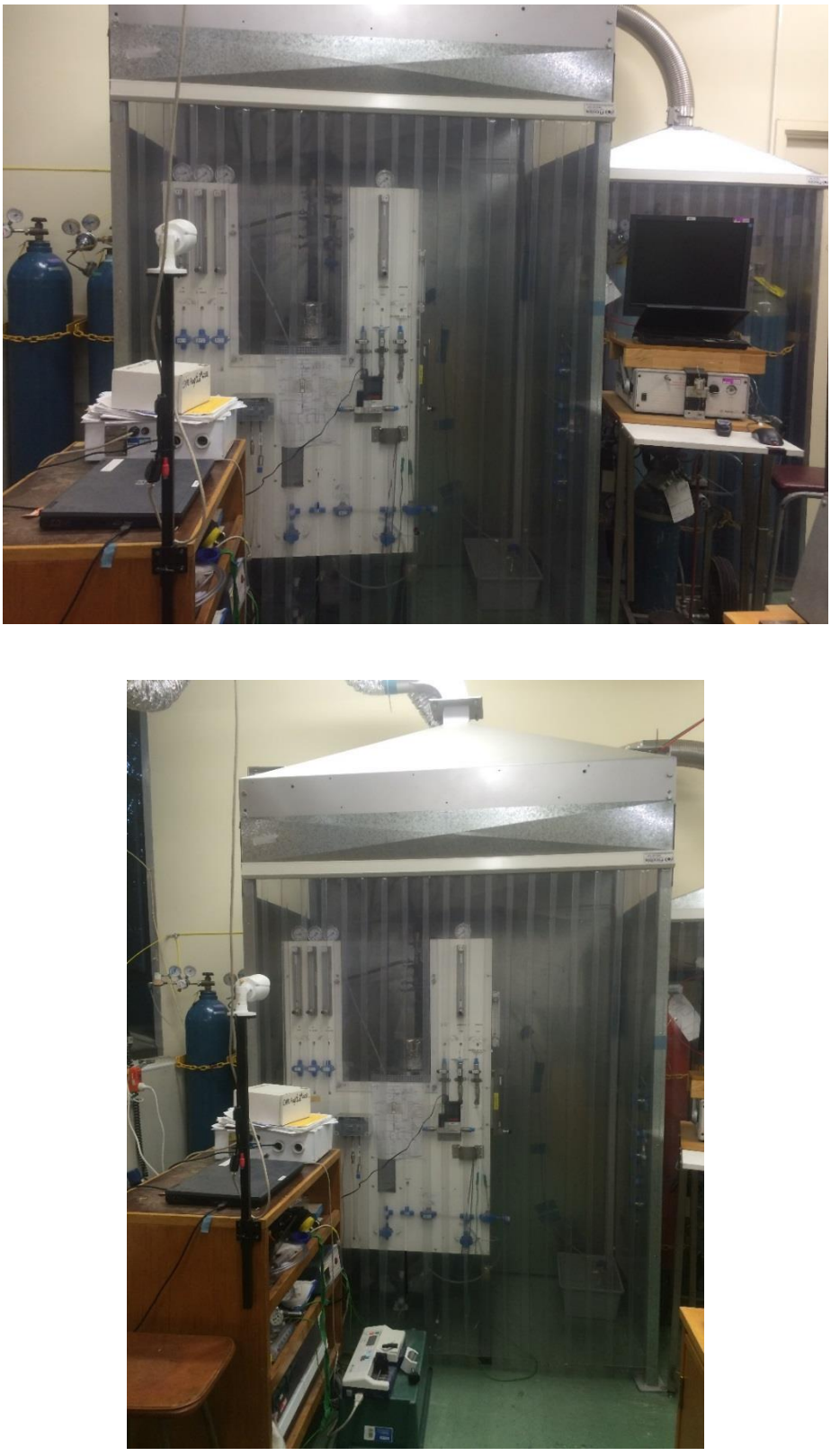

Figure 3.2 Pictures of the hot catalytic system.

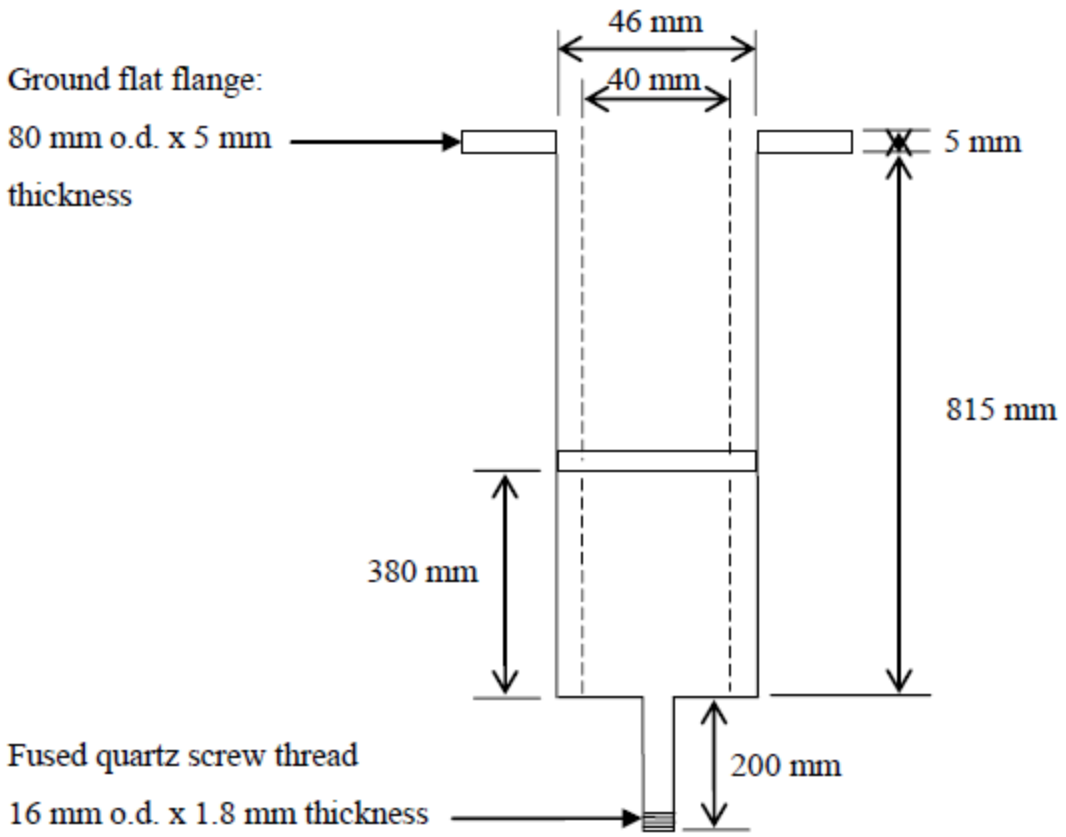

Figure 3.3 Schematic diagram of the quartz tube reactor [1].

3.3 Feed gas flow rate, H_2S and NH_3 concentrations in this research

3.3.1 Feed gas flow rate

Appropriate operation of the bubbling fluidised reactor requires the gas velocity to be higher than the minimum bubbling velocity (u_{mb}) but lower than the terminal velocity (u_t). u_{mb} is the gas velocity at which bubbling fluidization firstly occurs [1, 22], whereas u_t is the gas velocity at which the bed particles start to be carried out of the reactor [1, 22]. u_{mb} and u_t are strongly dependent on the sphericity, density and particle size of the bed material [1]. Based on the Geldart classification of particles [1, 23], titanomagnetite particle used in this study belongs to group B particles, for

which u_{mb} is equal to minimum fluidization velocity (u_{mf}) at which the bed particles start to fluidise [1, 22]. u_{mf} and u_t can be calculated using the following equations and properties of gases and solids as listed in Table 3.1 [1]. As the introduction in Hongrapipat's thesis [1], u_{mf} can be calculated by Eqs. (3.1), (3.2) and (3.3), whereas, u_t can be determined by Eqs. (3.4), (3.5) and (3.6).

$$\frac{1.75}{\varepsilon_{mf}^3 \cdot \phi_s} \cdot Re_{p,mf}^2 + \frac{150 \cdot (1-\varepsilon_{mf})}{\varepsilon_{mf}^3 \cdot \phi_s^2} \cdot Re_{p,mf} = Ar \tag{3.1}$$

$$Re_{p,mf} = \frac{d_p \cdot u_{mf} \cdot \rho_g}{\mu} \tag{3.2}$$

$$Ar = \frac{d_p^3 \cdot \rho_g \cdot (\rho_s - \rho_g) \cdot g}{\mu^2} \tag{3.3}$$

$$d_p^* = d_p \cdot \left[\frac{\rho_g \cdot (\rho_s - \rho_g) \cdot g}{\mu^2} \right]^{1/3} = Ar^{1/3} \tag{3.4}$$

$$u_t^* = \left[\frac{18}{(d_p^*)^2} + \frac{2.335 - 1.744 \cdot \phi_s}{(d_p^*)^{0.5}} \right]^{-1}, \quad 0.5 < \varphi_s < 1 \tag{3.5}$$

$$u_t = u_t^* \left[\frac{\mu \cdot (\rho_s - \rho_g) \cdot g}{\rho_g^2} \right]^{1/3} \tag{3.6}$$

Where,

ε_{mf} is the voidage of particle;

ϕ_s is the sphericity of particle;

$Re_{p,mf}$ is the particle Reynolds number at minimum fluidization;

Ar is the Archimedes number, dimensionless;

d_p is the particle diameter, m;

ρ_g is the gas density, kg/m^3;

ρ_s is the particle density, kg/m^3;

μ is the gas viscosity, kg/(m·s);

g is the acceleration of gravity, m/s^2;

d_p^* is the dimensionless particle size, m;

u_t^* is the dimensionless gas terminal velocity, m/s.

Table 3.2 shows the calculated results of u_{mf} and u_t for different gases by using titanomagnetite as sorbent/catalyst at 500°C, and 1 bar. u_{01} and u_{02} are the gas velocities for gas flow rates of 3.4 and 3.65 L/min, respectively. It is observed that u_{01} and u_{02} are both between u_{mf} and u_t, which confirms that the operation conditions were bubbling fluidization when gas flowrates of 3.4 and 3.65 L/min were used. The calculation details for the u_{mf} and u_t of Ar, H_2, CO, CO_2, and CH_4 gases can be found in Appendix A.

Table 3.1 Parameters used for u_{mf} and u_t calculation by using titanomagnetite as sorbent/catalyst [1].

Properties of gas	**Affecting factors**
Gas density (ρ_g), kg/m^3	Depend on the gas type, temperature and pressure
Gas viscosity (μ), kg/(m·s)	Depend on the gas type, temperature and pressure
Properties of particle	**Input values**
Particle	Titanomagnetite
Particle density (ρ_s), kg/m^3	4540
Sphericity of particle (ϕ_s)	0.86
Particle diameter (d_p), m	180×10^{-6}-250×10^{-6} (average particle diameter will be used for the calculations)
Voidage (ε_{mf})	0.44
Other parameters and constants	**Input values**
Quartz tube reactor inner diameter (d_t), m	0.04
Bed cross-sectional area (A_t), m^2	0.00126
Acceleration of gravity (g), m/s^2	9.8

Table 3.2 u_{mf} and u_t for different gases by using titanomagnetite as sorbent/catalyst (500°C, 1 bar).

Gas type	Gas flowrate 1 (L/min)	Gas flowrate 2 (L/min)	ρ_g (kg/m^3)	$\mu \times 10^5$ (kg/(m·s))	u_{mf} (m/s)	u_{01} (m/s)	u_{02} (m/s)	u_t (m/s)
Ar	3.4	3.65	0.6303	4.64	0.033	0.128	0.137	1.611
H_2			0.0318	1.69	0.091			5.100
CO			0.2532	3.56	0.043			2.235
CO_2			0.6985	3.42	0.045			1.905
CH_4			0.4416	2.33	0.066			2.608

3.3.2 H_2S and NH_3 concentrations in the feed gas

As reviewed in Chapter 2, the H_2S concentrations in producer gas from gasification of woody biomass are in the range of 20-230 ppmv [1, 24-28], and the NH_3 concentrations are 2300 ppmv or lower [29-33]. Therefore, H_2S concentration of 230 ppmv and NH_3 concentration of 2300 ppmv were considered as the worst cases and selected in this study for investigation. However, due to the safety concerns, only certified gas compositions of 5 vol.% H_2S in Ar gas and 50 vol.% NH_3 in Ar gas were supplied by a commercial company, BOC in Australia [1]. Hence, H_2S concentration of 230 ppmv or NH_3 concentration of 2300 ppmv in the feed gas was achieved by adjusted flow rate of the gas mixture of 5 vol.% H_2S in Ar gas or that of the gas mixture of 50 vol.% NH_3 in Ar gas into the feed gas.

It should be pointed out that the H_2S removal experiments in Chapter 4 were conducted before the Alicat scientific mass flow controller installed to the system, and all of the gas flow rates in these experiments were adjusted by the ABB rotameters.

The 230 ppmv H_2S in the feed gas was obtained by feeding the gas mixture of 5 vol.% H_2S in Ar gas at the flow rate of 0.017 L/min into the test feeding gas at the flow rate of 3.65 L/min. The levels of two separate ABB rotameters' floats were determined based on the ABB software (CAL-AP3) to achieve the required flowrates. However, after the more accurate and reliable Alicat mass flow controller was installed to the experimental system, the feed gas flow rates used for the previous H_2S removal experiments were checked and it was found the actual feed gas flow rates were 3.4±0.1 L/min instead of 3.65 L/min as targeted. Therefore, in result analysis of this part of study, feed gas flow rate of 3.4±0.1 L/min have been used and will be reported in Chapter 4. This results in H_2S concentration of 240±20 ppmv (rather than 230 ppmv) which was further verified by a separate Ion Selective Electrode (ISE) method which will be discussed in Section 3.4 of this chapter.

In Chapters 5 and 6, to achieve the target NH_3 concentration (2300 ppmv) in the test gases, the flow rates of test gases were reliably controlled as 3.65 L/min by the Alicat mass flow controller if the test gas was supplied from one gas bottle, or by Alicat mass flow controller and ABB rotameters with adjustment if the test gas was a mixture from different gas bottles. The flow rate of NH_3 and Ar mixture (50 vol% NH_3 in Ar gas) was set at 0.017 L/min and controlled by an ABB rotameter. The NH_3 concentrations in the tested gases were measured by ISE method which the results were 2300±200 ppmv and reported in this work.

3.4 H_2S and NH_3 sampling and analysis

3.4.1 Methodology for analysis of H_2S in a gas or a gas mixture

There are three methods available for analysis of H_2S in a gas or a gas mixture, namely GC method [34], ISE method [18] and iodometric titration method [35]. GC with suitable detector columns can directly analyse the H_2S concentration in the gas. However, the micro-GC available in our lab cannot examine the H_2S concentration directly. Furthermore, considering the low concentration of H_2S in the gases (230 ppmv) and the complexity of the tested gases, GC method was not selected in this research. ISE and iodometric titration methods are operated to analyse the solution with sulphur ion (S^{2-}) which is available by impinging the H_2S-containing gas into the solution or through contacting of the H_2S-containing gas with the solution. The ISE method was selected in this research because there is a sulphide ISE available in our lab and this method also has the advantages of high sensitivity and simple operation. By using ISE method, the S^{2-} concentration in the solution can be easily determined by the electrode potential (mV scale) on a pH meter. In addition, it has been found that this method had high sensitivity and consistency for testing 230 ppmv H_2S in Ar gas [1]. The gas sampling method and ISE analysis will be introduced in Sections 3.4.3 and 3.4.4 and was applied in Chapter 4 for determining the H_2S concentrations in all the test gases.

3.4.2 Methodology for analysis of NH_3 in a gas or a gas mixture

For the determination of the low concentration of NH_3 in the gas, GC method [36, 37], ISE method [18], UV-VIS spectrophotometer method [38], and photometry method [35], can be used. Again, considering the low concentration of NH_3 in the gases ($\leq$ 2300 ppmv) and the complexity of the tested gases in this research (especially H_2 in the gases), GC method was not selected for the

analysis of NH_3 concentration. Moreover, due to the advantages of ISE method as mentioned for the H_2S analysis, this method was selected in this research for analysing the concentration of NH_3 in different gases. In addition, it has been proven by Hongrapipat [1] that the NH_3 concentration in Ar gas tested by ISE method was highly consistent with the results tested by a micro-GC. The sampling method and the ISE analysis will be introduced in Sections 3.4.3 and 3.4.5 which were applied in Chapter 5 and Chapter 6 for analysing the NH_3 concentrations in different gas mixtures.

3.4.3 Methodology for gas sampling

When ISE method was used for analysing the H_2S and NH_3 concentrations in the test gases, suitable gas sampling system should be developed for absorbing the H_2S and NH_3 in the tested gases. In the thesis of Hongrapipat [1], 0.05M H_2SO_4 solution was found to be suitable for sampling of 2000 ppmv NH_3 in Ar gas, and 0.05M NaOH solution was suitable for sampling of the 230 ppmv H_2S also in Ar gas, respectively. Therefore, 0.05M of NaOH solution will be used for H_2S absorption and 0.05M H_2SO_4 solution will be used for NH_3 absorption in this study. Feed gas flow rate, and H_2S and NH_3 concentrations in the feed gases have been discussed in the above Sections 3.3.1 and 3.3.2. Accordingly, volumes of the 0.05M NaOH and 0.05M H_2SO_4 solutions in the sampling train were trialled and determined in this study for sufficiently absorbing H_2S and NH_3 in the test gases.

Firstly, two 250 mL Scott gas washing bottles containing 200 mL 0.05M NaOH solution in each bottle were employed as sampling train for trapping 240 ppmv H_2S in the 3.4 L/min Ar gas for 6 min, and the sampling train was in the ice water bath during the test. The outlet gas after the second sampling bottle was collected by a gas bag and analysed by an AreaRAE Steel Z1 H_2S detector under the fume hood. H_2S gas was analysed by the H_2S detector which proved that the sampling

train was insufficient for trapping all H_2S in the gas. Afterwards, three 250 mL Scott gas washing bottles containing 200 mL 0.05M NaOH solution in each bottle were tested using the above method and H_2S was found in the outlet gas of the third sampling bottle again. Finally, a 900 mL Scott gas washing bottle containing 800 mL 0.05M NaOH solution was used for the H_2S containing gas sampling and, in this case, no more H_2S was detected after the sampling bottle by the H_2S detector even after 6 min. Therefore, a 900 mL Scott gas washing bottle containing 800 mL 0.05M NaOH solution as shown in Figure 3.4 was used as the first bubbler which was followed by a 2000 mL Scott gas washing bottle containing 1600 mL 0.05M NaOH solution as the second bubbler for sampling H_2S (240 ppmv) containing test gases. Each sampling run lasted for 4 or 6 min, from which only the solution in the first bubbler was analysed for determination of H_2S concentration in the test gas.

The second bubbler with 1600 mL 0.05M NaOH solution was added to the impinging system because it could ensure that any escaped H_2S from the first bubbler be captured to resolve safety concerns. Since there was almost no H_2S escaped from the first bubbler, the second bubbler has been used for the whole period of experiment (3-5 hours) without the need to replace the solution inside. After the whole period of experiment, the solution in the second bubbler was tested by the ISE analytical method and the quantity of S^{2-} was found to be insignificant which corresponded to approximately 1 ppmv of H_2S in the test gas. This has been included in analysis of test error.

Similarly, the impinging system of two bubblers with 800 mL 0.05M H_2SO_4 solution in the first bubbler followed by the second bubbler with 1600 mL 0.05M H_2SO_4 solution was tested for sampling of NH_3 at a concentration of 2300 ppmv in Ar gas with the gas flow rate of 3.65 L/min. After sampling for 6 min, no NH_3 was detected out in the outlet gas of the first bubbler by a ToxiRAE Pro detector. Therefore, the impinging system of two bubblers with 800 mL 0.05M

H_2SO_4 solution in the first bubbler and 1600 mL 0.05M H_2SO_4 solution in the second bubbler was used for sampling NH_3 (2300 ppmv) containing test gases in this research, and it is shown in Figure 3.5. Similarly, the solution in the second bubbler was also analysed at the end of each experiment, and it was found that only approximately 1 ppmv equivalent NH_3 was trapped in the second bubbler which was, again, considered in the experimental error analysis.

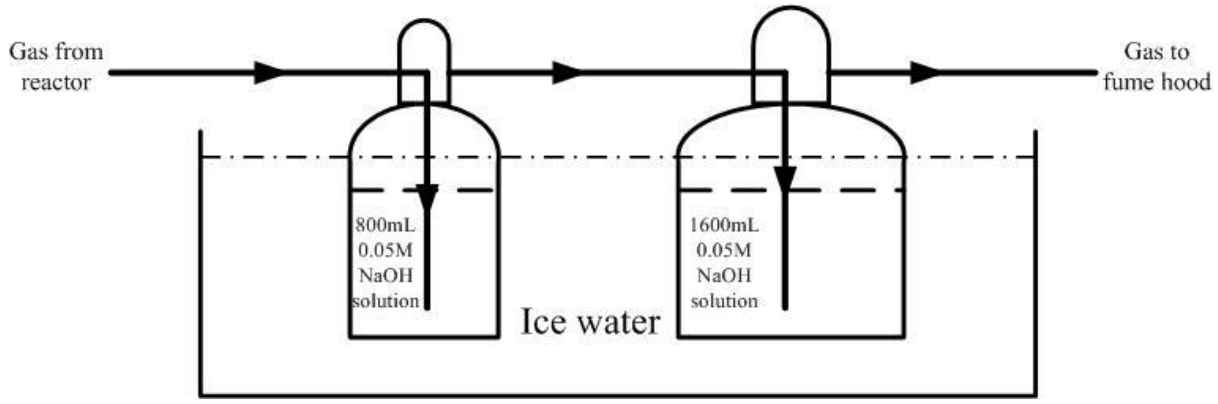

Figure 3.4 Impinging system of two bubblers for H_2S sampling with 800 mL 0.05M NaOH solution in the first bubbler and 1600 mL 0.05M NaOH solution in the second bubbler.

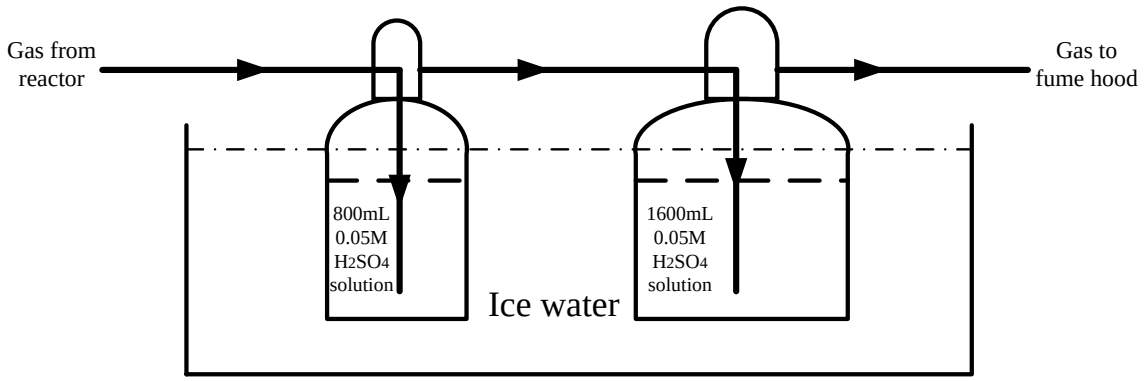

Figure 3.5 Two bubblers impinging system for NH_3 sampling with 800 mL 0.05M H_2SO_4 solution in the first bubbler and 1600 mL 0.05M H_2SO_4 solution in the second bubbler.

3.4.4 Gas analysis and calculation for H_2S adsorption

The sampled solutions (0.05M NaOH) with sulphur ions in the first bubblers from the above impinging method were analysed by a silver/sulphide ISE (Cat. No. 9616BNWP) according to the ASTM D 4658-09 standard [39]. More detailed introduction of the analysis method is also available elsewhere [1]. The concentration of H_2S in the gas (C_{H_2S}) was calculated by Eq. (3.7). The conversion of H_2S (λ) through the removal process was then calculated from the inlet and the outlet H_2S concentrations by using Eq. (3.8). To verify the analysis method (ISE) used in this study, a separate method of Dräger tubes was also employed. As expected, the discrepancies between these two methods were within ±5%, which proved that both methods are applicable for the analysis.

$$C_{H_2S} = \frac{\frac{C_{solution} \times V}{M_s} \times R \times T}{P_{system} \times F \times t} \times 10^6 \quad (3.7)$$

$$\lambda = \frac{C_{(Inlet\ H_2S)} - C_{(Outlet\ H_2S)}}{C_{(Inlet\ H_2S)}} \times 100\% \quad (3.8)$$

Where:

C_{H_2S} is the concentration of H_2S in the gas, ppmv;

$C_{(Inlet\ H2S)}$ is the H_2S concentration in the inlet gas, ppmv;

$C_{(Outlet\ H2S)}$ is the H_2S concentration in the outlet gas, ppmv;

$C_{solution}$ is the concentration of ion sulphur in the sampling solution, which was tested by ISE, $g \cdot L^{-1}$;

V is the volume of 0.05M sodium hydroxide solution in the first bubbler, 0.8 L;

M_S is the molecular weight of sulphur, 32.06 g/mol.

R is gas constant, 8.314 J·K-1mol^{-1};

T is the temperature of gas, K;

P_{system} is the absolute pressure in the system, Pa;

F is the flowrate of the gas, m^3/min;

t is the time for sampling, min;

3.4.5 Gas analysis and calculation for NH_3 decomposition

The impinged solutions (0.05M H_2SO_4) with NH_3 in the first bubblers, which was described in Section 3.4.3, were analysed by a high-performance ammonia ISE (Cat. No. 9512HPBNWP) according to the standard test method of ASTM D1426-08 [40]. A detailed description of this method can also be found elsewhere [1]. The concentration of NH_3 in the gas (C_{NH_3}) was calculated by Eq. (3.9), and the conversion of NH_3 (η) was calculated from the inlet and outlet NH_3 concentrations using Eq. (3.10). To verify the analysis method (ISE) used in this study, a separate method of Dräger tubes was also utilized in the experiments by using Ar as the feed gas. The discrepancies between these two methods were also found low within ±5%, which proved that both methods are applicable for the analysis.

$$C_{NH_3} = \frac{\frac{C_{solution} \times V}{M_N} \times R \times T}{P \times F \times t} \times 10^6 \qquad (3.9)$$

$$\eta = \frac{C_{(Inlet\ NH_3)} - C_{(Outlet\ NH_3)}}{C_{(Inlet\ NH_3)}} \times 100\% \quad (3.10)$$

Where:

C_{NH_3} is the NH_3 concentration in the gas, ppmv;

$C_{(Inlet\ NH3)}$ is the NH_3 concentration in the inlet gas, ppmv;

$C_{(Outlet\ NH3)}$ is the NH_3 concentration in the outlet gas, ppmv;

$C_{solution}$ is the concentration of NH_3 in the sampling solution, which was tested by the ISE, g N in NH_3 /L;

V is the volume of 0.05M H_2SO_4 solution in the first bottle, 0.8L;

M_N is the molecular weight of nitrogen, 14 g/mol;

R is the gas constant, 8.314 $J \cdot K^{-1} \cdot mol^{-1}$;

T is the standard temperature, 273.15 K;

P is the standard pressure, 100000 Pa;

F is the standard flowrate of the gas, m^3/min;

t is the time for gas sampling, min.

3.5 Gas analysis by micro-GC

The major gas species in the producer gas including H_2, CO, CO_2, CH_4 and other minor gas components (N_2 and O_2) were analysed by an Agilent 3000 micro-GC in this research which is shown in Figure 3.6. More detailed information about the columns utilized in the micro-GC can

be found elsewhere [1]. Calibrations of the micro-GC for the above gases were performed by diluting each of the gases in Ar gas to different concentrations which were achieved by accurately controlling the gas flow rates of the interested gas and Ar gas by Alicat mass flow controllers. The calibration curves for the above six gases are given in Figures 3.7 to 3.9 as follows.

Figure 3.6 Agilent 3000 micro-GC system.

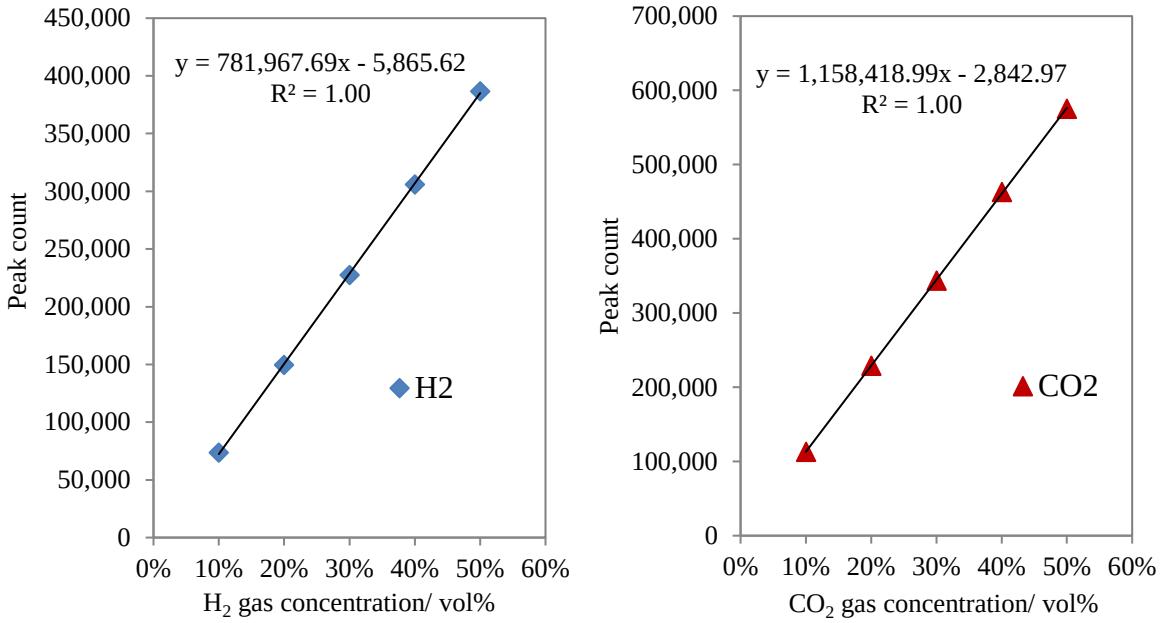

Figure 3.7 Calibration curves for H_2 and CO_2 gases.

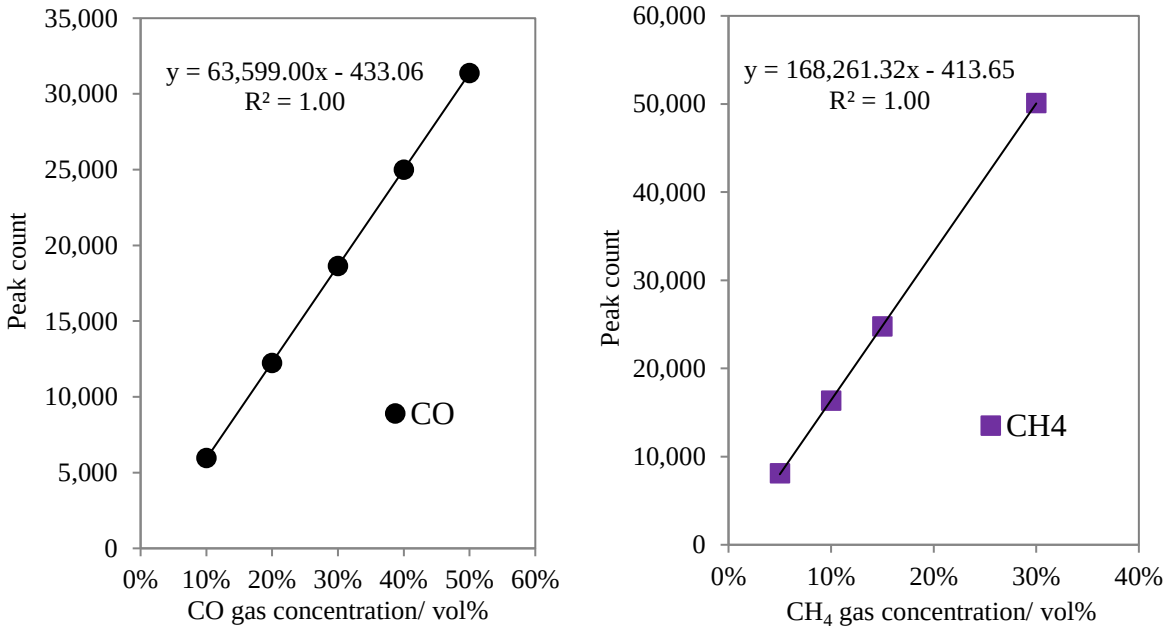

Figure 3.8 Calibration curves for CO and CH_4 gases.

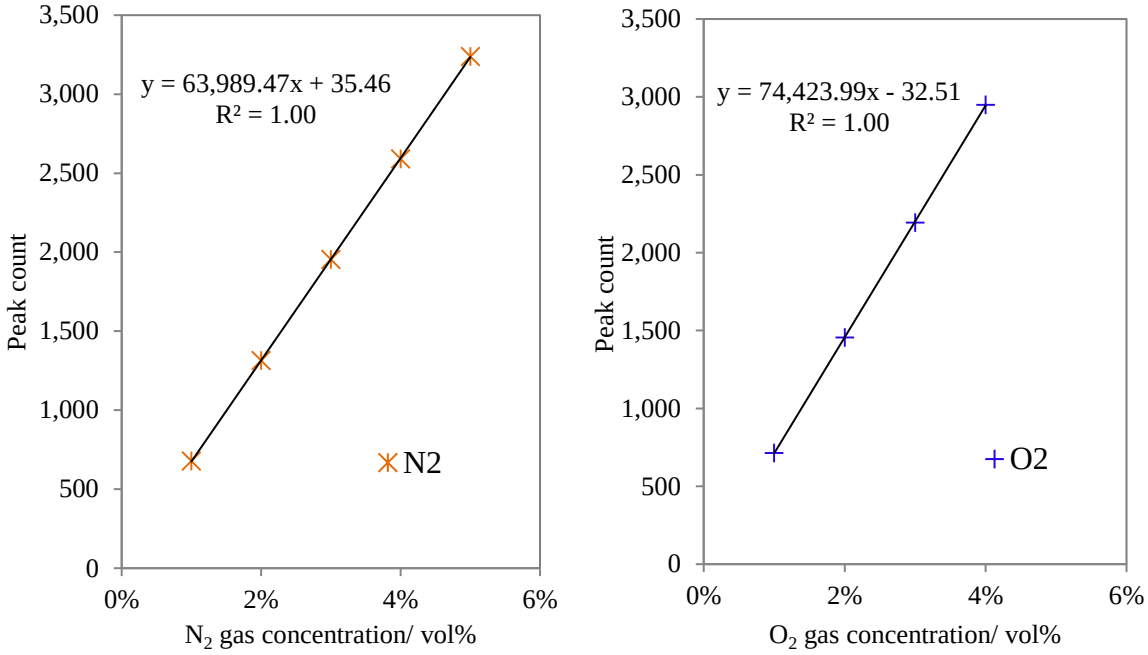

Figure 3.9 Calibration curves for N_2 and O_2 gases.

3.6 Experimental procedures

In brief, the complete experimental procedures for H_2S/NH_3 removal can be divided into six phases. 1). Material preparation and experimental system setup; 2). Reactor heat-up and/or H_2 reduction; 3) H_2S/NH_3 removal process; 4) System shutdown; 5) Sampling solution analysis; 6) Reactor cleaning. Description of each phase is given as below.

(1) Material preparation and experimental system setup

Before each experimental run, sufficient sampling bubblers with the suitable impinging solution are prepared and stored in the refrigerator. For example, if the experiment lasts for 4 hours for H_2S removal, at least eleven 900 mL-bubblers with 800 mL of 0.05M NaOH solution in each and one 2000 mL-bubbler with 1600 mL of 0.05M NaOH solution should be prepared. Three of those

eleven 900 mL-bubblers are used for inlet gas samplings and the left eight are used for eight times of outlet gas samplings (approximately 30 min interval).

After the titanomagnetite sand being received, the titanomagnetite is sieved to particle size range of 180-250 μm and the particles selected in this size range are then dried in an oven at 105°C for 2 hours. After these pre-treatments, 100g dried titanomagnetite is directly applied to the quartz tube reactor as shown in Figure 3.1 and the bed depth at static state is 28.3 mm. The equipment fittings and connections are then put together, after which any possibility of system leakage is checked by applying soap bubbles on each pipeline connection with 3.65 L/min Ar gas flowing through the pipelines and reactor. If the unprocessed titanomagnetite is the required as a sorbent/catalyst for the experiment, thus reactor will be heated up to the target temperature and followed by H_2S/NH_3 removal process (see the information in phase (2) and (3)). However, if the reduced titanomagnetite is used for the experiment, H_2 reduction process will be conducted firstly (see the information in phase (2)).

(2) Reactor heat up and/or H_2 reduction

For the heating process, instrumental grade Ar gas (0.5 L/min) is first introduced to the reactor to purge air out of the system and the outlet gas is tested by the micro-GC to monitor the O_2 concentration. Once there is no O_2 found in the outlet gas, the reactor is started to be heated up with the temperature ramping rate of 10 °C/min until the target temperature is reached.

If the reduced titanomagnetite is required for the experiment, air in the reactor is purged out by instrumental grade Ar gas until there is no O_2 detected out by the micro-GC. Afterwards, the afterburner is ignited on and the Ar gas is switched off. Meanwhile, the gas mixture of 36.5 vol.% H_2 in Ar gas is obtained by setting Ar gas at 2.35 L/min and H_2 gas at 1.35 L/min and introduced

into the reactor. Next, the reactor is heated by a ramping rate of 10°C up to 810°C, which is maintained for 6 hours until titanomagnetite is reduced completely [1]. Since it is not allowed to conduct experiment overnight, the reduced titanomagnetite in the reactor is purged by instrumental grade Ar gas overnight and cooled down to the room temperature, thus used for H_2S/NH_3 removal experiment next day. The reactor will be heated up again to the target experimental temperature by following the reactor heat-up process.

(3) H_2S/NH_3 removal process

Just before the H_2S/NH_3 removal process, firstly, the CO monitor and H_2S/NH_3 detector are turned on near the reactor. Secondly, the micro-GC is turned on and connected to the system. Finally, the afterburner is flamed on. After these preparations, the H_2S/NH_3 removal is started.

The Ar gas used for reactor heat-up process is switched off (unless it is the test gas), and thus the test gas and H_2S/NH_3 containing gas with pre-set gas flow rates are switched on and introduced to the system. Almost at the same time, the micro-GC is started to inject and analyse the outlet gas online. Next, the outlet gas is sampled approximately every 30 min for once until the H_2S/NH_3 removal process is completed. When the H_2S/NH_3 process is finished, the test gas and H_2S/NH_3 containing gas are switched to the inlet gas sampling line (Figure 3.1) for inlet gas samplings. Meanwhile, the welding grade Ar gas is switched on and introduced to the reactor. After the last inlet gas sampling, the system is ready for shutdown. For the NH_3/H_2S concentrations analysis by Dräger tubes, the outlet/inlet gases are collected by gas bags which are tested by Dräger tubes under the fume hood.

(4) System shutdown

For the system shutdown, the furnace is turned off firstly. All of the gas bottles except the welding grade Ar gas bottle are switched off successively. However, micro-GC and afterburner are kept on until there is only Ar gas tested out by the micro-GC. Gas monitors are turned off after the micro-GC is shut down. During the whole H_2S/NH_3 removal process and reactor cooled down process, the temperature in the reactor is monitored and recorded automatically. The temperature monitor and welding grade Ar gas bottle is shut down until the temperature in the reactor is close to room temperature.

(5) Sampling solution analysis

After the last gas sampling is completed, the solution in the sampling bottles is started to be analysed by the ISE methods which can be found in Sections 3.4.4 and 3.4.5.

(6) Reactor cleaning

The quartz tube reactor is cleaned after each experimental run to remove any fine particle and residuals on the quartz frit and reactor wall. Firstly, the quartz frit is soaked by 80 mL fresh aqua regia solution (3 volume parts of concentrated hydrochloric acid (HCl) and 1 volume part of concentrated nitric acid (HNO_3) under a fume hood at room temperature for one day. Next, the reactor wall is carefully rinsed with the aqua regia a few of time, and thus the used aqua regia is discarded to a great amount of water which will be handled appropriately. Secondly, the reactor is rinsed with a great amount of water a few of times. Afterwards, approximately 40 mL of 35% of hydrogen peroxide (H_2O_2) solution and a suitable amount of potassium hydroxide (KOH) pellets are added to the reactor, which will be soaked for overnight. Thirdly, the H_2O_2 plus KOH solution is poured out of the reactor into a great amount of water, which is disposed of rightly. The reactor is flushed with a great amount of tap water and rinsed with deionized water (DI water) twice.

Finally, the wet reactor is dried by putting the tube reactor to the tube furnace at 130°C for 1-2 hours until the reactor is completely dry. Therefore, the dried and clean quartz tube reactor is ready for another experimental run.

3.7 Reference

[1] J. Hongrapipat, "Removal of NH_3 and H_2S from biomass gasification producer gas," Doctor of Philosophy, Chemical and Procees Engineering, University of Canterbury, Christchurch, New Zealand, 2014.

[2] H.-L. Fan, C.-H. Li, and C.-H. Li, "Testing of iron oxide sorbent for high-temperature coal gas desulfurization," *Energy sources,* vol. 27, no. 3, pp. 245-250, 2005.

[3] Y.-H. Lin, Y.-C. Chen, and H. Chu, "The mechanism of coal gas desulfurization by iron oxide sorbents," *Chemosphere,* vol. 121, pp. 62-67, 2015.

[4] C. Lin, W. Qin, and C. Dong, "H_2S adsorption and decomposition on the gradually reduced α-Fe_2O_3(001) surface: A DFT study," *Applied Surface Science,* vol. 387, pp. 720-731, 2016.

[5] B. Zeng *et al.*, "Desulfurization Behavior of Fe–Mn-Based Regenerable Sorbents for High-Temperature H_2S Removal," *Energy & Fuels,* vol. 29, no. 3, pp. 1860-1867, 2015.

[6] R. Zhang, J. Huang, J. Zhao, Z. Sun, and Y. Wang, "Sol-gel auto-combustion synthesis of zinc ferrite for moderate temperature desulfurization," *Energy & Fuels,* vol. 21, no. 5, pp. 2682-2687, 2007.

[7] V. Girard *et al.*, "Innovative low temperature regenerable zinc based mixed oxide sorbents for synthesis gas desulfurization," *Fuel,* vol. 140, pp. 453-461, 2015.

[8] M. Chomiak, J. Trawczyński, Z. Blok, and P. Babiński, "Monolithic Zn-Co-Ti based sorbents for hot syngas desulfurization," *Fuel Processing Technology,* vol. 144, pp. 64-70, 2016.

[9] A. Hachimi, L. Vilcocq, C. Courson, and A. Kiennemann, "Study of olivine supported copper sorbents performances in the desulfurization process in link with biomass gasification," *Fuel Processing Technology,* vol. 118, pp. 254-263, 2014.

[10] P. Dhage, A. Samokhvalov, M. L. McKee, E. C. Duin, and B. J. Tatarchuk, "Reactive adsorption of hydrogen sulfide by promoted sorbents Cu-ZnO/SiO_2: active sites by experiment and simulation," *Surface and interface analysis,* vol. 45, no. 5, pp. 865-872, 2013.

[11] D. Liu, W. Zhou, and J. Wu, "CuO-CeO_2/ZSM-5 composites for reactive adsorption of hydrogen sulphide at high temperature," *The Canadian Journal of Chemical Engineering,* vol. 9999, pp. 1-6, 2016.

[12] P. N. Bhandari, A. Kumar, D. D. Bellmer, and R. L. Huhnke, "Synthesis and evaluation of biochar-derived catalysts for removal of toluene (model tar) from biomass-generated producer gas," *Renewable Energy,* vol. 66, pp. 346-353, 2014.

[13] L. F. Guo, K. L. Pan, H. M. Lee, and M. B. Chang, "High-Temperature Gaseous H_2S Removal by Zn-Mn-based Sorbent," *Industrial & Engineering Chemistry Research,* vol. 54, no. 44, pp. 11040-11047, 2015.

[14] Z. Wang and M. Flytzani-Stephanopoulos, "Cerium oxide-based sorbents for regenerative hot reformate gas desulfurization," *Energy & fuels*, vol. 19, no. 5, pp. 2089-2097, 2005.

[15] M. Flytzani-Stephanopoulos, M. Sakbodin, and Z. Wang, "Regenerative adsorption and removal of H_2S from hot fuel gas streams by rare earth oxides," *Science*, vol. 312, no. 5779, pp. 1508-1510, 2006.

[16] D. Liu, W. Zhou, and J. Wu, "CeO_2-MnOx/ZSM-5 sorbents for H_2S removal at high temperature," *Chemical Engineering Journal*, vol. 284, pp. 862-871, 2016.

[17] K. Svoboda *et al.*, "Thermodynamic Possibilities and Limits for Producer Gas Desulfurization and HCl Related Interferences for Zn, Mn, Ce and La Based Sorbents of Sulfur Compounds," in *Key Engineering Materials*, 2015, vol. 656, pp. 101-106: Trans Tech Publ.

[18] J. Hongrapipat, A. C. K. Yip, A. T. Marshall, W. L. Saw, and S. Pang, "Investigation of simultaneous removal of ammonia and hydrogen sulphide from producer gas in biomass gasification by titanomagnetite," *Fuel*, vol. 135, pp. 235-242, 2014.

[19] R. B. Slimane and J. Abbasian, "Utilization of metal oxide-containing waste materials for hot coal gas desulfurization," *Fuel Processing Technology*, vol. 70, no. 2, pp. 97-113, 2001.

[20] L. Reeve, "Desulphurization of coke oven gas at Appleby-Frodingham," *Journal of the Institute of Fuel*, vol. 31, pp. 319-324, 1958.

[21] J. Swisher and K. Schwerdtfeger, "Review of metals and binary oxides as sorbents for removing sulfur from coal-derived gases," *Journal of Materials Engineering and Performance*, vol. 1, no. 3, pp. 399-407, 1992.

[22] K. Daizo and O. Levenspiel, "Fluidization engineering," 1991.

[23] D. Geldart, "Types of gas fluidization," *Powder technology,* vol. 7, no. 5, pp. 285-292, 1973.

[24] W. Torres, S. S. Pansare, and J. G. Goodwin, "Hot Gas Removal of Tars, Ammonia, and Hydrogen Sulfide from Biomass Gasification Gas," *Catalysis Reviews,* vol. 49, no. 4, pp. 407-456, 2007.

[25] X. Meng, W. de Jong, R. Pal, and A. H. M. Verkooijen, "In bed and downstream hot gas desulphurization during solid fuel gasification: A review," *Fuel Processing Technology,* vol. 91, no. 8, pp. 964-981, 2010.

[26] M. Jazbec, K. Sendt, and B. S. Haynes, "Kinetic and thermodynamic analysis of the fate of sulphur compounds in gasification products," *Fuel,* vol. 83, no. 16, pp. 2133-2138, 2004.

[27] A. Van der Drift, J. Van Doorn, and J. Vermeulen, "Ten residual biomass fuels for circulating fluidized-bed gasification," *Biomass and Bioenergy,* vol. 20, no. 1, pp. 45-56, 2001.

[28] H. Boerrigter and R. Rauch, "Review of applications of gases from biomass gasification," *ECN Biomassa, Kolen en Milieuonderzoek,* vol. 20, 2006.

[29] J. Hongrapipat, W. L. Saw, and S. Pang, "Removal of ammonia from producer gas in biomass gasification: integration of gasification optimisation and hot catalytic gas cleaning," *Biomass Conversion and Biorefinery,* vol. 2, pp. 327-348, 2012.

[30] J. Corella, J. M. Toledo, and R. Padilla, "Olivine or dolomite as in-bed additive in biomass gasification with air in a fluidized bed: which is better?," *Energy & Fuels,* vol. 18, no. 3, pp. 713-720, 2004.

[31] W. Wang, N. Padban, Z. Ye, G. Olofsson, A. Andersson, and I. Bjerle, "Catalytic hot gas cleaning of fuel gas from an air-blown pressurized fluidized-bed gasifier," *Industrial & engineering chemistry research,* vol. 39, no. 11, pp. 4075-4081, 2000.

[32] H. Cui, S. Q. Turn, V. Keffer, D. Evans, T. Tran, and M. Foley, "Contaminant estimates and removal in product gas from biomass steam gasification," *Energy & Fuels,* vol. 24, pp. 1222-1233, 2010.

[33] M. Jeremiáš, M. Pohořelý, P. Bode, S. Skoblia, Z. Beňo, and K. Svoboda, "Ammonia yield from gasification of biomass and coal in fluidized bed reactor," *Fuel,* vol. 117, pp. 917-925, 2014.

[34] T. K. Tseng, H. C. Chang, H. Chu, and H. T. Chen, "Hydrogen sulfide removal from coal gas by the metal-ferrite sorbents made from the heavy metal wastewater sludge," *Journal of Hazardous Materials,* vol. 160, no. 2–3, pp. 482-488, 2008.

[35] D. Schweitzer *et al.*, "Steam gasification of wood pellets, sewage sludge and manure: Gasification performance and concentration of impurities," *Biomass and Bioenergy,* 2017.

[36] N. Tsubouchi, H. Hashimoto, and Y. Ohtsuka, "Sulfur tolerance of an inexpensive limonite catalyst for high temperature decomposition of ammonia," *Powder Technology,* vol. 180, pp. 184-189, 2008.

[37] N. Tsubouchi, H. Hashimoto, and Y. Ohtsuka, "Catalytic performance of limonite in the decomposition of ammonia in the coexistence of typical fuel gas components produced in an air-blown coal gasification process," *Energy & Fuels*, vol. 21, pp. 3063-3069, 2007.

[38] A. Sarıoğlan, Y. Durak-Çetin, H. Okutan, and F. Akgün, "Decomposition of ammonia: The effect of syngas components on the activity of zeolite Hβ supported iron catalyst," *Chemical Engineering Science*, vol. 171, pp. 440-450, 2017.

[39] *Standard Test Method for Sulfide Ion in Water*.

[40] *Standard Test Methods for Ammonia Nitrogen In Water*.

4 H_2S Removal from the Simulated Producer Gas of Biomass Gasification by Titanomagnetite

This Chapter presents the fundamental research of H_2S removal from the simulated producer gas of biomass gasification by titanomagnetite. Two different types of titanomagnetites, the reduced and unprocessed titanomagnetites, were investigated in both Ar gas and the simulated producer gas firstly to choose the suitable type of titanomagnetite for H_2S adsorption. Thus, the selected type of titanomagnetite, the unprocessed titanomagnetite, was studied at the temperature range of 350-750°C to find the effect of temperature on H_2S removal in the simulated producer gas and the most effective operation temperatures for H_2S adsorption. Finally, the effects of steam and CO on the H_2S removal were studied using the gas mixtures of 2.2 vol.% steam in Ar gas and 20.6 vol.% CO in Ar gas, respectively.

4.1 Introduction

The combination of biomass gasification and Fischer-Tropsch (FT) process is a promising technology to convert renewable resource, biomass, into pure liquid fuel [1]. However, the producer gas from biomass gasification contains tars and other gaseous contaminants such as NH_3 and H_2S which adversely affects the downstream processes. These gaseous contaminants, although at low levels of concentration, will poison catalysts used for FT process [2, 3]. H_2S concentration is normally lower than NH_3 [2], however, it is the primary gaseous nuisance for poisoning the catalyst [4]. It is known that H_2S comes from the conversion of S-containing biomass during the gasification which details can be found elsewhere [4]. Approximately 93%-96% of sulphur in the biomass is converted to H_2S with the rest to COS [5].

The H_2S concentration in the producer gas varies with biomass resources, gasifier type and operation conditions of the gasification. van der Drift et al. [6] tested ten types of biomass in a circulating fluidised bed gasifier, and found the H_2S concentrations in the producer gas varied between 20-230 ppmv where the producer gas from gasification of public garden wood had the highest H_2S content. Harold Boerrigter et al. [7] reported that the H_2S concentration was 100 ppmv in the producer gas from gasification of wood chips at an air-blown circulating fluidised bed gasifier at an operation temperature of 850°C. In another study by Hongrapipat [2], pellets of *Pinus radiata* sawdust were tested at a 100 kWth dual fluidised bed (DFB) gasifier where three different bed materials were used. It was found that the H_2S concentration in the producer gas ranged from 19 to 122 ppmv. In most of the reported studies, the H_2S concentrations in the producer gas from woody biomass gasification were between 20 and 230 ppmv; however, with gasification of pulp and paper residues (largely lignin), the H_2S concentration in the producer gas can be as high as 2000 to 3000 ppmv [4].

However, for application of the producer gas in FT process, H_2S concentration in the feeding gas needs to meet the stringent standard of less than 1 ppmv [1, 8-10]. For this application, H_2S concentrations in the producer gas from biomass gasification are higher than this requirement thus H_2S removal is necessary before it is used in the FT synthesis process.

As discussed in Chapter 2 and Chapter 3, the hot catalytic clean-up system using titanomagnetite as the sorbent has been employed for the H_2S removal. The objectives of this part of study project were: 1) to investigate the performance of titanomagnetite as a sorbent for removing H_2S in the simulated producer gas of biomass gasification; 2) to investigate the effect of operation temperature (350-750°C) and thus find the most effective operation temperatures; and 3) to

investigate the effect of water vapour and CO in the producer gas on H_2S removal, and to understand the mechanisms of these impacts.

4.2 Materials and methods

4.2.1 Sorbent material and preparation

Titanomagnetite was selected as the H_2S adsorption precursor in this research. Characterization and preparation of titanomagnetite have been introduced in Section 3.1.4 and Section 3.6 of Chapter 3.

4.2.2 Gases

Four types of gases were tested in this chapter and, in each run of the experiment, H_2S was introduced to the test gas at controlled very low flow rate by an ABB rotameter so that the H_2S concentration was 240±20 ppmv. The four gases were: (1) pure Ar gas, (2) simulated producer gas, (3) Ar gas with 2.2±0.1 vol.% steam in it, and (4) Ar gas with 20.6±0.4 vol.% CO in it. The H_2S gas was supplied from a gas bottle with 5.0 vol.% H_2S in Ar. The simulated producer gas was comprised of 21.2±0.4 vol.% CO, 20.5±0.4 vol.% CO_2, 15.5±0.3 vol.% CH_4 and the remaining was H_2. The composition of the simulated producer gas was similar to that of the producer gas from biomass steam gasification in a 100 kW DFB gasifier developed in this research group at the University of Canterbury [11, 12]. In the No. 2 tested gas (simulated producer gas), there was an insignificant amount of Ar introduced from the H_2S and Ar mixture, but the Ar quantity was very small thus it was not considered. The gas mixture of H_2S and Ar, and the simulated producer gas were both supplied by BOC Group Ltd., Australia. The steam was supplied from a steam generator with water being supplied and flowrate controlled by an IVAC P2000 syringe pump.

4.2.3 Experimental operation and procedures

The hot catalytic clean-up system in this research has been introduced in Section 3.2, Chapter 3. For each run, Ar gas was first introduced to purge out the air in the reactor and pre-heat the reactor with temperature ramping rate of 10°C/min until the target temperature was reached. After this, the Ar gas was switched off (except that Ar was used as the test gas), test gas as well as 5.0 vol.% H_2S in Ar gas were switched on and introduced into the reactor. To achieve the target H_2S concentration in the test gas, the flow rate of test gas into the reactor was controlled at 3.4±0.1 L/min, and the flow rate of H_2S and Ar mixture (5.0 vol% H_2S in Ar gas) was set as 0.017±0.001 L/min. Details of the experimental procedures is available in Section 3.6 of Chapter 3.

The inlet and the outlet gases were sampled by the impinging method in which two bubblers in an ice bath were used as trappers. The first bubbler was filled with 800 mL of 0.05M NaOH solution and the second bubbler was filled with the same solution of 1600 mL. Details of the impinging method has been introduced in Section 3.4.3, Chapter 3. The sampled solution containing sulphur ion in the first bubbler was analysed by ISE analysis method, which can be found in Section 3.4.4, Chapter 3.

In order to investigate the effect of operation temperature, the reactor temperature was maintained constant at the pre-set value which varied from 350 to 750°C for different runs. In each run, after the measurements were completed, the system was cooled down with purging of welding grade Ar gas until the system temperature was close to the room temperature. After this, the used titanomagnetite was taken out from the reactor, and analysed by analysers of X-Ray Diffraction (XRD) and Total Organic Carbon (TOC). Furthermore, the quartz reactor with solid residues was cleaned following the procedures introduced in Section 3.6 of Chapter 3.

4.2.4 Characterisation of catalyst, liquid and gas

A Philips PW1700 series diffractometer with Co $K\alpha_1$ radiation was used for analysis of the used catalyst in crystal phases at an X-ray wavelength of 1.78896 Å. A Phillips PW2400 sequential wavelength dispersive X-ray fluorescence spectrometer was employed to identify the sulphur element absorbed by the used catalyst. A SSM-5000A TOC-L analyser of SHIMADZU was used to detect the total carbon on the catalyst. During the experiments, liquid was formed and trapped in a condenser after the reactor, and an ATAGO NAR-3T Abbe refractometer was used for analysis of the liquid collected. The composition of the gas samples was measured by an Agilent 3000 micro-GC, which has been calibrated and the calibration curves for different gas species are available in Section 3.5, Chapter 3.

4.3 Results and discussion

4.3.1 Effects of titanomagnetite reduction on H_2S removal in pure Ar gas and simulated producer gas

Both unprocessed and H_2-reduced titanomagnetites were tested for H_2S removal in pure Ar gas and in simulated producer gas. This was to determine if the reduction of the sorbent has a positive impact on the H_2S removal. The experiments using pure Ar gas were conducted at 600°C while the experiments for using simulated gas were conducted at 500°C and 600°C, respectively. The conversions of H_2S were calculated by Eq. (3.7) in Chapter 3 and the results are shown in Figure 4.1 from which it is found that H_2S in the pure Ar gas was almost completely removed by the reduced titanomagnetite during the operation time of 260 min. However, at the same temperature, the conversion of H_2S in the pure Ar gas by using the unprocessed titanomagnetite was initially 94.7% and was then increased to almost 100% in 72 min. These results are in agreement with those

reported by Hongrapipat et al. [3] who showed that H_2S in Ar gas with a concentration of 230 ppmv were removed by almost 100% by using the reduced titanomagnetite at 500°C. Hongrapipat et al. [3] also conducted experiments at 700 and 800°C using the reduced titanomagnetite and found that the H_2S conversion in the same atmosphere (Ar gas) was reduced to 98% at these high temperatures.

The results from the present study show that the conversion of H_2S in the simulated producer gas was significantly reduced as compared to that for Ar gas at the same temperature (600°C) although the conversion was initially high for the reduced titanomagnetite. The reduced titanomagnetite initially showed higher H_2S conversion than the unprocessed titanomagnetite, however, the H_2S conversion by the reduced titanomagnetite dropped dramatically and, after approximate 66 min, it was lower than that of the unprocessed titanomagnetite. As the H_2S conversion in the simulated gas was unsatisfactory at 600°C by using both unprocessed and reduced titanomagnetites, these sorbents were further tested at a lower temperature of 500°C. The result of H_2S removal by the unprocessed titanomagnetite at 500°C is also included in Figure 4.1 from which it is found that the unprocessed titanomagnetite could maintain higher H_2S conversion in the simulated gas at the lower temperature. This finding shows that the temperature had a significant effect and this will be further discussed in Section 4.3.2. When the reduced sand was tested at 500°C, significant carbon deposit was observed which blocked the system. In this case, H_2S removal is unpractical and the used sand was analysed to understand the mechanism.

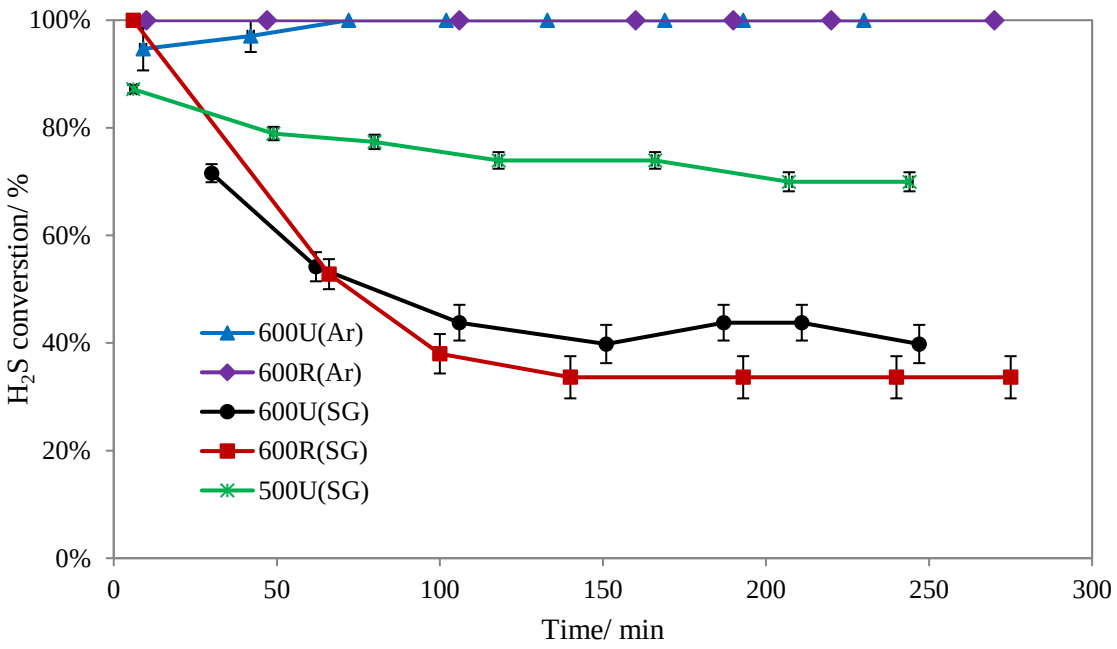

Figure 4.1 H_2S removal in argon (Ar) and simulated producer gas (SG) at 500°C and 600°C by using unprocessed (U) and reduced (R) titanomagnetites.

During the experiments with simulated producer gas, liquid was formed which was initially found in the outlet gas tube. In the following tests, an ice bath was added to condense the vapour in the outlet gas from which the liquid product was accumulated and finally collected at the end of each run of the experiment. After this, the collected liquid was weighed and analysed by Abbe refractometer, which result proved that the liquid product was water. Based on the quantity of water collected and the condensation duration, average water formation rates were calculated for different operation temperatures (500 and 600°C) and different sorbents (unprocessed and reduced titanomagnetites). The results are given in Table 4.1.

After the experiments, the used sorbents from tests with simulated producer gas were tested by TOC-L analyser to determine carbon formed and results of average carbon production rates are

also included in Table 4.1, which were calculated from the total quantities (mols) of carbon produced divided by the experiment duration.

From Table 4.1, it is found that the water production rate in the simulated producer gas was highly dependent on operation temperature and sorbent type used. For example, for unprocessed titanomagnetite, the water production rate at 600°C was 8 times more than that at 500°C. At the same temperature of 600°C, the water production rate using reduced titanomagnetites was almost double that using unprocessed titanomagnetite.

Temperature and sorbent type also showed pronounced impact on carbon formation, but in different trends from those of water production. The carbon production rate using reduced titanomagnetite was higher than using unprocessed titanomagnetite at the same temperature. For the same sorbent, the carbon formation rate at 500°C was much higher than that at 600°C. There was a similar result in the research of Tamhankar et al. [13] who found that carbon deposited rapidly on the iron catalyst in the presence of H_2 and CO when the temperature was below 600°C. These authors attributed the carbon formation to the following reaction (Eq. 4.1).

$$H_2 + CO \leftrightarrow H_2O + C \qquad (4.1)$$

Table 4.1 Water and carbon production rates at 500°C and 600°C for both unprocessed and reduced titanomagnetites in the simulated producer gas.

Titanomagnetite	Water production rate (mol/min)	Carbon production rate (mol/min)
Unprocessed at 500°C	0.00019	0.00018
Reduced at 500°C	Not available	0.00753
Unprocessed at 600°C	0.00167	0.00001
Reduced at 600°C	0.00325	0.00007

Based on Eq. (4.1), when more water was formed, more carbon should have been formed as well. However, the experimental results from the present study do not show consistent trends between water formation and carbon formation. Nevertheless, by comparing the H_2S removal results shown in Figure 4.1 with the results of water/carbon formation given in Table 4.1, it appeared that the formation of water and carbon deposition had adverse effects on the H_2S removal in the simulated producer gas.

To understand the mechanisms of carbon formation and its effect on the H_2S removal, the fresh titanomagnetites (both unprocessed and reduced) and the used titanomagnetites in the simulated producer gas at 500°C were analysed by the XRD analyser, respectively. The XRD graphs are shown in Figures 4.2 to 4.5, respectively, for fresh unprocessed, fresh reduced, used unprocessed and used reduced titanomagnetites. Comparing Figures 4.2 with 4.3, significant Fe_3O_4 phase was found on the fresh unprocessed sorbent (Figure 4.2), however, the Fe_3O_4 phase was much reduced and transformed to α-Fe phase after the H_2 reduction process (Figure 4.3). These sorbent analysis

results can be used to explain the results of H_2S removal presented in Figure 4.1 and Table 4.1. From experiments using Ar gas, the Fe_3O_4 phase on the unprocessed titanomagnetite and the α-Fe phase on the reduced titanomagnetite all had high activity to remove H_2S as shown in Figure 4.1. On the other hand, in the simulated gas, the α-Fe phase on the reduced titanomagnetite tended to promote carbon formation at both temperatures (Table 4.1) and thus to reduce the H_2S removal efficiency (Figure 4.1).

By comparing the XRD results between fresh and used titanomagnetites at 500°C, it is found that there was significant carbide (Fe_3C) formed on the used titanomagnetites. This was more significant for the used reduced titanomagnetite than that for the used unprocessed titanomagnetite. Interestingly, the α-Fe phase was also observed on the used unprocessed titanomagnetite. Based on these findings, it is believed that in H_2S removal from the simulated producer gas, active phases of Fe_3O_4 and α-Fe were transferred to less active phase Fe_3C on the titanomagnetites, thus their activity for H_2S removal was reduced. The Fe_3O_4 on the unprocessed titanomagnetite may have been transformed to α-Fe first and then to Fe_3C as H_2 existed in the simulated gas. As the α-Fe phase on the reduced titanomagnetite was more likely to transform to Fe_3C, the H_2S conversion efficiency of the reduced titanomagnetite was lower than the unprocessed titanomagnetite at the same temperature.

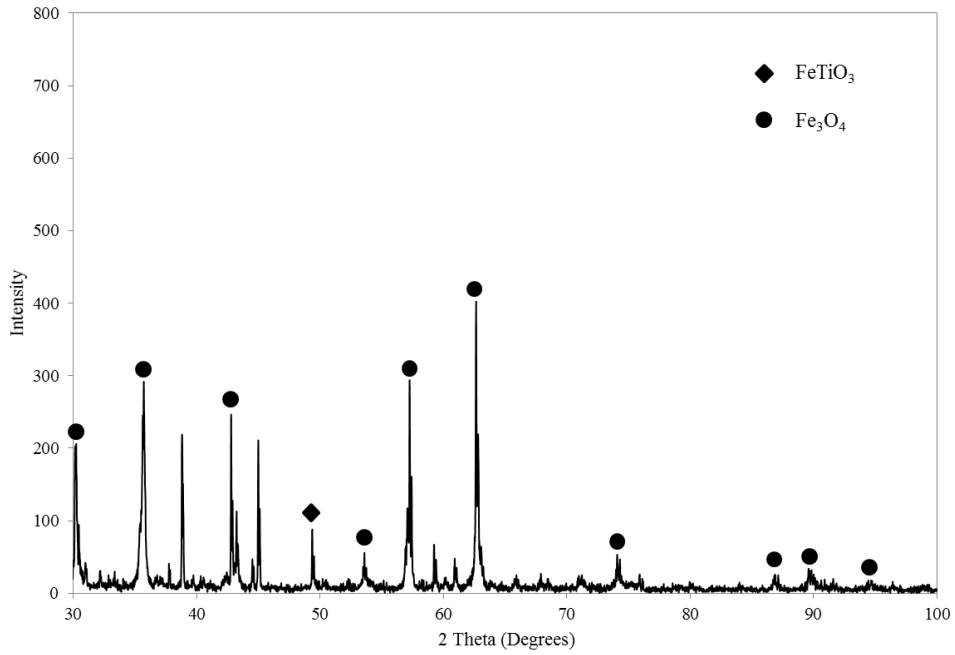

Figure 4.2 The XRD graph of the fresh unprocessed titanomagnetite.

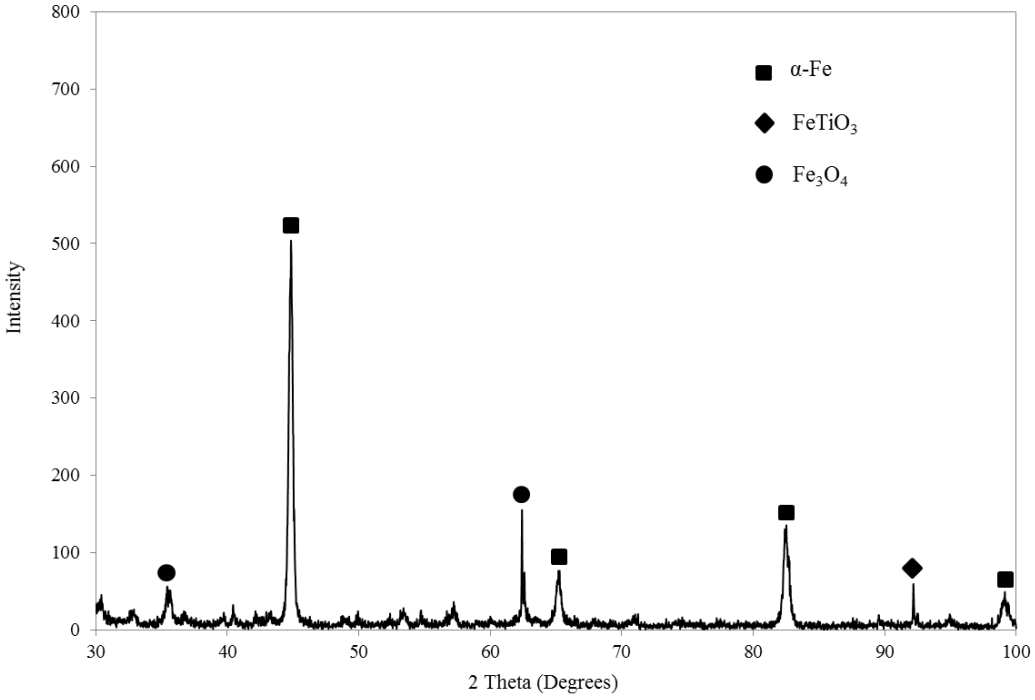

Figure 4.3 The XRD graph of the fresh reduced titanomagnetite.

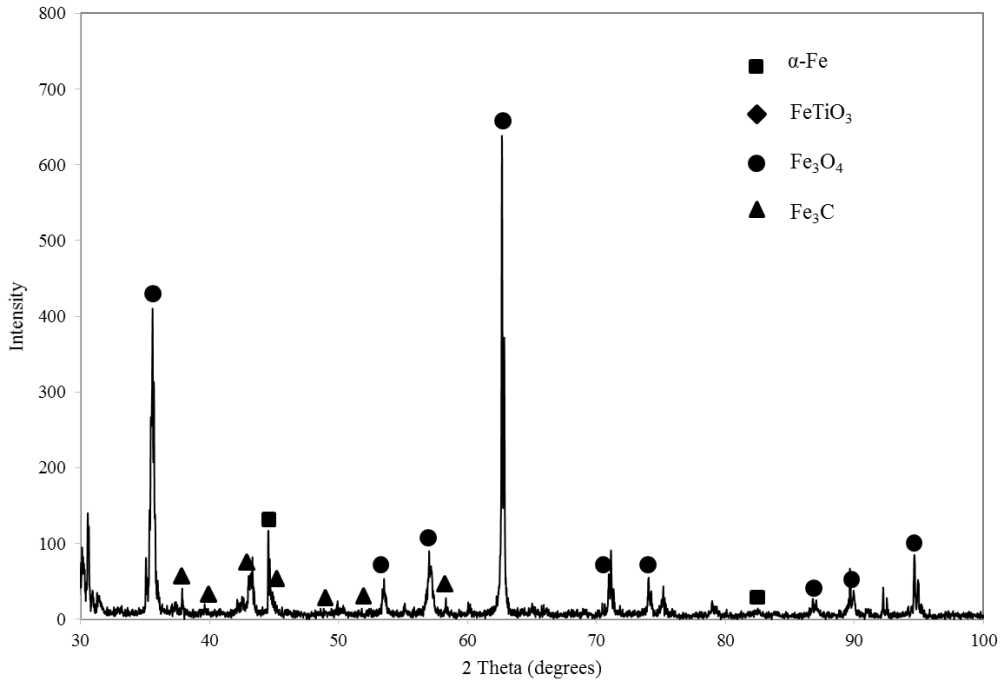

Figure 4.4 XRD graph for the used unprocessed titanomagnetite at 500°C.

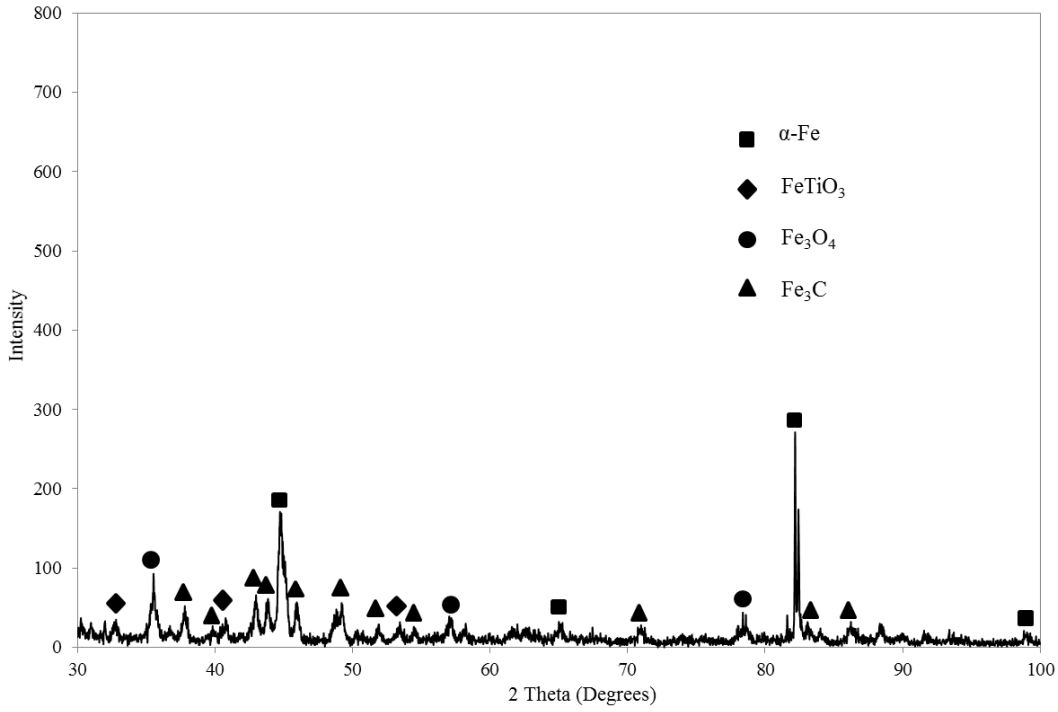

Figure 4.5 XRD graph for the used reduced titanomagnetite at 500°C.

4.3.2 Influence of operation temperature on H_2S removal in the simulated gas by using unprocessed titanomagnetite

Since the unprocessed titanomagnetite had better performance on the H_2S removal than the reduced titanomagnetite in the simulated producer gas at the tested temperatures (500 and 600°C), the unprocessed titanomagnetite was selected for further investigation. In this part of the study, experiments were performed on H_2S removal in the simulated producer gas using unprocessed titanomagnetite at temperatures from 350°C to 750°C, and the results are shown in Figure 4.6. From this figure, it is found that the operation temperature has a significant influence on the H_2S removal. Based on the results of H_2S conversion over 3 hours of operation, the unprocessed titanomagnetite was found to be most effective at the operation temperatures of 400 and 450°C, at which the H_2S conversion maintained at over 85%. When the operation temperatures was higher than 450°C, the H_2S conversion was decreased and this could be as low as 20% at 750°C. At a temperature of 350°C, the H_2S conversion was initially very high, close to 100%, but this dropped rapidly to 73.8% after about 3 hours which may be attributed to the reduced diffusivity of the gases within the sorbent at lower temperatures. A similar finding was also observed by Reeve [14] that the desulphurization ability of an iron ore sorbent was reduced when tested at 400 to 325°C in a fluidized bed reactor for coke-oven gas. Tamhankar et al. [15] noted that diffusion played a vital role in the desulphurization reaction and the effective diffusivity increased with the temperature increasing.

In order to check the reliability in the determination of H_2S conversions based on inlet gas flow rates and outlet gas analysis using ISE, H_2S concentrations in inlet and outlet gases were measured using Dräger tubes in the H_2S removal experimental run at 400°C for simulated gas using the unprocessed titanomagnetite.The result from this confirmation test is also included in Figure 4.6

from which it was found that the H_2S conversion was in close agreement with that determined by ISE.

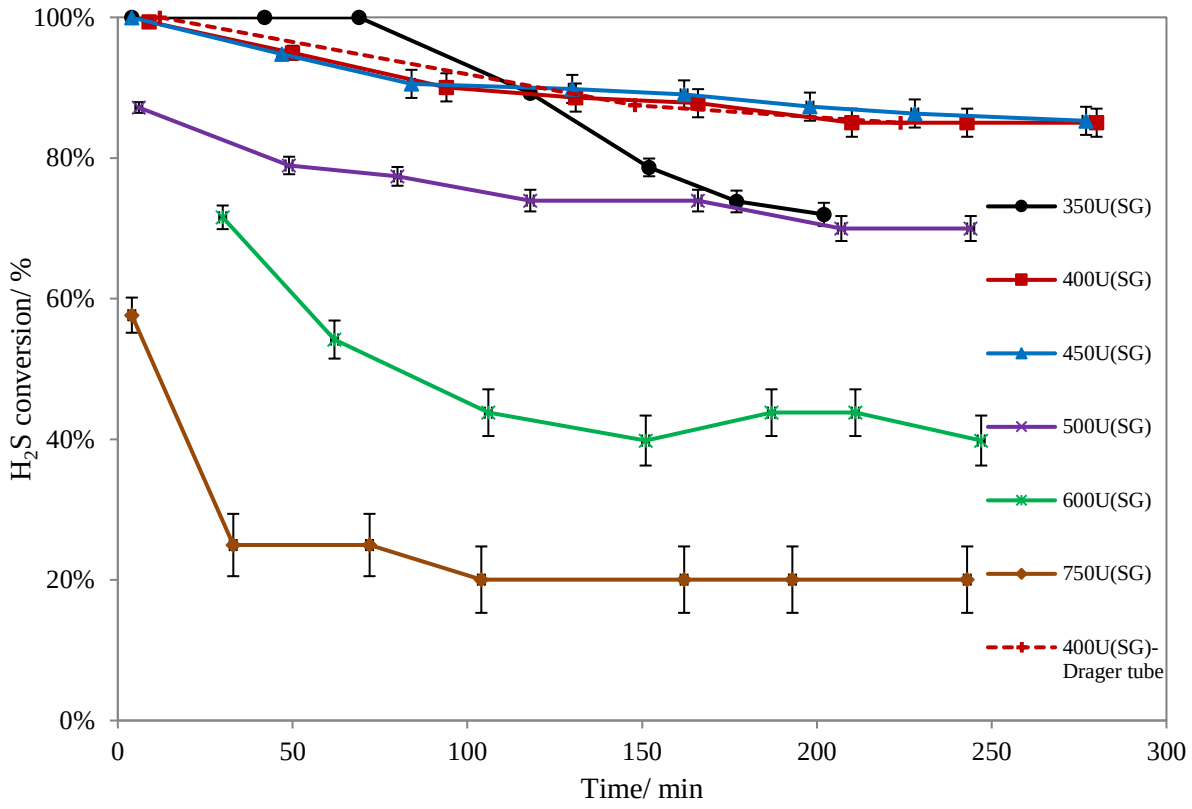

Figure 4.6 The conversion of H_2S in simulated gas by unprocessed titanomagnetite at temperatures from 350 to 750 °C (the dash line represents the result tested by Dräger tubes and other lines are tested by ISE).

Table 4.2 shows the results of water and carbon production rates during the H_2S removal from simulated producer gas using unprocessed titanomagnetite at different operation temperatures. It is seen that at operation temperatures of 450°C or lower, water was undetectable. However, water production rate was increased rapidly from 500°C to 750°C, confirming that high temperature promoted the production of water. Interestingly, the carbon formation rate was the highest at 500°C.

Table 4.3 lists possible reactions (Eq.4.2 – 4.9) which were involved in the H_2S removal from simulated producer gas, which consists of H_2, CO, CO and CH_4. Based on the experimental results in the present study and analysis reported in literature [2, 13, 16], the dominant reactions involved in the removal of H_2S were most likely to be the reverse water-gas shift reaction (Eq.4.2) and the Boudouard reaction (Eq.4.3). In addition, the reduction reactions of the unprocessed titanomagnetite by H_2 and CO also played an important role when the simulated producer gas was used.

In the present study, it has been observed that high temperature promoted water production for which the reverse water-gas shift reaction was most likely to be responsible as this is the only endothermic reaction to produce water. All the other reactions for possible H_2O generation, Eqs. (4.4), (4.5), (4.8) and (4.9), are all exothermic and were thus favoured at low temperatures.

Based on the fact that elemental carbon was detected on the used unprocessed and used reduced titanomagnetites, it is expected that the Boudouard reaction was responsible for the carbon formation as suggested by Yasuo et al. [16]. The methane cracking reaction (Eq. 4.7) may also be possible at high temperatures of above 680°C [17]. The observation that the carbon formation rate on the used unprocessed sand was the highest at 500°C (Table 4.2) can be explained by chemisorption of CO on the iron catalysts which was reported to be the maximum at 500-600°C. The CO absorption promoted carbon formation through the Boudouard reaction [18].

Table 4.2 The water and carbon production rates at different temperatures.

Temperature (°C)	Water production rate (mol/min)	Carbon production rate (mol/min)
350	undetectable	0.00001
400	undetectable	0.00001
450	undetectable	0.00001
500	0.00019	0.00018
600	0.00167	0.00001
750	0.00793	0.00000

Table 4.3 The possible reactions in the reactor for H_2S removal.

Reaction formula	ΔH_{298K} (kJ/mol)	Reaction type
$CO_2+H_2 \leftrightarrow CO+H_2O$	+41.2	(4.2) Reverse water gas shift reaction
$2CO \leftrightarrow C+CO_2$	-172.4	(4.3) Boudouard reaction
$CO+3H_2 \leftrightarrow CH_4+H_2O$	-206.1	(4.4) CO methanation
$CO_2+4H_2 \leftrightarrow CH_4+2H_2O$	-165.0	(4.5) CO_2 methanation
$2CO+2H_2 \leftrightarrow CH_4+CO_2$	-247.3	(4.6) Inversed methane CO_2 reforming
$CH_4 \leftrightarrow 2H_2+C$	+74.8	(4.7) Methane cracking
$CO+H_2 \leftrightarrow C+H_2O$	-131.3	(4.8) Carbon monoxide reduction
$CO_2+2H_2 \leftrightarrow C+2H_2O$	-90.1	(4.9) Carbon dioxide reduction

Furthermore, the used unprocessed titanomagnetite at 750°C was analysed by the XRD analyser and the results are shown in Figure 4.7. By comparing the results in Figure 4.7 (750°C) with those in Figure 4.4 (500°C), higher α-Fe phase was found on the used unprocessed titanomagnetite at 750°C than that at 500°C. This can be attributed to the reduction reactions, Eq. (4.10) and (4.11) which was promoted at high temperatures with reduction gases of H_2 and CO in the system. The increased α-Fe phase at higher temperature is expected to enhance the production of water as well. Moreover, there was less Fe_3O_4 phase on the used unprocessed titanomagnetite at 750°C than that at 500°C, therefore, the H_2S removal was reduced at high temperatures.

$$Fe_3O_4 + 4H_2 \leftrightarrow 3Fe + 4H_2O \quad (4.10)$$

$$Fe_3O_4 + 4CO \leftrightarrow 3Fe + 4CO_2 \quad (4.11)$$

Other researchers also reported that the H_2S absorption efficiency of the iron oxide was decreased when the temperature was higher than 500°C; however, inconclusive interpretations were given in literature. Tamhankar et al. [15] reported that iron oxide was easily reduced to spongy iron with fast reduction, which had low reaction rate to adsorb H_2S from the gas. Tseng et al. [19] illustrated that high temperatures above 600°C caused reduction of iron oxide to Fe and FeO which had lower desulphurization equilibrium. Gangwal et al. [20] demonstrated that high temperature led to excessive reduction and iron carbide formation which damaged the sorbent severely.

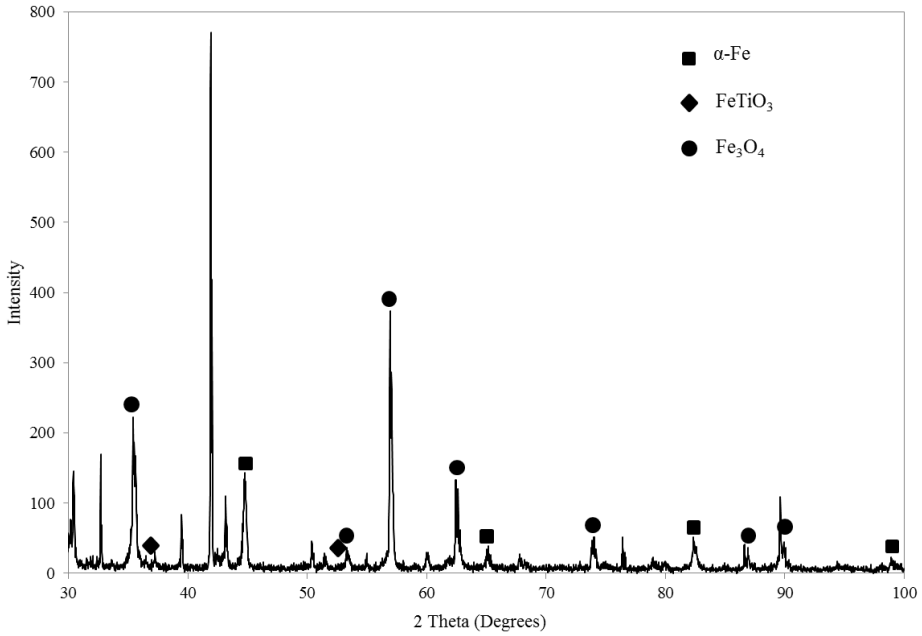

Figure 4.7 XRD graph for the used unprocessed titanomagnetite at 750°C.

4.3.3 Effects of steam and CO in the gas mixture on H_2S removal using unprocessed titanomagnetite

In order to examine the effect of H_2O on H_2S removal, 2.2 vol.% steam was added into the pure Ar gas for the experiment to remove H_2S using unprocessed titanomagnetite at an operation temperature of 600°C. A separate experiment was also conducted to investigate the effect of CO (20.6%) in the Ar gas at 600°C. The H_2S concentration was also controlled at 240±20 ppmv. The results from these experiments are shown in Figure 4.8 in which the experimental results from pure Ar gas tests are also included for comparison. From Figure 4.8, it is found that with 2.2 vol.% steam in the Ar gas, H_2S conversion decreased dramatically from initial 92.5% to 9% in 237 min from the start. However, when the steam feeding was turned off at this time, the H_2S conversion increased to 69% in less than 10 min. The results show that H_2O was one of the major factors adversely affecting the H_2S removal efficiency of the titanomagnetites. This finding may be used

to explain the results in Figure 4.6 that higher temperatures promoted the production of H_2O thus reduced the efficiency of H_2S removal. Sasaoka et al. [21] also found that H_2O had an adverse effect on an iron ore (hematite) for H_2S absorption at 400°C. The authors explained that H_2O limited the equilibrium of the following reaction, Eq. (4.12). Moreover, Tamhankar et al. [15] reported that H_2O suppressed the H_2S absorption by an iron oxide sorbent; however, the authors revealed that H_2O inhibited the iron oxide reduction by H_2 and CO in the atmosphere to Fe by reaction of Eq. (4.13), thus reduced the desulfurization rate of Fe successively. Nevertheless, from the above findings, H_2O in the producer gas and the formation of H_2O should be minimised when iron oxide is used as the sorbent for H_2S adsorption.

$$Fe_3O_4 + 3H_2S + H_2 \leftrightarrow 3FeS + 4H_2O \quad (4.12)$$

$$Fe_xO_y + y(H_2 + CO) \leftrightarrow xFe + y(H_2O + CO_2) \quad (4.13)$$

Furthermore, CO in the gas also lowered the H_2S removal efficiency, but its effect was much less significant compared with the effect of steam as shown in Figure 4.8. In the experiment on the gas mixture of CO and Ar, the H_2S removal efficiency was 97% at the start and then reduced to 92% in 226 min. These results confirm the experimental results shown in Figure 4.1 and Figure 4.6 that the H_2S removal efficiency using unprocessed titanomagnetite was higher at 500°C although more carbon was formed in comparison with higher temperatures. This is because more water was formed at 600 and 750°C which was a dominant factor.

In the experiments for a gas mixture of CO and Ar, H_2 and CO_2 were also found in the outlet gas which were detected by using Agilent 3000 micro-GC. It is believed that the H_2 was from H_2S decomposition which also produced FeS on the sorbent through the reaction $xFe+yH_2S \leftrightarrow yH_2+Fe_xS_y$. The FeS on the used unprocessed titanomagnetites was measured by XRF

qualitative scan which showed 0.3 wt.% S on the sorbent after 258 min operation at 500°C. CO_2 was produced through the Boudouard reaction which also formed carbon.

H_2 formed from the H_2S decomposition may have double-sided effects. On one side, more H_2S was decomposed which improved H_2S removal; but on the other side, FeS formation may hinder the reactivity of sorbent for H_2S absorption. In future studies, the effect of H_2 on H_2S removal should be investigated.

Based on the measured CO_2 concentration, the volumetric (or mole) percentage of CO converted to CO_2 through the Boudouard reaction has been calculated and the results are presented in Figure 4.9, which shows 2.0-2.5 vol.% of CO was converted to CO_2 during the experiment. The conversion of CO to CO_2 decreased with the increase of reaction time.

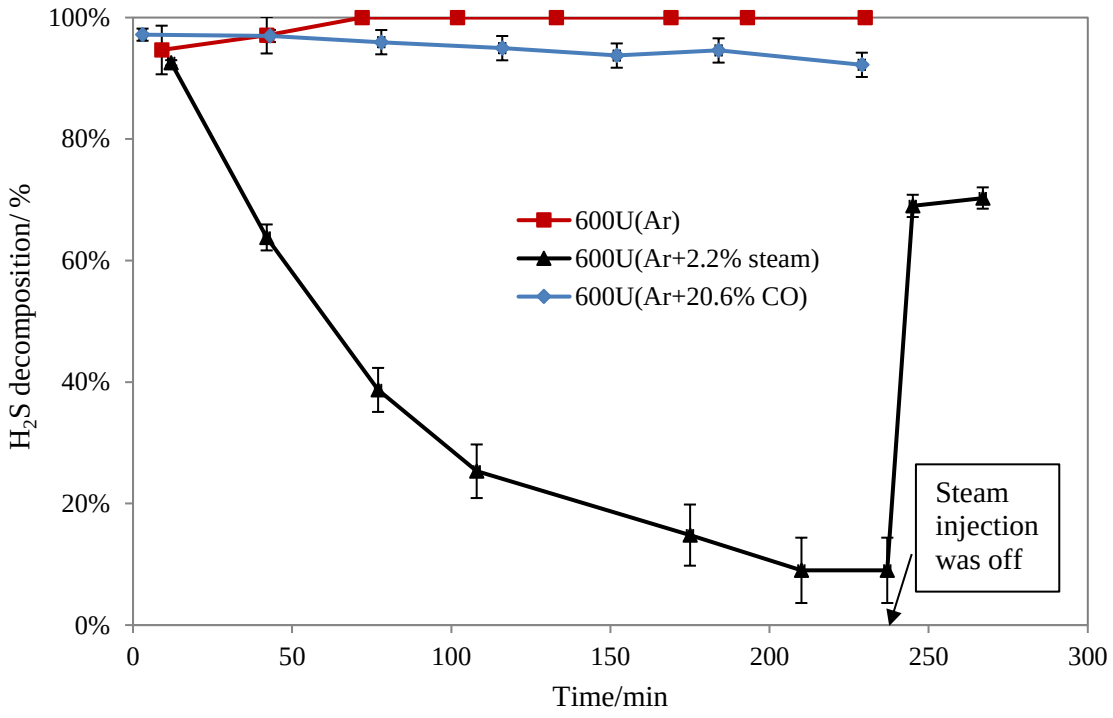

Figure 4.8 The comparison of H_2S conversion in different gases at 600°C.

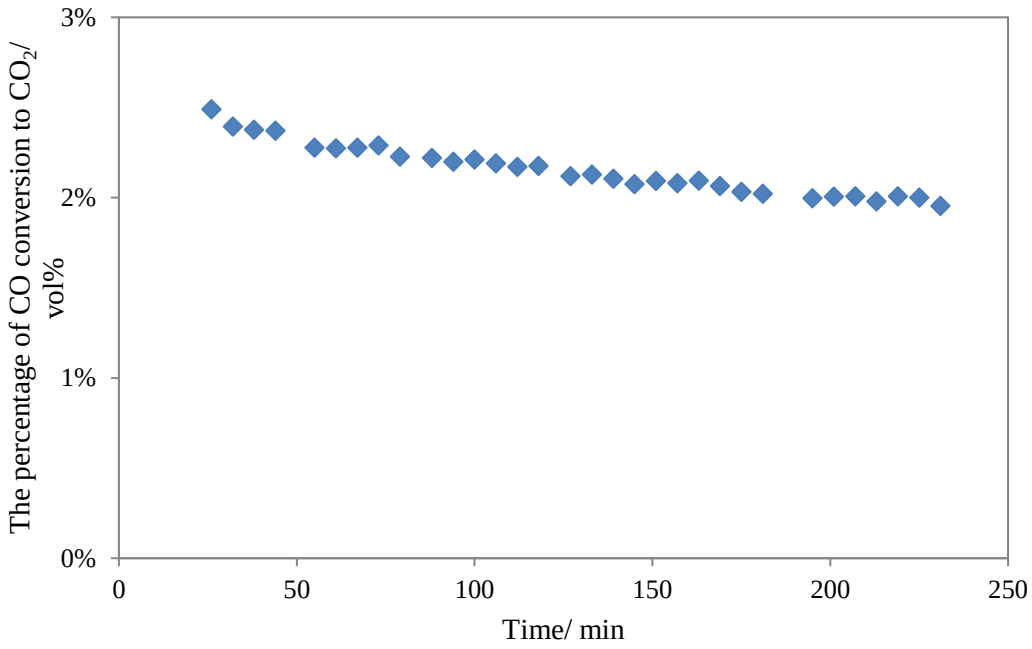

Figure 4.9 The percentage of CO converted into CO_2 as a function of elapsed time.

4.4 Conclusions

The removal of H_2S in simulated producer gas from biomass gasification was investigated in this part of study by using unprocessed and H_2-reduced titanomagnetites. H_2S concentrations in the inlet and outlet gases were measured by an effective impinging method with two bubblers to trap H_2S and the solution with sulphur ion (S^{2-}) was analysed by the ISE method. Effects of operation temperature and gas species (H_2O and CO) were investigated. Inert gas was tested for comparison with the simulated gas.

This study shows that the unprocessed titanomagnetite and the reduced titanomagnetite are highly effective in removing H_2S from pure Ar gas at 600°C, but their performance is suppressed in the simulated producer gas, where the unprocessed sand is more effective than the reduced sand. It is believed that the reduced sand has more α-Fe phase transformed from active Fe_3O_4 phase on the

fresh titanomagnetite. The α-Fe phase is more likely to be transformed to carbide (Fe_3C) which reduces the reactivity of titanomagnetite.

Reaction temperature has a significant impact on the H_2S removal of the unprocessed sand. In the temperature range tested (350 - 750°C), the most effective operation temperatures are found to be between 400 and 450°C. The exact optimal temperature can be investigated in the future studies. Both steam and carbon formation has negative effects on the H_2S removal efficiency of the unprocessed titanomagnetite and steam is the dominant factor adversely affecting the H_2S removal. The dominant reactions involved in the H_2S removal from simulated producer gas by using the titanomagnetite are reverse gas-water shift reaction and the Boudouard reaction.

To improve the titanomagnetite performance on H_2S removal in the simulated producer gas or in the actual producer gas of biomass steam gasification, H_2O in the producer gas should be minimised during the tar removal stage prior to the H_2S removal. Reducing CO_2 content in the producer gas is also helpful because CO_2 is the reactant for the reverse water gas shift reaction. The other gas species in the producer gas (H_2, CO_2, CH_4 and NH_3) may also affect the H_2S removal efficiency using titanomagnetite sorbent and this should be confirmed in future studies.

4.5 References

[1] H. P. C. H. Boerrigter, D.J. Slort, H. Bodenstaff, A.J. Kaandorp, H. den Uil, L.P.L.M. Rabou, "Gas Cleaning for Integrated Biomass Gasification (BG) and Fischer-Tropsch (FT) Systems," in "Energy Research Centre of the Netherlands (ECN), Petten, The Netherlands, report RX-04-041," May 2004.

[2] J. Hongrapipat, "Removal of NH_3 and H_2S from biomass gasification producer gas," Doctor of Philosophy, Chemical and Procees Engineering, University of Canterbury, Christchurch, New Zealand, 2014.

[3] J. Hongrapipat, A. C. K. Yip, A. T. Marshall, W. L. Saw, and S. Pang, "Investigation of simultaneous removal of ammonia and hydrogen sulphide from producer gas in biomass gasification by titanomagnetite," *Fuel*, vol. 135, pp. 235-242, 2014.

[4] X. Meng, W. de Jong, R. Pal, and A. H. M. Verkooijen, "In bed and downstream hot gas desulphurization during solid fuel gasification: A review," *Fuel Processing Technology*, vol. 91, no. 8, pp. 964-981, 2010.

[5] K. Liu, C. Song, and V. Subramani, *Hydrogen and syngas production and purification technologies*. Wiley Online Library, 2010.

[6] A. Van der Drift, J. Van Doorn, and J. Vermeulen, "Ten residual biomass fuels for circulating fluidized-bed gasification," *Biomass and Bioenergy*, vol. 20, no. 1, pp. 45-56, 2001.

[7] H. Boerrigter, H. den Uil, and H.-P. Calis, "Green diesel from biomass via Fischer-Tropsch synthesis: new insights in gas cleaning and process design," ed: CPL Press: Newbury, UK, 2003, pp. 371-383.

[8] P. L. Spath and D. C. Dayton, "Preliminary screening-technical and economic assessment of synthesis gas to fuels and chemicals with emphasis on the potential for biomass-derived syngas," National Renewable Energy Lab Golden Co2003.

[9] T. Bui, R. Loof, and S. Bhattacharya, "Multi-stage reactor for thermal gasification of wood," *Energy*, vol. 19, no. 4, pp. 397-404, 1994.

[10] M. Asadullah, "Biomass gasification gas cleaning for downstream applications: A comparative critical review," *Renewable and sustainable energy reviews,* vol. 40, pp. 118-132, 2014.

[11] W. L. Saw and S. Pang, "The influence of calcite loading on producer gas composition and tar concentration of radiata pine pellets in a dual fluidised bed steam gasifier," *Fuel,* vol. 102, pp. 445-452, 2012.

[12] W. L. Saw and S. Pang, "Co-gasification of blended lignite and wood pellets in a 100kW dual fluidised bed steam gasifier: The influence of lignite ratio on producer gas composition and tar content," *Fuel,* vol. 112, pp. 117-124, 2013.

[13] S. Tseng, S. Tamhankar, and C. Wen, "Kinetic studies on the reactions involved in the hot gas desulfurization using a regenerable iron oxide sorbent—II: reactions of iron sulfide with oxygen and sulfur dioxide," *Chemical Engineering Science,* vol. 36, no. 8, pp. 1287-1294, 1981.

[14] L. Reeve, "Desulphurization of coke oven gas at Appleby-Frodingham," *Journal of the Institute of Fuel,* vol. 31, pp. 319-324, 1958.

[15] S. Tamhankar, M. Hasatani, and C. Wen, "Kinetic studies on the reactions involved in the hot gas desulfurization using a regenerable iron oxide sorbent-I: Reduction and sulfidation of iron oxide," *Chemical Engineering Science,* vol. 36, no. 7, pp. 1181-1191, 1981.

[16] Y. Ohtsuka, C. Xu, D. Kong, and N. Tsubouchi, "Decomposition of ammonia with iron and calcium catalysts supported on coal chars," *Fuel,* vol. 83, pp. 685-692, 2004.

[17] M. A. Ermakova, D. Y. Ermakov, A. L. Chuvilin, and G. G. Kuvshinov, "Decomposition of methane over iron catalysts at the range of moderate temperatures: the influence of structure of the catalytic systems and the reaction conditions on the yield of carbon and morphology of carbon filaments," *Journal of catalysis,* vol. 201, pp. 183-197, 2001.

[18] P. Walker Jr, J. Rakszawski, and G. Imperial, "Carbon mixture over iron catalysts. II. Rates of carbon formation," *The Journal of Physical Chemistry,* vol. 63, pp. 140-149, 1959.

[19] T. K. Tseng, H. C. Chang, H. Chu, and H. T. Chen, "Hydrogen sulfide removal from coal gas by the metal-ferrite sorbents made from the heavy metal wastewater sludge," *Journal of Hazardous Materials,* vol. 160, no. 2–3, pp. 482-488, 2008.

[20] S. Gangwal, S. Harkins, M. Woods, S. Jain, and S. Bossart, "Bench-scale testing of high-temperature desulfurization sorbents," *Environmental Progress & Sustainable Energy,* vol. 8, no. 4, pp. 265-269, 1989.

[21] E. Sasaoka, T. Ichio, and S. Kasaoka, "High-temperature hydrogen sulfide removal from coal-derived gas by iron ore," *Energy & Fuels,* vol. 6, no. 5, pp. 603-608, 1992.

5 Investigation of NH_3 Removal from the Simulated Producer Gas of Biomass Gasification by Titanomagnetite

In this chapter, the selected catalyst, titanomagnetite, was examined for NH_3 removal from the simulated producer gas of biomass gasification. First of all, the unprocessed and reduced titanomagnetites were tested in Ar gas at different temperatures to observe the effects of temperature and titanomagnetite reduction on NH_3 decomposition. Secondly, the selected reduced titanomagnetite with better performance was investigated at 500, 750 and 850°C, respectively to evaluate its performance in the simulated producer gas for NH_3 removal. Meanwhile, the side reactions occurred during the NH_3 removal in the simulated producer gas were assessed through comparison of products and reagents, and equilibrium calculation. Finally, the effects of 230 ppmv H_2S on the reduced titanomagnetite for NH_3 removal from the simulated producer gas were studied at 750°C.

5.1 Introduction

From the literature review in section 2.1.2 of Chapter 2, the concentration of NH_3 in the producer gas is strongly dependent on the N contents in the feedstock, gasifier types and gasification operating conditions [1, 2]. It is reported that 60-80% of nitrogen in the feedstock could be liberated as NH_3 which is the major N-containing compound and the primary gaseous contaminant in the producer gas of biomass gasification [3]. It is also reported that the NH_3 concentration ranges from 100 to 5000 ppmv in the producer gas of biomass gasification but, in most cases, the NH_3 concentration is lower than 2300 ppmv for woody biomass gasification [1, 2, 4, 5]. NH_3 is known as the toxin for the catalysts used in downstream processes and the precursor of NO_x when the oxidation process occurs [6]. When the producer gas is used for Fischer-Tropsch (FT) process, the

concentration of ammonia in the producer gas should meet stringent specification of less than 1 ppmv [7-10].

To remove NH_3 in the producer gas of biomass gasification, both physical and chemical methods can be used. Among the physical methods, the wet scrubber is the most attractive method and has been investigated extensively, from which different NH_3 removal efficiencies have been reported. Boerrigter et al. [7] reported that a water scrubber following the "OLGA" system had an NH_3 removal efficiency of 99.3% which reduced the NH_3 concentration from 1304 to 8.5 ppmv. Pino et al. [11] used a scrubber system to cool down the producer gas and, at the same time, to remove NH_3 in the producer gas using the condensed water, and they found that the NH_3 removal efficiency could be higher than 90%. Loipersböck et al. [12] also found that a biodiesel scrubber at low temperatures with the assistance of condensed water from the producer gas from a DFB steam blown gasifier had a remarkable capacity to absorb NH_3 in the producer gas with removal efficiency of 99.7%. However, in a separate study by Pröll et al. [13], only 50% of 500 ppmv NH_3 in the producer gas of biomass gasification was removed by using a wet scrubber using a mixture of an organic solvent with condensed water from the same producer gas. In the study of Pröll et al. [13], when the NH_3 concentration was increased to 2000 ppmv, the NH_3 removal efficiency was reduced to 30%. The wet scrubber method has disadvantages of waste solution generation and low NH_3 removal efficiency if the inlet NH_3 concentration was high [14]. Therefore, an alternative hot-catalytic method was investigated in this part of the research.

Hot catalytic gas cleaning technology is an effective method for NH_3 removal downstream the gasifier. Its advantages include high NH_3 removal efficiency, no waste liquid being generated and effective processes available for catalyst regeneration. In previous studies, Fe-based catalysts, such as iron sinter, ferrous dolomite, limonite and magnetite, have attracted increasing attention in the

past few decades because of their performance and low cost. Tsubouchi et al. [15] reported that reduced limonite (α-FeOOH) showed effective NH_3 removal in helium gas (99.9% NH_3) at 500°C. However, its NH_3 removal efficiency was inhibited by the presence of CO and H_2 [16] or H_2S [17] which resulted from the carbon deposition of the Boudouard reaction, equilibrium reduction and the sulphur poisoning. On the other hand, Tsubouchi et al. [15], in the subsequent studies, found that addition of CO_2 and H_2O along with the syngas (CO and H_2 mixture) improved the catalytic performance by reducing the carbon deposition significantly. For further improvement of the NH_3 removal, the limonite was reformed by adding 3 wt.% Mg on the catalyst, which showed a significant increase in efficiency and stability for NH_3 removal [18]. In a separate study at a 5 MW updraft gasifier, Leppälahti et al. [19] found that iron-based materials like ferrous dolomite, iron sinter and iron pellet showed the NH_3 removal efficiency being higher than dolomite and limestone.

Furthermore, the previous study by Hongrapipat et al. [23] has investigated the performance of the Fe-based catalyst, named titanomagnetite, in decomposition of NH_3 in Ar gas and showed high efficiency for NH_3 removal. Titanomagnetite is cheap and can be found in natural form, therefore, it has promising future in commercial applications. However, its performance in the simulated producer gas and the effects of the gas composition are unknown. The objective of this chapter is to investigate the NH_3 removal efficiency of titanomagnetite both in the original form and in the reduced form in an inert gas, Ar, and then to investigate the performance of the selected titanomagnetite in simulated producer gas from biomass gasification. Influence of producer gas composition will also be examined and possible reactions in the NH_3 removal will be explored. In addition, the effect of H_2S in the simulated producer gas on NH_3 decomposition by the reduced titanomagnetite will be also investigated in this chapter.

5.2 Materials and methods

5.2.1 Catalyst material and preparation

Titanomagnetite, Fe-based sand, was purchased from a local supplier in New Zealand and used as a catalyst in the experiments. Catalyst characterization, preparation and H_2 reduction process can be found in section 3.1.4 and section 3.6 of Chapter 3.

5.2.2 Gases

Pure instrumental grade Ar gas, simulated producer gas, and simulated producer gas containing 230±20 ppmv H_2S were tested in this study, in which 50.0 vol.% NH_3 in Ar gas was introduced at a controlled low flow rate based on the required NH_3 concentration of 2300±100 ppmv in all of the test gases. In practical gasification of woody biomass, NH_3 concentrations in most of the producer gases are lower than 2300 ppmv, therefore, the selected NH_3 concentration in this research represents the worst case [20].

The simulated producer gas was purchased from the BOC group, Australia, and its composition was 18.9±0.4 vol.% CO, 19.1±0.4 vol.% CO_2, 14.4±0.3 vol.% CH_4 and 47.6±0.4 vol.% H_2. This composition was chosen based on reported studies by this research group on biomass steam gasification on a dual fluidised bed (DFB) gasifier [21, 22], and this was also close to that from other studies although it was affected by operation conditions and application of catalytic bed materials [12, 13, 23, 24].

The 230±20 ppmv H_2S in simulated producer gas was obtained by mixing the simulated producer gas and a specified gas mixture of 5 vol.% H_2S in Ar gas with controlled flow rates through gas flowmeters. In this case, there was a slight amount of Ar gas in the tested simulated producer gases

which from the NH_3 and/or H_2S containing gas bottles; however, the amount was too low to be considered in the study. Overall, there were three types of gases tested in this chapter which the gas flow rates of different gases for mixing them are shown in Table 5.1.

Table 5.1 Gas flow rates of different gases for mixing the three tested mixture gases in this chapter.

Gas type	Ar gas containing 2300 ppmv NH_3	Simulated producer gas containing 2300 ppmv NH_3	Simulated producer gas containing 2300 ppmv NH_3 and 230 ppmv H_2S
Ar gas (L/min)	3.65±0.002	0.00	0.00
Simulated producer gas (L/min)	0.00	3.65±0.002	3.65±0.002
50.0 vol% NH_3 in Ar gas (L/min)	0.017±0.001	0.017±0.001	0.017±0.001
5 vol.% H_2S in Ar gas (L/min)	0.000	0.000	0.017±0.001

5.2.3 Experimental operation and procedures

The hot catalytic gas cleaning system used in this study is shown in Figure 3.1, Chapter 3. Details of the experimental procedures can be found in section 3.6, Chapter 3.

The inlet and the outlet gases were sampled by an impinging method where two bubblers in ice bath were used as trappers. The first bubbler was filled with 800 mL of 0.05M sulphuric acid solution and the second bubbler was filled with 1600 mL of the same solution, as shown in Figure 3.5, Chapter 3. This sampling method had been proved to be an appropriate method to trap the

NH_3 in the inlet and outlet gases which details can be found in section 3.4.3, Chapter 3. The sampled solution containing NH_3 in the first bubbler was analysed by the ISE method which has been given in section 3.4.5 of Chapter 3. This system was also used to check the NH_3 concentration (volume fraction) in the inlet gas that was found to be 2300±100 ppmv, which was very close to the controlled concentration of 2318 ppmv by gas flow rate meters.

In order to investigate the effect of temperature, operation temperature of the reactor was varied from 500 to 850°C, respectively. The temperature on the furnace was maintained constant for each test. After an experimental run, the reactor was cooled down with purging of welding grade Ar gas until the system temperature was close to the room temperature. Furthermore, the quartz reactor with solid residues was cleaned by following the procedures in section 3.6 of Chapter 3 after each run.

5.2.4 Solid, liquid and gas characterisation

A Philips PW1700 series diffractometer with Co $K\alpha_1$ radiation was used to get the crystal phases of the sands at an X-ray wavelength of 1.78896 Å. An ATAGO NAR-3T Abbe refractometer was used for analysing the liquid which was trapped in a condenser after the reactor. The gas composition was analysed by an Agilent 3000 micro-GC. A SSM-5000A TOC-L analyser of SHIMADZU was used to detect the total carbon amount on the catalyst. The H_2S concentrations in the inlet and outlet gases were measured by Dräger tubes from Dräger Safety AG & Co. KGaA.

5.3 Results and discussion

5.3.1 Effects of temperature and titanomagnetite reduction on NH_3 decomposition in Ar gas

Experiments on NH_3 decomposition in Ar gas were conducted at four different temperatures of 500, 600, 750 and 850°C, respectively, in the quartz reactor. The experiments were first conducted with empty rector to examine if there was any significant thermal cracking of NH_3. After this, unprocessed titanomagnetite and H_2-reduced titanomagnetite were tested, respectively. The experimental results are shown in Figure 5.1 from which it is found that the thermal cracking of NH_3 in an empty reactor was 2.1% at 500°C but this was increased to 10.1% at 600°C, 21.5% at 750°C and 23.9% at 850°C. Importantly, the experimental results show that the H_2-reduced titanomagnetite has a significantly higher activity for NH_3 decomposition than the unprocessed titanomagnetite at the same operation temperature. As observed in Figure 5.1, with the application of reduced titanomagnetite, the decomposition of NH_3 was 97.8% at 500°C, 99.7% at 600°C and 100% at 750°C and 850°C. However, when the unprocessed titanomagnetite was used as the catalyst, the corresponding NH_3 decomposition rates were 31.6% at 500°C, 34.0% at 600°C, 83.9% at 750°C and 93.2% at 850°C. To understand the performance differences between the unprocessed and the reduced titanomagnetites, these catalysts were analysed before their use by XRD analyser and the results are shown in Figure 5.2 for the unprocessed titanomagnetite and in Figure 5.3 for the reduced titanomagnetite. For these figures, it is found that there was a significant quantity of Fe_3O_4 phase on the unprocessed sand whereas the Fe_3O_4 phase was transferred to α-Fe phase on the reduced sand. The α-Fe phase is believed to have higher activity to decompose NH_3 than the Fe_3O_4 phase on the unprocessed sand.

In the experiments with Ar gas, the outlet gas was analysed by a micro-GC from which H_2 and N_2 gases were detected and their concentrations determined. As the inlet gas only contained NH_3 and Ar, the resultant H_2 and N_2 must have come from the ammonia decomposition reaction as follows.

Ammonia decomposition reaction: $2NH_3 \leftrightarrow N_2 + 3H_2$ (5.1)

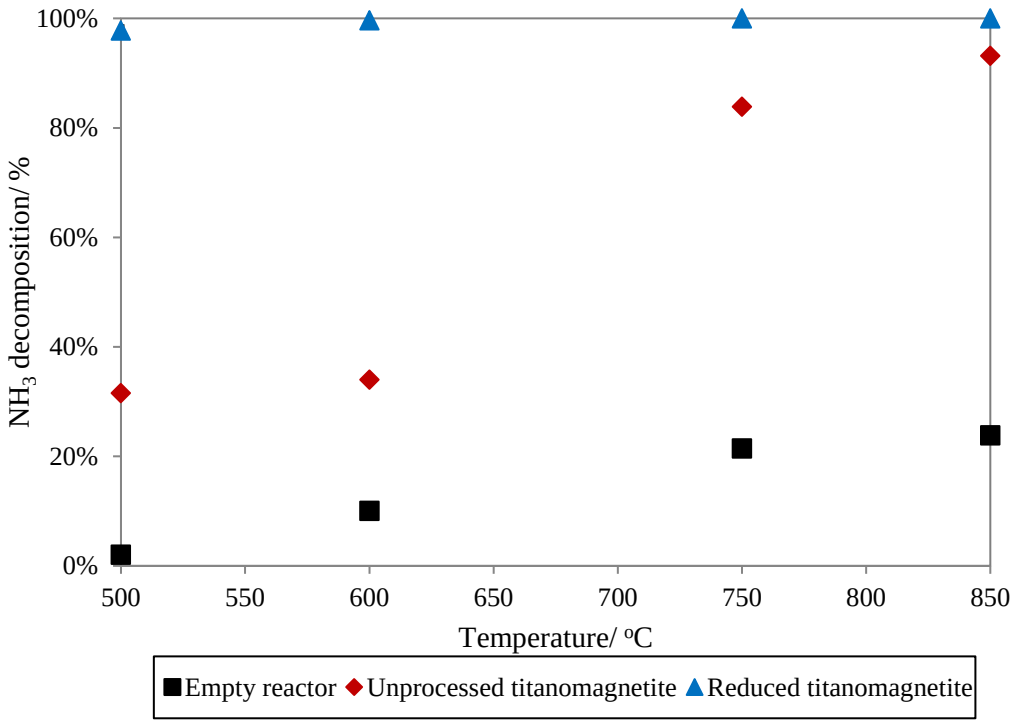

Figure 5.1 NH_3 decomposition in Ar gas at different temperatures with and without catalyst. In the figure, each point represents the average value of two measurements.

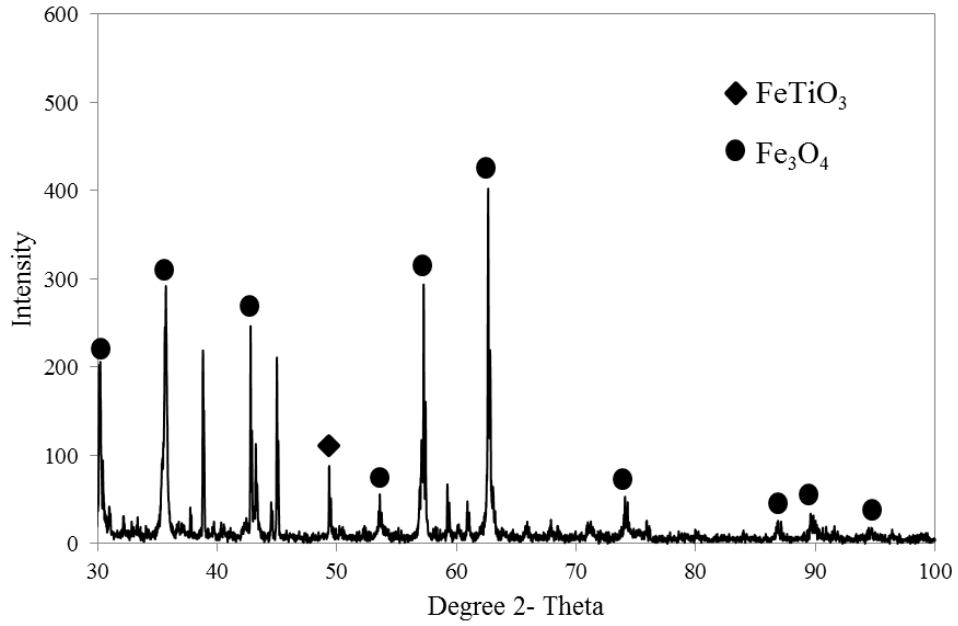

Figure 5.2 The XRD graph of the unprocessed titanomagnetite.

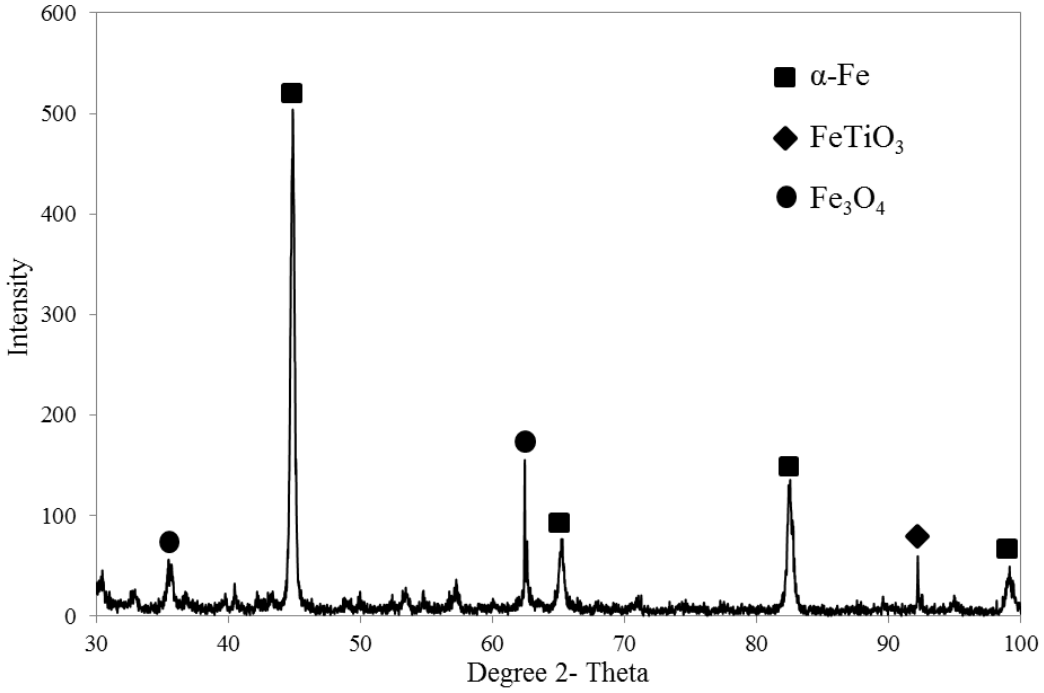

Figure 5.3 The XRD graph of the reduced titanomagnetite.

5.3.2 NH_3 removal from the simulated producer gas (without H_2S) by the reduced titanomagnetite

5.3.2.1 NH_3 decompositions in the simulated producer gas

The experiments of NH_3 removal in the simulated producer gas were carried out with H_2-reduced titanomagnetite at 500, 750 and 850°C, respectively. The results are shown in Figure 5.4 from which it is found that the average NH_3 decompositions are 28.4±3.4%, 94.7±2.8% and 98.4±0.4%, respectively, at 500, 750 and 850°C. These results illustrate that the reduced titanomagnetite is more effective to remove NH_3 at high temperatures. However, the efficiency for the NH_3 removal in the simulated producer gas was lower than that in Ar gas, which was believed to be due to the effects of side reactions and the other gas species (H_2, CO, CO_2 and CH_4) in the simulated producer gas. This assumption was supported by the study of Sarioğlan et al. [25] who investigated the effects of gas composition in the mixture of H_2, CO, CO_2, CH_4 and N_2 on NH_3 decomposition using an iron catalyst (Fe/HZβ). In the study of Sarioğlan et al. [25], side reactions were also identified which will be further discussed in the following sections of this chapter.

Comparing with other catalysts reported in the literature, the reduced titanomagnetite is found to have relatively higher activity at temperatures of 750-850°C for NH_3 decomposition in the simulated producer gas. It was reported that an iron catalyst (Fe/HZβ) only had the ability to remove 46% of NH_3 at 700°C with inlet concentration of 800 ppmv in the simulated producer gas (20 vol.% CO, 20 vol.% CO_2, 30 vol.% H_2 and 5 vol.% CH_4 in N_2) [25]. In a separate study [16], reduced limonite ore was tested and its efficiency was 45-80% at 750°C for removing NH_3 with an inlet concentration of 2000 ppmv from the simulated producer gas (20 vol.% CO and 10 vol.% H_2 in helium). In this study [16], it was found that the NH_3 decomposition was increased to 90%

when 3 vol.% H_2O or 10 vol.% CO_2 was added to the simulated producer gas. Similar results were also reported by Ohtsuka et al. [26] who tested an iron catalyst with 2 wt.% Fe supported on coal char and found that this catalyst had very low (10%) efficiency at 750°C for NH_3 decomposition in the syngas of 2000 ppmv (NH_3, 20 vol.% CO and 10 vol.% H_2 in helium). However, its performance was improved significantly with 95% NH_3 decomposition when 7 vol.% CO_2 was added to the syngas [26].

Mojtahedi and Abbasian [27] tested three Ni-based catalysts with different Ni contents and a Ru-based catalyst for NH_3 reduction in the simulated producer gas from an air-blown gasifier (2100 ppmv NH_3 in the gas mixture of 15.1 vol.% H_2O, 16.7 vol.% H_2, 16.5 vol.% CO, 10.3 vol.% CO_2, and 4.6 vol.% CH_4 in N_2). The NH_3 decomposition was found to vary from 50% to 90%, depending on operation temperatures (700-900°C) and catalyst applied. These studies confirmed that the NH_3 decomposition by iron catalysts is affected by the gas composition.

In addition, the other components such as H_2S and tars in the practical producer gas of biomass gasification also have impacts on the performance of the catalysts for NH_3 decomposition. Hongrapipat et al. [28] reported that when 230 ppmv H_2S was added to the Ar gas, the NH_3 decomposition at 500°C by using the reduced titanomagnetite was reduced from 92% to 30%. However, the authors [28] also found that the effect of H_2S on NH_3 decomposition in Ar gas was mitigated when the temperature was increased to 700°C at which the NH_3 decomposition was slightly reduced from 100% to 96% when 230 ppmv H_2S was added. Tsubouchi et al. [17] found that there was no obvious negative effect of introducing 50-500 ppm H_2S to the gas on the reduced limonite for NH_3 decomposition in helium gas at 750°C. However, if 2000 ppm H_2S was introduced, the activity of the reduced limonite was significantly suppressed for NH_3 decomposition. Moreover, the authors [17] also noticed that at an operation temperature of 650°C,

the addition of 100 ppmv H_2S to the test gas had a remarkably negative effect on the NH_3 decomposition due to the conversion of active α-Fe phase to FeS phase on the reduced limonite whereas this conversion was insignificant at 750°C. The impact of 230 ppmv H_2S on the activity of the reduced titanomagnetite for NH_3 decomposition in the simulated gas will be discussed in Section 5.3.3 of this chapter.

Tar compounds in the producer gas also deactivated the catalysts for NH_3 decomposition due to carbon deposition from tar cracking at high temperatures [29]. It is recommended that when applying the reduced titanomagnetite in practical biomass gasification for NH_3 removal, tars and H_2S should be removed first. In addition, more investigations are recommended to determine the effects of individual gas species in the producer gas on NH_3 decomposition by the reduced titanomagnetite.

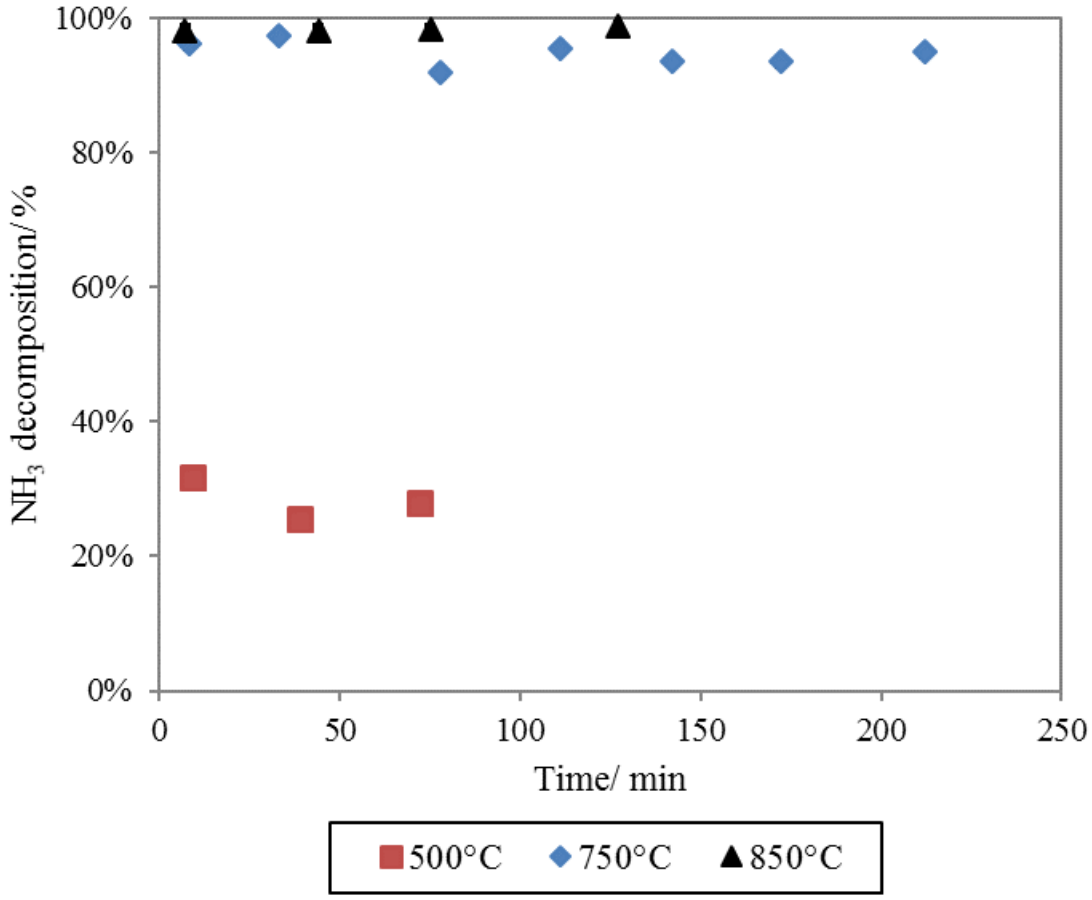

Figure 5.4 NH_3 decompositions using reduced titanomagnetite in the simulated producer gas at 500, 750 and 850°C. In the figure, each point represents the average value of two measurements.

5.3.2.2 Water and carbon formation

During the experiments, condensate was found in the outlet pipe. Therefore, a glass bottle in an ice bath was employed to condense the vapour product from the reactor, then the liquid product was weighed and analysed by Abbe refractometer. It was found that the liquid collected was water, which confirms that the reverse water-gas shift reaction as follows occurred during the NH_3 decomposition.

Reverse water-gas shift reaction: $H_2 + CO_2 \leftrightarrow H_2O + CO$ (5.2)

The rate of water vapour production was calculated as the total quantity (moles) of water collected in a run divided by the duration of valid time, which were 0.00017, 0.00018 and 0.00013 mol/s, respectively, for the operation temperatures of 500, 750 and 850°C. Although it is known that the reverse water-gas shift reaction is favoured at high temperatures and promoted by α-Fe catalyst [28], the H_2O production was not increased with operation temperature in these experiments, which indicates that other side reactions also occurred in the reactor.

In order to identify the other side reactions, the reduced titanomagnetites used in the experiments were analysed by XRD analyser and the results are shown in Figure 5.5, Figure 5.6 and Figure 5.7 for operation temperature of 500, 750 and 850°C, respectively. As observed in Figure 5.5, there was a significant amount of Fe_3C on the catalyst used at 500°C from which the active phase of α-Fe was almost disappeared. However, for catalysts used at 750 and 850°C, a great amount of α-Fe phase, which catalysed the NH_3 decomposition, still existed as observed in Figure 5.6 and Figure 5.7 in which Fe_3C phase was not found. These results show that carbon was formed during the NH_3 decomposition at 500°C. For quantification of the carbon formation, the catalyst used at 500°C was further analysed by TOC-L analyser and 16.3±1.0 wt.% of the used catalysts was found to be pyrolytic carbon. Based on this result and the catalyst mass, the rate of carbon formation was found to be 0.00010 mol/s. Part of the carbon measured may be formed from the Boudouard reaction [26, 30], which is favoured at low temperatures and enhanced by the applied Fe-based catalyst. In addition, Fe_3C could be formed from the reactions of α-Fe with CO in the simulated producer gas or the carbon produced in the reactor. The possible reactions related to carbon formation are shown as follows:

Boudouard reaction: $2CO \leftrightarrow CO_2 + C_s$ (5.3)

Fe-CO reaction: $3Fe + C_s \leftrightarrow Fe_3C$ (5.4)

Fe-C reaction: $3Fe + 2CO \leftrightarrow Fe_3C + CO_2$ (5.5)

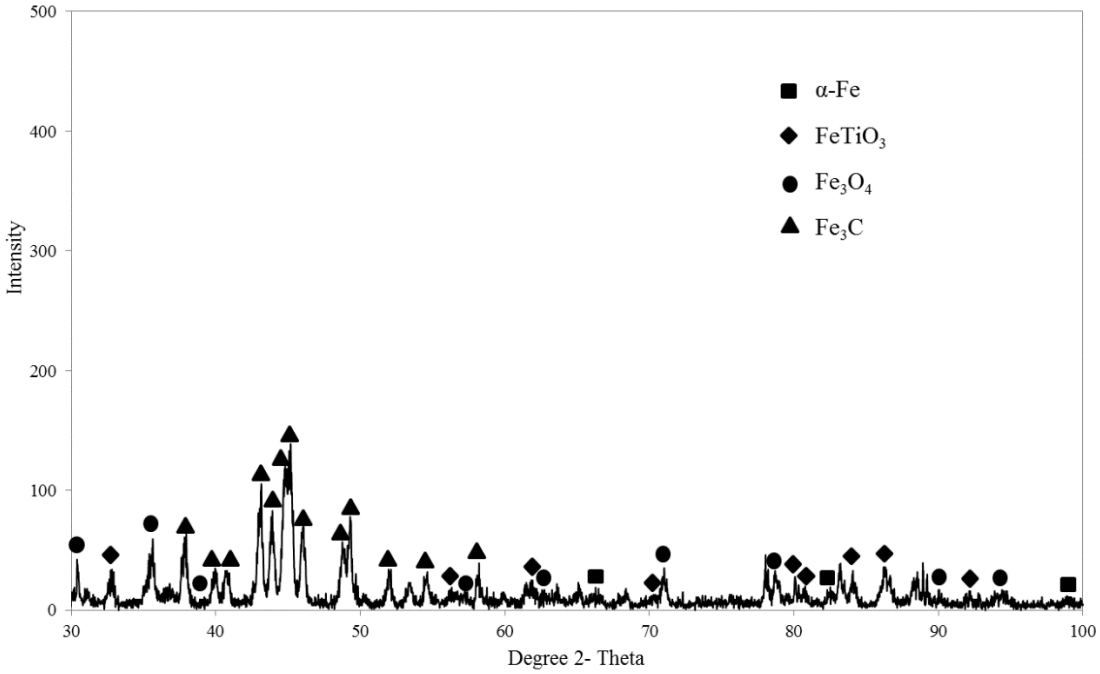

Figure 5.5 XRD graph for the reduced titanomagnetite used at 500°C in NH_3 removal from the simulated producer gas.

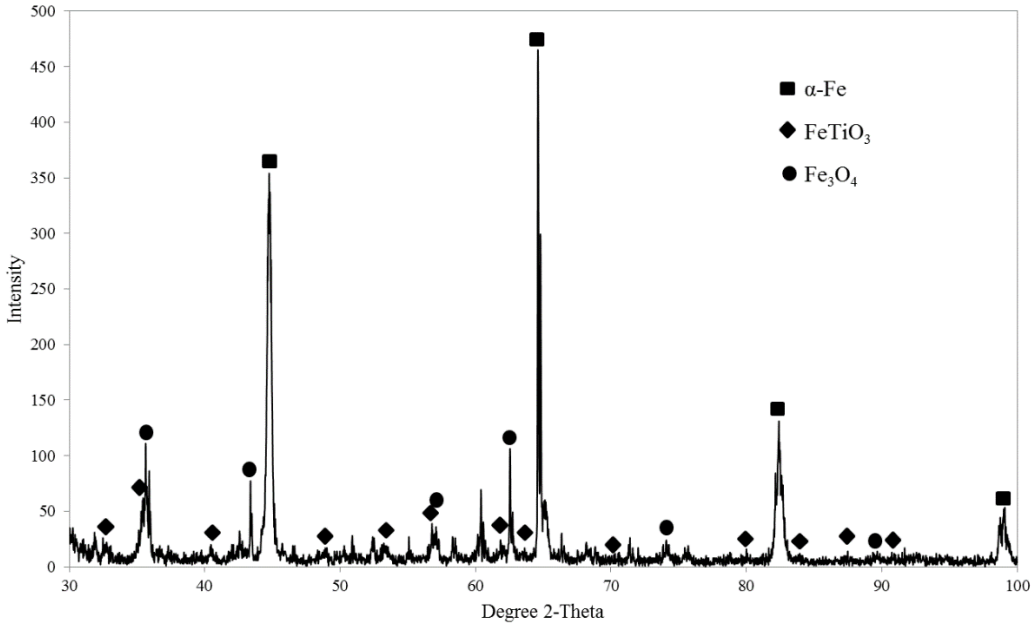

Figure 5.6 XRD graph for the reduced titanomagnetite used at 750°C in NH_3 removal from the simulated producer gas.

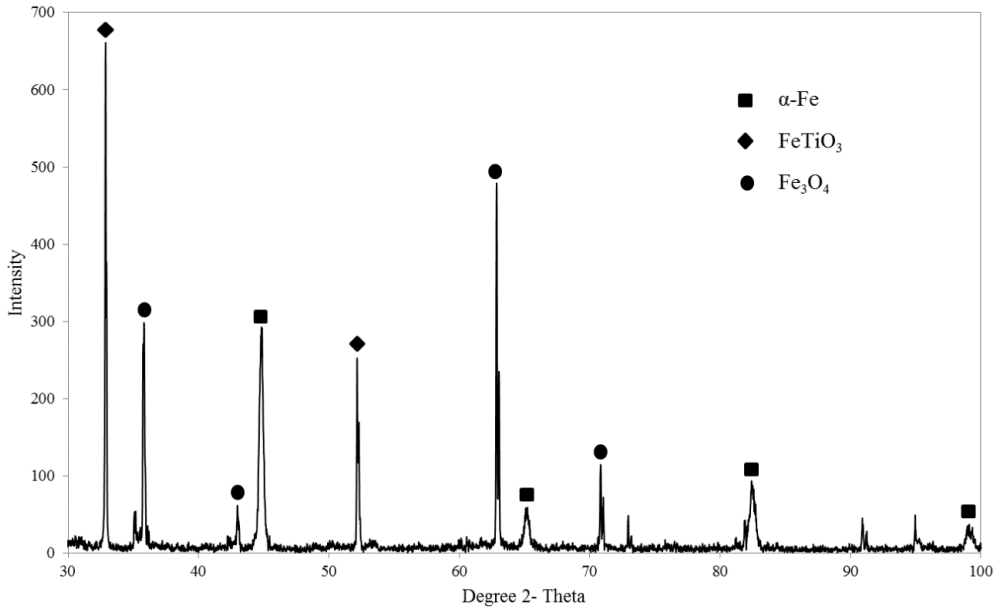

Figure 5.7 XRD graph for the reduced titanomagnetite used at 850°C in NH_3 removal from the simulated producer gas.

5.3.2.3 The side reactions in catalytic NH_3 decomposition from the simulated producer gas

The composition of water-free outlet gas from the reactor was analysed by the micro-GC, and the results are given in Table 5.2, Table 5.3 and Table 5.4, respectively, for operation temperatures of 500°C, 750°C and 850°C. From these tables, differences of the outlet gas compositions in different runs have been observed which are attributed to side chemical reactions. The H_2 and N_2 generated from NH_3 decomposition will not be included because their contributions to the concentrations of H_2 and N_2 in the outlet producer gas were so low which fall within the experimental errors.

At 500°C, the reverse water-gas shift reaction (Eq. 5.2) and the Boudouard reaction (Eq. 5.3) have already been confirmed to occur in the reactor because significant water and carbon were detected. As the methane concentration in the outlet gas was increased, the carbon Methanation reaction (Eq. 5.6) was also expected to occur which is favoured with the α-Fe catalyst at low temperatures under atmospheric pressure [31]. During the NH_3 removal in the simulated gas (21% CO, 16% H_2 and 3400 ppm NH_3 in N_2), Wang et al. [30] also proposed that these three reactions, the reverse water-gas shift reaction, the Boudouard reaction and the carbon Methanation reaction, were the basic and independent side reactions which may be combined to form other effective reactions. The authors [30] also reported that the Boudouard and the carbon Methanation reactions were thermodynamically favoured at low temperatures. From the above analysis, the Boudouard reaction, which caused carbon deposition and carbide formation on the catalyst, is believed to be the major contributor to the reduction of NH_3 decomposition by reduced titanomagnetite at 500°C in the simulated producer gas (Figure 5.4) as compared with that in Ar gas (Figure 5.1). Similar findings were reported elsewhere [26, 29].

Carbon Methanation reaction: $2H_2 + C \leftrightarrow CH_4$ (5.6)

Therefore, the reverse water-gas shift reaction (RWGSR), the Boudouard reaction (BR) and the carbon Methanation reaction (CMR) were used for the calculations for NH_3 decomposition at 500°C, and the results are presented in Table 5.2. For the tested simulated producer gas, it was assumed that the Ideal Gas Law was applicable in the range of conditions tested. In this way, the total inlet gas volumetric flow rate of 3.65 L/min at standard conditions was converted to the molar flow rate of 0.00268 mol/s. The molar flow rate of each gas component in the inlet simulated producer is shown in column 4 of Table 5.2. Since the three basic side reactions were independent, they can be used for the calculations of the product flow rate independently. For example, when the reverse water-gas shift reaction was first considered, H_2 and CO_2 were consumed while H_2O and CO were generated, and the corresponding molar flow rates and concentrations were changed. In the experiment at 500°C, the water production rate was measured to be 0.00017 mol/s which was used as the reference to determine changes in molar flow rates (column 5) and concentrations (column 6) of H_2, CO and CO_2 based on the reverse water-gas shift reaction. Secondly, the measured concentrations of CO (18.4 vol.% or 0.00044 mol/s) was used as the reference for the subsequent Boudouard reaction to determine changes in CO_2 molar flow rate as well as carbon formation rate (0.00012 mol/s), which results are shown in column 7. Finally, the carbon Methanation reaction was included and the measured carbon generation rate (0.00010 mol/s) was used as the reference to calculate changes of molar flow rates (column 9) and concentrations of H_2 and CH_4 (column 10). After having considered these three side reactions, the resultant molar flow rates and concentrations of all gaseous species, as well as generation rates of water and carbon, are determined as shown in the last two columns in Table 5.2. By comparing the calculated gas composition in column 10 with the measured composition of water-free outlet gas in column 3, it

is found that the calculated concentrations of all gaseous species are in close agreement with those measured from the experiments.

At 750°C, slightly more quantity of water (0.00018 mol/s) was found in the experimental outlet gas than that collected in the experiment of 500°C (0.00017 mol/s), but no carbon was detected on the catalyst. Therefore, the reverse water-gas shift reaction also occurred during the experiment, from which the produced H_2O is not expected to significantly affect the efficiency of NH_3 decomposition. It was also found that in the experiment the outlet concentration of CO was increased while those of CO_2 and CH_4 were decreased which indicates that the reverse Boudouard reaction and the reverse carbon Methanation reaction occurred at this higher temperature. These two reverse reactions can be combined to one effective reaction, termed as carbon dioxide reforming reaction (CDRR) as given in Eq. (5.7).

Carbon dioxide reforming reaction: $CH_4 + CO_2 \leftrightarrow 2CO + 2H_2$ (5.7)

Therefore, in analysis of the side reactions in the catalytic decomposition of NH_3 at 750°C, the reverse water-gas shift reaction was used to calculate the gas molar flow rates (column 5 in Table 5.3) and composition (column 6 in Table 5.3) in the outlet gas by using the water production rate (0.00018 mol/s) as the reference. The carbon dioxide reforming reaction (Eq. 5.7) was also included and the newly calculated gas flow rates and compositions are given in columns 7 and 8, respectively. By comparing the calculated concentrations of H_2 and CH_4 in column 8 with those measured in the experiment (column 3), very close agreement was observed.

However, the calculated CO_2 concentration was higher and the calculated CO concentration was lower than the corresponding measured values from the experiments. It is expected that CO_2 reacted with the α-Fe on the catalyst at high temperatures to produce CO. To verify this assumption, a separate experiment was conducted by using CO_2 and Ar mixture gas instead of

simulated gas at 750°C in which CO was detected by micro-GC in the outlet gas. From the previous discussion, it was found that there was more Fe_3O_4 phase on the used reduced titanomagnetite at 750°C in simulated gas (Figure 5.6) than the fresh reduced titanomagnetite (Figure 5.3). Therefore, iron oxidation reaction with CO_2 (Eq. 5.8) occurred and was also included in the calculations of gaseous products in the outlet gas at 750°C, and the results of gas composition are given in the last column (column 9) of Table 5.3. By comparing the measured values of gas composition in column 3 with those calculated in column 9, very close agreement is found confirming the proposed side reactions in the NH_3 decomposition. Therefore, it can be concluded that the reverse water-gas shift reaction, the carbon dioxide reforming reaction and the iron oxidation reaction are the main side reactions occurred in the reactor at 750°C.

Iron oxidization reaction: $4CO_2 + 3Fe \leftrightarrow Fe_3O_4 + 4CO$ (5.8)

At 850°C the same side reactions occurred as those at 750°C, although the carbon dioxide reforming reaction was significantly boosted by the increased temperature. Similar calculations were performed for 850°C and the results are given in Table 5.4. The decreased concentrations of CO_2 and CH_4 in the simulated producer gas at 850°C are preferred for FT synthesis [32].

Table 5.2 Comparison of calculated and measured molar flowrates and concentrations of species in the outlet simulated producer gas in catalytic decomposition of NH_3 at 500°C.

1	2	3	4	5	6	7	8	9	10
Gas species and carbon	Inlet gas volume composition, vol%	Measured dry outlet gas volume composition by micro-GC, vol%	Inlet molar flow rate, mol/s	Calculated molar flow rate after RWGSR, mol/s	Calculated dry gas volume composition after RWGSR, vol%	Calculated molar flow rate after RWGSR and BR, mol/s	Calculated dry gas volume composition after RWGSR and BR, vol%	Calculated molar flow rate after RWGSR, BR and CMR, mol/s	Calculated dry gas volume composition after RWGR, BR and CMR, vol%
H_2	47.6±0.4	42.8±2	0.00128	0.00111	44.0	0.00110	46.2	0.00107	44.9
CO	18.9±0.4	18.4±2	0.00051	0.00068	27.0	0.00044	18.4	0.00044	18.6
CO_2	19.1±0.4	19.3±2	0.00051	0.00034	13.5	0.00046	19.2	0.00046	19.3
CH_4	14.4±0.4	19.5±2	0.00039	0.00039	15.5	0.00039	16.2	0.00041	17.2
H_2O	0.0	0.0	0.00000	**0.00017**	0.0	**0.00017**	0.0	**0.00017**	0.0
C	0.0	0.0	0.00000	0.00000	0.0	0.00012	0.0	**0.00010**	0.0
Note: RWGSR= Reverse Water-Gas Shift Reaction; BR= Boudouard Reaction; CMR= Carbon Methanation Reaction									

Table 5.3 Comparison of calculated and measured molar flowrates and concentrations of species in the outlet simulated producer gas in catalytic decomposition of NH_3 at 750°C.

1	2	3	4	5	6	7	8	9
Gas species	Inlet gas volume composition, vol%	Measured dry outlet gas volume composition, vol%	Inlet molar flow rate, mol/s	Calculated gas molar flow rate after RWGSR, mol/s	Calculated dry gas volume composition after RWGSR, vol%	Calculated gas molar flow rate after RWGSR and CDRR, mol/s	Calculated dry gas volume composition after RWGSR and CDRR, vol%	Calculated dry gas volume composition after RWGSR and CDRR as well as IOR, vol%
H_2	47.6±0.4	45.4±2	0.00128	0.00110	43.8	0.00118	45.7	45.7
CO	18.9±0.4	31.5±2	0.00051	0.00069	27.5	0.00077	29.8	31.4
CO_2	19.1±0.4	9.8±2	0.00051	0.00033	13.3	0.00029	11.2	9.6
CH_4	14.4±0.4	13.3±2	0.00039	0.00039	15.4	0.00034	13.3	13.3
H_2O	0.0	0.0	0.00000	**0.00018**	0.0	**0.00018**	0	0
Note: RWGSR= Reverse Water-Gas Shift Reaction; CDRR=Carbon Dioxide Reforming Reaction; IOR= Iron Oxidization Reaction								

Table 5.4 Comparison of calculated and measured molar flowrates and concentrations of species in the outlet simulated producer gas in catalytic decomposition of NH_3 at 850°C.

1	2	3	4	5	6	7	8	9
Gas species	Inlet gas volume composition, vol%	Measured dry outlet gas volume composition, vol%	Inlet molar flow rate, mol/s	Calculated gas molar flow rate after RWGSR, mol/s	Calculated dry gas volume composition after RWGSR, vol%	Calculated gas molar flow rate after RWGSR and CDRR, mol/s	Calculated dry gas volume composition after RWGSR and CDRR vol%	Calculated dry gas volume composition after RWGSR and CDRR as well as IOR, vol%
H_2	47.6±0.4	49.7±2	0.00128	0.00115	44.9	0.00142	50.2	50.2
CO	18.9±0.4	35.1±2	0.00051	0.00064	25.0	0.00091	32.1	35.0
CO_2	19.1±0.4	6.3±2	0.00051	0.00038	15.0	0.00025	8.8	5.9
CH_4	14.4±0.4	8.9±2	0.00039	0.00039	15.1	0.00025	8.9	8.9
H_2O	0.0	0.0	0.00000	**0.00013**	0.0	**0.00013**	0	0
Note: RWGSR= Reverse Water-Gas Shift Reaction; CDRR=Carbon Dioxide Reforming Reaction; IOR= Iron Oxidization Reaction								

5.3.2.4 Equilibrium gas composition with the three side reactions

In order to investigate the effect of operation temperature on gas composition, equilibrium gas composition has been calculated as a function of reaction temperature based on three independent side reactions: the reverse water-gas shift reaction, the (reverse) Boudouard reaction and the (reverse) carbon Methanation reaction. NH_3 decomposition reaction and the iron oxidation reaction were not included because their influence on the gas composition was insignificant. The operation pressure in the reactor during the experiments was 114 kPa which has been used for the equilibrium calculations. Details of the calculation are given in Appendix B. The results of calculated equilibrium gas composition at different temperatures are shown in Figure 5.8, in which the measured values (as discrete points) are included for comparison. From Figure 5.8, it is found that the measured gas composition follows the trends of equilibrium gas composition as a function of reaction temperature which further confirms that the three side reactions can reflect the process of NH_3 decomposition in the simulated producer gas using the catalyst of reduced titanomagnetite.

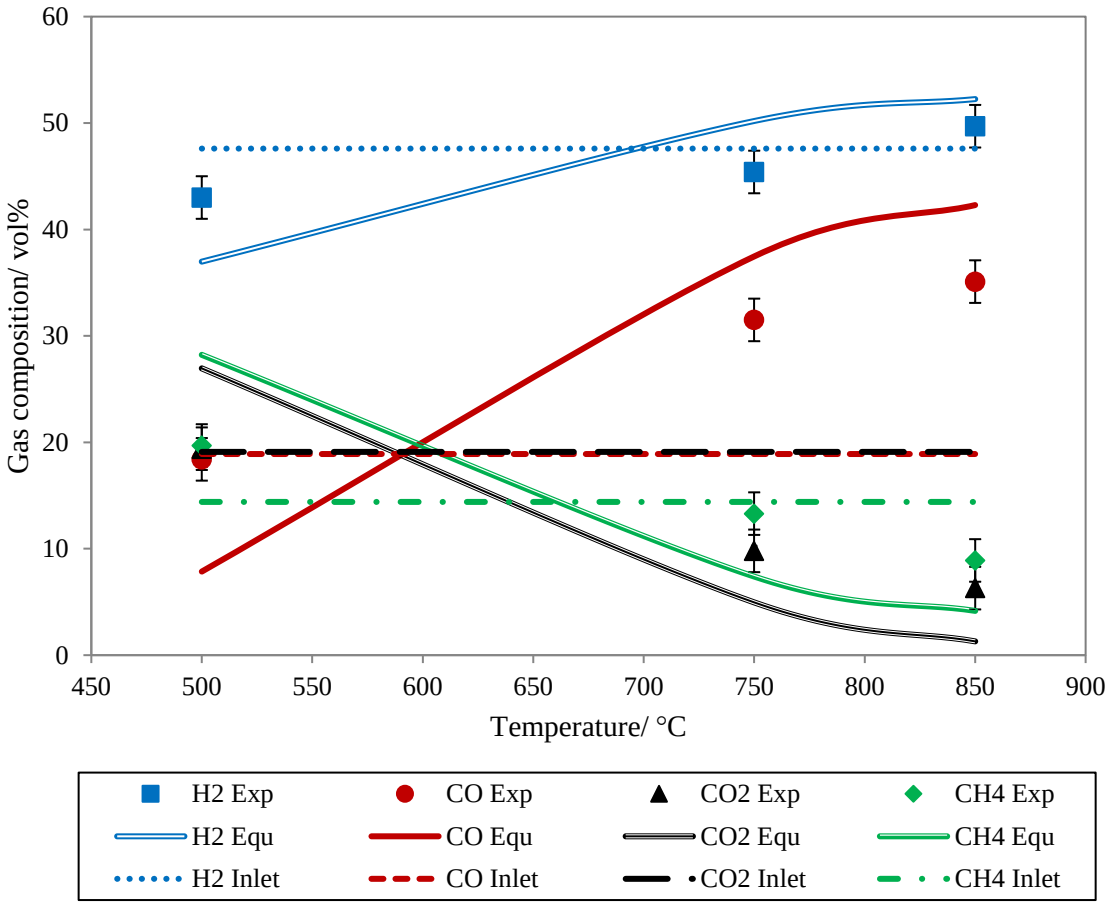

Figure 5.8 Calculated equilibrium gas composition and comparison with experimentally measured values at different reaction temperatures in simulated producer gas for NH_3 decomposition (The dotted lines represent the feed gas composition of the simulated gas).

5.3.3 The effect of H_2S on the NH_3 removal in the simulated producer gas

To study the effect of H_2S on the activity of the reduced titanomagnetite for NH_3 removal in the simulated producer gas, a gas mixture of 230±20 ppmv H_2S and 2300±100 ppmv NH_3 in the simulated producer gas was investigated firstly in this section. Figure 5.9 shows the NH_3 decompositions in the above gas mixture by the reduced titanomagnetite at 750°C with elapsed time. It is illustrated that H_2S of 230 ppmv concentration in the simulated producer gas had a

significantly adverse effect on the activity of reduced titanomagnetite for NH_3 decomposition, which was reduced gradually from 96.8% to 67.0% in 238 min. Hongrapipat et al. [28] did similar studies but in Ar gas, it was found that the NH_3 decomposition was reduced from 92% to 30% rapidly by the reduced titanomagnetite after 230 ppmv H_2S was added to the gas mixture of 2000 ppmv NH_3 in Ar gas at 500°C. However, the authors [28] also found that the effect of H_2S on NH_3 decomposition from Ar gas was mitigated when the temperature was increased to 700°C that the NH_3 decomposition was only reduced from almost 100% to 96-97% after 230 ppmv H_2S was added. Therefore, it can be concluded that effect of H_2S on the NH_3 decomposition by the reduced titanomagnetite pronouncedly depends on the experimental temperature and the gas atmosphere.

During the experiment, three NH_3 decompositions were also tested by NH_3 Dräger tubes purchased from Dräger Safety AG & Co. KGaA which the results showed very close agreement with those determined by ISE method. Moreover, the H_2S adsorptions by the reduced titanomagnetite were also measured by H_2S Dräger tubes which the results are presented in Figure 5.9 as well. It is indicated that reduced titanomagnetite at high temperature (750°C) was not favoured for H_2S adsorption in the simulated producer gas, which showed agreement with the findings in Chapter 4.

To determine the effect of H_2S on the reduced titanomagnetite, the used reduced titanomagnetite was analysed by XRD analyser after the experiment. The XRD graph is given in Figure 5.10, which shows that troilite (FeS) was formed during the NH_3 decomposition. Therefore, the FeS formation on the reduced titanomagnetite could be one of the reasons for the NH_3 decomposition reduction because it poisoned the active α-Fe sites on the catalyst. However, it is inconvincible to use this single reason to explain the significant reduction of NH_3 decomposition because there is still a great amount of α-Fe phase on the reduced titanomagnetite, shown in Figure 5.10, which

should still have high activity for NH_3 decomposition. Therefore, another plausible explanation is the competition between H_2S and NH_3 at the active α-Fe sites.

To determine the recoverability of the reduced titanomagnetite for NH_3 decomposition after exposed to 230 ppmv of H_2S for a period of time in the simulated producer gas, another experimental run was conducted at 750°C that the reduced titanomagnetite was exposed to 2300 ppmv NH_3 in the simulated producer gas in the initial 88 min (phase 1), and thus 230 ppmv H_2S was added to the gas mixture subsequently for 150 min (phase 2); afterwards, it was followed by using 2300 ppmv NH_3 in the simulated producer gas again for 116 min (phase 3). The NH_3 decompositions at those three phases are shown in Figure 5.11. In addition, at phase 3, H_2S concentrations in the outlet gas were tested by H_2S Dräger tubes which the results can be found in Figure 5.11 as well.

From the Figure 5.11, it is noticed that the NH_3 decomposition at phase 1 was as high as approximate 97% which was similar to the results at 750°C shown in Figure 5.4. However, the NH_3 decomposition was reduced to 77.1% with the presence of 230 ppmv H_2S at phase 2 which showed similar phenomenon in Figure 5.9 that H_2S could reduce the activity of reduced titanomagnetite for NH_3 decomposition gradually. After the 230 ppmv H_2S was deducted at phase 3, the NH_3 decomposition remained almost steadily around 80%. Hongrapipat et al. [28] reported that the activity of the reduced titanomagnetite for decomposing NH_3 in Ar gas was not restored but remained steadily for 2 hours (after which experiments were ceased) after it was exposed to 230 ppmv H_2S for 6 hours. However, in this experiment, phase 3 was only conducted for 116 min, it cannot be concluded that the activity of the reduced titanomagnetite will be maintained steadily afterward or will be recovered slowly over a long period of time.

Nevertheless, in this research, it is not suggested that using the reduced titanomagnetite to remove NH_3 in the simulated producer gas with the presence of high concentration of H_2S such as 230 ppmv. However, it also should be noticed that lower concentration of H_2S might have reduced adverse effect on the reduced titanomagnetite for NH_3 decomposition in the simulated producer gas, therefore, more studies should be conducted in the future to determine the H_2S concentration in the simulated producer gas that the reduced titanomagnetite can tolerate.

Furthermore, during phase 3, H_2S was found in the outlet gas even though there was no H_2S in the inlet gas. A similar finding was observed by Tsubouchi et al. [17] that H_2S was obtained when FeS was used for NH_3 conversion at 750°C. The authors explained that the H_2S was evolved from the reaction between FeS and H_2 in the atmosphere, and the reaction is shown in Eq. 5.9 as followed.

FeS reduction reaction: $FeS + H_2 \leftrightarrow Fe + H_2S$ (5.9)

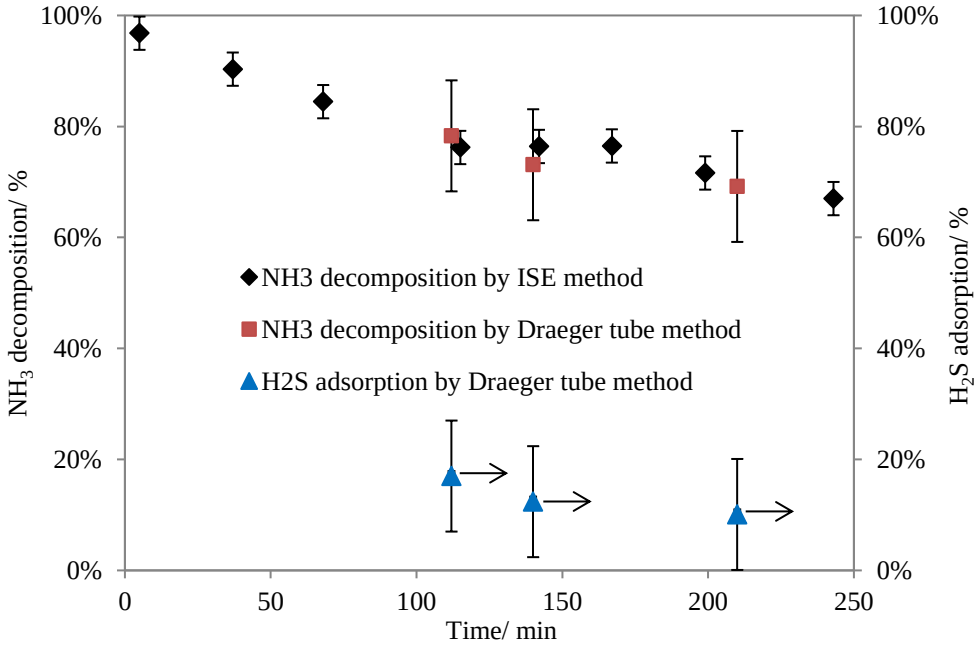

Figure 5.9 NH_3 decomposition and H_2S adsorption in the simulated gas containing 2300 ppmv NH_3 and 230 ppmv H_2S by reduced titanomagnetite at 750°C.

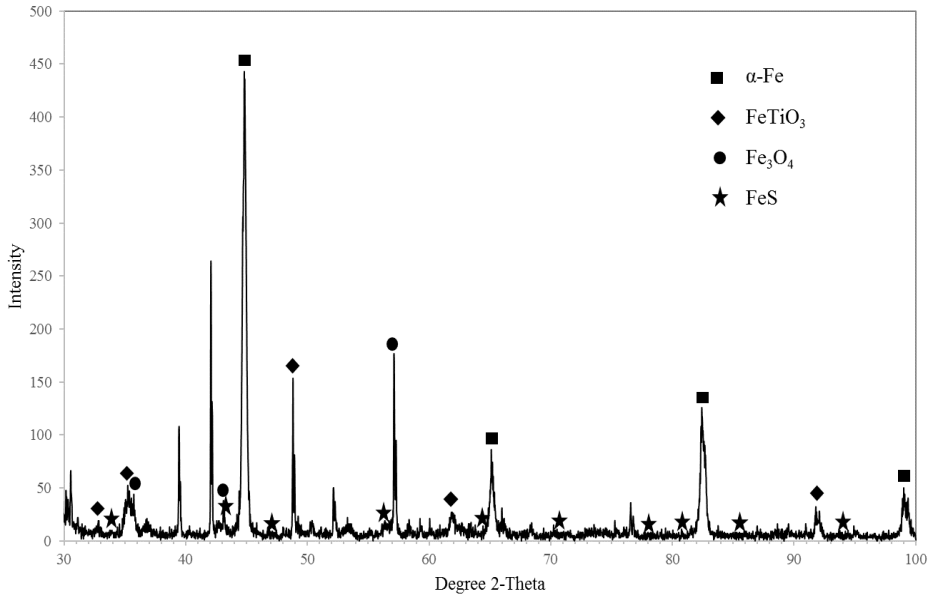

Figure 5.10 XRD graph for the reduced titanomagnetite used at 750°C for NH_3 removal from the simulated producer gas containing 2300 ppmv NH_3 and 230 ppmv H_2S.

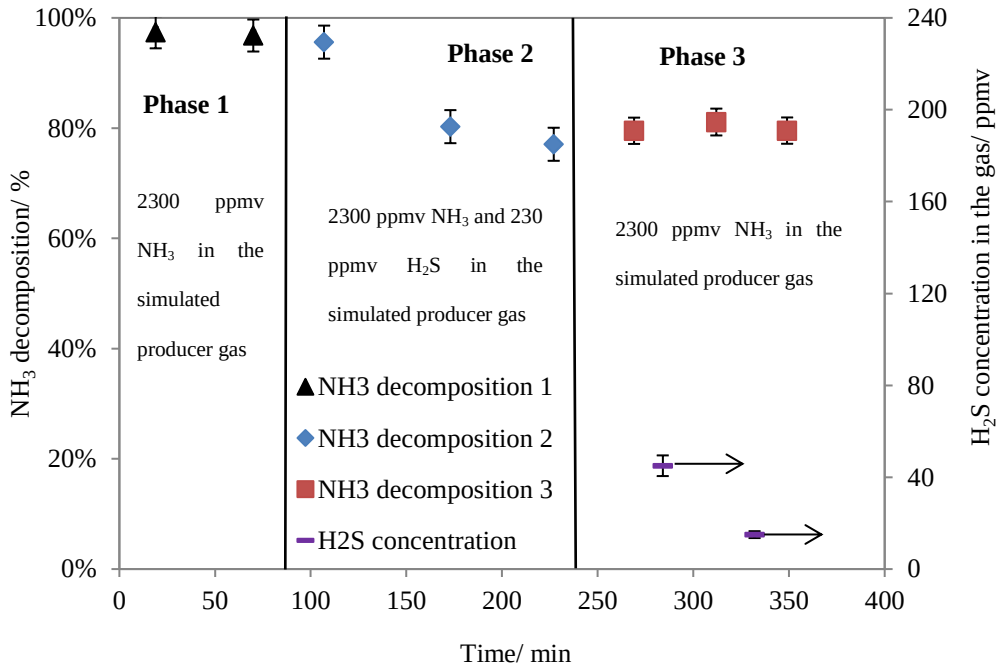

Figure 5.11 NH_3 decomposition in the simulated producer gas by reduced titanomagnetite at 750°C.

5.4 Conclusions

Both unprocessed and H_2-reduced titanomagnetites are effective to remove NH_3 in an inert gas (Ar) at high temperatures but the H_2-reduced titanomagnetite is more effective for the NH_3 removal at all temperatures. In the simulated producer gas from biomass gasification, the key reaction in the catalytic NH_3 removal is NH_3 decomposition to form H_2 and N_2. However, side reactions also occur which affect the NH_3 decomposition efficiency and the gas composition. In this study, three basic side reactions have been identified as the reverse water-gas shift reaction, the (reverse) Boudouard reaction and the (reverse) carbon Methanation reaction. The direction and the extent of these reactions are affected by the reaction temperature and feeding gas composition. At the lower temperature (500°C), the Boudouard reaction was found to be the main reaction for deactivating the reduced titanomagnetite. However, at higher temperatures (750°C and 850°C), the reverse carbon methanation reaction and the reverse Boudouard reaction are more important which reduce concentrations of CH_4 and CO_2 but increase the concentration of CO in the producer gas.

It is noticed that although the NH_3 can be effectively decomposed at 850°C, the NH_3 concentration in the reactor outlet gas may be still higher than the required level (<1 ppmv) for FT process. Moreover, in this research, 2300 ppmv NH_3 in the simulated producer gas was tested which is the worst scenario for steam gasification of most biomass. For biomass with high N content, the NH_3 concentrations in the producer gas could be higher than 2300 ppmv [4, 6]. In these cases, it is recommended that a second reactor or an alternative gas cleaning unit should be added following the proposed hot-catalytic reactor to further remove NH_3 thus to meet the required NH_3 concentration.

Furthermore, 230 ppmv H_2S in the simulated producer gas reduced the catalytic activity of the H_2-reduced titanomagnetite significantly for NH_3 decomposition at 750°C. Therefore, the proposed catalytic removal of NH_3 should follow the tar removal and H_2S removal when it is applied to a practical biomass gasification system for gas cleaning.

5.5 References

[1] J. Hongrapipat, W. L. Saw, and S. Pang, "Removal of ammonia from producer gas in biomass gasification: integration of gasification optimisation and hot catalytic gas cleaning," *Biomass Conversion and Biorefinery*, vol. 2, pp. 327-348, 2012.

[2] W. Wang, N. Padban, Z. Ye, G. Olofsson, A. Andersson, and I. Bjerle, "Catalytic hot gas cleaning of fuel gas from an air-blown pressurized fluidized-bed gasifier," *Industrial & engineering chemistry research*, vol. 39, no. 11, pp. 4075-4081, 2000.

[3] W. Mojtahedi, M. Ylitalo, T. Maunula, and J. Abbasian, "Catalytic decomposition of ammonia in fuel gas produced in pilot-scale pressurized fluidized-bed gasifier," *Fuel processing technology*, vol. 45, no. 3, pp. 221-236, 1995.

[4] J. Corella, J. M. Toledo, and R. Padilla, "Olivine or dolomite as in-bed additive in biomass gasification with air in a fluidized bed: which is better?," *Energy & Fuels*, vol. 18, no. 3, pp. 713-720, 2004.

[5] H. Cui, S. Q. Turn, V. Keffer, D. Evans, T. Tran, and M. Foley, "Contaminant estimates and removal in product gas from biomass steam gasification," *Energy & Fuels*, vol. 24, no. 2, pp. 1222-1233, 2010.

[6] J. Zhou, S. M. Masutani, D. M. Ishimura, S. Q. Turn, and C. M. Kinoshita, "Release of fuel-bound nitrogen during biomass gasification," *Industrial & engineering chemistry research,* vol. 39, no. 3, pp. 626-634, 2000.

[7] H. P. C. H. Boerrigter, D.J. Slort, H. Bodenstaff, A.J. Kaandorp, H. den Uil, L.P.L.M. Rabou, "Gas Cleaning for Integrated Biomass Gasification (BG) and Fischer-Tropsch (FT) Systems," in "Energy Research Centre of the Netherlands (ECN), Petten, The Netherlands, report RX-04-041," May 2004.

[8] P. L. Spath and D. C. Dayton, "Preliminary screening-technical and economic assessment of synthesis gas to fuels and chemicals with emphasis on the potential for biomass-derived syngas," National Renewable Energy Lab Golden Co2003.

[9] T. Bui, R. Loof, and S. Bhattacharya, "Multi-stage reactor for thermal gasification of wood," *Energy,* vol. 19, no. 4, pp. 397-404, 1994.

[10] M. Asadullah, "Biomass gasification gas cleaning for downstream applications: A comparative critical review," *Renewable and sustainable energy reviews,* vol. 40, pp. 118-132, 2014.

[11] F. Pinto, H. Lopes, R. N. André, M. Dias, I. Gulyurtlu, and I. Cabrita, "Effect of experimental conditions on gas quality and solids produced by sewage sludge cogasification. 1. Sewage sludge mixed with coal," *Energy & Fuels,* vol. 21, no. 5, pp. 2737-2745, 2007.

[12] J. Loipersböck, M. Lenzi, R. Rauch, and H. Hofbauer, "Hydrogen production from biomass: The behavior of impurities over a CO shift unit and a biodiesel scrubber used as

a gas treatment stage," *Korean Journal of Chemical Engineering*, vol. 34, no. 8, pp. 2198-2203, 2017.

[13] T. Pröll, I. G. Siefert, A. Friedl, and H. Hofbauer, "Removal of NH3 from biomass gasification producer gas by water condensing in an organic solvent scrubber," *Industrial & engineering chemistry research*, vol. 44, no. 5, pp. 1576-1584, 2005.

[14] N. Abdoulmoumine, S. Adhikari, A. Kulkarni, and S. Chattanathan, "A review on biomass gasification syngas cleanup," *Applied Energy*, vol. 155, pp. 294-307, 2015.

[15] N. Tsubouchi, H. Hashimoto, and Y. Ohtsuka, "High catalytic performance of fine particles of metallic iron formed from limonite in the decomposition of a low concentration of ammonia," *Catalysis letters*, vol. 105, pp. 203-208, 2005.

[16] N. Tsubouchi, H. Hashimoto, and Y. Ohtsuka, "Catalytic performance of limonite in the decomposition of ammonia in the coexistence of typical fuel gas components produced in an air-blown coal gasification process," *Energy & Fuels*, vol. 21, pp. 3063-3069, 2007.

[17] N. Tsubouchi, H. Hashimoto, and Y. Ohtsuka, "Sulfur tolerance of an inexpensive limonite catalyst for high temperature decomposition of ammonia," *Powder Technology*, vol. 180, pp. 184-189, 2008.

[18] N. Tsubouchi, H. Hashimoto, and Y. Ohtsuka, "High catalytic performance of magnesium cations-added limonite in the decomposition of ammonia in a simulated syngas-rich fuel gas," *Journal of Molecular Catalysis A: Chemical*, vol. 407, pp. 75-80, 2015.

[19] J. Leppälahti, P. Simell, and E. Kurkela, "Catalytic conversion of nitrogen compounds in gasification gas," *Fuel Processing Technology*, vol. 29, no. 1, pp. 43-56, 1991.

[20] J. Hongrapipat, "Removal of NH_3 and H_2S from biomass gasification producer gas," Doctor of Philosophy, Chemical and Procees Engineering, University of Canterbury, Christchurch, New Zealand, 2014.

[21] W. L. Saw and S. Pang, "The influence of calcite loading on producer gas composition and tar concentration of radiata pine pellets in a dual fluidised bed steam gasifier," *Fuel,* vol. 102, pp. 445-452, 2012.

[22] W. L. Saw and S. Pang, "Co-gasification of blended lignite and wood pellets in a 100kW dual fluidised bed steam gasifier: The influence of lignite ratio on producer gas composition and tar content," *Fuel,* vol. 112, pp. 117-124, 2013.

[23] K. Göransson, U. Söderlind, P. Engstrand, and W. Zhang, "An experimental study on catalytic bed materials in a biomass dual fluidised bed gasifier," *Renewable Energy,* vol. 81, pp. 251-261, 2015.

[24] A. Alamia, A. Larsson, C. Breitholtz, and H. Thunman, "Performance of large-scale biomass gasifiers in a biorefinery, a state-of-the-art reference," *International Journal of Energy Research,* 2017.

[25] A. Sarıoğlan, Y. Durak-Çetin, H. Okutan, and F. Akgün, "Decomposition of ammonia: The effect of syngas components on the activity of zeolite Hβ supported iron catalyst," *Chemical Engineering Science,* vol. 171, pp. 440-450, 2017.

[26] Y. Ohtsuka, C. Xu, D. Kong, and N. Tsubouchi, "Decomposition of ammonia with iron and calcium catalysts supported on coal chars," *Fuel,* vol. 83, pp. 685-692, 2004.

[27] W. Mojtahedi and J. Abbasian, "Catalytic decomposition of ammonia in a fuel gas at high temperature and pressure," *Fuel*, vol. 74, no. 11, pp. 1698-1703, 1995.

[28] J. Hongrapipat, A. C. K. Yip, A. T. Marshall, W. L. Saw, and S. Pang, "Investigation of simultaneous removal of ammonia and hydrogen sulphide from producer gas in biomass gasification by titanomagnetite," *Fuel*, vol. 135, pp. 235-242, 2014.

[29] P. Simell, E. Kurkela, P. Ståhlberg, and J. Hepola, "Catalytic hot gas cleaning of gasification gas," *Catalysis Today*, vol. 27, no. 1, pp. 55-62, 1996.

[30] W. Wang, N. Padban, Z. Ye, A. Andersson, and I. Bjerle, "Kinetics of ammonia decomposition in hot gas cleaning," *Industrial & engineering chemistry research*, vol. 38, pp. 4175-4182, 1999.

[31] C. Xu, N. Tsubouchi, H. Hashimoto, and Y. Ohtsuka, "Catalytic decomposition of ammonia gas with metal cations present naturally in low rank coals," *Fuel*, vol. 84, no. 14, pp. 1957-1967, 2005.

[32] C. H. Boerrigter H, Slort DJ, Bodenstaff H, Kaandorp AJ, denUil H, Rabou LPLM, "Gas cleaning for integrated biomass gasification (BG) and Fischer-Tropsch (FT) systems: experimental demonstration of two BG-FT systems ("Proof-of-Principle")," the Energy research Centre of the Netherlands (ECN), the NetherlandsECN-C-04-056, 2004.

6 The Effects of Temperature and Gas Species on NH_3 Removal in the Simulated Producer Gas of Biomass Gasification by H_2-Reduced Titanomagnetite

To understand the effects of the gas species in the simulated producer gas on the reduced titanomagnetite for NH_3 removal, the gas mixtures of H_2 in Ar, CO in Ar, CO_2 in Ar, and CH_4 in Ar were tested firstly at both 500 and 750°C. Afterwards, the gas mixtures of H_2 and CO in Ar and H_2, CO, and CO_2 in Ar were investigated at 500 and 750°C, respectively, to find out the combined effects of the gas species on NH_3 removal using the reduced titanomagnetite.

6.1 Introduction

Chapter 5 indicated that the activity of H_2-reduced titanomagnetite for NH_3 decomposition was reduced in the simulated producer gas compared with in Ar gas, which was due to side reactions and the gas species of the simulated producer gas. However, it was unclear that how did the side reactions and gas species affect the performance of H_2-reduced titanomagnetite for NH_3 decomposition at different temperatures.

Recently, Sarioglan et al. [1] reported the effects of H_2, CO, CO_2, CH_4, H_2S and their combinations on NH_3 decomposition with an iron catalyst, which is helpful to understand the effects of each gas and the side reactions on NH_3 decomposition. However, the NH_3 decomposition from this study was only 46.3% from the simulated gas. Moreover, this study was only for a constant operation temperature of 700°C.

Therefore, in this chapter, the effects of individual gas species (H_2, CO, CO_2 and CH_4) and their mixtures on the NH_3 decomposition using the H_2-titanomagnetite as well as the effect of operation temperatures were studied. Side reactions in the NH_3 decomposition was examined for a better understanding the mechanism of activity reduction of the catalyst when applied to practical producer gas of biomass gasification.

6.2 Materials and methods

6.2.1 Catalyst material and preparation

The H_2-reduced titanomagnetite was further employed as the catalyst for NH_3 decomposition in this chapter. The properties of titanomagnetite are available in the Section 3.1.4 of Chapter 3. The titanomagnetite preparation and H_2 reduction process have been given in Section 3.6 of Chapter 3.

6.2.2 Gases

Seven gas mixtures were prepared and tested in this chapter. These gas mixtures include: 1). simulated producer gas consisting of H_2, CO, CO_2 and CH_4; 2). H_2 in Ar; 3). CO in Ar; 4). CO_2 in Ar; 5). CH_4 in Ar; 6). H_2, CO and Ar; and 7). H_2, CO, CO_2 and Ar. The NH_3 concentration in each test gas mixture was 2300±200 ppmv. The NH_3 concentration in each test gas mixture was controlled by maintaining flow rate of a specified gas mixture of 50 vol.% NH_3 in Ar at desired value from a gas bottle which was supplied by BOC group, Australia. The simulated producer gas (No. 1) was specified based on composition of producer gas from biomass steam gasification in a dual fluidised bed (DFB) gasifier [2, 3], which was also supplied by BOC group, Australia. The gas mixtures No. 2 to No. 6 were obtained by mixing instrument grade gas species of H_2, CO, CO_2, CH_4 and Ar at pre-set flowrates of required individual gases. The composition of gas mixture No. 7 was obtained by controlling flowrate from a gas bottle purchased (50 vol.% H_2, 25 vol.% CO

and 25 vol.% CO_2) and flow rate of instrument grade Ar gas. For verifying the gas composition, the actual gas compositions were measured by an Agilent 3000 micro-GC and the uncertainties of the gas concentrations were within ±3.5%. The gas compositions of those eight gas mixtures are listed in Table 6.1.

Table 6.1 Gas compositions in dry basis of the seven gas mixtures tested in this study.

Gas I.D.	H_2, vol.%	CO, vol.%	CO_2, vol.%	CH_4, vol.%	Ar, vol.%
No. 1	47.6	18.9	19.1	14.4	0.0
No. 2	42.6	0.0	0.0	0.0	57.4
No. 3	0.0	22.2	0.0	0.0	77.8
No. 4	0.0	0.0	20.0	0.0	80.0
No. 5	0.0	0.0	0.0	15.0	85.0
No. 6	48.7	20.4	0.0	0.0	30.9
No. 7	42.8	21.3	23.7	0.0	12.2

6.2.3 Equipment setup and experimental procedures

The hot catalytic gas cleaning system introduced in Chapter 3 was still used in this study. The system information and the experimental procedures can be found in Section 3.2 and Section 3.6 of Chapter 3, respectively.

Once the operation was stable, inlet and the outlet gases were sampled by an impinging method where two bubblers in ice bath were used as trappers. The first bubbler was filled with 800 mL of 0.05M sulphuric acid (H_2SO_4) solution and the second bubbler was filled with 1600 mL of the

same solution. Details of this sampling system is available in Section 3.4.3, Chapter 3. The sampled solution containing NH_3 in the first bubbler was tested by the ISE method which has been introduced in Section 3.4.5, Chapter 3. This system was also used to determine the NH_3 concentration (volume fraction) in the inlet gas that was found to be 2300±200 ppmv, which was very close to the concentration of 2318 ppmv based on the controlled gas flow rates.

In the experiments, the flow rate of each tested gas mixture was controlled at 3.65±0.20 L/min and the flow rate of NH_3 and Ar mixture (50.0 vol% NH_3 in Ar gas) was set at 0.017±0.001 L/min. The temperature of the furnace was maintained at the pre-set value (500°C or 750°C) for all the test gases. After each experimental run was completed, the system was cooled down with purging of welding grade Ar gas until the system temperature was close to the room temperature.

6.2.4 Characterisation of used catalysts and liquid product, and analysis of outlet gases

The used catalysts after the experiment runs were ground by a ROCKLABS ringmill with a model of P.B. and a serial number of 1007. Then the ground samples were mounted in ID 0.25 mm Quartz GC column fragments and carried out on a Rigaku SuperNova X-Ray Diffractometer (XRD) with Atlas diffractometer using Cu Kα (λ = 1.5418Å) radiation. Data were collected over a 360-degree rotation and the baseline was removed manually. A SSM-5000A TOC-L analyser of SHIMADZU was used to detect the total carbon formed and deposited on the catalyst. An ATAGO NAR-3T Abbe refractometer was used for analysing the liquid which was trapped in a condenser after the reactor. The composition of inlet and outlet gases in the experiments was analysed by an Agilent 3000 micro-GC.

6.3 Results and discussion

6.3.1 NH_3 decompositions in the simulated producer gas (No.1)

In Chapter 5, experiments of NH_3 decomposition by the reduced titanomagnetite in the simulated producer gas (No. 1) of biomass gasification have been conducted at 500 and 750°C, respectively, and the results are shown in Figure 6.1 again and used to be compared with the other gas mixtures in this chapter. As the findings in Chapter 5, condensate was found in the outlet pipe, an ice bath glass bottle was then installed after the reactor to trap the vapour product as shown in Figure 3.1 in Chapter 3. The liquid was weighed by balance and analysed by refractometer, which proved that the condensate was water. To check and quantify solid carbon produced during the process, the used catalysts were also analysed by TOC analyser. The water production rate and the carbon production rate were then determined from the total quantities (moles) of water and carbon produced during the experiment over a certain period of time. The results can be found in Table 6.2. For the other experimental runs, the water and carbon production rates were determined by the above method as well.

The experimental results show that the operation temperature had a significant impact on NH_3 decomposition in the simulated producer gas which was 28.4% at 500°C and 94.7% at 750°C. The effect of operation temperature can be attributed to its influence on the reactions involved and reaction direction in the NH_3 decomposition process. Consequently, the products and gas composition of the outlet gases were also different at different operation temperatures as given in Table 6.2. From the table, it is found that both carbon and water were produced at an operation temperature of 500°C, whereas no carbon was detected at 750°C. Based on the results and discussion in Chapter 5, the reverse water-gas shift reaction, the (reverse) Boudouard reaction, the

(reverse) carbon Methanation reaction and the iron oxidization reaction were involved in the NH_3 decomposition process, but the direction and the kinetics of these reactions were significantly influenced by operation temperature. These reactions are shown as follows in Eqs. (6.1) to (6.4).

Reverse water-gas shift reaction: $H_2 + CO_2 \leftrightarrow H_2O + CO$ (6.1)

Boudouard reaction: $2CO \leftrightarrow CO_2 + C_s$ (6.2)

Carbon Methanation reaction: $C + 2H_2 \leftrightarrow CH_4$ (6.3)

Iron oxidization reaction: $4CO_2 + 3Fe \leftrightarrow Fe_3O_4 + 4CO$ (6.4)

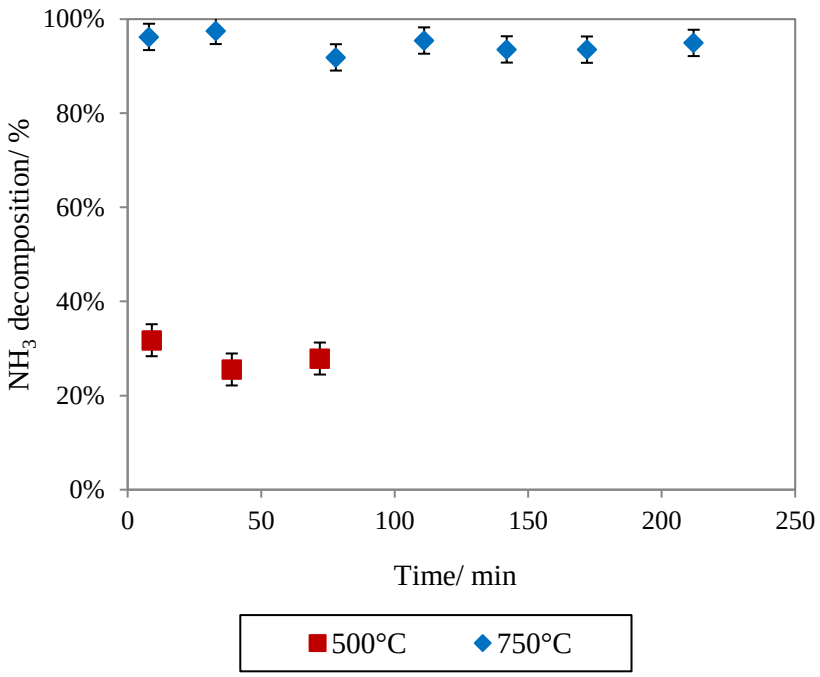

Figure 6.1 NH_3 decompositions in the simulated producer gas (No. 1) at 500 and 750°C.

Table 6.2 Inlet and outlet gas compositions as well as other reaction products in NH_3 decomposition from the simulated producer gas (No.1) at 500 and 750°C.

	H_2/ vol.%	CO/ vol.%	CO_2/ vol.%	CH_4/ vol.%	C/ mol/min	H_2O/ mol/min
Inlet	47.6	18.9	19.1	14.4	0	0
Outlet at 500°C	42.8	18.4	19.3	19.5	0.0060	0.0104
Outlet at 750°C	45.4	31.5	9.8	13.3	0	0.0105

In order to investigate the effects of individual gas species, namely H_2, CO, CO_2 and CH_4, and their combinations in the simulated producer gas on NH_3 decomposition using reduced titanomagnetite, experiments were conducted, respectively, for various gas species and mixtures (No. 2 to No. 7). The results are presented in the following six sections from 6.3.2 to 6.3.7.

6.3.2 Effect of H_2 on NH_3 decompositions

Figure 6.2 shows that the NH_3 decompositions in a gas mixture of H_2 and Ar (No. 2). It is observed that the reaction temperature also had a significant impact on the NH_3 decomposition as observed for the simulated producer gas. At 750°C, the average NH_3 decomposition was 99.1%; however, this was reduced to 16.5% at 500°C. The temperature effect, in this case, was largely due to the effect of temperature on equilibrium concentrations of reactant and products in the NH_3 decomposition reaction ($2NH_3 \rightarrow 3H_2 + N_2$). These results are in agreement with those of Ohtsuka et al. [4] who predicted the concentrations of NH_3 in the gas mixture at different temperatures

based on thermodynamic equilibrium. In comparison with the results in the simulated producer gas, the NH_3 decomposition in gas mixture H_2 and Ar was higher at 750°C but lower at 500°C, therefore, other gas species played a role in the process.

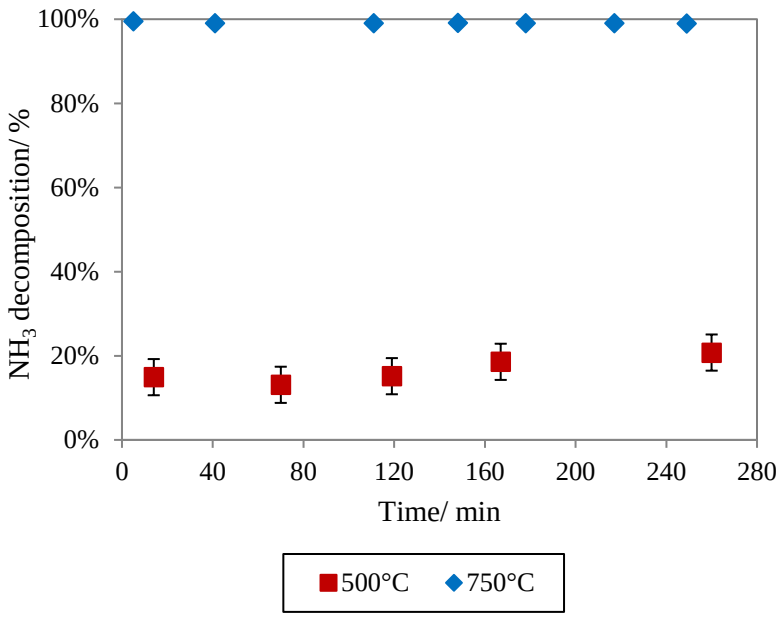

Figure 6.2 NH_3 decompositions in the gas mixture of H_2 and Ar (No. 2) at 500 and 750°C.

6.3.3 Effect of CO on NH_3 decompositions

Figure 6.3 shows the results of NH_3 decompositions in the gas mixture of CO and Ar (No. 3). Once again, the temperature had a significant impact, but in a different manner in comparison to the gas mixture of H_2 and Ar (No. 2). At 750°C, NH_3 was almost completely decomposed throughout the experiment. However, at 500°C, the NH_3 decomposition dropped rapidly from an initial value of 98% to 32.8% in 240 min. Compared with the NH_3 decomposition results in the simulated producer gas, the NH_3 decompositions in mixture gas CO and Ar (No. 3) were higher at both 500 and 750°C

within the experimental period. Therefore, other gas species such as H_2, CO_2 and CH_4 increased the negative effects on NH_3 decomposition.

It is believed that the Boudouard reaction (Eq. 6.2) was the dominant reaction involved in the NH_3 decomposition when CO was present and this can be confirmed by the measured inlet and outlet gas compositions as well as carbon formation on the used catalysts. However, the kinetics and the equilibrium of the Boudouard reaction were significantly affected by reaction temperature. Figure 6.4 and Figure 6.5 show the changes of CO and CO_2 concentrations in the reactor with elapsed time at pre-set temperatures of 500 and 750°C, respectively. At 500°C, the CO concentration decreased from 22.2% to 15.7% in 40 min and then increased until 100 min, after which it slowly increased to the inlet value. In the meantime, CO_2 concentration increased in the first 40 min and then dropped to a very low value after 100 min. The above trends of changes in CO and CO_2 concentrations confirm that the Boudouard reaction rate increased in the initial 40 min and then decreased to an insignificant level after approximate 100 min. At 750°C, however, the Boudouard reaction was steady throughout the experiment in which the CO_2 concentration maintained at approximately 1.3 vol.%. To quantify the carbon produced in the experiment, the used catalysts were analysed by the TOC analyser. Surprisingly, the average carbon production rate at 750°C (0.0013 mol/min) was higher than that at 500°C (0.0009 mol/min), even though the Boudouard reaction is theoretically favoured at low temperatures.

To interpret the above phenomena, the used catalysts were also analysed by the XRD analyser and the results are shown in Figure 6.6. At 500°C, most of the α-Fe phase on the reduced titanomagnetite was converted to carbide after the reaction. However, at 750°C, there was still significant α-Fe phase found at 44.7, 65.1, 82.4 and 99.0 2-Theta degrees. Based on these results, it is believed that the chemisorption of CO on the iron catalysts was higher at lower temperatures

with the maximum CO decomposition rate occurring between 500 and 600°C [5]. In addition, the carbide formation (Eq. 6.5) rate was higher than its decomposition (Eq. 6.6) rate at 500°C, which resulted in α-Fe phase converting to carbide [6]. When most of the α-Fe phase was converted to carbide, CO decomposition ceased [7]. Correspondingly, the Boudouard reaction was almost ceased after approximate 100 min of the experiment at 500°C as shown in Figure 6.4. Meanwhile, the decrease of α-Fe phase on the reduced titanomagnetite at 500°C caused the significant reduction of NH_3 decomposition (Figure 6.3). At 750°C, however, the carbide decomposition was faster than the rate of carbide formation and the α-Fe phase was stable throughout the experiment [6]. The α-Fe phase on the reduced titanomagnetite at 750°C, which is shown in Figure 6.6, maintained consistent activity for CO decomposition and high activity for NH_3 decomposition. Therefore, it can be concluded that the higher carbon production rate at 750°C than at 500°C is due to the consistent CO decomposition at 750°C. However, the CO decomposition at 500°C was almost ceased after 100 min.

Carbide formation reaction on an iron-based catalyst: $2CO + 3Fe \leftrightarrow Fe_3C + CO_2$ (6.5)

Carbide decomposition reaction on an iron-based catalyst: $Fe_3C \leftrightarrow 3Fe + C_s$ (6.6)

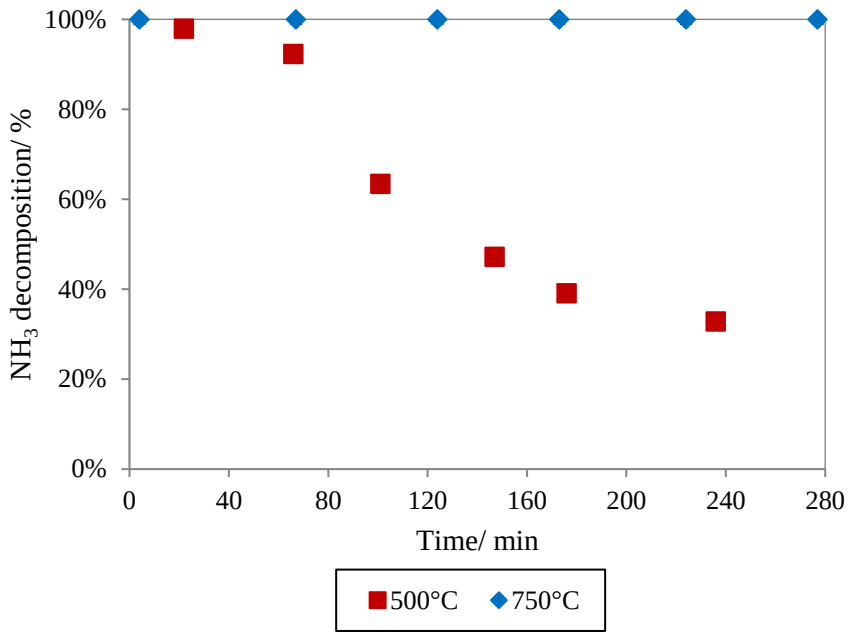

Figure 6.3 NH_3 decompositions in the gas mixture of CO and Ar (No. 3) at 500 and 750°C.

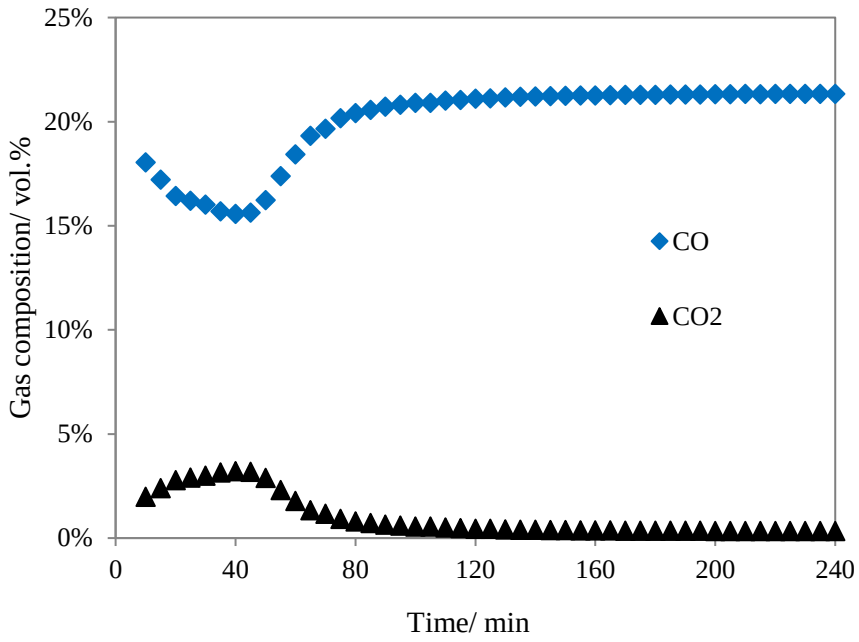

Figure 6.4 Changes in CO and CO_2 concentrations with elapsed time during NH_3 decomposition in the gas mixture of CO and Ar (No. 3) at 500°C.

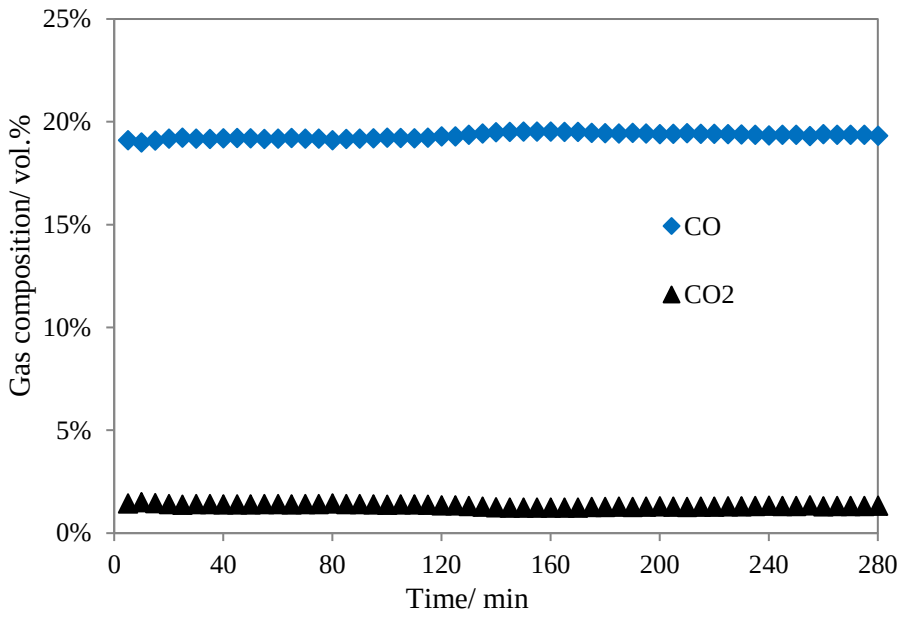

Figure 6.5 Changes in CO and CO_2 concentrations with elapsed time during NH_3 decomposition in the gas mixture of CO and Ar (No. 3) at 750°C.

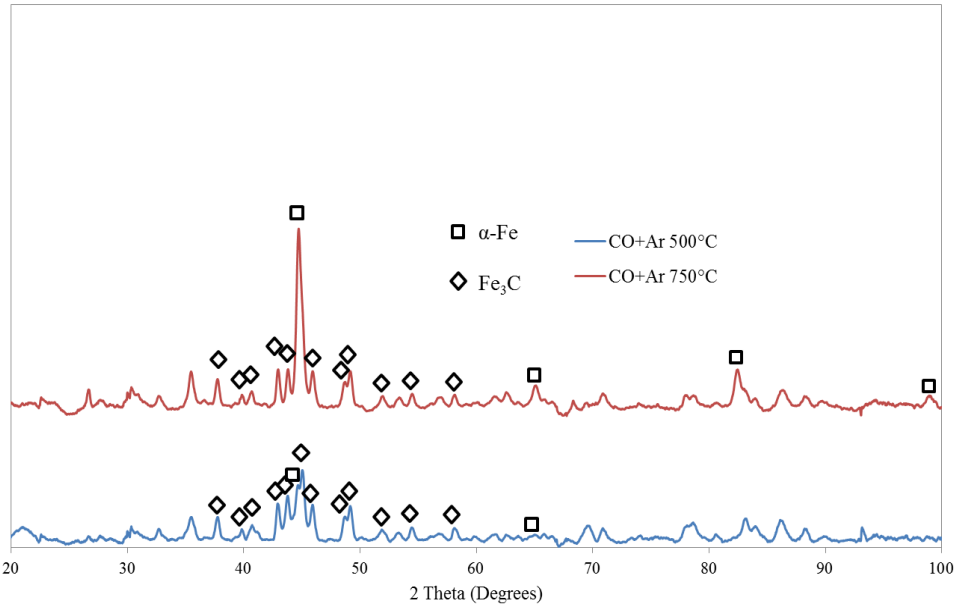

Figure 6.6 XRD analysis results for the used catalysts at 500 and 750°C in the gas mixture of CO and Ar (No. 3) for NH_3 decomposition.

6.3.4 Effects of CO_2 on NH_3 decompositions

To understand the effect of CO_2 on NH_3 decomposition by using the reduced titanomagnetite, experiments were conducted in the gas mixture of CO_2 and Ar (No. 4) at 500 and 750°C, respectively. The results are shown in Figure 6.7 and Figure 6.8 which show CO in the outlet gases at both temperatures. CO should be generated from the iron oxidization reaction (Eq. 6.4) and this is supported by the results in Chapter 5 and the research of Sarioglan et al. [1] who found that CO_2 oxidized the α-Fe sites to form iron oxide on the Fe-based catalyst. As Figure 6.7 and 6.8 reveal, the iron oxidization reaction rate was initially fast then slowed down approaching a steady rate after 150 min (500°C) and 90 min (750°C). Correspondingly, the NH_3 decompositions were initially high at both temperatures (close to 100%) and then decreased to 42% at 500°C and 91% at 750°C. This phenomenon can be explained by the oxidization of the metallic iron (α-Fe) on the reduced titanomagnetite by CO_2. The steady NH_3 decomposition after the rapid iron oxidization reaction illustrated that the oxidized iron catalyst still had an activity to decompose NH_3 at both 500 and 750°C; however, the activity was lower than the fresh reduced titanomagnetite. Furthermore, the activity of the oxidized catalyst for NH_3 decomposition was much higher at 750°C than at 500°C. These conclusions are supported by the results in Chapter 5 that the reduced titanomagnetite (mainly α-Fe phase) had a higher activity for NH_3 decomposition in Ar gas than that of the unprocessed titanomagnetite (mainly iron oxide phase). In addition, high temperature promoted the NH_3 decomposition in Ar gas by both two types of titanomagnetites.

In comparison with the NH_3 decompositions in the simulated producer gas (No. 1), the NH_3 decomposition during the steady period in the gas mixture of CO_2 and Ar (No. 4) was higher at 500°C, but lower at 750°C. These results indicate that the other gas species (H_2, CO and CH_4) also negatively affected the NH_3 decomposition at 500°C; however, at 750°C, H_2 in the producer gas

may have positive effect of mitigating oxidization of α-Fe sites on the catalyst by CO_2, which demonstrated favourable effects on NH_3 decomposition.

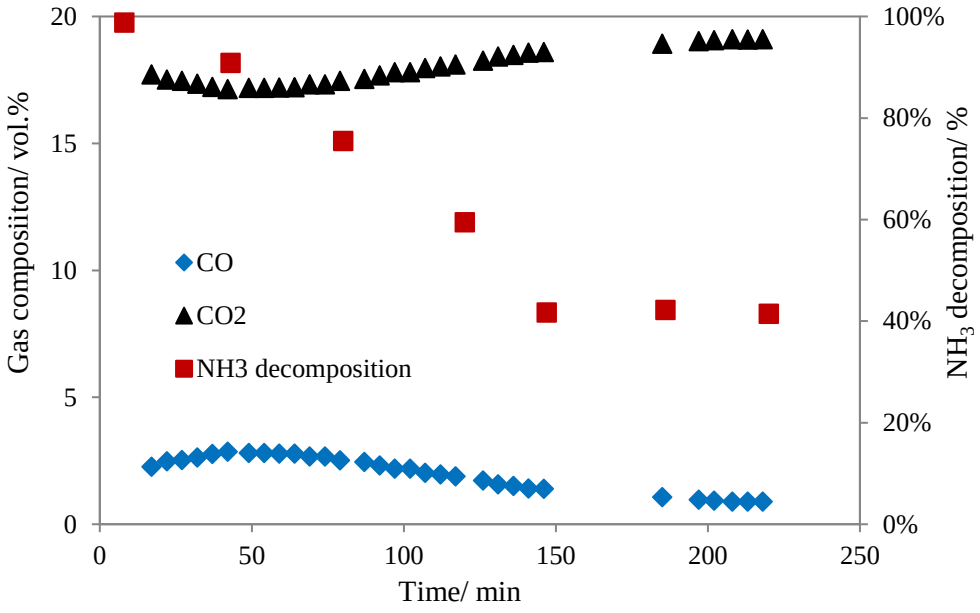

Figure 6.7 NH_3 decompositions and outlet gas composition for NH_3 decomposition in the gas mixture of CO_2 and Ar (No. 4) at 500°C.

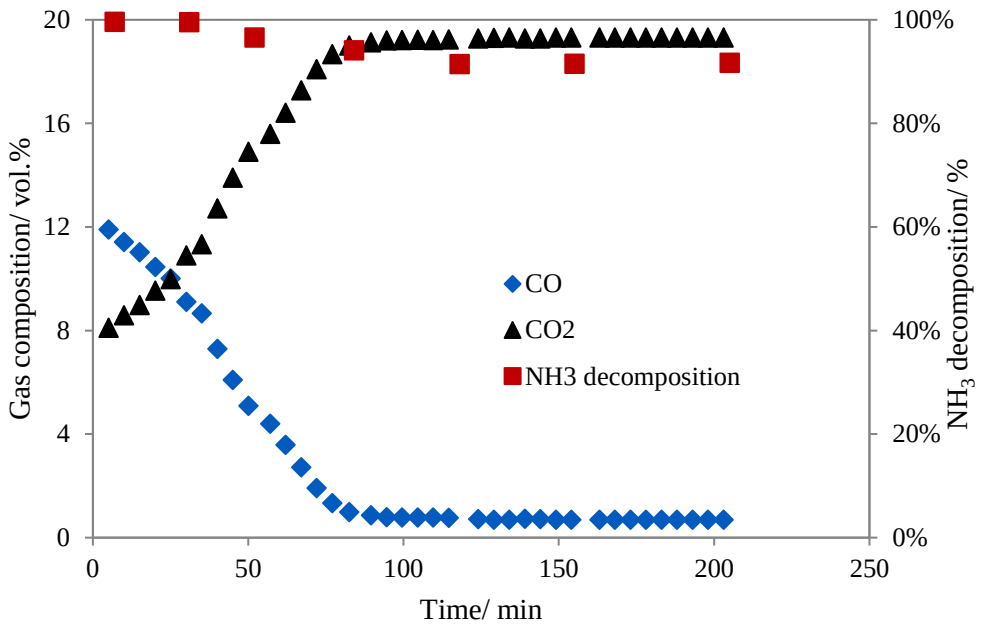

Figure 6.8 NH_3 decomposition and outlet gas composition for NH_3 decomposition in the gas mixture of CO_2 and Ar (No. 4) at 750°C.

6.3.5 Effects of CH_4 on NH_3 decompositions

Effects of CH_4 in the gas mixture CH_4 and Ar (No. 5) on the activity of reduced titanomagnetite for decomposing NH_3 were investigated at 500 and 750°C, respectively, and the results are shown in Figure 6.9. At 500°C, the NH_3 decomposition decreased slightly from 99.4% to 95% in approximate 30 min, after which was steady throughout the rest of experiment. At 750°C, the NH_3 decomposition was ~99% consistently throughout the entire experiment. Compared with the other three gases (H_2, CO, and CO_2) as discussed in previous sections, CH_4 had the minimum negative effect on the activity of the reduced titanomagnetite for NH_3 decomposition at both temperatures.

To examine if there was carbon formation on the catalysts in the CH_4 gas, the used catalysts were analysed by TOC analyser. There was undetectable carbon on the used catalyst at 500°C. Interestingly, there was significantly measurable carbon formation at 750°C and the average

carbon production rate was 0.0078 mol/min; however, the activity of the reduced titanomagnetite for NH_3 decomposition was still as high as 99%. To understand the mechanism of this phenomenon, the used catalysts were also analysed by XRD analyser and the results are shown in Figure 6.10. It is observed that there was significant α-Fe phase on the used catalysts at both temperatures; however, the α-Fe peaks on the used catalyst at 750°C were larger than the used catalyst at 500°C. Therefore, the higher α-Fe phase on the used catalyst at 750°C and the higher temperature are believed to maintain high NH_3 decomposition at 750°C. It is interesting to note that at 750°C, the α-Fe phase on the used catalyst in the gas mixture of CH_4 and Ar (No. 5) was much higher than the used catalyst in the gas mixture of CO and Ar (No. 3). However, the NH_3 decomposition for the gas mixture No. 5 was 99% and that for the gas mixture No. 3 was almost 100%. From the measured outlet gas composition of gas mixture No. 5 at 750°C, H_2 was found to be 12.3±1.0 vol.% (average) which lowered the NH_3 decomposition equilibrium.

At 750°C, the carbon formation and H_2 production confirm that the reverse carbon Methanation reaction occurred (Eq. 6.7); however, this reaction was insignificant at 500°C based on insignificant H_2 in the outlet gas and undetectable carbon formation on the catalyst. This finding is consistent with the study of Ermakova et al. [6] who claimed that CH_4 decomposition was unlikely to occur on the iron catalyst at 400 to 600°C. The CH_4 decomposition was only possible at or above 680°C when the carbide could be transformed into its metastable state [6].

Reverse carbon Methanation or Methane decomposition reaction: $CH_4 \leftrightarrow C + 2H_2$ (6.7)

The carbon formation at 750°C has been explained by a theory of "carbide cycle" [6]. However, the carbide generated from the CH_4 decomposition on the α-Fe sites was different from the carbide formed from the CO decomposition. The former was much more unstable than the latter at high

temperatures. Comparing the XRD graphs of Figure 6.10 with those of Figure 6.6, it is found that at 750°C, the used catalysts in the gas mixture of CH_4 and Ar (No. 5) had much less carbide than that used in the gas mixture of CO and Ar (No. 3). However, the carbon production rate in the gas mixture No. 5 was more than that in the gas mixture No. 3 at 750°C. It can be interpreted by the following theory. At 750°C, the carbide formed from the CH_4 decomposition on the iron catalyst particle was extremely unstable and CH_4 decomposition led to graphite nuclei on the particle. Since the nucleation had to overcome a high activation barrier, other graphite formed around the former nucleus. Thus the "carbide cycle" was repeated on the graphite nucleus which ended with abundant carbon deposition [6].

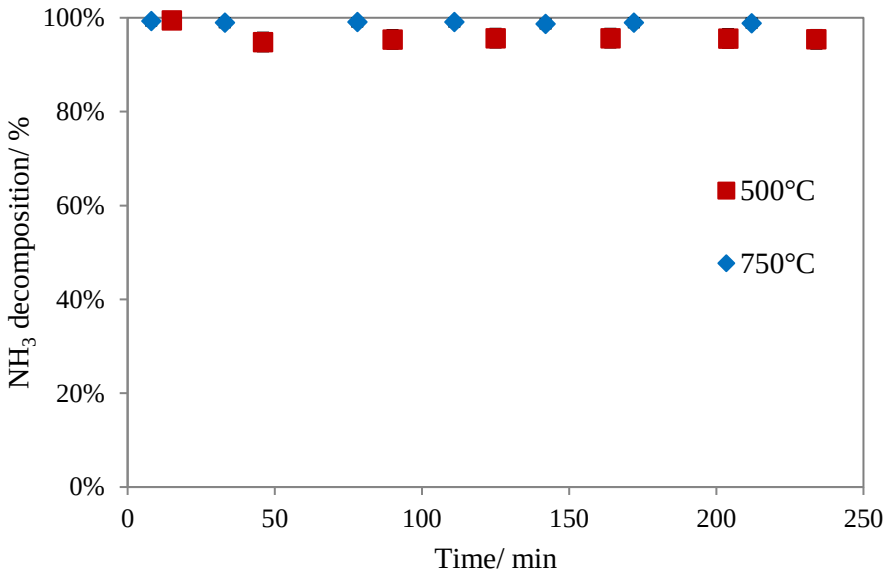

Figure 6.9 NH_3 decompositions by the reduced titanomagnetite in the gas mixture of CH_4 and Ar (No. 5) at 500 and 750°C.

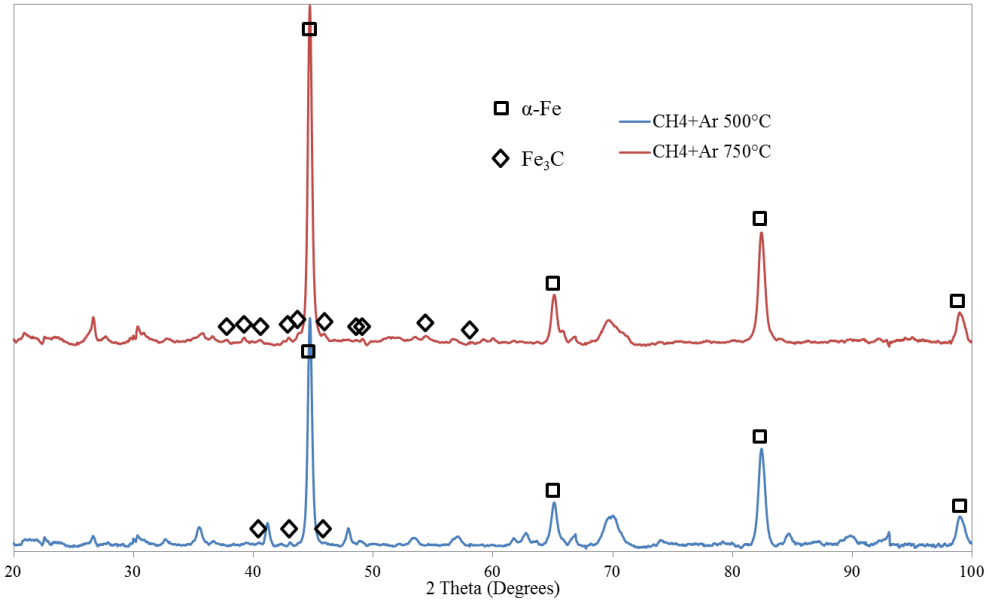

Figure 6.10 XRD results of the used catalysts at 500 and 750°C in the gas mixture of CH_4 and Ar (No. 5).

From the above four sections (Section 6.3.2 to 6.3.5), it is found that H_2, CO, CO_2 and CH_4 separately demonstrated unfavourable effects on NH_3 decomposition by using the reduced titanomagnetite at 500 and 750°C. Moreover, the reduced titanomagnetite had a lower activity for NH_3 decomposition at 500°C than at 750°C. In order to investigate if there were combined effects of gas species, a mixture of H_2 and CO (gas mixture No. 6) and a gas mixture of H_2, CO and CO_2 (gas mixture No. 7) were also tested and results are presented in the following two sections.

6.3.6 NH_3 decompositions in the gas mixture of H_2, CO and Ar (No. 6)

Figure 6.11 shows the experimental results of NH_3 decomposition in the gas mixture of H_2, CO and Ar (No. 6) at both 500 and 750°C. At 750°C, the NH_3 decomposition was steady at 97% throughout the whole experiment. However, at a lower temperature of 500°C, the NH_3 decomposition decreased rapidly with elapsed time, from 68.9% to 32.1% in 124 min. The used

catalysts at 500 and 750°C were analysed by the XRD analyser and the results are shown in Figure 6.12. The significant reduction of α-Fe sites on the used catalyst by converting to carbide was a significant reason for the decrease of NH_3 decomposition in gas mixture No. 6 at 500°C.

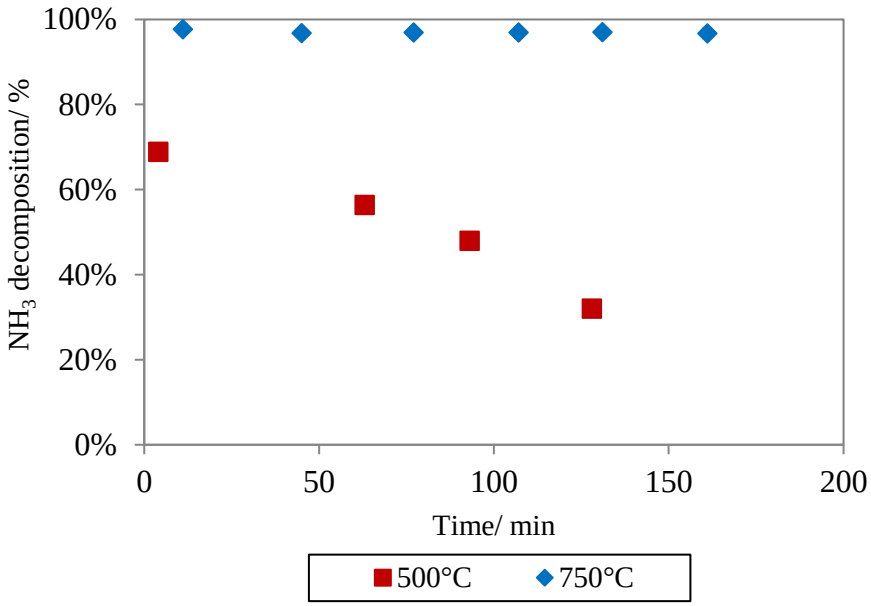

Figure 6.11 NH_3 decompositions in the gas mixture of H_2, CO and Ar (No. 6) at 500 and 750°C.

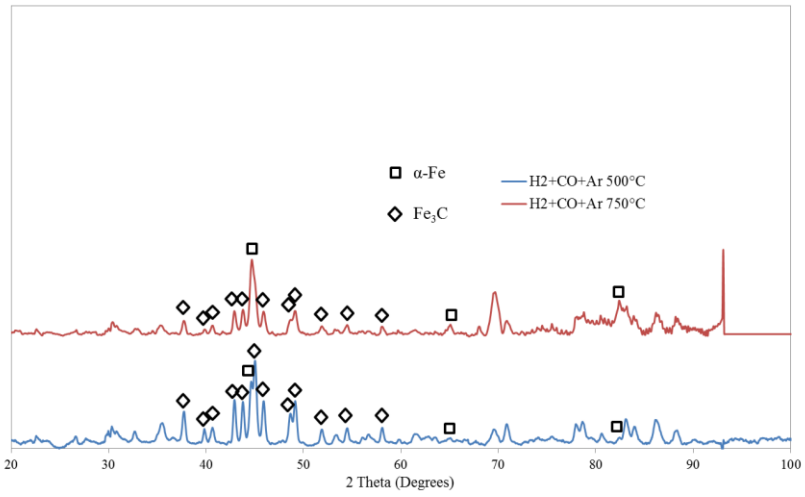

Figure 6.12 XRD results of the used catalysts at 500 and 750°C for NH_3 decomposition in the gas mixture of H_2, CO and Ar (No. 6).

Table 6.3 lists the inlet and outlet gas compositions as well as other reaction products in NH_3 decomposition for a gas mixture of H_2, CO and Ar (No. 6) at 500 and 750°C. In addition, the content ratios of CO_2/CO and (2*CH_4)/H_2 in the dry basis are also given in Table 6.3. From the table, it is found that water, carbon, CO_2 and CH_4 were produced at both 500 and 750°C. These products indicate that the NH_3 decomposition involved three basic reactions as given in Eqs. (6.1) to (6.3) or combination of them. The following reaction, Eq. (6.8), which is the combination of reverse water-gas shift reaction (Eq. 6.1) and Boudouard reaction (Eq. 6.2) and was also involved and has been reported to be a fast reaction in H_2 and CO gas mixture to produce water and carbon with iron catalysts [1, 5, 7, 8].

Reverse water gas reaction: $CO + H_2 \leftrightarrow C + H_2O$ (6.8)

Wang et al. [9] also proposed that the three reactions of Eqs. (6.1), (6.2) and (6.3), were basic reactions in NH_3 decomposition in the CO and H_2 gas mixture. The reaction kinetics of these reactions were significantly different at two different temperatures, which was confirmed by the differences in the outlet gas composition and the generation rates of the products such as water and carbon. At 500°C, the carbon production rate (0.0099 mol/min) was 5 times more than that at 750°C (0.0019 mol/min) and the water production at 500°C (0.0055 mol/min) was also more than that at 750°C (0.0011 mol/min).

Table 6.3 Inlet and outlet gas compositions in dry basis as well as other reaction products in NH_3 decomposition for the gas mixture of H_2, CO and Ar (No. 6) at 500 and 750°C.

	H_2/ vol.%	CO/ vol.%	CO_2/ vol.%	CH_4/ vol.%	Ar/ vol.%	C/ mol/min	H_2O/ mol/min	CO_2/CO ratio	$(2*CH_4)/H_2$ ratio
Inlet	48.7	20.4	0	0	30.9	0	0	0	0
Outlet at 500°C	45.5	8.3	4.0	1.3	40.9	0.0099	0.0055	0.4816	0.0571
Outlet at 750°C	43.7	16.9	1.1	1.2	37.1	0.0019	0.0011	0.0637	0.0549

The carbon and water formation during the NH_3 decomposition can be explained by Reaction (6.2) and Reaction (6.8). In steel manufacturing process and other processes with Fe-based catalysts, it was observed that CO reacted with H_2 (Eq. 6.8) to form water and carbon and CO decomposed (Eq. 6.2) to form carbon and CO_2 [7, 10]. Sarioglan et al. [1] and Ohtsuka et al. [4] explained the measurable carbon produced in the gas mixture of H_2, CO and N_2 was only due to Reaction (6.8). However, Reaction (6.8) itself cannot explain the uneven mole production rates of carbon and water which were found at both 500 and 750°C in this study. Olsson and Turkdogan [8] considered both Reaction (6.2) and Reaction (6.8) which is much more convincible. The authors [8] also reported that Reaction (6.8) played an important role to produce carbon when H_2 was added and the concentration was high, and the carbon formation rate at 500°C was much higher than at 750°C. It is supported by the results in this study that the carbon production rates in a gas mixture of H_2,

CO and Ar (No. 6) were higher than those in a gas mixture of CO and Ar (No. 3) at both two temperatures. Additionally, the carbon formation rate was higher at 500°C than at 750°C in gas mixture No. 6. The carbon formation rates in gas mixture No. 6 were 0.0099 and 0.0019 mol/min at 500 and 750°C, respectively. However, the carbon production rates in gas mixture No. 3 were only 0.0009 and 0.0013 mol/min at 500 and 750°C, respectively. It illustrates that the carbon formation was boosted by adding H_2 to the gas mixture of CO and Ar. Moreover, in Table 6.3, more water was produced at 500°C than at 750°C that can be due to Reaction (6.8), which is favoured at 500°C. Furthermore, the higher carbon production rates than the water production rates at both 500 and 750°C indicated that the Boudouard reaction (Eq. 6.2) is another reaction for carbon generation. To compare the ratios of CO_2/CO in the outlet gases of 500°C and 750°C, it was found that the CO_2/CO in the outlet gas of 500°C was much higher than that of 750°C which illustrated the Boudouard reaction was more favoured at 500°C than 750°C.

From Table 6.3, it is also found that CH_4 was produced at two temperatures which may be formed from carbon and H_2 by the carbon Methanation reaction (Eq. 6.3) and CO Methanation reaction (Eq. 6.9). However, the experimental results on concentrations of CO_2 and CH_4 in the outlet gases were inconsistent with the expected results only based on the CO Methanation reaction (Eq. 6.9) as reported by Sarioglan et al. [1]. Furthermore, in comparison with the $(2*CH_4)/H_2$ ratios in the outlet gases of 500°C and 750°C, it was found that the $(2*CH_4)/H_2$ ratio was slightly higher than that at 750°C which indicated that the carbon Methanation reaction or the CO Methanation reaction was slightly promoted at 500°C than 750°C in the gas mixture of H_2, CO and Ar.

CO Methanation reaction: $2CO + 2H_2 \leftrightarrow CH_4 + CO_2$ (6.9)

Compared the NH_3 decompositions in gas mixture of H_2, CO and Ar (No. 6) with those in gas mixture H_2 and Ar (No. 2) and gas mixture CO and Ar (No. 3) at both 500 and 750°C, at 750°C, it is found that the NH_3 decomposition in gas mixture No. 6 (97%) was lower than those in gas mixture No. 2 (99.1%) and gas mixture No. 3 (100%), which demonstrates that the combined effect of H_2 and CO was more unfavourable than the separate effects from H_2 and CO. At 750°C, the NH_3 decomposition equilibrium was insignificantly reduced by H_2. However, adding H_2 into CO gas could boost the carbon and carbide formation on the iron-based catalyst by reactions (6.8) and (6.5), which reduced the activity of the iron catalyst for NH_3 decomposition in gas mixture No. 6. At 500°C, the NH_3 decomposition in gas mixture No. 6 had similar reduction trend as that in gas mixture No. 3. However, it was lower in gas mixture No. 6 than that in gas mixture No. 3. It is illustrated that the H_2 in gas mixture No. 6 caused an additional negative effect on NH_3 decomposition, which is supported by the severely unfavourable effect of H_2 on NH_3 decomposition in gas mixture No. 2 at 500°C (Figure 6.2). Furthermore, the carbon production rate in gas mixture No. 6 was also higher than that in gas mixture No. 3 at 500°C, which might be another reason for the reduction of NH_3 decomposition.

In comparison with the NH_3 decompositions in the simulated producer gas (No. 1) at both 500 and 750°C, the NH_3 decompositions in the gas mixture No. 6 were higher than those in gas mixture No.1. Therefore, CO_2 and CH_4 had additional negative effects on NH_3 decomposition as presented in Section 6.3.7.

6.3.7 NH_3 decompositions in the gas mixture of H_2, CO, CO_2 and Ar (No. 7)

Gas mixture No.7 aimed to investigate the combined effect of a gas mixture of H_2, CO and CO_2 or the effect without CH_4 in comparison with the simulated producer gas on the NH_3

decomposition. In this gas mixture, concentrations of H_2, CO and CO_2 maintained similar as those in the simulated producer gas while CH_4 was substituted by Ar gas. The results are shown in Figure 6.13 from which it is found that the average NH_3 decompositions were 29.2% at 500°C and 95.2% at 750°C, respectively, which were close to those from the simulated gas mixture (No. 1). Therefore, it is concluded that CH_4 only had an insignificant effect on NH_3 decomposition at both temperatures, which is consistent with the results of gas mixture CH_4 and Ar (No. 5) as presented in Section 6.3.5. However, a different result was reported by Sarioglan et al. [1] who found that at 700°C, CH_4 had a positive effect on NH_3 decomposition with decomposition rate increasing from 43.8% to 53.8%.

Additionally, in comparison with the NH_3 decompositions for gas mixture of H_2, CO and Ar (No. 6) in Figure 6.11, it is found that the NH_3 decomposition in gas mixture No.7 (95.2%) was slightly lower than that in gas mixture No. 6 (97%) at 750°C. This reduction in NH_3 decomposition was due to the addition of CO_2, which may have oxidized the active α-Fe phase on the reduced titanomagnetite. At 500°C, the negative effect of CO_2 was significant with the average NH_3 decomposition of 29.2% for gas mixture No.7 in comparison to the NH_3 decomposition trend in gas mixture No. 6 decreasing from an initial value of 68.9% to 32.1% in 124 min.

From the above comparison and analysis, it is found that all of the gas species, H_2, CO, CO_2 and CH_4, participated in reducing NH_3 decompositions in the simulated producer gas at both 500 and 750°C. It is found that CH_4 had the least negative effect on NH_3 decomposition. The negative effect from CO can be boosted by H_2; however, the negative effect from CO_2 can be mitigated by H_2. Therefore, the rank for the unfavourable effects of the gas species in the simulated producer gas was $CH_4 < CO_2 <$ (CO and H_2).

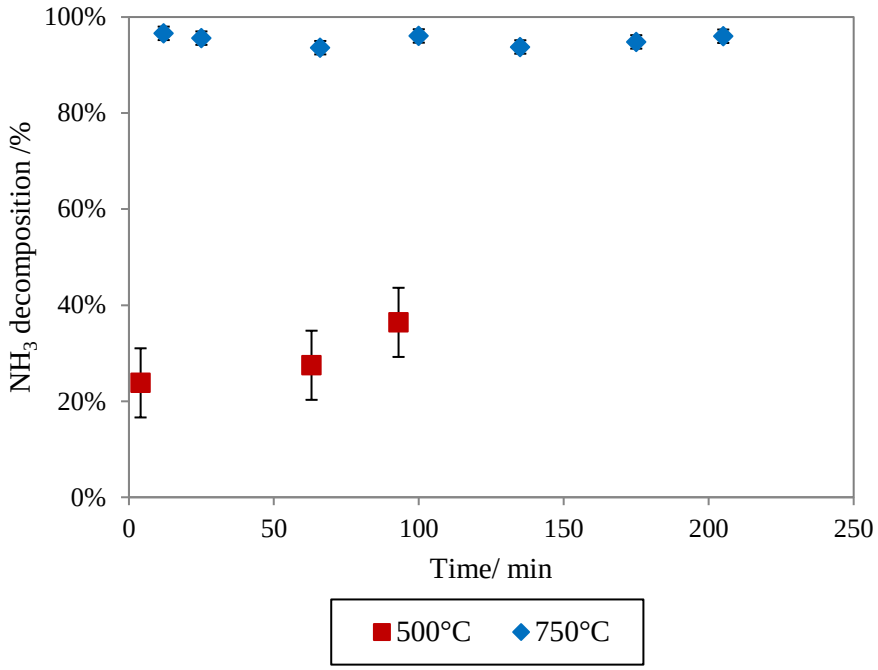

Figure 6.13 NH_3 decompositions in the gas mixture H_2, CO, CO_2 and Ar (No. 7) at 500 and 750°C.

The concentrations of the inlet and outlet gas compositions, CO_2/CO ratios and (2*CH_4)/H_2 ratios are given in in Table 6.4 for understanding the mechanisms of NH_3 decomposition process and side-reactions. Water was formed during the NH_3 decomposition process likely from the reverse water-gas shift reaction (Eq. 6.1). Moreover, the higher water production rate and lower CO_2/CO ratio in the outlet gas at 750°C than those at 500°C demonstrated that the reverse water-gas shift reaction was promoted at high temperature. Carbon was also observed at 500°C and this should be the product of the Boudouard reaction (Eq. 6.2). At 500°C, in the outlet gas, CH_4 was also found even there was no CH_4 in the inlet gas which means the carbon Methanation reaction (Eq. 6.3) occurred with carbon and H_2 as reactants.

However, no carbon was detected on the used catalyst in the experiment at 750°C, which indicates that the Boudouard reaction was retarded at this temperature when CO_2 and H_2O existed in the gas. Walker et al. [5] explained this phenomenon by reduced chemisorption of CO on the iron catalyst when the temperature was higher than 600°C. Olsson and Turkdogan [8] also reported that H_2O and CO_2 inhibited carbon formation on the iron catalyst at 600°C. In the present study, CH_4 was hardly detected at 750°C which can be expected as there was no carbon formed on the catalyst. As the carbon Methanation reaction is an exothermal reaction, it was retarded at high temperatures. Sarioglan et al. [1] also reported that CH_4 was not found in NH_3 decomposition at 700°C for the gas mixture of H_2, CO, CO_2 and N_2 by using zeolite Hβ supported iron catalyst. The authors thought this was due to the high concentration of CO_2 in the gas mixture which inhibited the production of CH_4 through the CO Methanation reaction (Eq. 6.9). However, in this study, CH_4 was found at a lower temperature of 500°C which means the CH_4 generation was dependent on both temperature and the gas composition in the atmosphere.

By comparing the results of gas mixture No. 7 with those of gas mixture No. 6, CO_2 in the gas mixture tends to inhibit the carbon formation from the Boudouard reaction (Eq. 6.2). From Comparing Table 6.4 with Table 6.3, it is found that the carbon production rate in the gas mixture No. 7 was much lower than those in the gas mixture No. 6 both at 500 and at 750°C. Similar trend has been reported by Tsubouchi et al. [11] who found that addition of CO_2 with a concentration of 10 vol.% to the syngas (20 vol.% CO and 10 vol.% H_2 in He) decreased the carbon deposition on the reduced limonite at 750°C and thus improved the catalytic performance. However, the addition of 23.7 vol.% CO_2 to the gas mixture of H_2, CO and Ar in this present study reduced the NH_3 decompositions at both 500 and 750°C by comparing the results in Figure 6.11 with Figure 6.13. It can be explained that the negative effect of CO_2 for oxidizing the reduced titanomagnetite

suppressed the positive effect of reducing the carbon deposition on the catalyst. Therefore, the concentration of CO_2 in the gas mixture may be a significantly important factor to affect the catalytic activity for NH_3 decomposition. Further experiments can be conducted to research the suitable concentration of CO_2.

Table 6.4 Inlet and outlet gas compositions in dry basis, as well as other reaction products in NH_3 decomposition for gas mixture H_2, CO, CO_2 and Ar (No. 7) at 500 and 750°C.

	H_2/ vol%	CO/ vol%	CO_2/ vol%	CH_4/ vol%	Ar/ vol%	C/ mol/min	H_2O/ mol/min	CO_2/CO ratio	(2*CH_4)/H_2 ratio
Inlet	42.8	21.3	23.7	0	12.2	0	0	1.1127	0
Outlet at 500°C	37.7	21.7	23.3	1.2	16.1	0.0051	0.0084	1.0737	0.0637
Outlet at 750°C	36.3	32.9	14.6	0	16.2	0.0000	0.0092	0.4438	0

6.4 Conclusions

Effect of temperature and the gas species in the producer gas of biomass gasification on NH_3 removal have been experimentally investigated by using H_2-reduced titanomagnetite. It was found that the reduced titanomagnetite had much higher NH_3 decomposition rate at 750°C than at 500°C. All of the gas species, H_2, CO, CO_2 and CH_4, in the simulated producer gas had negative effects on the NH_3 decompositions although their effects were at different magnitudes. The unfavourable

effects of the gas species can be ranked as CH_4 < CO_2 < (CO and H_2). Mechanisms and side reactions involved were investigated in this study.

H_2 had a negative effect on NH_3 decomposition due to the increased H_2 equilibrium concentration in the products, which effect was more pronounced at 500°C than at 750°C. The negative effect from CO was caused by carbon formation and converting α-Fe phase on the iron catalyst to carbide by CO decomposition, and the carbide had extremely low or no activity to decompose NH_3. Moreover, the formed carbide was much more stable on the catalyst at 500°C than at 750°C, which resulted in lower activity of the iron catalyst at 500°C than at 750°C. When CO_2 was present at the gas, it oxidized the α-Fe phase on the reduced titanomagnetite to form iron oxide. The iron oxide reduced the catalyst activity to decompose NH_3. This negative effect by CO_2 was worse at 500°C than at 750°C. Compared with the above three gas species, CH_4 had the minimum effect on NH_3 decomposition. Although there was measurable carbon deposition on the iron catalyst at 750°C in the CH_4 gas, the NH_3 decomposition was still as high as 99%.

The combined effects of these gas species of H_2, CO, CO_2, and CH_4 were complicated and can be explained by NH_3 decomposition reaction, side reactions and decomposition equilibrium. H_2 was the most dominant gas species which affected the NH_3 decomposition equilibrium and promoted carbon formation when it coexisted with CO. However, H_2 also protected the α-Fe phase on the iron-based catalyst from being oxidized by CO_2 and suppressed carbon formation from the CH_4 decomposition reaction. The next important gas species was CO_2 which had both positive and negative effect. CO_2 oxidized the α-Fe phase on the catalyst which reduced the NH_3 decomposition, but it reduced carbon formation by inhibiting the Boudouard reaction which was favourable for the NH_3 decomposition.

6.5 References

[1] A. Sarıoğlan, Y. Durak-Çetin, H. Okutan, and F. Akgün, "Decomposition of ammonia: The effect of syngas components on the activity of zeolite Hβ supported iron catalyst," *Chemical Engineering Science,* vol. 171, pp. 440-450, 2017.

[2] W. L. Saw and S. Pang, "The influence of calcite loading on producer gas composition and tar concentration of radiata pine pellets in a dual fluidised bed steam gasifier," *Fuel,* vol. 102, pp. 445-452, 2012.

[3] W. L. Saw and S. Pang, "Co-gasification of blended lignite and wood pellets in a 100kW dual fluidised bed steam gasifier: The influence of lignite ratio on producer gas composition and tar content," *Fuel,* vol. 112, pp. 117-124, 2013.

[4] Y. Ohtsuka, C. Xu, D. Kong, and N. Tsubouchi, "Decomposition of ammonia with iron and calcium catalysts supported on coal chars," *Fuel,* vol. 83, pp. 685-692, 2004.

[5] P. Walker Jr, J. Rakszawski, and G. Imperial, "Carbon mixture over iron catalysts. II. Rates of carbon formation," *The Journal of Physical Chemistry,* vol. 63, pp. 140-149, 1959.

[6] M. A. Ermakova, D. Y. Ermakov, A. L. Chuvilin, and G. G. Kuvshinov, "Decomposition of methane over iron catalysts at the range of moderate temperatures: the influence of structure of the catalytic systems and the reaction conditions on the yield of carbon and morphology of carbon filaments," *Journal of catalysis,* vol. 201, pp. 183-197, 2001.

[7] E. Turkdogan and J. Vinters, "Catalytic effect of iron on decomposition of carbon monoxide: I. carbon deposition in H_2-CO Mixtures," *Metallurgical and Materials Transactions B,* vol. 5, pp. 11-19, 1974.

[8] R. Olsson and E. Turkdogan, "Catalytic effect of iron on decomposition of carbon monoxide: II. Effect of additions of H_2, H_2O, CO_2, SO_2 and H_2S," *Metallurgical and Materials Transactions B*, vol. 5, pp. 21-26, 1974.

[9] W. Wang, N. Padban, Z. Ye, A. Andersson, and I. Bjerle, "Kinetics of ammonia decomposition in hot gas cleaning," *Industrial & engineering chemistry research*, vol. 38, pp. 4175-4182, 1999.

[10] N. Bost, M. Ammar, M. Bouchetou, and J. Poirier, "The catalytic effect of iron oxides on the formation of nano-carbon by the Boudouard reaction in refractories," *Journal of the European Ceramic Society*, vol. 36, pp. 2133-2142, 2016.

[11] N. Tsubouchi, H. Hashimoto, and Y. Ohtsuka, "Catalytic performance of limonite in the decomposition of ammonia in the coexistence of typical fuel gas components produced in an air-blown coal gasification process," *Energy & Fuels*, vol. 21, pp. 3063-3069, 2007.

7 Equipment, Materials, and Preliminary Experiments of an Oil Scrubber for Tar Removal

7.1 Introduction

From the literature review in Chapter 2, the producer gas from biomass gasification for Fisher-Tropsch (FT) synthesis is required to have tar concentration below the dew point (<0.1 mg/Nm^3), and the tar concentration from a practical gasification process is normally at 0.7-16.8 g/Nm^3 even with application of primary measures to minimise the tar concentration [1, 2]. Therefore, secondary measures (downstream measures) have to be used for tar removal from the producer gas of biomass gasification. Among the secondary measures, the oil scrubber method for tar removal was selected in this research because of its high efficiency for tar removal, easy operation, low cost, and no waste solution treatment [3]. This chapter will firstly introduce the solvents used for tar absorption in the scrubber, and the verification and modification of an oil scrubber system. Secondly, calculations of the operating range of the oil scrubber, tar sampling and analysis methods, and experimental procedures will be described. Finally, the preliminary experimental results using biodiesel and canola oil, in the oil scrubber for tar removal will be presented and discussed.

7.2 Materials

Biodiesel (tallow methyl esters) and canola oil were selected as the solvents in the oil scrubber for tar removal in this research because they are effective for tar absorption [4-6], cheap and widely available.

7.2.1 Biodiesel

The biodiesel used in this research was produced from tallow and obtained from Haarslev Industries Ltd. in New Zealand [7]. The fatty acid composition and the main properties of the biodiesel are given in Table 7.1 and 7.2, respectively. The numbers in the brackets in the first column of Table 7.1 represent the carbon numbers and double bonds numbers of the chemical. For example, oleic acid (18:1) has eighteen carbons and one double bond.

Table 7.1 Composition of tallow biodiesel [8, 9].

Fatty acid in biodiesel	Molecular formula	Molecular weight/ g/mol	Composition/ wt.%
Myristic acid (14:0)	$C_{14}H_{26}O_2$	228.38	3
Palmitic acid (16:0)	$C_{16}H_{32}O_2$	256.43	26
Palmitoleic acid	$C_{16}H_{30}O_2$	254.42	3
Stearic acid (18:0)	$C_{18}H_{36}O_2$	284.48	14
Oleic acid (18:1)	$C_{18}H_{34}O_2$	282.47	47
Linoleic acid (18:2)	$C_{18}H_{32}O_2$	280.46	3
Linolenic acid (18:3)	$C_{18}H_{30}O_2$	278.44	1
Other acids			3
Average molecular weight g/mol		~272.31	

Table 7.2 Properties of the biodiesel used in this research [7].

Parameters of biodiesel	Values
Ester content, mass%	96.9
Density, kg/m^3	876.7
Viscosity at 40°C, mm^2/s	5.0
Flashpoint, °C	175
Water content, mg/kg	592
Total contamination, mg/g	10.9
Total glycerol, mass%	0.657

7.2.2 Canola oil

Clear fry canola oil used in this research was purchased from the local supermarket which was manufactured and produced in Canada and imported and distributed by Cookright Filtering Services, Ltd. The fatty acid composition and main properties of canola oil are cited from literature and given in Table 7.3 and 7.4, respectively.

Table 7.3 Composition of canola oil [9, 10].

Fatty acid in canola oil	Molecular formula	Molecular weight/ g/mol	Composition/ wt.%
Myristic acid (14:0)	$C_{14}H_{26}O_2$	228.38	0.1
Palmitic acid (16:0)	$C_{16}H_{32}O_2$	256.43	3.9
Stearic acid (18:0)	$C_{18}H_{36}O_2$	284.48	3.1
Oleic acid (18:1)	$C_{18}H_{34}O_2$	282.47	60.2
Linoleic acid (18:2)	$C_{18}H_{32}O_2$	280.46	21.1
Linolenic acid (18:3)	$C_{18}H_{30}O_2$	278.44	11.1
Erucic acid (22:1)	$C_{22}H_{42}O_2$	338.58	0.5
Average molecular weight g/mol		280.71	

Table 7.4 Properties of canola oil [11-13].

Parameters of canola oil	Values
Density, kg/m^3	905
Viscosity at 40°C, mm^2/s	3.67
Flashpoint, °C	290.5
Surface tension (σ), mN/m (30-50°C)	30-32

7.3 Description and modification of an oil scrubber

The packed tower is suitable for removal of corrosive, hazardous gases, vapours, and particulates from a gas stream [14]. It also has advantages of low energy consumption and occupying a reasonably small space [14]. The packed tower filled with random packing materials is shown in Figure 7.1 which was used in this study. In the counter-current packed column, liquid flows down via gravity through the random packing materials to form droplets or a trickle film, whereas the gas flows upwards through the packing materials to contact with the liquid droplets or film [15].

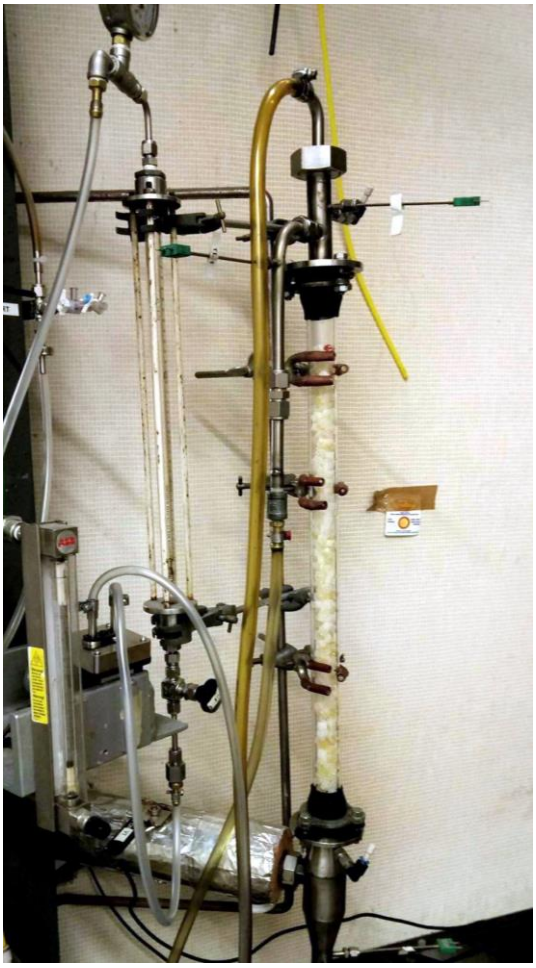

Figure 7.1 Photo of the packed oil scrubber with random packing materials used in this study.

7.3.1 Henry's law

The oil scrubber for absorbing tars involves the absorption of the gaseous tars in the producer gas into the liquid oil solvents. The solubility of tars in the liquid oil solvent is governed by Henry's law if the system is an ideal gas-liquid mixture and the tars in the gas phase is very dilute [16]. Henry's law can be expressed by the equation as follows [16]:

$$\frac{H}{P} = \frac{y_i}{x_i} \tag{7.1}$$

Where, H is Henry's constant for a given system, atm;

P is the total pressure of the system, atm;

yi is the mole fraction of tars in the gaseous phase;

xi is the mole fraction of tars in the liquid phase;

The H/P at the right side of Eq. (7.1) is called the equilibrium coefficient [17], which is the ratio of mole fractions of a tar compound in the gas and liquid phase at equilibrium [16]. The equilibrium coefficient for each of the tar compound can be determined through a non-random two-liquid (NRTL) model [16].

7.3.2 The oil scrubber system in this research group

An oil scrubber system used in this study was available before this study, but it was not in working condition and it had not been operated successfully due to some design problems. Therefore, verification and modification were firstly conducted with the assistance of two research students of this group.

To verify the oil scrubber, design instructions for a packed tower in the book of MASS-TRANSFER OPERATIONS [18] was followed. The packed tower (scrubber) is mainly comprised of a tower shell, packing elements, a packing support, a packing restrainer, an entrainment eliminator, and a liquid distributor. For the oil scrubber, these components were designed and described in Table 7.5. After modification, the oil scrubber system was experimentally tested and the details can be found in Section 7.3.2.

Apart from the packed tower (scrubber), the oil scrubber system also includes other sections for gas introduction, oil circulation, and gas sampling. The schematic diagram of the oil scrubber is shown in Figure 7.2. The gas introduction section consists of a pipe with tracing heat, a temperature monitor, and a cyclone. The pipe with tracing heat is used for connecting the DFB gasifier and the oil scrubber at a controlled temperature of 200°C so that the tars would not condense in the pipe. The pipe is covered by an insulation layer. Following the pipe with tracing heat, the gas goes into a cyclone with a trap which is for capturing particulates in the producer gas before it flows into the oil scrubber.

For the oil circulation section, it is comprised of an oil tank, a ball valve, a 3-way valve, a peristaltic pump, and an oil sampling bottle. The peristaltic pump, purchased from Cole-Parmer Instrument Company with the model number of 7521-57, is used for pumping oil from the oil tank to the liquid distributor at the top of the packed column.

Furthermore, the gas sampling section includes a gas sampling train, a rotameter, and a diaphragm pump. The gas sampling train consists of three gas washing bottles in an ice bath. A diaphragm pump, supplied by Charles Austen Pumps Ltd. with the model number of CAPEX V2, is used for

driving the producer gas from the DFB gasifier through the oil scrubber and the gas sampling train to the afterburner and fume hood.

Table 7.5 Components of the oil scrubber in this research.

Item	Description	Requirements in the book of MASS-TRANSFER OPERATIONS [18]	Picture
Packing elements	Partition ring of 7.5 mm in length, 8 mm of inner diameter (ID) and 9 mm of out diameter (OD)	1. Provide large interfacial surface between liquid and gas; 2. Process desirable fluid-flow characteristics; 3. Be chemically inert to fluids being processed; 4. Have structural strength to permit easy handling and installation; 5. Low cost.	
Tower shell/column	Glass tube of 55.88 cm height and 2.54 cm in ID	1. Strong and inert to the liquid and gas; 2. Usually circular.	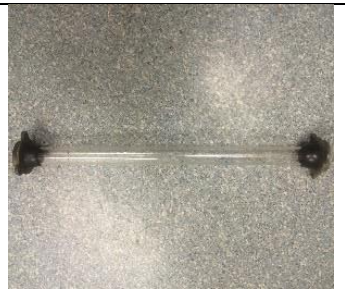
Packing support	A large hole mesh	1. Being sufficiently strong to carry the weight of a reasonable height of packing; 2. Having ample free area to allow liquid and gas flow with minimum restriction.	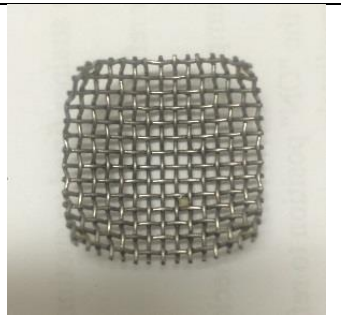

Packing restrainer	Mesh screen	Have the ability to guard against the packing elements.	
Liquid distributor	Perforated pipe	1. Distribute the liquid adequately at the top of the packing; 2. The perforated pipe can be used for small packing tower.	
Entrainment eliminator	Steel wool	1. Have the ability to remove mist at the top of packing tower; 2. Anti-corrosive to the gas and liquid.	

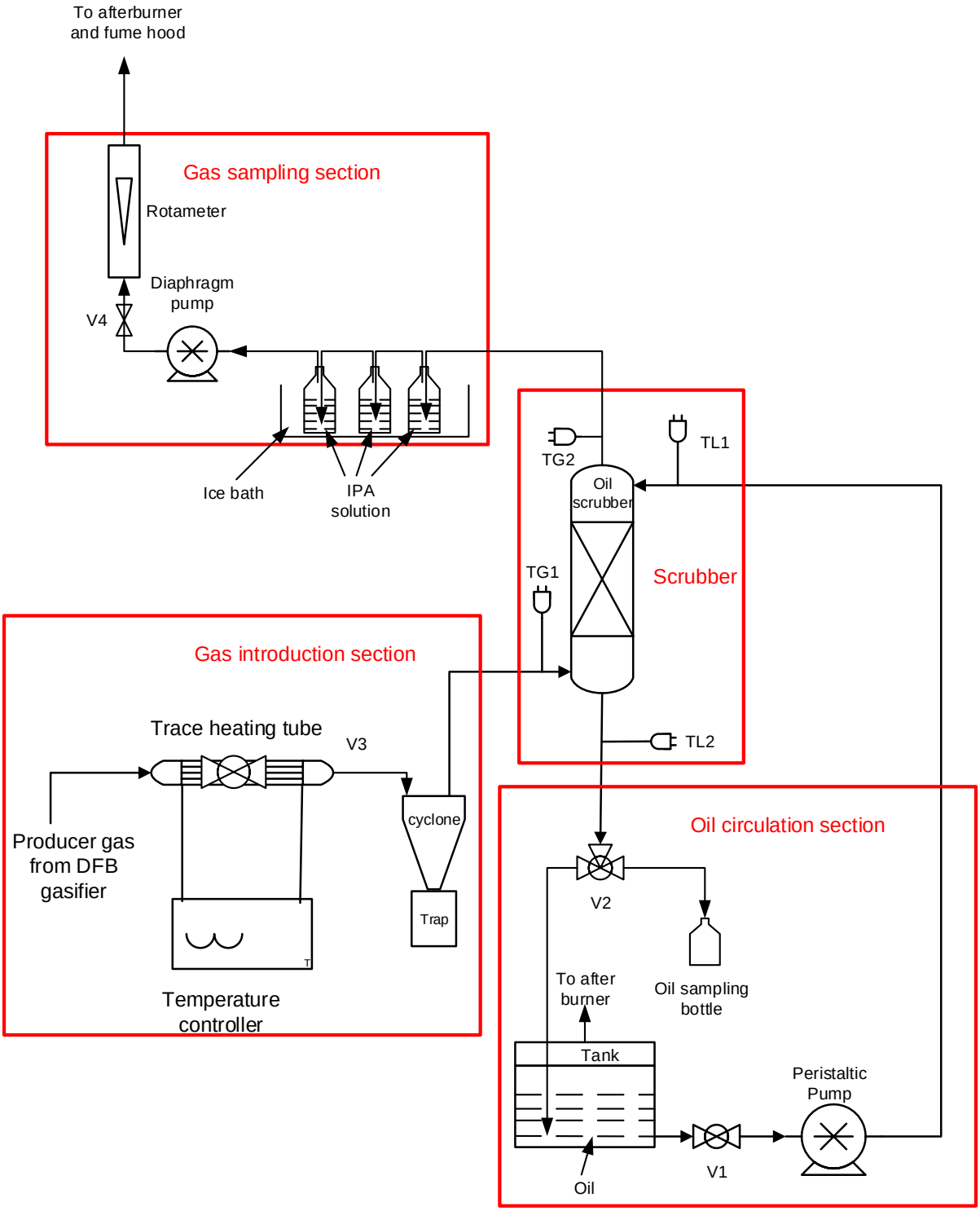

Figure 7.2 Flow diagram of the old oil scrubber system available before this research.

7.3.3 Modification and calibration of the oil scrubber system

Before experiments were conducted on the oil scrubber system, the gas sampling section of the oil scrubber system was modified. It was found that the rotameter itself needed calibration because the rotameter was specified for air, not for producer gas. Moreover, the composition of producer gas varied with gasification operation conditions and application of different bed materials as well as the type of biomass feedstock for gasification. Therefore, an anti-corrosion drum (wet) type flowmeter was added after the rotameter in the gas sampling section for measuring the producer gas volume. Thus, the gas flow rate could be calibrated from the total volume of producer gas divided by the time for gas collection. The calibration curve is shown in Figure 7.3 which was used to determine the gas flow rate during the experiment.

During the system assessment experiments, it was found that the cyclone was easily blocked by tars and fine particulates in the producer gas. Therefore, the cyclone was removed from the system as shown in Figure 7.4. It was thought that there may be a problem when the particulates existed in the inlet gas to the oil scrubber; however, after a few of assessment runs, it was found that the particulates concentration was low and these could be removed effectively by the oil scrubber as well.

Moreover, to improve the ability of the sampling train to absorb tars in the outlet gas, the sampling train was adjusted to five sampling bottles that contained isopropyl alcohol (IPA) in the first three bottles (150 mL IPA in the first bottle and 100 mL IPA in the second and third bottles respectively) and two empty bottles for restricting overflow. In addition, the ice bath was changed to contain ethylene glycol and water mixture (50/50 v/v), which was maintained at −20°C during gas sampling by a digital temperature controller that was purchased from PolyScience. The schematic diagram of the modified system is shown in Figure 7.4 and its photos are given in Figure 7.5.

Furthermore, calibrations of the peristaltic pump for the biodiesel and canola oil, respectively, were performed by controlling the pump settings, thus the oil for a certain time was collected by the oil sampling bottle and measured by a 500 mL graduated cylinder. The calibration curves are shown in Figure 7.6.

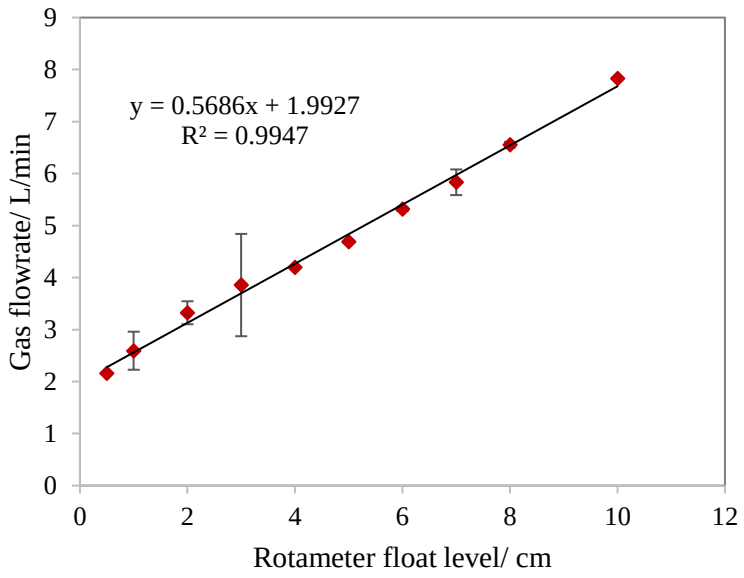

Figure 7.3 Calibration of the rotameter by using producer gas from a DFB gasifier.

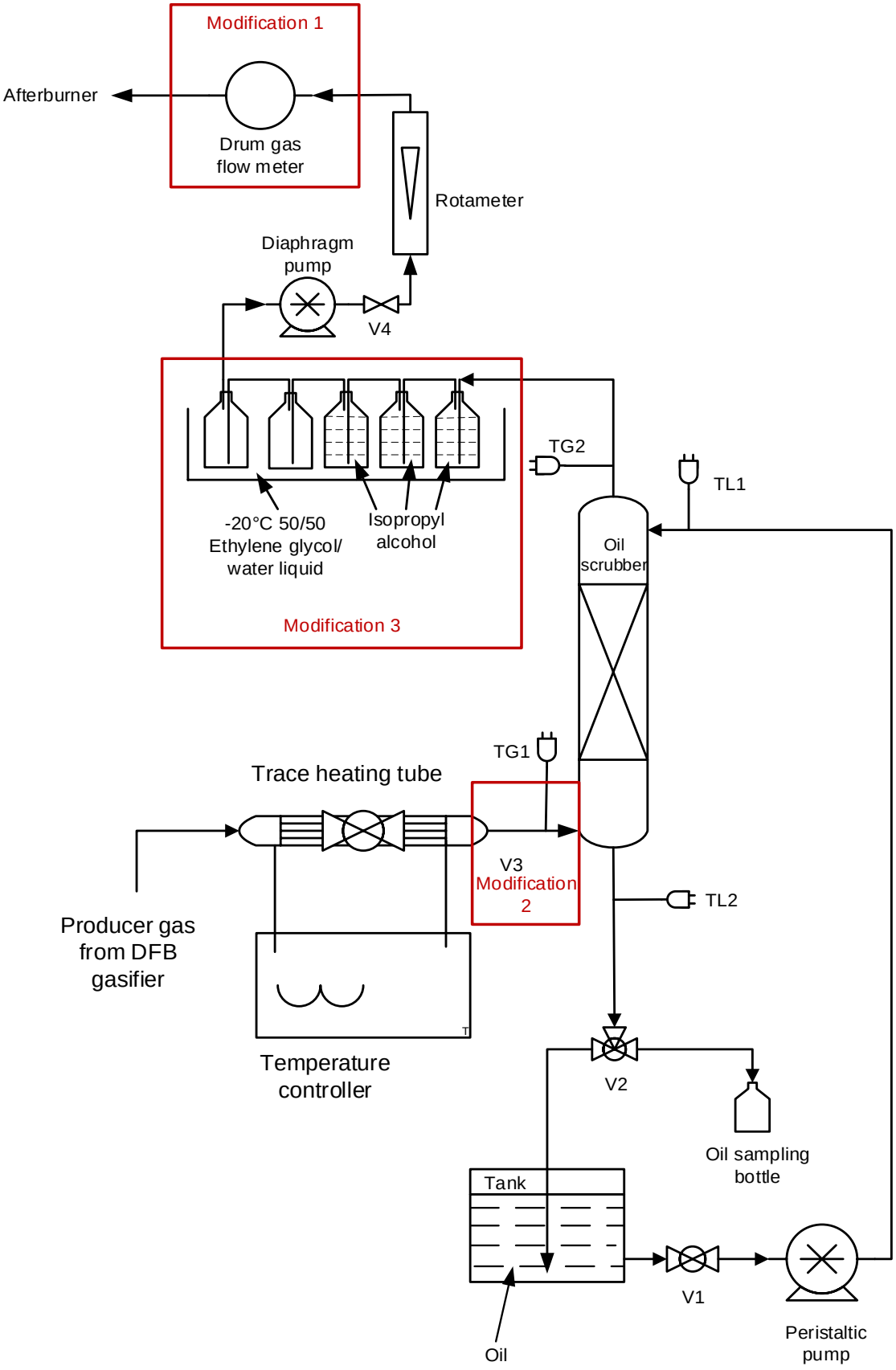

Figure 7.4 Diagram of oil scrubber system for tar removal.

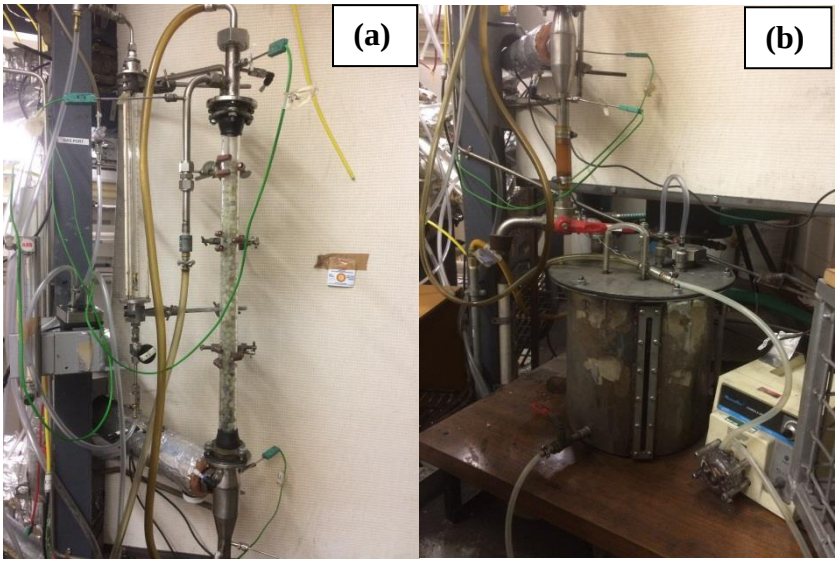

Figure 7.5 Pictures of oil scrubber system for tar removal. Picture (a) mainly contains the packed column part. Picture (b) mainly contains the oil tank and the peristaltic pump.

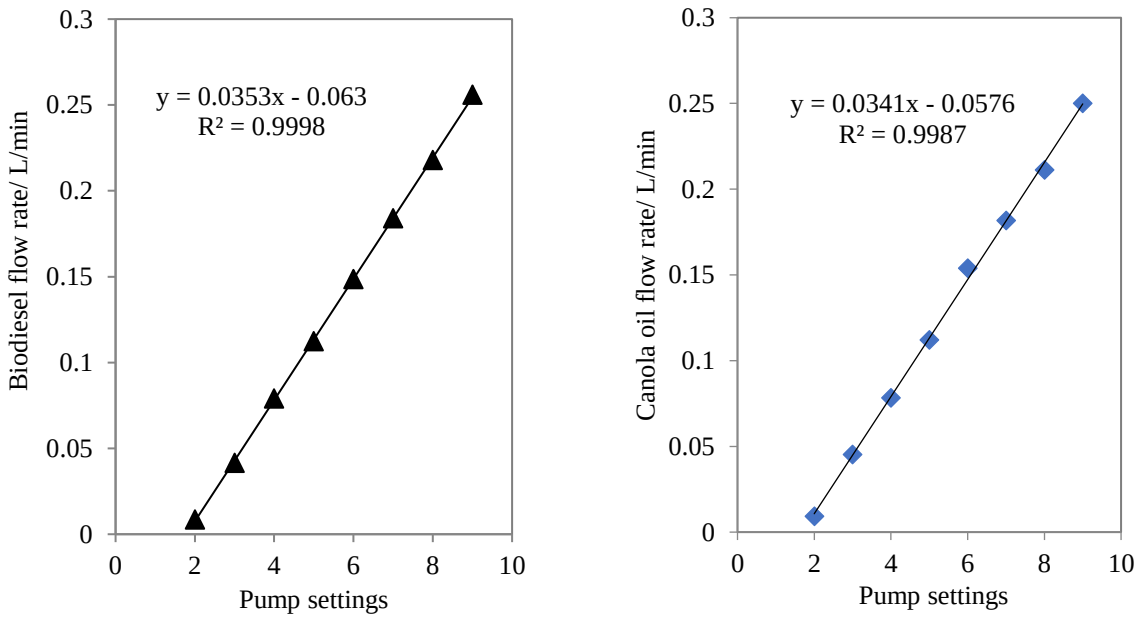

Figure 7.6 Calibration curves for biodiesel and canola oil by using the peristaltic pump.

7.4 Operation range of the oil scrubber

In scrubber design, if the operating gas flow rate (G) and liquid flow rate (L) are known, the diameter and height of the packed column can be determined using methods given in Chemical

Engineers textbooks. In this research, the available column was selected with known dimensions of 55.88 cm in height and 2.54 cm in inner diameter. Therefore, the range of gas and liquid flow rates on this scrubber were calculated based on the method in Treybal's book [18].

As the packing elements were randomly packed in the scrubber, the flooding boundaries can be calculated by the following graph of Figure 7.7.

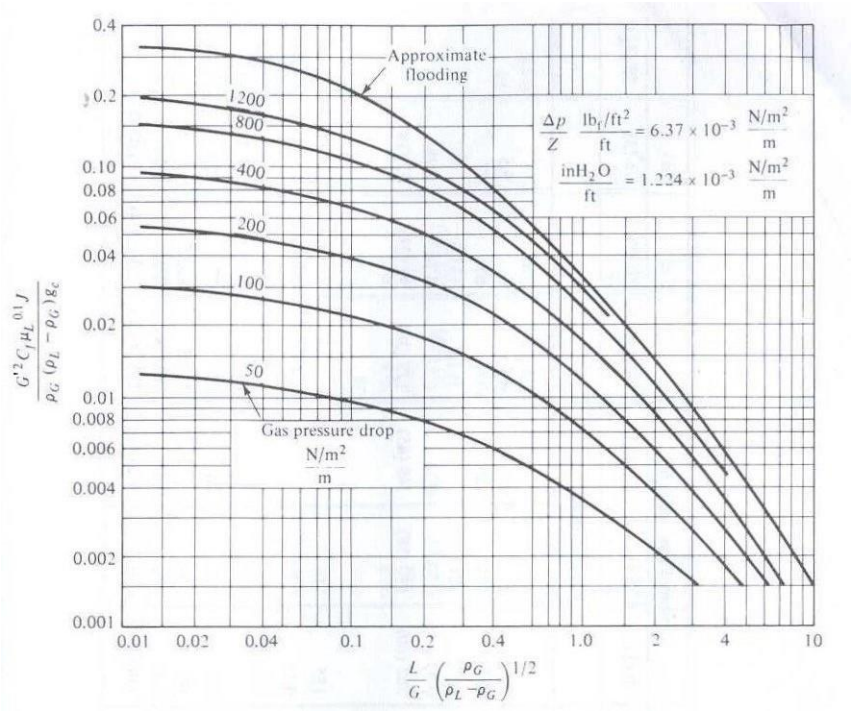

Figure 7.7 Flooding and pressure drop in random-packed towers [16].

The x-axis of Figure 7.7 represents the flow parameter (F_{LG}) and its correlation is shown as below.

$$F_{LG} = \frac{L}{G}\left(\frac{\rho_G}{\rho_L}\right)^{0.5} \tag{7.2}$$

Where,

L is the liquid flow rate, m^3/s;

G is the gas flow rate, m^3/s;

ρ_G is the gas density, kg/ m^3;

ρ_L is the liquid density, kg/ m^3.

The y-axis of Figure 7.7 represents the capacity parameter (CP), of which correlation is shown below.

$$CP = \frac{G'^2 \cdot C_f \cdot \mu_L{}^{0.1} \cdot J}{\rho_G \cdot (\rho_L - \rho_G) \cdot g_c} \tag{7.3}$$

Where,

G' is the calculated gas flow rate, $kg/(m^2 \cdot s)$;

C_f is one of the parameters of packing elements;

μ_L is liquid viscosity, m^2/ s;

For J and g_c in Eq. (7.3), g_c=1, and J=1 in SI.

$$G' = \pi \cdot \frac{D^2}{4} \cdot F_{G'} \tag{7.4}$$

Where,

π is the mathematical constant;

D is the diameter of the column, m;

$F_{G'}$ is the gas flow rate, kg/s.

To obtain the values of properties of the producer gas, the gas composition of the producer gas and tar concentration should be known. However, the gas composition and tar concentration of

the producer gas from a DFB gasifier was affected by operation conditions, applied catalyst, and type of biomass feedstock. In the calculations, gas composition of the producer gas from a typical experimental run of biomass steam gasification was used as shown in Table 7.6 [1]. The tar content in the producer gas was 0.2 vol.% (approximately 12.7 g/m^3) which is the maximum level from previous gasification experiments [1, 19-21]. The average molecular weight of the tars was calculated based on the tar composition analysed by a Varian CP-3800 gas chromatography (GC) and the parameters used for the calculations are listed in Table 7.7.

During the calculations, it was found that at high liquid flow rates and low gas flow rates, flooding was likely to occur which can be explained by Figure 7.8. From Figure 7.8, it is found that at a given liquid velocity (u_L), the liquid hold-up (h_L) in the packed column is almost independent of the gas velocity (u_V) if the gas velocity is lower than the maximum value identified by the line AA. However, when u_V is higher than the values on the AA line, the liquid hold-up (h_L) increases with the gas velocity significantly. If the gas velocity (u_V) reaches a critical value at the CC line, flooding will occur and the system cannot operate successfully. The CC line is called the flooding line. If the gas velocity at the flooding point ($u_{v,Fl}$) is known, the maximum gas velocity at line AA can be calculated which is approximately 65% of the $u_{v,Fl}$ [15]. The operating range of the gas velocity is usually between 30 and 80% of $u_{v,Fl}$ [15]. Furthermore, it was observed from Figure 7.8 that if u_L is increased, $u_{v,Fl}$ will decrease.

For example, if the biodiesel flow rate is 0.15 L/min which is equivalent to a liquid velocity of 0.0049 m/s, the producer gas flow rate at flooding point is calculated to be 8.0 L/min, equivalent to the gas velocity of 0.2633 m/s. The calculation details can be found in Appendix C. Therefore, the calculated operating range of the producer gas flow rate should be in the range of 2.4 – 6.4 L/min.

However, when the operating range was experimentally verified by running biodiesel at a flow rate of 0.15 L/min through the oil scrubber and increasing the producer gas flow rate from low to high levels, it was found that flooding occurred when the producer gas flow was approximately 3.4 L/min. This was much lower than the calculated flooding gas flow rate of 8.0 L/min. Therefore, further investigation should be performed to explain this phenomenon and revise the calculations.

Table 7.5 Gas composition of producer gas from one experimental run on the DFB gasifier [1].

Gases	Volume concentration/ vol.%	Molecular weight/ kg/kmol
Helium (He)	1.2	4
Hydrogen (H_2)	34.5	2
Nitrogen (N_2)	3.0	28
Methane (CH_4)	11.0	16
Carbon monoxide (CO)	24.0	28
Carbon dioxide (CO_2)	22.6	44
Ethylene (C_2H_4)	3.0	28
Ethane (C_2H_6)	0.7	30
Average gas molecular weight		21

Table 7.6 Parameters used for the operation range calculation.

Parameters of gas phase	Value	Parameters of liquid phase	Value
Producer gas temperature at the inlet of oil scrubber, K	473.15	Biodiesel density at 323K, kg/m^3	857
Density of tar, kg/m^3	1060	Biodiesel viscosity, Pa·s	0.05
Average tar molecular weight, kg/kmol	157.4		
Average producer gas weight with tars, kg/kmol	21.3		
Density of the producer gas with tars at 473K, kg/ m^3	0.536		

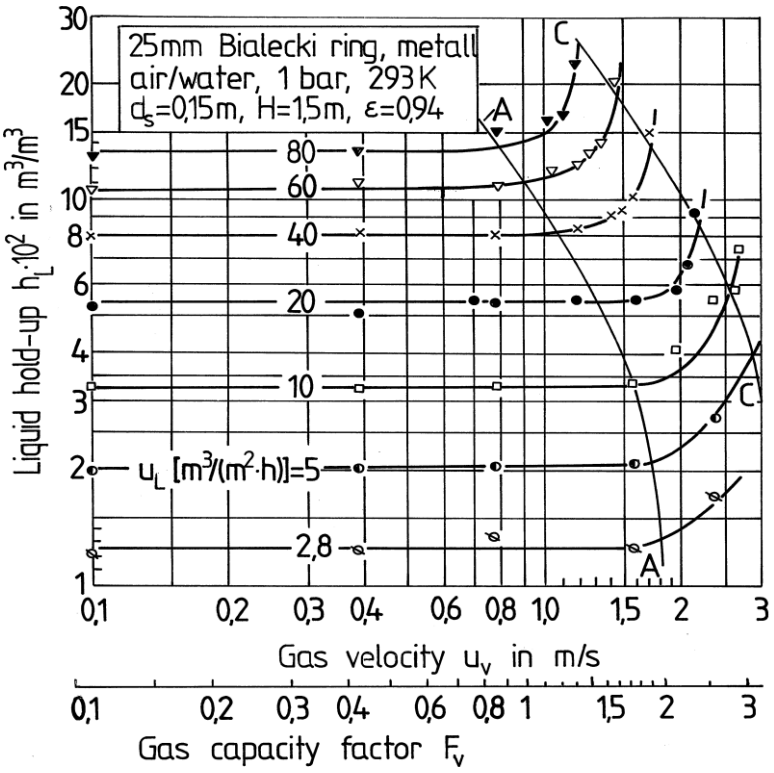

Figure 7.8 Example of liquid hold-up (h_L) as a function of gas velocity (u_V) and gas capacity factor (F_V) [15].

7.5 Methods of tar sampling and analysis

To determine the tar removal efficiency of the oil scrubber, tar concentrations in the inlet and outlet gases of the oil scrubber should be known. Therefore, the raw producer gas from the gasifier (inlet gas of the oil scrubber) and the cleaned gas after the oil scrubber (outlet gas of the oil scrubber) were sampled at a similar time but by different sampling methods. For analysing the tar concentration of the inlet gas, during the biomass gasification run on the DFB gasifier, a certain volume of producer gas (200 mL) was extracted by a syringe through a 3 mL Supelclean LC-NH_2 solid phase extraction (SPE) column, where tars were trapped. Thus, tars were eluted from the SPE column by 1 mL of dichloromethane (DCM) with 40 ppm of n-dodecane as internal standard (IS) and 1 mL of DCM and IPA mixture (50/50 v/v) with 40 ppm IS, respectively, to two 2 mL vials. Afterwards, the tar solution samples were analysed by the Varian CP-3800 GC from which the concentrations of 31 tar compounds were analysed. These 31 compounds of tars were categorised into 4 classes according to the methods proposed by Kiel et al. [22] which are shown in Table 7.8. More details about the sampling and analysis methods of tars in the producer gas of biomass gasification can be found elsewhere [20, 23]. The column information of the Varian CP-3800 GC is available in the publications of Saw and Pang [20, 23]. These works were completed by Rahman Jinar Hadi in our group who conducted the experiments on the DFB gasifier.

In addition, the cleaned gas after the oil scrubber was impinged by a sampling train in a −20°C chilled bath as shown in Figure 7.4. During the experiment, the total volume of the sampling gas drawn through the sampling bottles was measured by the drum type flowmeter at atmospheric pressure and the sampling time was recorded by a stopwatch. After each sampling run, all the IPA solution in the sampling bottles was mixed together completely. Thus, 10 mL of the mixed solution was spiked with 40 ppm of IS and 1 mL of the spiked solution was

pipetted to a 2 mL vial and analysed by the Varian CP-3800 GC. Peaks of those 31 compounds on the GC graph were identified and their concentrations were calculated.

Table 7.7 31 typical compounds of the tars in the producer gas of biomass gasification.

No.	Name	Tar classification
1	Pyridine	Class 2
2	Phenol	Class 2
3	o-cresol	Class 2
4	(m+p)-cresol	Class 2
5	Quinoline	Class 2
6	Isoquinoline	Class 2
7	Toluene	Class 3
8	p-xylene + Ethylbenzene	Class 3
9	m-xylene	Class 3
10	o-xylene	Class 3
11	Styrene	Class 3
12	Indene	Class 4
13	Naphthalene	Class 4
14	2-Methylnaphthalene	Class 4
15	1-Methylnaphthalene	Class 4
16	Biphenyl	Class 4
17	Acenaphthylene	Class 4
18	Acenapthene	Class 4

19	Fluorene	Class 4
20	Phenanthrene	Class 4
21	Anthracene	Class 4
22	Fluoranthene	Class 5
23	Pyrene	Class 5
24	Benz(a)anthracene	Class 5
25	Chrysene	Class 5
26	Benso(b)fluoranthene	Class 5
27	Benso(k)fluoranthene	Class 5
28	Benso(a)Pyrene	Class 5
29	Indeno(1,2,3-cd)pyrene	Class 5
30	Benso(g,h,i)perylene	Class 5
31	Dibenso(a,h)anthracene	Class 5

7.6 Experimental procedures

The complete experimental procedures for the oil scrubber experiments for tar removal can be divided into five parts. 1). Material preparation and equipment setup; 2). Tar removal process; 3). System shutdown; 4). System cleaning; 5) Sample analysis. Detailed information of each part is described as below.

(1) Material preparation and equipment setup

Before each experimental run, approximately 2 L biodiesel/canola oil is weighed and poured into the oil tank as shown in Figure 7.4 which will be used for a whole experimental run. The

tank is then sealed with a rubber ring and tightened well. The clean and dry packing elements are put into the column, and the oil scrubber is set up by attaching the appropriate connections. Afterwards, thermocouple sensors are attached to the oil scrubber and ensure all of the pipelines are in correct places and connected when needed. After the system setup is completed, the pump for oil circulation is turned on and the oil is circulated for 5 minutes to check if there is oil leakage. If there is no leakage, the system is ready for the experimental run.

(2) Tar removal process

Before the experiment on the tar removal, the temperature of the heat tracing pipe is turned on and the temperature is set at 200°C. Then the digital temperature controller for chilling the sampling train bath is turned on and set to −20°C. Sampling bottles are filled with IPA solution as per description in Section 7.5. Finally, the CO detector and the monitor which connect to the thermal couples on the oil scrubber are turned on.

After the biomass gasification is at steady running mode, and temperature on the heat tracing pipe as well as the chilling bath have reached their target points, tar removal experiment is started by turning on the peristaltic pump with a pre-set oil flow rate. Moreover, the valve on the heat tracing pipe connecting the oil scrubber the DFB gasifier is turned on and gas flows through the oil scrubber. Almost at the same time, the diaphragm pump is turned on and the gas flow rate is controlled by a valve before the rotameter. The gas flow rate is determined by the rotameter float level based on the calibration curve as given in Figure 7.3. However, an accurate gas volume for each sampling run is later determined by the drum type flowmeter and the time recorded by a stopwatch. After a stable run for a period of time, the sampling train is disconnected, the solution is mixed thoroughly and stored in a glass bottle for further analysis. Following this, the gas washing bottle is rinsed and filled with new IPA solution and another sampling run is conducted. At the end of the last sampling run, the system is ready to be shut down.

(3) System shutdown

For system shutdown, the diaphragm pump and peristaltic pump are turned off first. Then the temperature controller/monitor that is connected to the heat tracing pipe and the digital temperature controller are turned off.

(4) System cleaning

Since the oil scrubber is attached to the gasifier, system cleaning is carried out after the gasification experiment is finished and the gasifier system has been cooled down. Normally, it is one night after the experiment. For the system cleaning, the most important parts are the heat tracing pipe, the oil scrubber, the oil tank and the diaphragm pump. Firstly, the oil scrubber is disconnected, removed and disassembled, and thus each part can be thoroughly cleaned and dried. Secondly, the heat tracing pipe is disconnected from the gasifier and the oil scrubber, and a specially designed long bush is used to clean it until there are no fine particles observed in the pipe. Thirdly, all the contaminated oil is drawn out by the peristaltic pump and weighed on a balance. Finally, the diaphragm pump is disconnected from the system and disassembled carefully, then IPA solvent is used to clean each piece of the pump under the fume hood. After they are cleaned and dried, the diaphragm pump is reassembled.

(5) Sample analysis

All of the samples from the experiments are analysed by the method described in Section 7.5.

7.7 Results and discussion of the preliminary experiments

7.7.1 Tar removal by the oil scrubber with biodiesel

Biodiesel was first employed in the oil scrubber for experiments on tar removal from the producer gas of biomass steam gasification on a DFB gasifier. To study the effects of different liquid/gas (L/G) ratios on the efficiency of the tar removal, different ratios of biodiesel molar

flow rate to producer gas molar flow rate were examined during the experiments, as shown in Table 7.9. The inlet and outlet gases of the biodiesel scrubber for each run were sampled and analysed by the methods introduced in Section 7.5 of this chapter. The sampling times for the outlet gas of each run are also given in Table 7.9. As the analysis methods are the same for all experimental runs, results from run No. 3 will be presented and discussed in this section, and the results on tar removal efficiencies in each run are finally summarized.

The GC results for tar analysis in the inlet and outlet gases of run No. 3 are shown in Figure 7.9 in which the 31 tar compounds as listed in Table 7.8 are indicated. Interestingly, in the GC graphs of outlet gas tars, it was found that an obvious peak, named compound x, with the retention time of 20.176 min was much larger than the other tar compounds (benzene is not a tar compound). When comparing the GC graph of the outlet gas tars with that of the inlet gas tars, it was found that most of the tar compounds in the inlet gas were significantly removed by the biodiesel scrubber. Furthermore, it was observed from Figure 7.9 that the tar species in the inlet gas (the producer gas of biomass gasification) were more than those 31 tar compounds as listed in Table 7.8 which could not be identified due to the lack of reference standard although those unidentified compounds were at minor concentrations. Therefore, there are limitations of the tar analysis methods in this research because only 31 tar compounds were analysed.

To further identify the compound x in the outlet gas, the blue rectangle area in Figure 7.9 was enlarged for clarity, as shown in Figure 7.10. It was found that the compound x had a high possibility of being benz(a)anthracene based on the peak shape and retention time. Thus, the concentration of benz(a)anthracene in the outlet gas was calculated by the calibration curve of benz(a)anthracene. The benz(a)anthracene concentration in the outlet gas was 2.59 g/m^3. However, its concentration in the inlet gas was only 0.56 g/m^3. This is unexpected as the oil scrubber is a physical process and the operation temperature was low (~50°C) in which

polymerisation and depolymerisation or decomposition should be minimum. Therefore, further tests are recommended to examine the reasons for this finding.

Due to the uncertainty of compound x, it was not included in the calculations of tar removal efficiency (ε) of the biodiesel scrubber by using Eq. (7.5), where the concentrations of those tar compounds in Table 7.8 except for benz(a)anthracene in the inlet gas and outlet gas were used. The efficiency of the oil scrubber at different L/G ratios are presented in Figure 7.11 from which it was observed that the L/G ratio between 1.28 and 4.35 barely affected the efficiency of the biodiesel scrubber for tar removal and the average efficiency was 96.8±1.4%. It was also found that the efficiency of sample No. 7 was slightly lower than those of the other runs. Hence, the efficiency of the biodiesel scrubber with elapsed time is shown in Figure 7.12. A plausible explanation for the slightly lower efficiency of No. 7 sample run might be due to the deterioration of biodiesel with increasing tars in it. This is easily understood using the Henry's law. As shown in the Eq. (7.1), the equilibrium coefficient is a constant number for each of the tar compound, if the tar concentration in the liquid phase is increased with time elapsed, the tar concentration in the gaseous phase at equilibrium is increased as well. In other words, the efficiency of the oil scrubber is lowered. A process model using the Aspen Plus software was developed by Bhoi [16] to calculate the tar removal efficiency of a soybean oil scrubber based on the equilibrium stage of tar absorption. It was found that the tar removal efficiency was decreased with the increase of time [16].

$$\varepsilon = \frac{C_{30\ \text{tar compounds in the inlet gas}} - C_{30\ \text{tar compounds in the outlet gas}}}{C_{30\ \text{tar compounds in the inlet gas}}} \quad (7.5)$$

Where,

$C_{30\ \text{tar compounds in the inlet gas}}$ is the total concentration of the tar compounds listed in Table 7.8 except for benz(a)anthracene in the inlet gas;

$C_{30\ tar\ compounds\ in\ the\ outlet\ gas}$ is the total concentration of the tar compounds listed in Table 7.8 except for benz(a)anthracene in the outlet gas.

Furthermore, at the end of the experiment, the total mass of water and contaminants that the biodiesel scrubber removed from the producer gas was measured to be 113.4 g. These contaminants included water, tars and particles which were absorbed in the biodiesel. Based on this result and the total volume of producer gas that this scrubber cleaned, it was found that this biodiesel scrubber had the ability to remove 1.02 kg of water and contaminants from 1 m^3 of the producer gas of biomass gasification.

Table 7.8 Sampling time, producer gas and biodiesel flow rates, and L/G ratio of each sample run on the biodiesel scrubber.

Sample No.	Sampling time/ min	Biodiesel volume flow rate/ L/min	Gas volume flow rate/ L/min	L/G/ (mol/s)/(mol/s)
1	2	0.0782	4.84	1.28
2	2	0.1135	3.39	2.65
3	2	0.1488	2.71	4.35
4	2	0.0782	3.47	1.78
5	2	0.1135	2.80	3.20
6	2	0.1135	3.55	2.53
7	10	0.1135	3.48	2.58

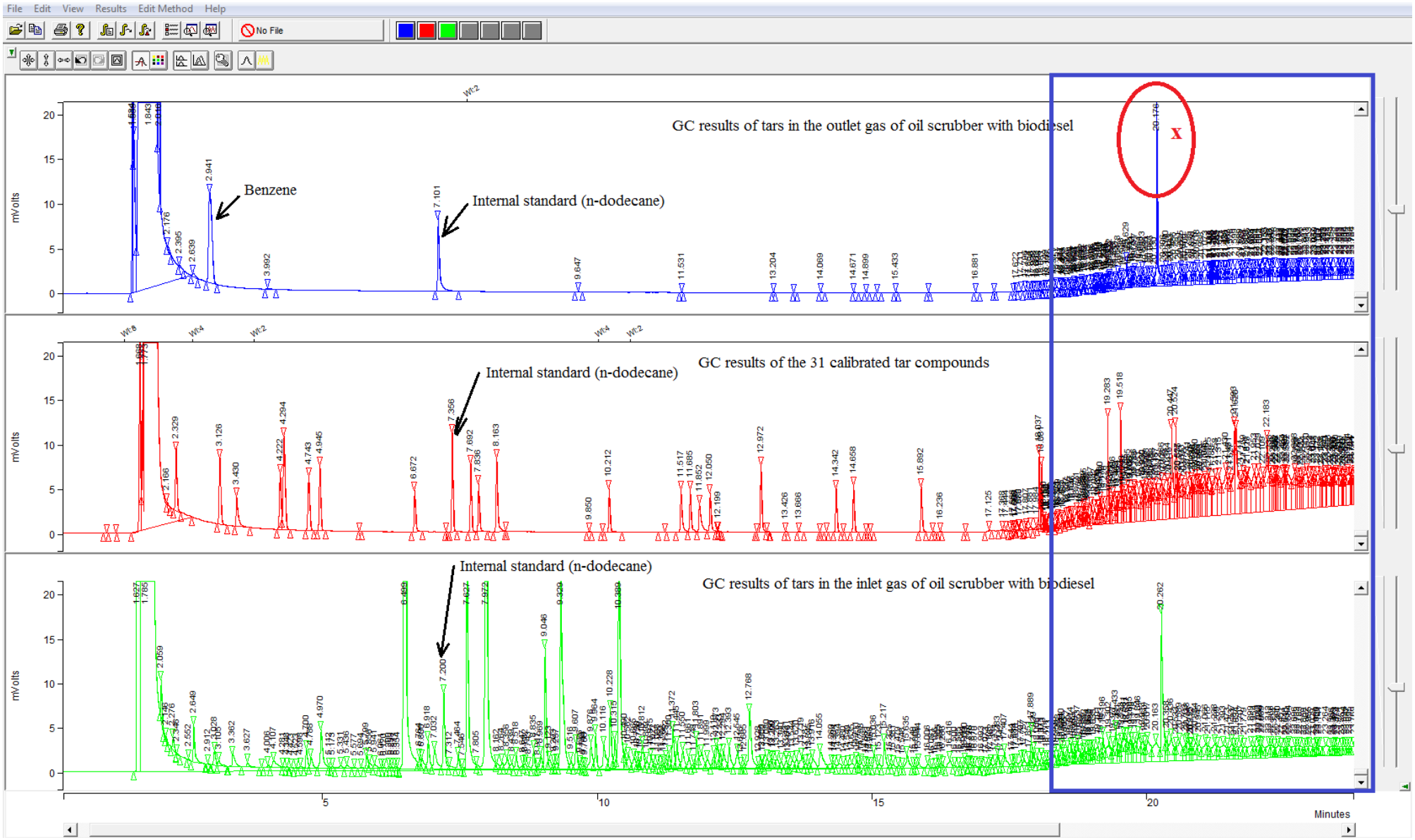

Figure 7.9 GC results of tars in the inlet and outlet gases of Sample No.3 on the biodiesel scrubber, and the GC result of those 31 calibrated tar compounds.

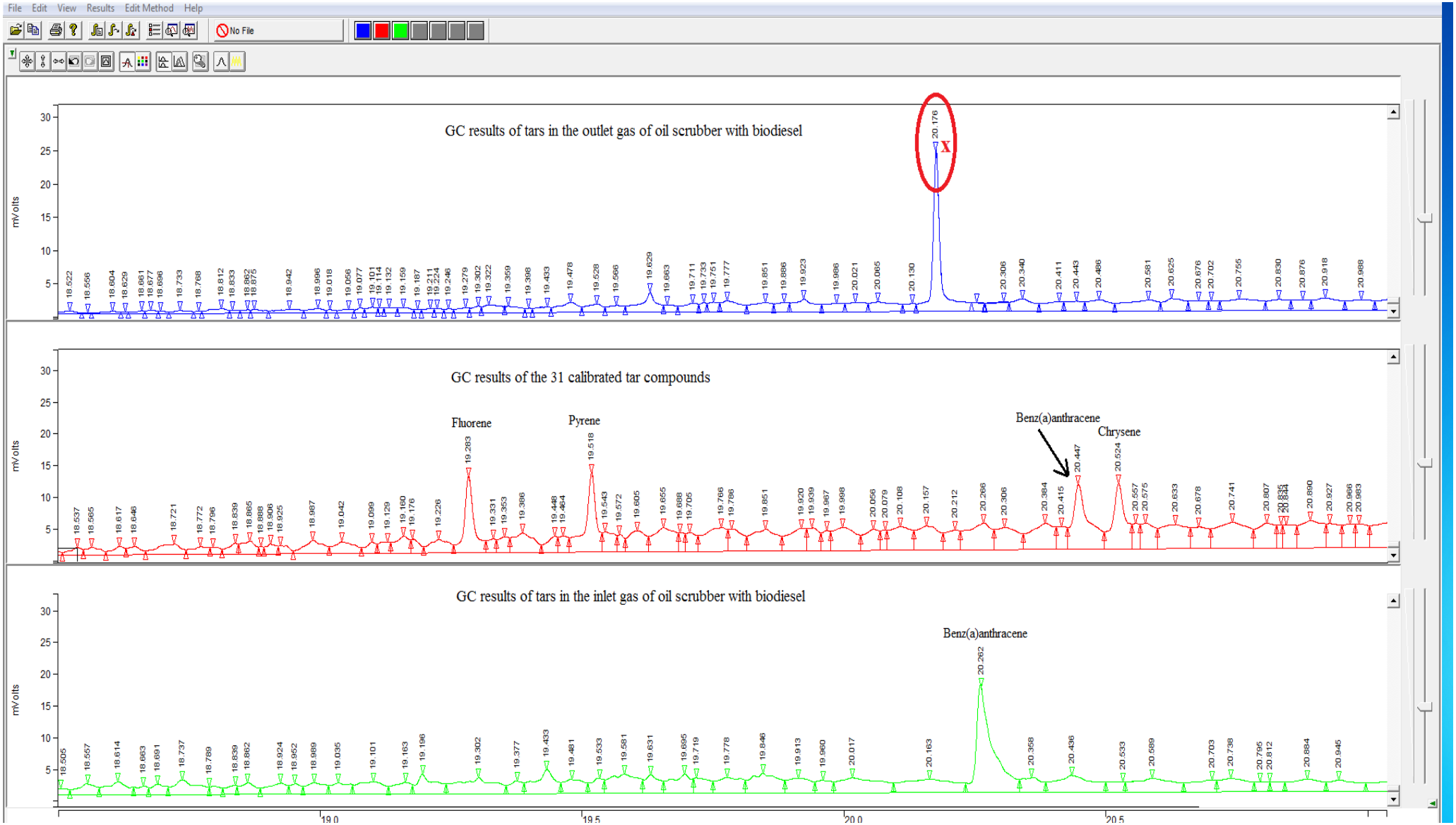

Figure 7.10 The enlarged blue rectangle area of Figure 7.9.

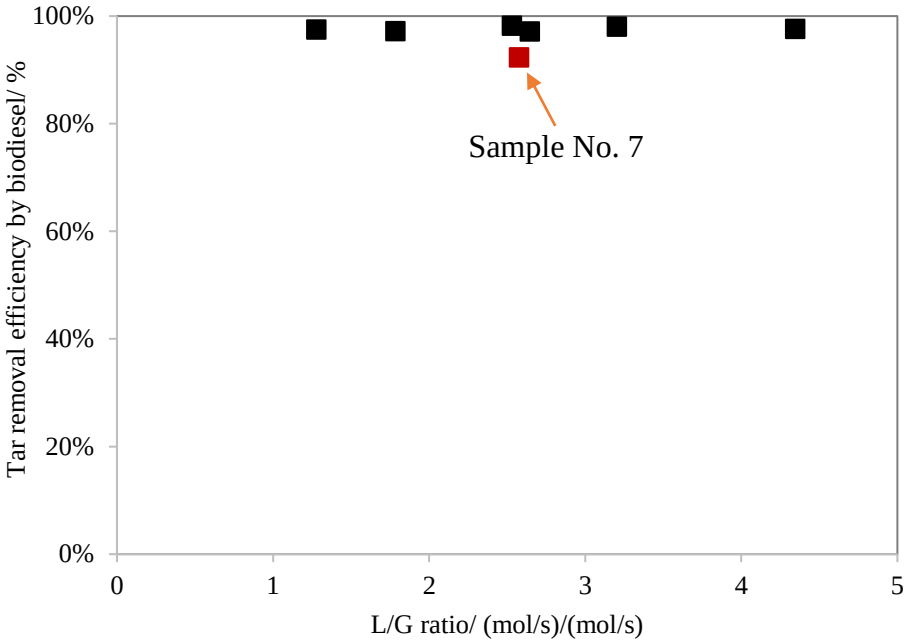

Figure 7.11 The efficiency of the biodiesel scrubber for tar removal at different L/G ratios.

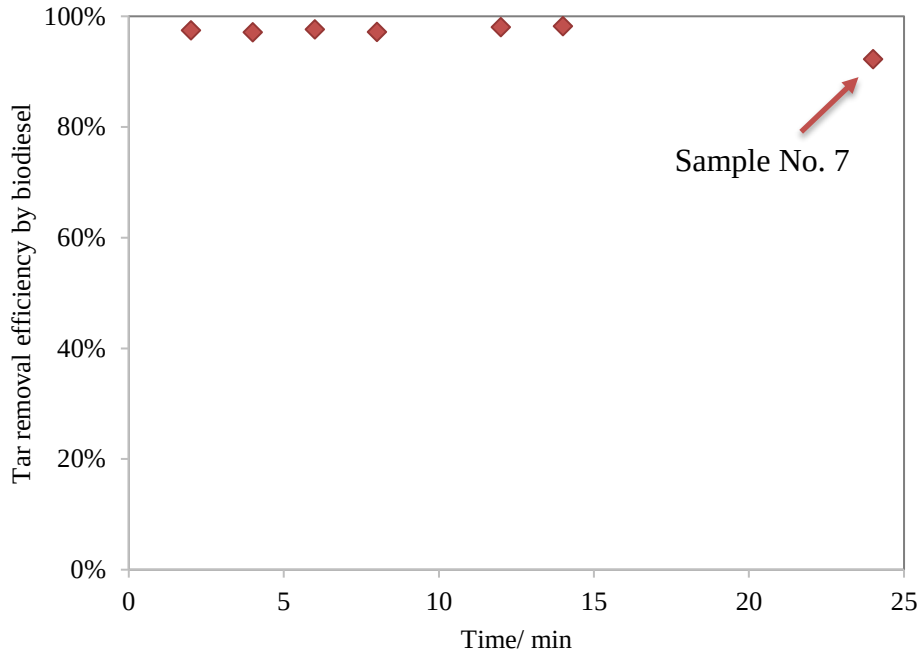

Figure 7.12 The efficiency of the biodiesel scrubber for tar removal with elapsed time.

7.7.2 Tar removal by the oil scrubber with canola oil

In a similar way to bio-diesel removal of tars, canola oil was tested in the oil scrubber as well. The sampling times, flow rates of producer gas and canola oil, and L/G molar ratios used in the experiments are presented in Table 7.10. The inlet gas and outlet gas of each experimental run were sampled and tested by the methods described in Section 7.5 of this chapter. As the analysis methods are the same for all experimental runs, results from run No. 1 will be presented and discussed in this section, and the results on tar removal efficiencies in each run are finally summarized.

The GC results of the inlet gas tars and outlet gas tars of Sample No. 1 are shown in Figure 7.13, where the 31 calibrated tar compounds as listed in Table 7.8 are indicated. From Figure 7.13, it was found that an obvious big peak at the retention time of 20.190 min was shown in the GC graph of the outlet gas tars, and it was named as compound y. This was similar to the results of the biodiesel scrubber.

To identify the compound y, the same method used for identifying compound x was utilized. It was also found that the compound y had a high possibility of being benz(a)anthracene. Thus, its concentration in the outlet gas was calculated by the calibration curve of benz(a)anthracene which was 1.53 g/m^3. However, the benz(a)anthracene concentration in the inlet gas was 0.73 g/m^3, which was again unexpected that it was less than the concentration in the outlet gas.

Nevertheless, the concentrations of those tar compounds in Table 7.8 except for benz(a)anthracene in the inlet and outlet gases were calculated. The efficiency of the canola oil scrubber was calculated by Eq. (7.5) for each run, and the results are presented in Figure 7.15. It was found that the canola oil scrubber had similar efficiency to the biodiesel scrubber for tar removal from the producer gas of biomass gasification that 96.3±1.6% tars can be removed.

Moreover, Figure 7.15 also shows that the efficiency of the canola oil scrubber increased slightly with the increase of L/G ratio, which was different from that of the biodiesel scrubber.

Furthermore, the efficiency of the canola oil scrubber for tar removal with the elapsed time is given in Figure 7.16. It was observed that the efficiency of the canola oil scrubber was decreased gradually which may be due to the deterioration of canola oil with more tars absorbed into it.

At the end of the experiment, the total mass of water and contaminants such as tars and particles that absorbed by the canola oil scrubber from the producer gas was measured. It was found that the canola oil scrubber had the ability to remove 1.21 kg water and contaminants from 1 m^3 of the producer gas, which was higher than that of the biodiesel scrubber.

Table 7.9 Sampling time, producer gas and canola oil flow rates, and L/G ratio of each sample run on the canola oil scrubber.

Sample No.	Sampling time/ min	Canola oil volume flow rate/ L/min	Producer gas volume flow rate/ L/min	L/G/ (mol/s)/(mol/s)
1	2	0.0788	4.02	1.55
2	2	0.1464	2.68	4.33
3	2	0.1126	3.34	2.67
4	2	0.1126	3.41	2.62
5	10	0.0788	2.76	2.26
6	10	0.0788	2.75	2.27
7	10	0.0788	2.77	2.25

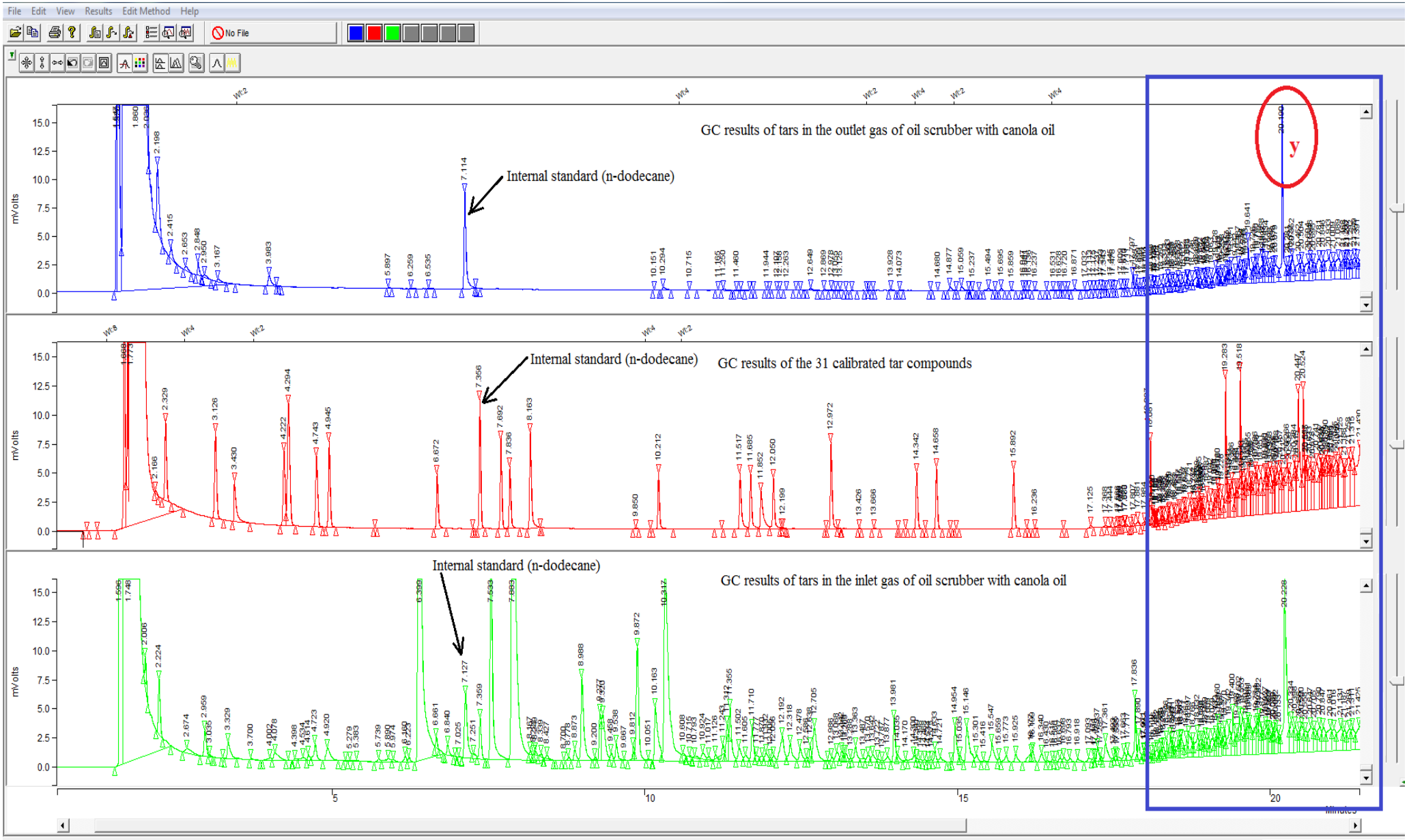

Figure 7.13 GC results of tars in the inlet and outlet gases of Sample No. 1 on the canola oil scrubber, and the GC result of those 31 calibrated tar compounds.

Figure 7.14 The enlarged blue rectangle area of Figure 7.13.

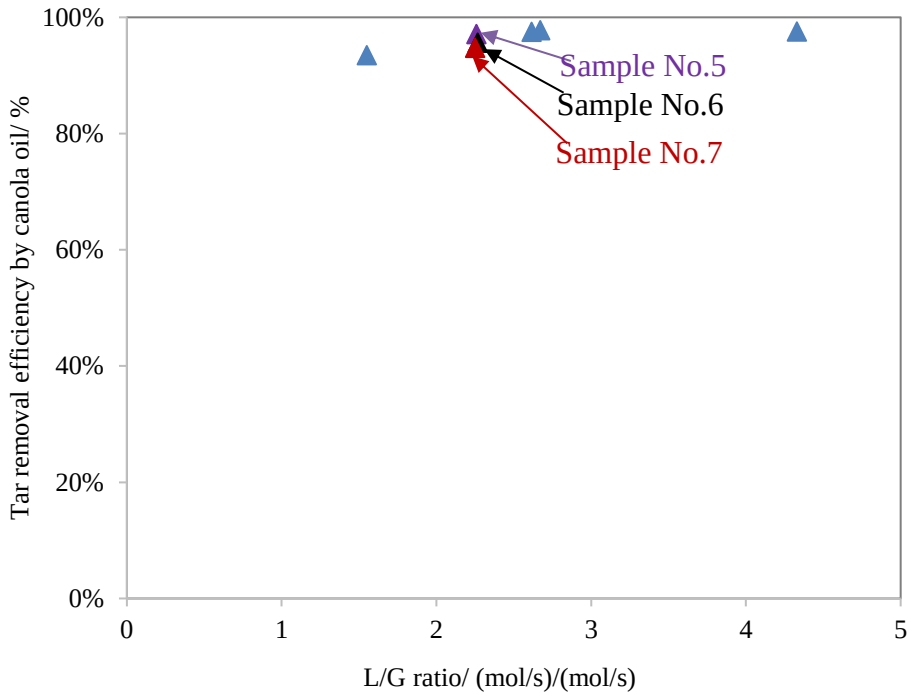

Figure 7.15 The efficiency of the canola oil scrubber for tar removal at different L/G ratios.

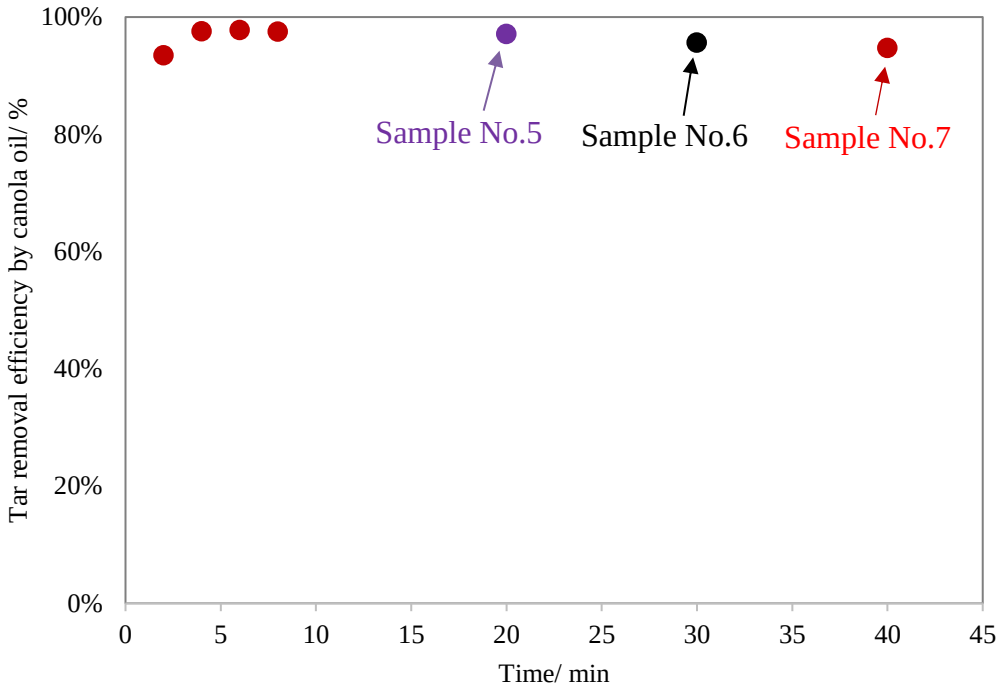

Figure 7.16 The efficiency of the canola oil scrubber for tar removal with elapsed time.

7.8 Conclusions and recommendations

An oil scrubber system in this research group was verified and modified to be applied for tar removal from the producer gas of biomass steam gasification on a DFB gasifier. From the preliminary experiments on this oil scrubber, it was found that except for an unknown compound and its unexpected increase in the outlet gases of the oil scrubber, this oil scrubber either with biodiesel or canola oil can achieve effective removal of tar compounds at an efficiency of ~96% GC-detectable tars from the producer gas of biomass gasification. This oil scrubber could also remove water, GC-undetectable tars, and particles from the producer gas. Further improvements and experiments are recommended as follows.

Firstly, it was found that the oil scrubber easily had flooding during the experiments. One possible reason might be because of the plastic partition rings used in the oil scrubber, which were non-perforated packing elements. They had a low void fraction and contained dead space, thus limited the operation range of the oil scrubber. Therefore, packing elements with large void fraction could be tried in the future. In addition, a new column with a larger diameter could be considered in the future to avoid flooding. Secondly, it is recommended that the sampling train should be designed on a bypass line. This modification would permit to do gas sampling while keeping the oil scrubber under continuous operation. Thirdly, the unknown compound in the outlet gas of the oil scrubber should be identified, and its source and concentration increase should be investigated and confirmed. If this is the product of polymerisation and depolymerisation of other tar compounds, then the operation condition of oil scrubber should be adjusted. If this is the compound of solvent, different solvents should be used. Otherwise, the majority of this compound should be condensed and filtered out after the oil scrubber. Finally, the efficiency of the oil scrubber for removing water-soluble contaminants such as NH_3 and H_2S can be studied in the future.

7.9 Reference

[1] W. L. Saw and S. Pang, "The influence of calcite loading on producer gas composition and tar concentration of radiata pine pellets in a dual fluidised bed steam gasifier," *Fuel,* vol. 102, pp. 445-452, 2012.

[2] M. Virginie *et al.*, "Effect of Fe–olivine on the tar content during biomass gasification in a dual fluidized bed," *Applied Catalysis B: Environmental*, vol. 121-122, pp. 214-222, 2012.

[3] T. Tarnpradab, S. Unyaphan, F. Takahashi, and K. Yoshikawa, "Tar removal capacity of waste cooking oil absorption and waste char adsorption for rice husk gasification," *Biofuels*, vol. 7, no. 4, pp. 401-412, 2016.

[4] T. Phuphuakrat, T. Namioka, and K. Yoshikawa, "Absorptive removal of biomass tar using water and oily materials," *Bioresource Technology,* vol. 102, no. 2, pp. 543-549, 1// 2011.

[5] A. Paethanom, S. Nakahara, M. Kobayashi, P. Prawisudha, and K. Yoshikawa, "Performance of tar removal by absorption and adsorption for biomass gasification," *Fuel Processing Technology,* vol. 104, pp. 144-154, 2012.

[6] S. Nakamura, S. Kitano, and K. Yoshikawa, "Biomass gasification process with the tar removal technologies utilizing bio-oil scrubber and char bed," *Applied Energy,* vol. 170, pp. 186-192, 2016.

[7] P. B. Tissa Fernando, and Brian Earl, "Application of reactive distillation to produce methyl esters from tallow," Flo-Dry Engineering Ltd.

[8] J. Bitman, "Status Report on the Alteration of Fatty Acid and Sterol composition in Lipids in Meat, Milk, and Eggs," in *Fat content and Composition of Animal Products*, Washington, DC, 1976.

[9] S. K. Hoekman, A. Broch, C. Robbins, E. Ceniceros, and M. Natarajan, "Review of biodiesel composition, properties, and specifications," *Renewable and sustainable energy reviews,* vol. 16, no. 1, pp. 143-169, 2012.

[10] W. Yuan, A. Hansen, and Q. Zhang, "Vapor pressure and normal boiling point predictions for pure methyl esters and biodiesel fuels," *Fuel,* vol. 84, no. 7, pp. 943-950, 2005.

[11] B. Sajjadi, A. A. A. Raman, and H. Arandiyan, "A comprehensive review on properties of edible and non-edible vegetable oil-based biodiesel: composition, specifications and prediction models," *Renewable and Sustainable Energy Reviews,* vol. 63, pp. 62-92, 2016.

[12] B. Esteban, J.-R. Riba, G. Baquero, R. Puig, and A. Rius, "Characterization of the surface tension of vegetable oils to be used as fuel in diesel engines," *Fuel,* vol. 102, pp. 231-238, 2012.

[13] M. O'Meara, "Determination of the Interfacial Tension between Oil-Steam and Oil-Air at Elevated Temperatures," 2012.

[14] J. Ralph F. Strigle, *Packed Tower Design and Applications: random and structured packings*, 2nd ed. 1994, p. 340.

[15] J. Mackowiak, "Fluid dynamics of packed columns," *Principles of the Fluid Dynamic Design of Columns for Gas/Liquid and Liquid/Liquid Systems, London, New York,* 2010.

[16] P. R. Bhoi, "Wet scrubbing of biomass producer gas tars using vegetable oil," Oklahoma State University, 2014.

[17] G. Mwandila, "Determination of Design Parameters and Investigation on Operation Performance for an Integrated Gas Cleaning System to Remove Tars from Biomass Gasification Producer Gas," 2010.

[18] R. E. Treybal, *Mass-Transfer Operations*, 3rd ed. 1981, p. 784.

[19] W. Saw, H. McKinnon, I. Gilmour, and S. Pang, "Production of hydrogen-rich syngas from steam gasification of blend of biosolids and wood using a dual fluidised bed gasifier," *Fuel,* vol. 93, pp. 473-478, 2012.

[20] W. L. Saw and S. Pang, "Co-gasification of blended lignite and wood pellets in a 100kW dual fluidised bed steam gasifier: The influence of lignite ratio on producer gas composition and tar content," *Fuel,* vol. 112, pp. 117-124, 2013.

[21] Z. Zhang and S. Pang, "Experimental investigation of biomass devolatilization in steam gasification in a dual fluidised bed gasifier," *Fuel,* vol. 188, pp. 628-635, 2017.

[22] P. S. Kiel JHA, Neeft JPA, Devi L, Ptasinski KJ, Janssen FJJG, Meijer R, Berends RH, Temmink HMG, Brem G, Padban N, Bramer EA, "Primary measures to reduce tar formation in fluidised-bed biomass gasifiers," 2004.

[23] W. Saw and S. Pang, "Influence of mean gas residence time in the bubbling fluidised bed on the performance of a 100-kW dual fluidised bed steam gasifier," *Biomass Conversion and Biorefinery,* vol. 2, no. 3, pp. 197-205, 2012.

8 Conclusions and Recommendations

8.1 Conclusions

In this study, secondary measures were selected and experimentally investigated for removal of H_2S, NH_3, and tars from the simulated or actual producer gas of biomass gasification. The simulated producer gas has similar composition and gaseous contaminants to that from steam gasification of woody biomass on a dual fluidized bed (DFB) gasifier and the gas is targeted to be used in Fischer-Tropsch (FT) process for liquid fuel production. A hot gas cleaning reactor (bubbling fluidised bed reactor) was modified and employed for H_2S adsorption and NH_3 decomposition from the simulated producer gas of biomass gasification, respectively. A natural iron-based sand, titanomagnetite, was selected as the sorbent for H_2S adsorption and the catalyst for NH_3 decomposition. Investigations of H_2S and NH_3 removal included: (1). Investigation of the performance of the unprocessed and reduced titanomagnetite as sorbents for H_2S adsorption and catalysts for NH_3 decomposition; (2). Examination of the effects of temperature on H_2S adsorption and NH_3 decomposition in the simulated producer gas; 3). Identification of the side reactions and investigation of the effect of gaseous species in the simulated producer gas on the activity of the sorbent/catalyst for H_2S adsorption and NH_3 decomposition. An oil scrubber system was modified and used for tar removal from the actual producer gas produced from the DFB gasifier. The efficiencies of two different solvents, biodiesel and canola oil, for tar removal were investigated in the oil scrubber. From this study, the following conclusion can be drawn:

1. H_2S removal study

The effectiveness of both the unprocessed and reduced titanomagnetites for H_2S adsorption was investigated in Ar gas and the simulated produced gas, respectively, for removing 240 ppmv H_2S.

It is found that both the unprocessed and reduced titanomagnetites were highly effective for removal H_2S in Ar gas at 600°C. The H_2S was almost completely removed by the reduced titanomagnetite throughout the whole experiment. The unprocessed titanomagnetite had a slightly lower activity initially that 94.7% of 240 ppmv H_2S was removed, but its activity increased quickly that almost 100% H_2S was removed after 72 min. However, in the simulated producer gas, the effectiveness of both these two types of titanomagnetite was lowered significantly, where the unprocessed titanomagnetite had a better performance than that of the reduced titanomagnetite at both 500 and 600°C. The results indicate that the reduction of effectiveness is due to the negative effects of steam and carbon formation from the side reactions in the simulated producer gas, where the higher α-Fe phase on the reduced titanomagnetite promoted steam and carbon production significantly. It is also found that the steam was mainly generated by the reverse water-gas shift reaction and the carbon was produced by the Boudouard reaction.

Therefore, the unprocessed titanomagnetite was selected to determine the optimisation temperature of H_2S removal from the simulated producer gas. The temperature range of 350-750°C was investigated. It is found that the unprocessed titanomagnetite had the most effective activity to remove H_2S at the temperature of 400-450°C, at which more than 85% H_2S was removed in the experimental duration. When the temperature was 500°C and higher, steam was produced and its production rate was increased with the increase of temperature. The carbon formation manner was different from that of the steam formation that the highest carbon formation rate occurred at 500°C. Again, the steam and carbon formation was supposed to have negative impacts on H_2S adsorption by the unprocessed titanomagnetite at the temperature range of 500-750°C. When the temperature was 350°C, the reduced activity of the unprocessed titanomagnetite for H_2S adsorption was due to the reduced diffusivity of the gases within the sorbent.

In the last part of H_2S removal study, the effects of steam and CO on H_2S removal by the unprocessed titanomagnetite were studied in the gas mixtures of 2.2 vol.% steam in Ar and 20.6 vol.% CO in Ar, respectively, at 600°C. The results illustrate that both the CO and steam adversely affected the H_2S removal by the unprocessed titanomagnetite, whereas steam was the dominant factor. It is also found that the Boudouard reaction happened in the gas mixture of CO and Ar.

Overall, the unprocessed titanomagnetite is an effective sorbent for H_2S removal from the producer gas of biomass gasification. To maximize its effectiveness for H_2S removal, it should be applied at the temperature range of 400-450°C and steam in the producer gas should be removed before the H_2S removal process. However, the H_2S removal efficiency through this hot gas reactor is only $\geq$ 85%, which is impossible to meet the requirement of FT synthesis of H_2S concentration less than 1 ppmv. It is reported that a reactor with ZnO and activated carbon has the ability to reduce the H_2S at a low level (~ 24 ppmv) to be less than 20 ppbv [1]. Therefore, recommendations are given in Section of 8.2.

2. NH_3 removal study

Extensive investigation of NH_3 removal from the simulated producer gas of biomass gasification was carried out using titanomagnetite.

(1). The performance of the unprocessed and reduced titanomagnetites for NH_3 removal was investigated at the temperature range of 500-850°C in Ar gas. It is found that high temperature promoted the NH_3 decomposition by both two types of titanomagnetites. The reduced titanomagnetite had much higher efficiency for NH_3 decomposition than that of the unprocessed titanomagnetite because of the higher activity of α-Fe phase on the reduced titanomagnetite than that of Fe_3O_4 phase on the unprocessed titanomagnetite.

Therefore, the reduced titanomagnetite was selected as the catalyst for NH_3 decomposition in the subsequent study of NH_3 removal from the simulated producer gas at the temperatures of 500, 750 and 850°C. It is found that temperature had a significant effect on NH_3 removal that high temperatures enhanced the NH_3 removal from the simulated producer gas. However, the activity of the reduced titanomagnetite was decreased in the simulated producer gas compared to that in Ar gas. This study has confirmed that, in addition to the NH_3 decomposition reaction, three basic side reactions have occurred in the NH_3 decomposition which are the reverse water-gas shift reaction, the (reverse) Boudouard reaction, and the (reverse) carbon Methanation reaction. The direction and the extent of these reactions were affected by the reaction temperature and feeding gas composition. At 500°C, the Boudouard reaction was a critical reaction which adversely lowered the activity of the reduced titanomagnetite for NH_3 removal by carbon deposition and converting α-Fe to carbide. At 750 and 850°C, the reverse Boudouard reaction and the reverse carbon Methanation reaction were significant which reduced the concentrations of CO_2 and CH_4 and increased the concentrations of H_2 and CO in the simulated producer gas. However, the reverse water-gas shift reaction was a reaction to consume H_2 in the simulated producer gas. Moreover, the iron oxidation reaction by CO_2 happened at temperatures of 750°C and 850°C and it had a negative effect on NH_3 removal by oxidizing the α-Fe phase on the reduced titanomagnetite to Fe_3O_4 phase.

Furthermore, the tolerance of the reduced titanomagnetite for 230 ppmv H_2S was tested in the simulated producer gas for NH_3 removal. It is found that 230 ppmv H_2S in the simulated producer gas was extremely poisonous for the reduced titanomagnetite that it converted the α-Fe phase to FeS and also competed with NH_3 decomposition on the α-Fe sites.

(2). In the second part of NH_3 removal study, the effects of the gas species and the side reactions in the simulated producer gas were examined at 500 and 750°C by conducting NH_3 removal experiments in different gas mixtures using the reduced titanomagnetite.

It is found that the reduced titanomagnetite had much higher NH_3 decomposition rate at 750°C than that at 500°C in all of the test gas mixtures. All of the gas species, H_2, CO, CO_2 and CH_4, in the simulated producer gas had negative effects on the NH_3 decompositions although their effects were at different magnitudes. The unfavourable effects of the gas species can be ranked as CH_4 < CO_2 < (CO and H_2) at both two temperatures.

H_2 had a negative effect on NH_3 decomposition due to the increased H_2 equilibrium concentration in the products. The negative effect from CO was caused by carbon deposition and converting α-Fe phase on the reduced titanomagnetite to carbide by CO decomposition, and the carbide had extremely low or no activity to decompose NH_3. When CO_2 was present at the gas, it oxidized the α-Fe phase on the reduced titanomagnetite to form Fe_3O_4. The Fe_3O_4 reduced the catalyst activity to decompose NH_3. Compared with the above three gas species, CH_4 had the minimum effect on NH_3 decomposition.

The combined effects of these gas species of H_2, CO, CO_2, and CH_4 were complicated and can be explained by NH_3 decomposition reaction, side reactions and decomposition equilibrium. H_2 was the most dominant gas species which affected the NH_3 decomposition equilibrium and promoted carbon formation when it coexisted with CO. However, H_2 also protected the α-Fe phase on the reduced titanomagnetite from being oxidized by CO_2 and suppressed carbon formation from the CH_4 decomposition reaction. The next important gas species was CO_2 which had both positive and negative effects. CO_2 oxidized the α-Fe phase on the catalyst which reduced the NH_3

decomposition, but it reduced carbon formation by inhibiting the Boudouard reaction which was favourable for the NH_3 decomposition.

Overall, it is found that the reduced titanomagnetite is an effective catalyst for NH_3 decomposition from the simulated producer gas of biomass gasification that more than 94.7% NH_3 can be removed when it is used at a high temperature of no less than 750°C. Comparing with the other reported catalysts, such as a lab-synthesized iron catalyst (Fe/HZβ) [2], a reduced natural limonite ore [3, 4], and even some Ni-based catalysts [5], the reduced titanomagnetite has higher efficiency for NH_3 removal in the simulated gas atmosphere. Moreover, in comparison with the other NH_3 removal methods, a water scrubber [6] and an oil scrubber with condensed water [7], this hot catalytic reactor with the reduced titanomagnetite still have very high level of competitiveness to remove NH_3 in the producer gas of biomass gasification. However, it still has the disadvantages of H_2 consumption by the reverse water-gas shift reaction and the NH_3 concentration in the cleaned gas may be still higher than the requirement of FT process (NH_3 concentration <1 ppmv). Therefore, recommendations are provided in Section 8.2.

3. Tar removal study

The preliminary results from the tar removal study show that the oil scrubber using either biodiesel or canola oil had a high efficiency of ~96% to removal GC-detectable tar compounds from the producer gas of biomass gasification without taking into account an unknown compound. This efficiency of tar removal is slightly lower than the efficiency of the "OLGA" system in ECN and the rapeseed oil methyl ester (RME) scrubber in Güssing, Austria [8-10], but higher than the efficiencies of the oil scrubbers reported by Tokyo Institute of Technology, Japan [11-14]. Moreover, the oil scrubber method also had a good performance to remove the other unwanted components in the producer gas like GC-undetectable tars, particles, and water. However, the

cleaned producer gas of biomass gasification after this oil scrubber cannot meet the requirement of the FT synthesis specification that tar concentration should be lower than 0.1 mg/Nm^3.

Furthermore, there are still some issues for this oil scrubber system to remove tars from the actual producer gas of biomass gasification. The flooding happened easily in the oil scrubber during the experiments. Most importantly, an unknown compound was detected which concentration in the outlet gas of the oil scrubber was higher than that in the inlet gas. Therefore, improvement of the oil scrubber and further studies should be carried out to identify this unknown compound and determine the reasons for the increase of its concentration through the scrubber.

8.2 Recommendations

For the hot gas cleaning reactor for H_2S removal, it is important to further investigate the negative effects of other gas species in the producer gas on H_2S adsorption by using different gas mixtures. Thus, these negative effects can be mitigated or prevented during the industrial application. For example, it was found that H_2O had a significantly adverse effect on the H_2S adoption by the unprocessed titanomagnetite, thus the H_2S removal process can be applied after the oil scrubber, where the H_2O in the producer gas of biomass gasification is removed. In addition, it is recommended that the research of sorbent regeneration should be conducted to improve the durability of the unprocessed titanomagnetite for H_2S removal and to reduce the cost of the process.

The hot catalytic reactor with the reduced titanomagnetite at temperatures higher than 750°C is effective for NH_3 removal from the producer gas of biomass gasification. However, research about reducing the H_2 consumption and improving the NH_3 decomposition can be carried out by reducing the concentration of CO_2 in the producer gas. Moreover, optimisation of the operation temperature

of this reactor is necessary to improve the performance and durability of the reduced titanomagnetite.

For the oil scrubber system, firstly, it is recommended to further modify the oil scrubber system by using packing elements with large void fractions or/and enlarge the diameter of the scrubber column to avoid flooding and improve its performance. Secondly, the sampling train should be designed on a bypass line so that the sampling would not interrupt the tar removal operation. Thirdly, the unknown compound in the outlet gas of the oil scrubber should be determined and its production should be investigated and confirmed. Fourthly, optimisation of the operation conditions of the oil scrubber should be studied further to maximize its activity for tar removal. Fifthly, the study should be conducted to determine the ability of the oil scrubber system to remove NH_3 and H_2S, which will be helpful to design the subsequent H_2S and NH_3 cleaning reactors. Finally, the used solvent saturated with tars may be used in two ways: (1) The solvent with tars can be separated from water and the solvent with tar is used as supplementary fuel for the gasifier. (2) The solvent with tars can be treated by a stripper, where the tars will be released to the hot air. Thus, the tar-free solvent will be re-used in the oil scrubber and the hot air with tars will be injected for the combustion reactor in the dual fluidised bed gasification system.

Overall, these three reactors: oil scrubber, H_2S adsorption reactor, and NH_3 decomposition reactor, should be integrated downstream of the DFB gasifier to further assess their suitability for cleaning the actual producer gas of biomass gasification. It is recommended that the oil scrubber should be applied after the particle remover such as cyclone and filter. In this way, most of the contaminants like particles, tars, and water can be removed and their negative effects on the H_2S and NH_3 removal reactors will be minimised largely. Thus, the oil scrubber will be followed by the H_2S removal reactor which can reduce the concentration of H_2S in the producer gas significantly. The

NH_3 removal reactor is recommended to locate after the H_2S removal reactor so that the adverse effects of tars and H_2S on NH_3 decomposition will be significantly reduced. Furthermore, the ability of this integrated system to remove other contaminants such as HCN, HCl, COS, CS_2 should be investigated. If the concentrations of tars, H_2S, and NH_3 in the cleaned producer gas after the this integrated system are still higher than the required levels of the FT synthesis, a guard reactor with catalyst/sorbent such as ZnO and activated carbon should be installed before the FT synthesis reactor to further remove the contaminants.

8.3 Reference

[1] H. Boerrigter, H. Den Uil, and H.-P. Calis, "Green diesel from biomass via Fischer-Tropsch synthesis: new insights in gas cleaning and process design," ed: Citeseer, 2003, pp. 371-383.

[2] A. Sarıoğlan, Y. Durak-Çetin, H. Okutan, and F. Akgün, "Decomposition of ammonia: The effect of syngas components on the activity of zeolite Hβ supported iron catalyst," Chemical Engineering Science, vol. 171, pp. 440-450, 2017.

[3] N. Tsubouchi, H. Hashimoto, and Y. Ohtsuka, "Catalytic performance of limonite in the decomposition of ammonia in the coexistence of typical fuel gas components produced in an air-blown coal gasification process," Energy & Fuels, vol. 21, pp. 3063-3069, 2007.

[4] Y. Ohtsuka, C. Xu, D. Kong, and N. Tsubouchi, "Decomposition of ammonia with iron and calcium catalysts supported on coal chars," Fuel, vol. 83, pp. 685-692, 2004.

[5] W. Mojtahedi and J. Abbasian, "Catalytic decomposition of ammonia in a fuel gas at high temperature and pressure," Fuel, vol. 74, no. 11, pp. 1698-1703, 1995.

[6] H. P. C. H. Boerrigter, D.J. Slort, H. Bodenstaff, A.J. Kaandorp, H. den Uil, L.P.L.M. Rabou, "Gas Cleaning for Integrated Biomass Gasification (BG) and Fischer-Tropsch (FT) Systems," in "Energy Research Centre of the Netherlands (ECN), Petten, The Netherlands, report RX-04-041," May 2004.

[7] J. Loipersböck, M. Lenzi, R. Rauch, and H. Hofbauer, "Hydrogen production from biomass: The behavior of impurities over a CO shift unit and a biodiesel scrubber used as a gas treatment stage," Korean Journal of Chemical Engineering, vol. 34, no. 8, pp. 2198-2203, 2017.

[8] Z. RWR, "Gas cleaning downstream biomass gasification: status report 2009," the Energy research Centre of the Netherlands (ECN), the NetherlandsECN-E-08-078, 2009.

[9] R. Zwart, A. Van der Drift, A. Bos, H. Visser, M. Cieplik, and H. Könemann, "Oil-based gas washing—Flexible tar removal for high-efficient production of clean heat and power as well as sustainable fuels and chemicals," Environmental progress & sustainable energy, vol. 28, no. 3, pp. 324-335, 2009.

[10] H. Hermann, R. Reinhard, B. Klaus, K. Reinhard, and A. Christian, "Biomass CHP Plant Güssing–a success story," ed: Vienna, 2001.

[11] T. Phuphuakrat, T. Namioka, and K. Yoshikawa, "Absorptive removal of biomass tar using water and oily materials," Bioresource Technology, vol. 102, no. 2, pp. 543-549, 1// 2011.

[12] S. Nakamura, S. Kitano, and K. Yoshikawa, "Biomass gasification process with the tar removal technologies utilizing bio-oil scrubber and char bed," Applied Energy, vol. 170, pp. 186-192, 2016.

[13] T. Tarnpradab, S. Unyaphan, F. Takahashi, and K. Yoshikawa, "Tar removal capacity of waste cooking oil absorption and waste char adsorption for rice husk gasification," Biofuels, vol. 7, no. 4, pp. 401-412, 2016.

[14] A. Paethanom, S. Nakahara, M. Kobayashi, P. Prawisudha, and K. Yoshikawa, "Performance of tar removal by absorption and adsorption for biomass gasification," Fuel Processing Technology, vol. 104, pp. 144-154, 2012.

Appendix A

A.1 Calculations of bubbling fluidised bed regime

Table A.1 Properties of Ar, H_2, CO, CO_2 and CH_4 gases and properties of titanomagnetite.

Properties of gas	
Type of gas	Ar
Gas flow rate (F_g) at 273.15K, L/min	3.4 or 3.65
Gas density (ρ_g), kg/m^3	0.6303
Gas viscosity (μ) $\times 10^5$, kg/(m·s)	4.64
Type of gas	H_2
Gas flow rate (F_g) at 273.15K, L/min	3.4 or 3.65
Gas density (ρ_g), kg/m^3	0.0318
Gas viscosity (μ) $\times 10^5$, kg/(m·s)	1.69
Type of gas	CO
Gas flow rate (F_g) at 273.15K, L/min	3.4 or 3.65
Gas density (ρ_g), kg/m^3	0.2532
Gas viscosity (μ) $\times 10^5$, kg/(m·s)	3.56
Type of gas	CO_2
Gas flow rate (F_g) at 273.15K, L/min	3.4 or 3.65
Gas density (ρ_g), kg/m^3	0.6985
Gas viscosity (μ) $\times 10^5$, kg/(m·s)	3.42
Type of gas	CH_4
Gas flow rate (F_g) at 273.15K, L/min	3.4 or 3.65
Gas density (ρ_g), kg/m^3	0.4416
Gas viscosity (μ) $\times 10^5$, kg/(m·s)	2.33

Properties of particle	
Type of particle	Titanomagnetite
Particle density (ρ_s), kg/m^3	4540
Sphericity of Particle (ϕ_s)	0.86
Particle diameter (d_p), m	0.000215
Voidage (ε)	0.44
Other parameters and constants	
Bed or column diameter(d_t), m	0.04
Bed cross-sectional area (A_t), m^2	0.001256
Accelereation of gravity(g), m/s^2	9.8

Table A.2 u_{mf} and u_t calculations for Ar gas.

	Name	Symbol, unit	Equation	Number
1	Superficial gas velocity for Fg=3.4 L/min at 500°C	u_0, m/s	$u_0 = \frac{\frac{\mathrm{Fg}}{1000 * 60}}{\mathrm{At}} * 773/273$	0.128
2	Superficial gas velocity for Fg=3.65 L/min at 500°C	u_0, m/s	$u_0 = \frac{\frac{\mathrm{Fg}}{1000 * 60}}{\mathrm{At}} * 773/273$	0.137
3	Archimedes number	Ar	$\mathrm{Ar} = \frac{d_p^3 \cdot \rho_g \cdot (\rho_s - \rho_g) \cdot g}{\mu^2}$	129.434
4	Particle Reynolds number at minimum fluidization	$Re_{p,mf}$	$\frac{1.75}{\varepsilon_{mf}^3 \cdot \phi_s} \cdot \mathrm{Re}_{p,mf}^2 + \frac{150 \cdot (1-\varepsilon_{mf})}{\varepsilon_{mf}^3 \cdot \phi_s^2} \cdot \mathrm{Re}_{p,mf} = \mathrm{Ar}$	0.097
5	Minimum fluidization velocity	u_{mf}, m/s	$u_{mf} = \frac{R_{ep,mf} \cdot \mu}{d_p \cdot \rho_g}$	**0.033**
6	Dimensionless particle size	d_p^*, m	$d_p^* = d_p \cdot \left[\frac{\rho_g \cdot (\rho_s - \rho_g) \cdot g}{\mu^2}\right]^{1/3} = \mathrm{Ar}^{1/3}$	5.058
7	Dimensionless gas velocity	u_t^*, m/s	$u_t^* = \left[\frac{18}{(d_p^*)^2} + \frac{2.335 - 1.744 \cdot \phi_s}{(d_p^*)^{0.5}}\right]^{-1}, \quad 0.5 < \varphi_s < 1$	0.930
8	Terminal free-fall velocity	u_t, m/s	$u_t = u_t^* \left[\frac{\mu \cdot (\rho_s - \rho_g) \cdot g}{\rho_g^2}\right]^{1/3}$	**1.611**

Table A.3 u_{mf} and u_t calculations for H_2 gas.

	Name	Symbol, unit	Equation	Number
1	Superficial gas velocity for Fg=3.4 L/min at 500°C	u_0, m/s	$u_0 = \frac{\frac{\mathrm{Fg}}{1000 * 60}}{\mathrm{At}} * 773/273$	0.128
2	Superficial gas velocity for Fg=3.65 L/min at 500°C	u_0, m/s	$u_0 = \frac{\frac{\mathrm{Fg}}{1000 * 60}}{\mathrm{At}} * 773/273$	0.137
3	Archimedes number	Ar	$\mathrm{Ar} = \frac{d_p^3 \cdot \rho_g \cdot (\rho_s - \rho_g) \cdot g}{\mu^2}$	49.232
4	Particle Reynolds number at minimum fluidization	$Re_{p,mf}$	$\frac{1.75}{\varepsilon_{mf}^3 \cdot \phi_s} \cdot \mathrm{Re}_{p,mf}^2 + \frac{150 \cdot (1-\varepsilon_{mf})}{\varepsilon_{mf}^3 \cdot \phi_s^2} \cdot \mathrm{Re}_{p,mf} = \mathrm{Ar}$	0.037
5	Minimum fluidization velocity	u_{mf}, m/s	$u_{mf} = \frac{R_{ep,mf} \cdot \mu}{d_p \cdot \rho_g}$	**0.091**
6	Dimensionless particle size	d_p^*, m	$d_p^* = d_p \cdot \left[\frac{\rho_g \cdot (\rho_s - \rho_g) \cdot g}{\mu^2}\right]^{1/3} = \mathrm{Ar}^{1/3}$	3.665
7	Dimensionless gas velocity	u_t^*, m/s	$u_t^* = \left[\frac{18}{(d_p^*)^2} + \frac{2.335 - 1.744 \cdot \phi_s}{(d_p^*)^{0.5}}\right]^{-1}, \quad 0.5 < \varphi_s < 1$	0.563
8	Terminal free-fall velocity	u_t, m/s	$u_t = u_t^* \left[\frac{\mu \cdot (\rho_s - \rho_g) \cdot g}{\rho_g^2}\right]^{1/3}$	**5.100**

Table A.4 u_{mf} and u_t calculations for CO gas.

	Name	Symbol, unit	Equation	Number
1	Superficial gas velocity for Fg=3.4 L/min at 500°C	u_0, m/s	$u_0 = \frac{\frac{\mathrm{Fg}}{1000 * 60}}{\mathrm{At}} * 773/273$	0.128
2	Superficial gas velocity for Fg=3.65 L/min at 500°C	u_0, m/s	$u_0 = \frac{\frac{\mathrm{Fg}}{1000 * 60}}{\mathrm{At}} * 773/273$	0.137
3	Archimedes number	Ar	$\mathrm{Ar} = \frac{d_p^3 \cdot \rho_g \cdot (\rho_s - \rho_g) \cdot g}{\mu^2}$	88.336
4	Particle Reynolds number at minimum fluidization	$Re_{p,mf}$	$\frac{1.75}{\varepsilon_{mf}^3 \cdot \phi_s} \cdot \mathrm{Re}_{p,mf}^2 + \frac{150 \cdot (1-\varepsilon_{mf})}{\varepsilon_{mf}^3 \cdot \phi_s^2} \cdot \mathrm{Re}_{p,mf} = \mathrm{Ar}$	0.066
5	Minimum fluidization velocity	u_{mf}, m/s	$u_{mf} = \frac{R_{ep,mf} \cdot \mu}{d_p \cdot \rho_g}$	**0.043**
6	Dimensionless particle size	d_p^*, m	$d_p^* = d_p \cdot \left[\frac{\rho_g \cdot (\rho_s - \rho_g) \cdot g}{\mu^2}\right]^{1/3} = \mathrm{Ar}^{1/3}$	4.454
7	Dimensionless gas velocity	u_t^*, m/s	$u_t^* = \left[\frac{18}{(d_p^*)^2} + \frac{2.335 - 1.744 \cdot \phi_s}{(d_p^*)^{0.5}}\right]^{-1}, \quad 0.5 < \varphi_s < 1$	0.767
8	Terminal free-fall velocity	u_t, m/s	$u_t = u_t^* \left[\frac{\mu \cdot (\rho_s - \rho_g) \cdot g}{\rho_g^2}\right]^{1/3}$	**2.235**

Table A.5 u_{mf} and u_t calculations for CO_2 gas.

	Name	Symbol, unit	Equation	Number
1	Superficial gas velocity for Fg=3.4 L/min at 500°C	u_0, m/s	$u_0 = \frac{\frac{\mathrm{Fg}}{1000 * 60}}{\mathrm{At}} * 773/273$	0.128
2	Superficial gas velocity for Fg=3.65 L/min at 500°C	u_0, m/s	$u_0 = \frac{\frac{\mathrm{Fg}}{1000 * 60}}{\mathrm{At}} * 773/273$	0.137
3	Archimedes number	Ar	$\mathrm{Ar} = \frac{d_p^3 \cdot \rho_g \cdot (\rho_s - \rho_g) \cdot g}{\mu^2}$	264.025
4	Particle Reynolds number at minimum fluidization	$Re_{p,mf}$	$\frac{1.75}{\varepsilon_{mf}^3 \cdot \phi_s} \cdot \mathrm{Re}_{p,mf}^2 + \frac{150 \cdot (1-\varepsilon_{mf})}{\varepsilon_{mf}^3 \cdot \phi_s^2} \cdot \mathrm{Re}_{p,mf} = \mathrm{Ar}$	0.197
5	Minimum fluidization velocity	u_{mf}, m/s	$u_{mf} = \frac{R_{ep,mf} \cdot \mu}{d_p \cdot \rho_g}$	**0.045**
6	Dimensionless particle size	d_p^*, m	$d_p^* = d_p \cdot \left[\frac{\rho_g \cdot (\rho_s - \rho_g) \cdot g}{\mu^2}\right]^{1/3} = \mathrm{Ar}^{1/3}$	6.415
7	Dimensionless gas velocity	u_t^*, m/s	$u_t^* = \left[\frac{18}{(d_p^*)^2} + \frac{2.335 - 1.744 \cdot \phi_s}{(d_p^*)^{0.5}}\right]^{-1}, \quad 0.5 < \varphi_s < 1$	1.304
8	Terminal free-fall velocity	u_t, m/s	$u_t = u_t^* \left[\frac{\mu \cdot (\rho_s - \rho_g) \cdot g}{\rho_g^2}\right]^{1/3}$	**1.905**

Table A.6 u_{mf} and u_t calculations for CH_4 gas.

	Name	Symbol, unit	Equation	Number
1	Superficial gas velocity for Fg=3.4 L/min at 500°C	u_0, m/s	$u_0 = \frac{\frac{\mathrm{Fg}}{1000 * 60}}{\mathrm{At}} * 773/273$	0.128
2	Superficial gas velocity for Fg=3.65 L/min at 500°C	u_0, m/s	$u_0 = \frac{\frac{\mathrm{Fg}}{1000 * 60}}{\mathrm{At}} * 773/273$	0.137
3	Archimedes number	Ar	$\mathrm{Ar} = \frac{d_p^3 \cdot \rho_g \cdot (\rho_s - \rho_g) \cdot g}{\mu^2}$	359.644
4	Particle Reynolds number at minimum fluidization	$Re_{p,mf}$	$\frac{1.75}{\varepsilon_{mf}^3 \cdot \phi_s} \cdot \mathrm{Re}_{p,mf}^2 + \frac{150 \cdot (1-\varepsilon_{mf})}{\varepsilon_{mf}^3 \cdot \phi_s^2} \cdot \mathrm{Re}_{p,mf} = \mathrm{Ar}$	0.268
5	Minimum fluidization velocity	u_{mf}, m/s	$u_{mf} = \frac{R_{ep,mf} \cdot \mu}{d_p \cdot \rho_g}$	**0.066**
6	Dimensionless particle size	d_p^*, m	$d_p^* = d_p \cdot \left[\frac{\rho_g \cdot (\rho_s - \rho_g) \cdot g}{\mu^2}\right]^{1/3} = \mathrm{Ar}^{1/3}$	7.111
7	Dimensionless gas velocity	u_t^*, m/s	$u_t^* = \left[\frac{18}{(d_p^*)^2} + \frac{2.335 - 1.744 \cdot \phi_s}{(d_p^*)^{0.5}}\right]^{-1}, \quad 0.5 < \varphi_s < 1$	1.495
8	Terminal free-fall velocity	u_t, m/s	$u_t = u_t^* \left[\frac{\mu \cdot (\rho_s - \rho_g) \cdot g}{\rho_g^2}\right]^{1/3}$	**2.608**

Appendix B

B.1 Equilibrium gas composition with the three side reactions at 500°C

$T_{reactor}$=530°C=803.15 K, $P_{reactor}$=113kPa

Note: $T_{reactor}$ is the temperature in the reactor and $P_{reactor}$ is the pressure in the reactor during the experiment.

Table B.1 Information of the three side reactions.

Eq. No. in thesis	Name	Reaction					
		$\alpha A+\beta B\leftrightarrow\gamma C+\delta D$	α	β	γ	δ	$K^{\theta}_{803.15K}$
5.2	Reverse water-gas shift reaction	$H_2+CO_2\leftrightarrow H_2O+CO$	1	1	1	1	$K^{\theta}_{5.2}$
5.3	Boudouard reaction	$2CO\leftrightarrow CO_2+C_s$	2	1	1	0	$K^{\theta}_{5.3}$
5.6	Carbon Methanation reaction	$2H_2+C\leftrightarrow CH_4$	2	1	1	0	$K^{\theta}_{5.6}$

Table B.2 Useful equations used in the calculation.

Equation	
$\Delta H = \Delta H_0 + \Delta aT + \frac{\Delta b}{2}T^2 + \frac{\Delta c}{3}T^3$	(1)
$\ln K^{\theta} = -\frac{\Delta H_0}{RT} + \frac{\Delta a}{R}\ln(T) + \frac{\Delta b}{2R}T + \frac{\Delta c}{6R}T^2 + I$	(2)
$\Delta_r G_m^{\theta} = \Delta H_0 - \Delta aT\ln(T) - \frac{\Delta b}{2}T^2 - \frac{\Delta c}{6}T^3 - IRT$	(3)

Table B.3 Thermodynamic properties at 298.15 K and 100 kPa for the chemicals in those three side reactions.

		T=298.15 K, P=100 kPa					
		$\Delta_f H_m$	$\Delta_f G_m$	S_m	a	$b\times10^3$	$c\times10^6$
No.	Gas	kJ/mol	kJ/mol	J/(mol·K)	J/(mol·K)	J/(mol·K·K)	J/(mol·K·K·K)
1	H_2	0	0	130.68	26.88	4.347	-0.3265
2	CO_2	-393.51	-394.36	213.7	26.75	42.258	-14.25
3	H_2O	-241.82	-228.57	188.83	29.16	14.49	-2.022
4	CO	-110.52	-137.17	197.67	26.537	7.6831	-1.172
5	C	0	0	5.74	0	0	0
6	CH_4	-74.81	-50.72	188	14.15	75.496	-17.99

Table B.4 $\Delta_r H_m$ of three side reactions at 298.15 K and 100 kPa.

	T=298.15 K, P=100 kPa		
Eq. No. in thesis	Reaction	$\Delta_r H_m$, kJ/mol	$\Delta_r H_m$, kJ/mol
5.2	$H_2+CO_2\leftrightarrow H_2O+CO$	$-\Delta_f H_m(1)-\Delta_f H_m(2)+\Delta_f H_m(3)+\Delta_f H_m(4)$	41.17
5.3	$2CO\leftrightarrow CO_2+C_s$	$-2*\Delta_f H_m(4)+\Delta_f H_m(2)+\Delta_f H_m(5)$	-172.47
5.6	$2H_2+C\leftrightarrow CH_4$	$-2*\Delta_f H_m(1)-\Delta_f H_m(5)+\Delta_f H_m(6)$	-74.81

Table B.5 Δ_rG_m of three side reactions at 298.15 K and 100 kPa.

	T=298.15 K, P=100 kPa		
Eq. No. in thesis	Reaction	Δ_rG_m, kJ/mol	Δ_rG_m, kJ/mol
5.2	$H_2+CO_2\leftrightarrow H_2O+CO$	$-\Delta_fG_m(1)-\Delta_fG_m(2)+\Delta_fG_m(3)+\Delta_fG_m(4)$	28.62
5.3	$2CO\leftrightarrow CO_2+C_s$	$-2*\Delta_fG_m(4)+\Delta_fG_m(2)+\Delta_fG_m(5)$	-120.02
5.6	$2H_2+C\leftrightarrow CH_4$	$-2*\Delta_fG_m(1)-\Delta_fG_m(5)+\Delta_fG_m(6)$	-50.72

Table B.6 Δa of three side reactions at 298.15 K and 100 kPa.

	T=298.15 K, P=100 kPa		
Eq. No. in thesis	Reaction	Δa, J/(mol·K)	Δa, J/(mol·K)
5.2	$H_2+CO_2\leftrightarrow H_2O+CO$	-a(1)-a(2)+ a(3)+ a(4)	2.067
5.3	$2CO\leftrightarrow CO_2+C_s$	-2*a(4)+ a(2)+ a(5)	-26.324
5.6	$2H_2+C\leftrightarrow CH_4$	-2*a(1)- a(5)+ a(6)	-39.61

Table B.7 Δb of three side reactions at 298.15 K and 100 kPa.

	T=298.15 K, P=100 kPa		
Eq. No. in thesis	Reaction	Δb, J/(mol·K·K)	Δb, J/(mol·K·K)
5.2	$H_2+CO_2\leftrightarrow H_2O+CO$	-b(1)-b(2)+ b(3)+ b(4)	-0.0244319
5.3	$2CO\leftrightarrow CO_2+C_s$	-2*b(4)+ b(2)+ b(5)	0.0268918
5.6	$2H_2+C\leftrightarrow CH_4$	-2*b(1)- b(5)+ b(6)	0.066802

Table B.8 Δc of three side reactions at 298.15 K and 100 kPa.

	T=298.15 K, P=100 kPa		
Eq. No. in thesis	Reaction	Δc, J/(mol·K·K)	Δc, J/(mol·K·K)
5.2	$H_2+CO_2\leftrightarrow H_2O+CO$	-c(1)-c(2)+ c(3)+ c(4)	0.000011382
5.3	$2CO\leftrightarrow CO_2+C_s$	-2*c(4)+ c(2)+ c(5)	-0.000011906
5.6	$2H_2+C\leftrightarrow CH_4$	-2*c(1)- c(5)+ c(6)	-0.000017337

Table B.9 ΔH_0 of three side reactions at 298.15 K and 100 kPa.

	T=298.15 K, P=100 kPa, $\Delta_r H_m = \Delta H_0 + \Delta aT + \frac{\Delta b}{2}T^2 + \frac{\Delta c}{3}T^3$					
Eq. No. in thesis	Reaction	$\Delta_r H_m$, J/mol	Δa, J/(mol·K)	Δb, J/(mol·K·K)	Δc, J/(mol·K·K)	ΔH_0, J/mol
5.2	$H_2+CO_2\leftrightarrow H_2O+CO$	41.17×10^3	2.067	-0.0244319	1.13825E-05	41539.08
5.3	$2CO\leftrightarrow CO_2+C_s$	-172.47×10^3	-26.324	0.0268918	-0.000011906	-165711.57
5.6	$2H_2+C\leftrightarrow CH_4$	-74.81×10^3	-39.61	0.066802	-0.000017337	-65816.24

Table B.10 I of three side reactions at 298.15 K and 100 kPa.

	T=298.15 K, P=100 kPa, R=8.314 J/(mol·K), $\Delta_r G_m^\theta = \Delta H_0 - \Delta aT\ln(T) - \frac{\Delta b}{2}T^2 - \frac{\Delta c}{6}T^3 - IRT$					
Eq. No. in thesis	Reaction	$\Delta_r G_m$, J/mol	Δa, J/(mol·K)	Δb, J/(mol·K·K)	Δc, J/(mol·K·K)	I
5.2	$H_2+CO_2\leftrightarrow H_2O+CO$	28.62×10^3	2.067	-0.0244319	0.000011382	4.213
5.3	$2CO\leftrightarrow CO_2+C_s$	-120.02×10^3	-26.324	0.0268918	-0.000011906	-0.854
5.6	$2H_2+C\leftrightarrow CH_4$	-50.72×10^3	-39.61	0.066802	-0.000017337	19.888

Table B.11 Information used for $K^{\theta}_{803.15}$ at 100 kPa calculation.

		T=803.15 K, P=100 kPa, R=8.314 J/(mol·K), $\ln K^{\theta} = -\frac{\Delta H_0}{R}\frac{1}{T} + \frac{\Delta a}{R}\ln T + \frac{\Delta b}{2R}T + \frac{\Delta c}{6R}T^2 + I$														
Eq. No. in thesis	Reaction	$\ln(K^{\theta}_{803.15})$		$-\Delta H_0/R$			$\Delta a/R$			$\Delta b/(2R)$			$\Delta c/(6R)$			I
5.2	$H_2+CO_2 \leftrightarrow H_2O+CO$	$\ln(K^{\theta}_{5.2})$	=	-4996.281	1/T	+	0.248617	lnT	+	-0.001470	T	+	2.28E-07	+	T^2	4.213066
5.3	$2CO \leftrightarrow CO_2+C_s$	$\ln(K^{\theta}_{5.3})$	=	19931.629	1/T	+	-3.166226	lnT	+	0.001617	T	+	-2.39E-07	+	T^2	-0.853889
5.6	$2H_2+C \leftrightarrow CH_4$	$\mathrm{Ln}(K^{\theta}_{5.6})$	=	7916.315	1/T	+	-4.764253	lnT	+	0.004017	T	+	-3.48E-07	+	T^2	19.887792

Table B.12 $K^{\theta}_{803.15}$ at 100 kPa for three side reactions.

	T=803.15 K, P=100 kPa		
Eq. No. in thesis	Reaction	$K^{\theta}_{803.15K}$	$K^{\theta}_{803.15K}$
5.2	$H_2+CO_2 \leftrightarrow H_2O+CO$	$K^{\theta}_{5.2}$	0.251868052
5.3	$2CO \leftrightarrow CO_2+C_s$	$K^{\theta}_{5.3}$	51.18712237
5.6	$2H_2+C \leftrightarrow CH_4$	$K^{\theta}_{5.6}$	2.418400654

Table B.13 Inlet gas composition and gas molar flow rate.

	PV=nRT, P=100 kPa, V_{total}=3.65 L/min, R=8.314 J/(mol·K), T=273.15 K		
Gas	Inlet gas composition in dry basis, vol.%	Inlet gas molar flow rate, mol/s	
H_2	47.6	0.00128	M_{H2}
CO_2	19.1	0.00051	M_{CO2}
CO	18.9	0.00051	M_{CO}
CH_4	14.4	0.00039	M_{CH4}
Total	100	0.00268	M_{total}

Table B.14 K^{θ}_{113kPa} at 803.15 K for three side reactions.

Eq.	$K_P^{\theta} = K_{100kPa}^{\theta} \times (\frac{P}{100})^{\alpha+\beta-\gamma-\delta}$, P=113 kPa Note: α,β,γ,δ in the equation do not count the coefficients of liquid and solid chemicals at 803.15 K.								
5.2	H_2	+	CO_2	↔	H_2O	+	CO	K^{θ}_{100kPa} at 803.15 K	K^{θ}_{113kPa} at 803.15 K
M_{start}	0.00128		0.00051		0		0.00051	0.251868	A=0.251868
$M_{equilibrium}$	0.00128-x-2z		0.00051-x+y		x		0.00051+x-2y		
5.3	2CO			↔	CO_2	+	C_s		
M_{start}	0.00051				0.00051		0	51.187122	B=57.632093
$M_{equilibrium}$	0.00051+x-2y				0.00051-x+y		y-z		
5.6	$2H_2$	+	C	↔	CH_4				
M_{start}	0.00128		0		0.00039			2.418401	C=2.722901
$M_{equilibrium}$	0.00128-x-2z		y-z		0.00039+z				

Table B.15 Equilibrium equation for the three side reactions.

Eq.	Equation	
5.2	$\frac{x \cdot (M_{CO} + x - 2y)}{(M_{H2} - x - 2z) \cdot (M_{CO2)} - x + y)} = A$	(4)
5.3	$\frac{(M_{CO2} - x + y) \cdot (M_{total} - y - z)}{(M_{CO} + x - 2y)^2} = B$	(5)
5.6	$\frac{(M_{CH4} + z) \cdot (M_{total} - y - z)}{(M_{H2} - x - 2z)^2} = C$	(6)

Solver in the Excel was used to solve the three roots, x, y,z, in the above three equations in Table B.15.

Table B.16 The roots results.

x	0.000521886
y	0.000450078
z	7.49518E-05

Table B.17 Equilibrium gas composition at 803.15 K and 113 kPa.

Gas		Gas molar flow rate/ mol/s	Gas composition in dry basis/ vol.%
H_2	0.00128-x-2z	0.000603991	36.98
CO	0.00051+x-2y	0.00012829	7.85
CO_2	0.00051-x+y	0.000440112	26.95
CH_4	0.00039+z	0.000460902	28.22
H_2O	x	0.000521886	
Sum (H_2+CO+CO_2+CH_4)		0.001633295	100%

B.2 Equilibrium gas composition with the three side reactions at 750°

$T_{reactor}$=714°C=987.15 K, $P_{reactor}$=114 kPa

Table B.18 Information used for $K^{\theta}_{987.15K}$ at 100 kPa calculation.

		T=987.15 K, P=100 kPa, R=8.314 J/(mol·K), $\ln K^{\theta} = -\frac{\Delta H_0}{R}\frac{1}{T} + \frac{\Delta a}{R}\ln T + \frac{\Delta b}{2R}T + \frac{\Delta c}{6R}T^2 + I$														
Eq. No. in thesis	Reaction	$\ln(K^{\theta}_{987.15K})$		$-\Delta H_0/R$			$\Delta a/R$			$\Delta b/(2R)$			$\Delta c/(6R)$			I
5.2	$H_2+CO_2 \leftrightarrow H_2O+CO$	$\ln(K^{\theta}_{5.2})$	=	-4996.281	1/T	+	0.248617	lnT	+	-0.001470	T	+	2.28E-07	+	T^2	4.213066
5.3	$2CO \leftrightarrow CO_2+C_s$	$\ln(K^{\theta}_{5.3})$	=	19931.629	1/T	+	-3.166226	lnT	+	0.001617	T	+	-2.39E-07	+	T^2	-0.853889
5.6	$2H_2+C \leftrightarrow CH_4$	$\mathrm{Ln}(K^{\theta}_{5.6})$	=	7916.315	1/T	+	-4.764253	lnT	+	0.004017	T	+	-3.48E-07	+	T^2	19.887792

Table B.19 $K^{\theta}_{987.15K}$ at 100 kPa for three side reactions.

	T=987.15 K, P=100 kPa		
Eq. No. in thesis	Reaction	$K^{\theta}_{987.15}$	$K^{\theta}_{987.15}$
5.2	$H_2+CO_2 \leftrightarrow H_2O+CO$	$K^{\theta}_{5.2}$	0.695706
5.3	$2CO \leftrightarrow CO_2+C_s$	$K^{\theta}_{5.3}$	0.324299
5.6	$2H_2+C \leftrightarrow CH_4$	$K^{\theta}_{5.6}$	0.269030

Table B.20 Inlet gas composition and gas molar flow rate.

	PV=nRT, P=100 kPa, V_{total}=3.65 L/min, R=8.314 J/(mol·K), T=273.15 K		
Gas	Inlet gas composition in dry basis, vol.%	Inlet gas molar flow rate, mol/s	Symbol
H_2	47.6	0.00128	M_{H2}
CO_2	19.1	0.00051	M_{CO2}
CO	18.9	0.00051	M_{CO}
CH_4	14.4	0.00039	M_{CH4}
Total	100	0.00268	M_{total}

Table B.21 K^{θ}_{113kPa} at 987.15 K for three side reactions.

Eq. No. in thesis	$K_P^{\theta} = K_{100kPa}^{\theta} \times (\frac{P}{100})^{\alpha+\beta-\gamma-\delta}$, P=114 kPa Note: α,β,γ,δ in the equation do not count the coefficients of liquid and solid chemicals at 987.15 K.								
5.2	H_2	+	CO_2	↔	H_2O	+	CO	K^{θ}_{100kPa} at 987.15 K	K^{θ}_{113kPa} at 987.15 K
M_{start}	0.00128		0.00051		0		0.00051	0.695706	A=0.695706
$M_{equilibrium}$	0.00128-x-2z		0.00051-x+y		x		0.00051+x-2y		
5.3	2CO			↔	CO_2	+	C_s		
M_{start}	0.00051				0.00051		0	0.324299	B=0.369701
$M_{equilibrium}$	0.00051+x-2y				0.00051-x+y		y-z		
5.6	$2H_2$	+	C	↔	CH_4				
M_{start}	0.00128		0		0.00039			0.269030	C=0.306694
$M_{equilibrium}$	0.00128-x-2z		y-z		0.00039+z				

Table B.22 Equilibrium equation for the three side reactions.

Eq. No. in thesis	Equation	
5.2	$\frac{x \cdot (M_{CO} + x - 2y)}{(M_{H2} - x - 2z) \cdot (M_{CO2)} - x + y)} = A$	(4)
5.3	$\frac{(M_{CO2} - x + y) \cdot (M_{total} - y - z)}{(M_{CO} + x - 2y)^2} = B$	(5)
5.6	$\frac{(M_{CH4} + z) \cdot (M_{total} - y - z)}{(M_{H2} - x - 2z)^2} = C$	(6)

Solver in Excel was used to solve the three roots, x, y,z in the above three equations.

Table B.23 The roots results.

x	0.000136034
y	-0.000229937
z	-0.000168633

Table B.24 Equilibrium gas composition at 803.15 K and 113 kPa

Gas		Gas molar flow rate/ mol/s	Gas composition in dry basis/ vol.%
H_2	0.00128-x-2z	0.001477012	50.19
CO	0.00051+x-2y	0.001102467	37.46
CO_2	0.00051-x+y	0.00014595	4.96
CH_4	0.00039+z	0.000217318	7.39
H_2O	x	0.000136034	
Sum (H_2+CO+CO_2+CH_4)		0.002942747	100

B.3 Equilibrium gas composition with the three side reactions at 850°

$T_{reactor}$=791°C=1064.15 K, $P_{reactor}$=114 kPa

Table B.25 Information used for $K^{\theta}_{1064.15K}$ at 100 kPa calculation.

		T=1064.15 K, P=100 kPa, R=8.314 J/(mol·K), $\ln K^{\theta} = -\frac{\Delta H_0}{R}\frac{1}{T} + \frac{\Delta a}{R}\ln T + \frac{\Delta b}{2R}T + \frac{\Delta c}{6R}T^2 + I$														
Eq. No. in thesis	Reaction	$\ln(K^{\theta}_{1064.15.15\ K})$		$-\Delta H_0/R$			$\Delta a/R$			$\Delta b/(2R)$			$\Delta c/(6R)$			I
5.2	$H_2+CO_2 \leftrightarrow H_2O+CO$	$\ln(K^{\theta}_{5.2})$	=	-4996.281	1/T	+	0.248617	lnT	+	-0.001470	T	+	2.28E-07	+	T^2	4.213066
5.3	$2CO \leftrightarrow CO_2+C_s$	$\ln(K^{\theta}_{5.3})$	=	19931.629	1/T	+	-3.166226	lnT	+	0.001617	T	+	-2.39E-07	+	T^2	-0.853889
5.6	$2H_2+C \leftrightarrow CH_4$	$Ln(K^{\theta}_{5.6})$	=	7916.315	1/T	+	-4.764253	lnT	+	0.004017	T	+	-3.48E-07	+	T^2	19.887792

Table B.26 $K^{\theta}_{1064.15K}$ at 100 kPa for three side reactions.

	T=1064.15 K, P=100 kPa		
Eq. No. in thesis	Reaction	$K^{\theta}_{1064.15}$	$K^{\theta}_{1064.15}$
5.2	$H_2+CO_2 \leftrightarrow H_2O+CO$	$K^{\theta}_{5.2}$	0.946562
5.3	$2CO \leftrightarrow CO_2+C_s$	$K^{\theta}_{5.3}$	0.064666
5.6	$2H_2+C \leftrightarrow CH_4$	$K^{\theta}_{5.6}$	0.135768

Table B.27 Inlet gas composition and gas molar flow rate.

	PV=nRT, P=100 kPa, V_{total}=3.65 L/min, R=8.314 J/(mol·K), T=273.15 K		
Gas	Inlet gas composition in dry basis, vol.%	Inlet gas molar flow rate, mol/s	
H_2	47.6	0.00128	M_{H2}
CO_2	19.1	0.00051	M_{CO2}
CO	18.9	0.00051	M_{CO}
CH_4	14.4	0.00039	M_{CH4}
Total	100	0.00268	M_{total}

Table B.28 K^{θ}_{113kPa} at 1064.15 K for three side reactions.

Eq. No. in thesis	$K_P^{\theta} = K_{100kPa}^{\theta} \times (\frac{P}{100})^{\alpha+\beta-\gamma-\delta}$, P=114 kPa Note: α,β,γ,δ in the equation do not count the coefficients of liquid and solid chemicals at 1064.15 K.								
5.2	H_2	+	CO_2	↔	H_2O	+	CO	K^{θ}_{100kPa} at 1064.15 K	K^{θ}_{113kPa} at 1064.15 K
M_{start}	0.00128		0.00051		0		0.00051	0.946562	A=0.946562
$M_{equilibrium}$	0.00128-x-2z		0.00051-x+y		x		0.00051+x-2y		
5.3	2CO			↔	CO_2	+	C_s		
M_{start}	0.00051				0.00051		0	0.064666	B=0.073719
$M_{equilibrium}$	0.00051+x-2y				0.00051-x+y		y-z		
5.6	$2H_2$	+	C	↔	CH_4				
M_{start}	0.00128		0		0.00039			0.135768	C=0.154776
$M_{equilibrium}$	0.00128-x-2z		y-z		0.00039+z				

Table B.29 Equilibrium equation for the three side reactions.

Eq.	Equation	
5.2	$\frac{x \cdot (M_{CO} + x - 2y)}{(M_{H2} - x - 2z) \cdot (M_{CO2)} - x + y)} = A$	(4)
5.3	$\frac{(M_{CO2} - x + y) \cdot (M_{total} - y - z)}{(M_{CO} + x - 2y)^2} = B$	(5)
5.6	$\frac{(M_{CH4} + z) \cdot (M_{total} - y - z)}{(M_{H2} - x - 2z)^2} = C$	(6)

Solver in Excel was used to solve the three roots, x, y,z in the above three equations.

Table B.30 The roots results.

x	5.00872E-05
y	-0.000419004
z	-0.000248692

Table B.31 Equilibrium gas composition at 1064.15 K and 114 kPa.

Gas		Gas molar flow rate/ mol/s	Gas composition in dry basis/ vol.%
H_2	0.00128-x-2z	0.001723077	52.25
CO	0.00051+x-2y	0.001394655	42.29
CO_2	0.00051-x+y	4.28292E-05	1.30
CH_4	0.00039+z	0.000137258	4.16
H_2O	x	5.00872E-05	
Sum (H_2+CO+CO_2+CH_4)		0.003297819	100

B.4 Summary

Table B.32 Equilibrium gas composition of the outlet gas at 500, 750 and 850°C.

Temperature/ °C	H_2/ vol.%	CO/ vol.%	CO_2/ vol.%	CH_4/ vol.%
500	37.0	7.9	27.0	28.2
750	50.2	37.5	5.0	7.4
850	52.3	42.3	1.3	4.2

Table B.33 Experimental gas composition of the outlet gas at 500, 750 and 850°C.

Temperature/ °C	H_2/ vol.%	CO/ vol.%	CO_2/ vol.%	CH_4/ vol.%
500	42.8	18.4	19.3	19.5
750	45.4	31.5	9.8	13.3
850	49.7	35.1	6.3	8.9

Table B.34 Inlet gas composition at 500, 750 and 850°C.

Temperature/ °C	H_2/ vol.%	CO/ vol.%	CO_2/ vol.%	CH_4/ vol.%
500	47.6	18.9	19.1	14.4
750	47.6	18.9	19.1	14.4
850	47.6	18.9	19.1	14.4

Appendix C

C.1 Operation range of the oil scrubber

Useful information and equations for calculating the operation producer gas with the biodiesel flow rate of 0.15 L/min.

Table C.1 The detailed information for calculating the operation producer gas flow rate.

Information	Symbol	Value	unit	Equation	Biodiesel information		value	unit
Producer gas flow rate from gasifier	G	8	L/min		Density of biodiesel at 50 °C	ρ_L	857	kg/m^3
Producer gas flow rate from gasifier	F_G	0.000133	m^3/s	Eq. (C.1)				
Average producer gas molar weight	M_{PG}	21	g/mol		Liquid flow rate	L	0.15	L/min
Producer gas Temperature, 200°C	T	473.15	K		Liquid flow rate	F_L	0.00214	kg/s
Tar concentration in the producer gas	C_{tar}	0.2%			Viscosity	σ	5.00E-02	m^2/s
Density of tar	ρ_{tar}	1060	kg/m^3					
Average tar molar weight	M_{tar}	157.4	g/mol					
Average molar weight of producer gas containing tars	M_{total}	21.3	kg/kmol	Eq. (C.2)				
Producer gas density (with tar)	ρ_1	3.39E-06	kmol/s	Eq. (C.3)				
Producer gas density (with tar)	$F_{G'}$	7.21E-05	kg/s	Eq. (C.4)				
Producer gas density (with tar)	ρ_2	0.541	kg/m^3	Eq. (C.5)				
Assuming essentially complete absorption, Tar removed	F_{tar}	1.07E-06	kg/s	Eq. (C.6)				
Liquid leaving	F_{out}	0.00214	kg/s	Eq. (C.7)				
L/G(ρG/(ρL-ρG))^0.5	F_{LG}	0.75		Eq. (C.8)				
In Fig. 7.7 use flooding line to determine the ordinate	δ	0.032						
For 8 mm partition ring, Cf	Cf	1000						
Galculated gas flow rate	G'	0.141	$kg/(s \cdot m^2)$	Eq. (C.9)				
The tower cross-sectional area	A	0.000510	m^2	Eq. (C.10)				
Diameter	D	2.55	cm	Eq. (C.11)				

Table C.2 Equations used in Table C.1.

Equation	Equation number
$F_G = \frac{G}{1000 \times 60}$	(C.1)
$M_{total} = M_{tar} \times C_{tar} + M_{PG} \times (1 - C_{tar})$	(C.2)
$\rho_1 = F_G \times \frac{273.15}{T} \times \frac{0.987}{1} \times \frac{1}{22.41}$	(C.3)
$F_{G\prime} = M_{total} \times \rho_1$	(C.4)
$\rho_2 = \frac{F_{G\prime}}{F_G}$	(C.5)
$F_{tar} = \rho_1 \times C_{tar} \times M_{tar}$	(C.6)
$F_{out} = F_{tar} + F_L$	(C.7)
$F_{LG} = \frac{F_{out}}{F_{G\prime}} \times [\frac{\rho_2}{(\rho_L - \rho_2)}]^{0.5}$	(C.8)
$G' = (\frac{\delta \times \rho_2 \times (\rho_L - \rho_2) \times 1}{C_f \times \sigma^{0.1} \times 1})^{0.5}$	(C.9)
$A = \frac{F_{G\prime}}{G'}$	(C.10)
$D = (\frac{4A}{\pi})^{0.5} \times 100$	(C.11)